BioMed Research International

PGCCs Generating Erythrocytes to Form VM Structure Contributes to Tumor Blood Supply

Guest Editors: Shiwu Zhang, Xiaochun Xu, Siwei Zhu, and Jun Liu

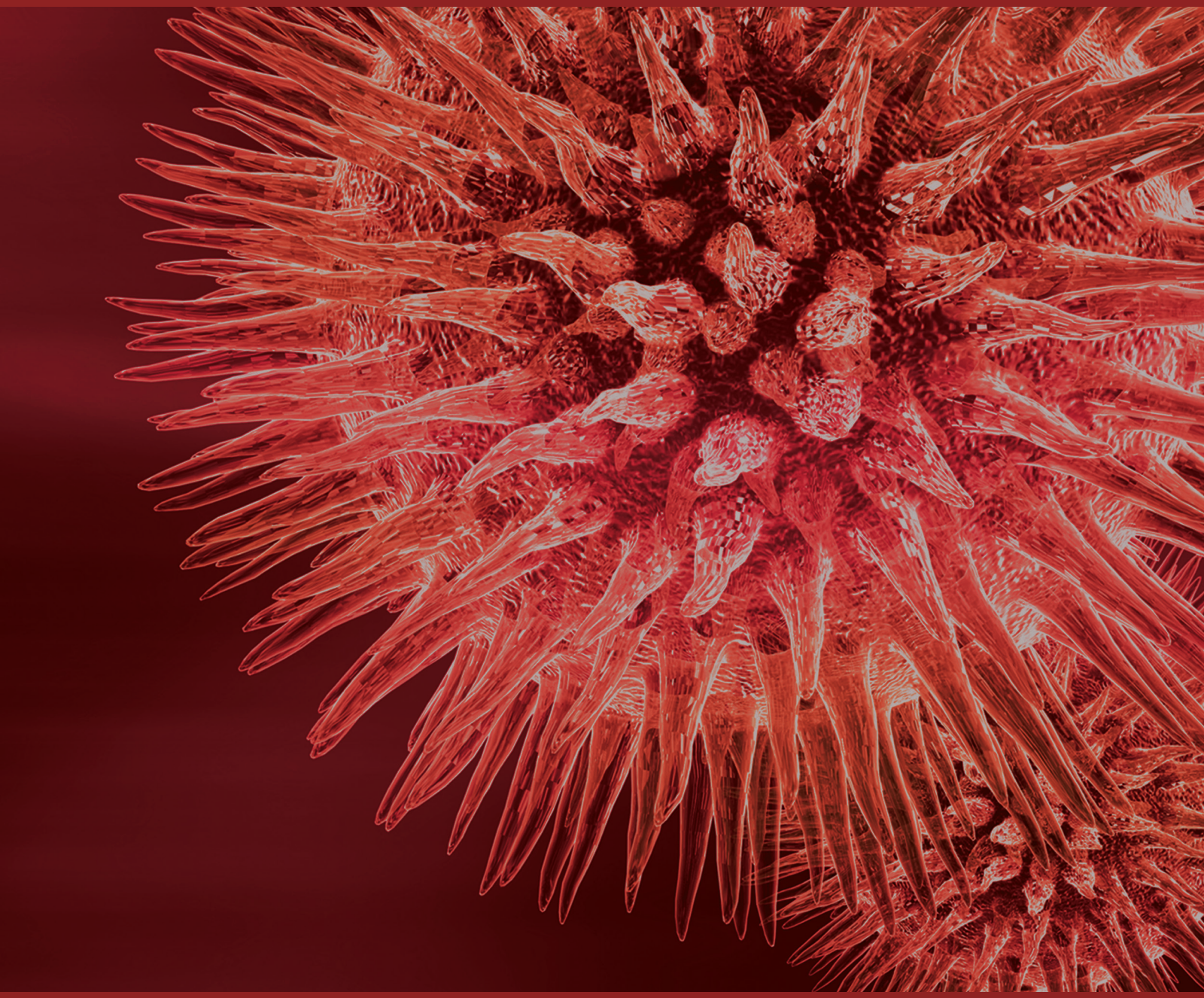

PGCCs Generating Erythrocytes to Form VM Structure Contributes to Tumor Blood Supply

BioMed Research International

PGCCs Generating Erythrocytes to Form VM Structure Contributes to Tumor Blood Supply

Guest Editors: Shiwu Zhang, Xiaochun Xu, Siwei Zhu, and Jun Liu

Contents

Hindawi Publishing Corporation
BioMed Research International
Volume 2015, Article ID 402619, 2 pages
http://dx.doi.org/10.1155/2015/402619

Editorial

PGCCs Generating Erythrocytes to Form VM Structure Contributes to Tumor Blood Supply

Shiwu Zhang,[1] Xiaochun Xu,[2] Siwei Zhu,[3] and Jun Liu[4]

[1]*Department of Pathology, Tianjin Union Medicine Center, Tianjin 300120, China*
[2]*Department of Clinical Cancer Prevention, University of Texas, M.D. Anderson Cancer Center, Houston, TX 77030, USA*
[3]*Department of Oncology, Nankai University, Tianjin 300121, China*
[4]*Department of Medical Imaging, Tianjin Union Medicine Center, Tianjin 300120, China*

Correspondence should be addressed to Shiwu Zhang; zhangshiwu666@aliyun.com

Received 16 December 2014; Accepted 16 December 2014

Over a century ago, it was found that cancer cells often have extra chromosomes; that is, normal human cells contain 46 chromosomes, whereas cancer cells contain abnormal numbers of chromosomes with cell-to-cell variability. Polyploid giant cancer cells (PGCCs) refer to a special subpopulation of cancer cells with giant and multinuclei and contribute to solid tumor heterogeneity. PGCCs differ from normal cells and even other cancer cells in cell size, morphology, proliferation pattern, expression of cell differentiation markers, and chromosome numbers and contribute to tumor formation and chemoradioresistance. The shape of PGCC nuclei is usually irregular and the size is at least three to five times larger than those of regular diploid cancer cells. PGCCs are the key contributor to the heterogeneity of human solid cancers and chromosome structural abnormalities, such as inversions, deletions, duplications, and translocations.

Mechanistically, PGCCs could be formed through end reduplication or cell fusion, reverting to regular cancer cells through splitting, budding, or burst-like mechanisms. PGCCs are divided asymmetrically and cycled slowly to form a dynamic population. However, these giant cells can also revert to regular-sized cancer cells through a reductive division, named as depolyploidization. Asymmetric cell division of giant cancer cells by meiosis-like depolyploidization had been previously proposed to explain the unexpected life cycle of these cells. In this special issue, D. Zhang et al. reported the asymmetric cell division in polyploid giant cancer cells and low eukaryotic cells and revealed the similarities in the budding process between yeast and PGCCs. This mechanism of PGCCs initialed the daughter cell generation which has also been reported in the normal growth of skeletal muscle and osteoclasts and in cells infected by virus or in vitro cell culture. Moreover, PGCCs were able to express certain normal and cancer stem cell markers and differentiate into the adipose tissue, cartilage, and bone. Single PGCC was able to form cancer spheroids in vitro and generate tumor xenograft in immunodeficient mice, indicating that these PGCCs had remarkable biologic features of cancer stem cells.

Furthermore, PGCCs are able to generate erythrocytes in vitro and in vivo besides their cancer stem cell properties. The difference of erythrocytes generated by bone marrow and PGCCs is the different forms of hemoglobin (see below). In human body, erythrocytes are produced in the bone marrow with a process known as hematopoiesis. The bone marrow stroma contains mesenchymal stem cells (MSCs) and hematopoietic stem cells (HSCs), which give rise to erythrocytes, leukocytes, and platelets. In adults, bone marrow is generally considered the main source of erythrocytes. However, PGCCs have an ability to generate erythrocytes in vitro and in vivo.

During cancer development, tumor cells undergo avascular growth. However, after a tumor mass reached a certain size, vasculogenic mimicry (VM) will connect with endothelium dependent vessels to obtain sufficient blood and oxygen supply to support further growth of tumor cells and support tumor invasion and metastasis. Accumulating evidence has

demonstrated that different types of cancer utilize VM to form a blood supply network to support their growth, invasion, and metastasis and, clinically, such a tumor is usually associated with poor prognosis. However, the source of erythrocytes in VM remains unclear. PGCCs can be induced by treatment of cancer cells with cobalt chloride (a hypoxia mimic) in vitro and hypoxia will increase self-renewal of cancer stem cells and promote the stem cell-like phenotype besides induction of PGCCs formation. Moreover, hypoxia also promotes the formation of vasculogenic mimicry (VM). B. Sun et al. showed that hypoxia inducible factor-1α plays an important role in the VM formation, while L. Zhang et al. provided the evidence that erythroid cells were localized in the cytoplasm of or around the PGCCs in serous ovarian carcinoma tissues and cancer cells in the VM structures and that these erythroid cells expressed hemoglobin-$\beta/\gamma/\varepsilon/\delta$ and hemoglobin-ζ detected by immunostaining. Thus, these VM structures can be formed by PGCCs or other cancer cells and their newly generated fetal erythrocytes with high O_2 binding affinity.

In addition, in this special issue, W. Wang et al. and L. Yao et al. demonstrated that epithelial-mesenchymal transition and Wnt signaling pathway could regulate the VM formation. Thus, elucidation of the molecular mechanisms of PGCC and VM formation could provide a novel insight into research in embryology, stem cells, and tumorigenesis. Identification of the PGCCs and tumor-derived erythrocytes could be a survival mechanism in hypoxia and targeting of PGCCs might be further developed as a potential therapeutic strategy for human cancers. Research focus on VM-targeted therapies could include dendritic cell vaccine and cytokine-induced killer cell therapy to conquer the recurrence and metastasis of aggressive cancers.

Shiwu Zhang
Xiaochun Xu
Siwei Zhu
Jun Liu

Hindawi Publishing Corporation
BioMed Research International
Volume 2015, Article ID 606752, 7 pages
http://dx.doi.org/10.1155/2015/606752

Clinical Study

Gemcitabine, Navelbine, and Doxorubicin as Treatment for Patients with Refractory or Relapsed T-Cell Lymphoma

Zhengzi Qian, Zheng Song, Huilai Zhang, Xianhuo Wang, Jing Zhao, and Huaqing Wang

Department of Lymphoma, Sino-US Center for Lymphoma and Leukemia, National Clinical Research Center of Cancer, Key Laboratory of Cancer Prevention and Therapy, Tianjin Medical University Cancer Institute and Hospital, Tiyuanbei, Huanhuxi Road, Hexi District, Tianjin 300060, China

Correspondence should be addressed to Huaqing Wang; huaqingw@163.com

Received 25 June 2014; Accepted 16 September 2014

Academic Editor: Shiwu Zhang

T-cell lymphoma (TCL) is resistant to conventional chemotherapy. We retrospectively evaluated the therapeutic efficiency and toxicity of gemcitabine, navelbine, and doxorubicin (GND) in patients with refractory or relapsed TCL. From 2002 to 2012, 69 patients with refractory or relapsed TCL received GND treatment in our hospital. The treatment protocol comprised gemcitabine (800 mg/m^2, group 1; 1000 mg/m^2, group 2) on days 1 and 8, navelbine (25 mg/m^2) on day 1, and doxorubicin (20 mg/m^2) on day 1, repeated every 3 weeks. The overall response rate (ORR) was 65.2%. The median overall survival (OS) was 36 months. The 5-year estimated OS rate was 32.4%. The GND regimen was well tolerated. Subgroup analysis demonstrated that the ORR and CR for group 1 were similar. A longer median OS was observed for group 1. Significant difference in grades 3-4 toxicities was observed between groups 1 and 2 ($P = 0.035$). Our study indicated that gemcitabine (800 mg/m^2) on days 1 and 8 every 21 days was favorable for pretreated TCL patients.

1. Introduction

T-cell lymphoma (TCL) belongs to a group of malignant, clonal hyperplastic diseases that is derived from T lymphocytes, and it is characterized by high heterogeneity, strong invasiveness, and a prominent association with Epstein-Barr virus and human T-lymphotropic virus type 1 infections as well as with specific chromosome translocations. The treatment outcomes of patients with B-cell lymphoma (BCL) have improved due to great advancements in chemotherapy combined with molecular targeted agents such as rituximab. However, due to its highly aggressive features, including local tumor invasiveness in early-stage disease, the outcomes of TCL patients are generally worse with poor long-term survival (5-year overall survival (OS): 20–30%) [1]. In addition, owing to resistance to conventional chemotherapeutic agents such as CHOP (cyclophosphamide, doxorubicin, vincristine, and prednisolone) or CHOP-like regimen, which is mediated by the expression of multidrug-resistance proteins, a substantial proportion of TCL patients develop refractory or relapsed disease. Although high-dose chemotherapy supported by autologous stem cell transplantation (ASCT) offers an advantage for some patients, the severe toxicities including cardiac and hematological adverse effects limit their widespread use. Even the introduction of novel drugs such as L-asparaginase cannot overcome the refractoriness completely. Therefore, additional trials and further studies are needed to develop safe and effective salvage chemotherapy regimens for patients with refractory or relapsed TCL.

Gemcitabine (2′,2′-difluoro-2′-deoxycytidine), which mainly acts on the synthesis phase of the cell cycle by inhibiting DNA synthesis, is a pyrimidine antimetabolite. It has been demonstrated that gemcitabine is one of the most effective agents when used either as a monotherapy agent or as part of a combination regimen for patients with relapsed or refractory Hodgkin lymphoma (HL) and non-Hodgkin lymphoma (NHL) [1–3]. Of particular importance, the National Comprehensive Cancer Network has incorporated this nucleoside metabolic inhibitor into its clinical practice guidelines.

Given the encouraging outcomes of previous studies, we investigated the effectiveness, safety, and toxicity of gemcitabine, navelbine, and doxorubicin (GND) combination chemotherapy in patients with refractory or relapsed TCL.

2. Patients and Methods

2.1. Patients. The subjects of this retrospective study are patients with refractory or relapsed TCL, who received GND treatment between January 2002 and December 2012 in the Tianjin Medical University Cancer Hospital. Patients were eligible according to the following criteria: histological with immunohistochemical diagnosis of TCL from professional pathologists according to the Revised European-American Lymphoma classification [4] and available pathological reports; complete blood counts showing white blood cell (WBC) counts $\geq 4 \times 10^9$/L, platelet (PLT) counts $\geq 100 \times 10^9$/L, neutrophil counts $\geq 1.5 \times 10^9$/L, and hepatic and renal function tests demonstrating aspartate aminotransferase and alanine transaminase levels ≤ 35 U/L and serum creatinine ≤ 80 μmol/L at the beginning of the treatment; no abnormalities with electrocardiography (ECG); refractory or relapsed after conventional therapeutic approaches including chemotherapy and/or radiotherapy; and accumulated dose of doxorubicin ≤ 350 mg/m^2 during the previous treatment. Exclusion criteria included a history of hepatitis B, hepatitis C, human immunodeficiency virus, uncontrolled infection or significant cardiac dysfunction, or central nervous system lymphoma at the time of GND administration. We collected the following clinical characteristics of enrolled patients retrospectively: patient demographics, time until relapse, histopathologic subtypes, Eastern Cooperative Oncology Group performance status, extent of disease involvement, Ann Arbor stage, International Prognostic Index, serum β2 microglobulin (β2-MG) levels, lactate dehydrogenase (LDH) levels, previous treatment regimens, deadline of the follow-up examination, and cause of death.

2.2. Treatment Protocol. From our archived clinical records, we established a cohort of 69 patients who received 2–6 cycles (median, 4 cycles) of the GND regimen every 3 weeks. All drugs were diluted in normal saline solution and administered through the subclavian vein. The treatment protocol consisted of gemcitabine (800 mg/m^2 or 1000 mg/m^2) on days 1 and 8, navelbine (25 mg/m^2) on days 1 and 8, and doxorubicin (20 mg/m^2) on day 1. In addition, 17 patients received local radiotherapy (36 Gy) for lymphoma masses after the completion of chemotherapy. Prophylactic 5-HT3 receptor antagonist (ramosetron and granisetron) and dexamethasone were administered routinely 30 minutes before every cycle. All patients were required to undergo a routine examination including physical examination, standard blood counts, liver and kidney function tests, urine routine analysis, and ECG on day 1 of each cycle. If the results showed no marked abnormalities, the subsequent cycle of chemotherapy was continued. Otherwise, patients whose WBC counts were $<4 \times 10^9$/L and neutrophil counts were $<1.5 \times 10^9$/L received recombinant human granulocyte colony-stimulating factor (G-CSF) at a dose of 100 μg/d and patients with PLT counts $<100 \times 10^9$/L received thrombopoietin (TPO) at the discretion of the treating physician, resulting in a treatment delay for 3–7 days.

2.3. Response Evaluation. All patients underwent a reevaluation with complete physical examination, laboratory tests, and previously positive radiographic examinations such as computed tomography (CT), magnetic resonance imaging, and positron emission tomography-CT imaging after every 2 cycles of the GND regimen. The tumor response was classified as complete remission (CR), unconfirmed complete remission (CRu), partial remission (PR), stable disease (SD), and progressive disease (PD), according to the International Workshop criteria for NHL [5]. The overall response rate (ORR) consists of CR, CRu, and PR. Adverse effects were also observed and graded from degree 1 to degree 4, according to the National Cancer Institute Common Terminology Criteria for Adverse Events v3.0. Overall survival (OS) was measured from the first day of GND treatment to the date of death due to any cause or the date of the last follow-up visit (30 June 2013).

2.4. Statistical Method. The SPSS software (Statistical Package for Social Science for Windows, version 17.0) for Windows was used for data analysis. Statistical significance was defined at P values < 0.05 by using a two-sided significance test. The survival rate was estimated and the survival curve was drawn simultaneously with the Kaplan-Meier method. Comparisons between response rates were performed by using the Chi-squared test (χ^2-test). The median OS is shown with 95% confidence interval (CI) limits and estimators for 1-, 3-, and 5-year OS were determined concomitantly. To compare the potential association between variables and prognosis, the log-rank test was performed. Variables showing P values < 0.05 in univariate analyses were candidates for multivariate analysis, which was performed by using the Cox proportional hazard regression model.

3. Results

3.1. Patient Characteristics. The clinical characteristics of 69 patients that were retrieved from clinical and pathological reports are summarized in Table 1. First, patients were stratified into 2 groups according to the different doses of gemcitabine, which were administered at either 800 mg/m^2 in group 1 ($n = 49$) or 1000 mg/m^2 in group 2 ($n = 20$). The time until recurrence from the initial diagnosis was calculated, and a cut-off of 12 months [6] was used to distinguish early relapse (48 patients (37 from group 1; 11 from group 2)) from late relapse (21 patients (12 from group 1; 9 from group 2)). Among all patients, peripheral TCL-unspecified (PTCL-U) is the most common histopathologic subtype (59.4%) followed by extranodal natural killer/T-cell lymphoma (33.3%), anaplastic large cell lymphoma (4.4%), and subcutaneous panniculitis-like TCL (2.9%). There was a male preponderance (42/69) in the cohort, and the median age was 59 years

Table 1: Clinical characteristics and prognostic factors for overall survival (OS) of all patients.

Characteristics	Number of patients (%)			Univariate	Multivariate		
	Group 1	Group 2	Total	*P* value	*P* value	HR	95% CI
Total	49 (71%)	20 (29%)	69 (100%)				
Recurrent time				0.021			
Early relapse	37 (75.5%)	11 (55%)	48 (69.6%)				
Late relapse	12 (24.5%)	9 (45%)	21 (30.4%)				
Pathology							
PTCL-U	28 (57.1%)	13 (65%)	41 (59.4%)				
NK/T	18 (36.7%)	5 (25%)	23 (33.3%)				
Subcutaneous panniculitis-like T-cell lymphoma	2 (4.1%)	0 (0%)	2 (2.9%)				
ALCL	1 (2.1%)	2 (10%)	3 (4.4%)				
Sex							
Male	30 (61.2%)	12 (60%)	42 (60.9%)				
Female	19 (38.8%)	8 (40%)	27 (39.1%)				
Age, years							
Median (range)	50 (10–79)	58 (19–80)	59 (10–80)				
≤60	20 (40.8%)	9 (45%)	29 (42.0%)				
>60	29 (59.2%)	11 (55%)	40 (58.0%)				
B-symptoms				0.014			
Present	27 (55.1%)	10 (50%)	37 (53.6%)				
Absent	22 (44.9%)	10 (50%)	32 (46.4%)				
Marrow involvement				0.000	0.042	3.816	1.049–13.886
Present	9 (18.4%)	5 (25%)	14 (20.3%)				
Absent	40 (81.6%)	15 (75%)	55 (79.7%)				
Splenomegaly				0.010			
Present	29 (59.2%)	11 (55%)	40 (58.0%)				
Absent	20 (40.8%)	9 (45%)	29 (42.0%)				
ECOG performance status							
0-1	19 (38.8%)	8 (40%)	27 (39.1%)				
2	26 (53.1%)	11 (55%)	37 (53.6%)				
≥3	4 (8.1%)	1 (5%)	5 (7.3%)				
Stage				0.004			
I-II	24 (49.0%)	7 (35%)	31 (44.9%)				
III-IV	25 (51.0%)	13 (65%)	38 (55.1%)				
IPI							
0-1 (low-risk group)	19 (38.8%)	2 (10%)	21 (30.4%)				
2-3 (intermediate-risk group)	25 (51.0%)	14 (70%)	39 (56.5%)				
4-5 (high-risk group)	5 (10.2%)	4 (20%)	9 (13.1%)				
Lymphocyte counts				0.005	0.000	5.305	2.100–13.403
$\geq 1 \times 10^9$/L	36 (73.5%)	16 (80%)	52 (75.4%)				
$<1 \times 10^9$/L	13 (26.5%)	4 (20%)	17 (24.6%)				
β2-MG				0.001			
>Upper limit of normal	26 (53.1%)	13 (65%)	39 (56.5%)				
Normal	23 (46.9%)	7 (35%)	30 (43.5%)				
LDH				0.002	0.018	2.538	1.172–5.493
>Upper limit of normal	31 (63.3%)	15 (75%)	46 (66.7%)				
Normal	18 (36.7%)	5 (25%)	23 (33.3%)				
Previous therapeutic regimen							
Radiotherapy	9 (18.4%)	3 (15%)	12 (17.4%)				
Chemotherapy	29 (59.2%)	13 (65%)	42 (60.9%)				
Chemoradiotherapy	11 (22.4%)	4 (20%)	15 (21.7%)				

PTCL-U: peripheral T-cell lymphoma-unspecified, NK/T: extranodal natural killer/T-cell lymphoma, ALCL: anaplastic large cell lymphoma, ECOG: Eastern Cooperative Oncology Group, LDH: lactate dehydrogenase, β2-MG: serum β2 microglobulin, IPI: International Prognostic Index, HR: hazard ratio, and 95% CI: 95% confidence interval. B-symptoms include unexplained fever over 38°C (100.4°F) for 1-2 weeks, unintentional weight loss of >10% of normal body weight over a period of 6 months or less, and drenching sweats, especially at night. IPI scores were calculated by summing the number of risk factors (age > 60 years, stage III/IV, involved extranodal sites > 1, ECOG performance status > 1, and elevated LDH levels).

Table 2: The clinical results for the two groups.

Response	Number of patients (%)		
	Group 1 (n = 49)	Group 2 (n = 20)	Total (n = 69)
CR	15 (30.6%)	5 (25%)	20 (29.0%)
PR	17 (34.7%)	8 (40%)	25 (36.2%)
ORR (CR + PR)	32 (65.3%)	13 (65%)	45 (65.2%)
SD	8 (16.3%)	3 (15%)	11 (15.9%)
PD	9 (18.4%)	4 (20%)	13 (18.9%)

CR: complete response, PR: partial response, ORR: overall response rate, SD: stable disease, and PD: progressive disease.

(range, 10–80 years). A majority of patients experienced B-symptoms and splenomegaly (53.6% and 58.0%, resp.). At baseline, 31 patients were classified as stages I-II and 38 patients were classified as stages III-IV. Remarkably, most patients showed elevated β2-MG levels (56.5%), LDH levels (66.7%), and most frequently elevated lymphocyte counts (75.4%). The previous chemotherapy treatments included CHOP or CHOP-like regimens (COP, CHOEP, ECHOP, and CHOPT), Hyper-CVAD (cyclophosphamide, vincristine, Adriamycin, and dexamethasone), DICE (dexamethasone, ifosfamide, carboplatin, and etoposide), and ICE (ifosfamide, carboplatin, and etoposide) with a median of 3 cycles (range, 2–6 cycles).

3.2. Response to GND. Table 2 demonstrates the clinical results of the two groups. Overall, objective responses to the GND regimen were obvious in 45 out of 69 evaluable patients with 20 patients achieving CR (29.0%) and 25 patients achieving PR (36.2%), resulting in an ORR of 65.2%. A total of 11 and 13 patients responded and developed SD (15.9%) or PD (18.9%), respectively. In addition, among 20 patients who achieved CR, 3 patients proceeded to receive ASCT and 5 patients received biotherapy. In subgroup analysis, the ORR was similar between patients from group 1 and group 2 (65.3% versus 65.0%, P = 0.981), although patients from group 1 achieved a higher CR rate than patients from group 2 (30.6% versus 25.0%, P = 0.641). Higher PR rates were observed in patients from group 2 versus group 1 (34.7% versus 40.0%, P = 0.677). There were no statistically significant response rate differences between the two different groups (by using χ^2-test).

3.3. Survival Analysis. At the cut-off date of the follow-up examination (30 June 2013), the median follow-up time was 3.5 years for all patients and 4 years for surviving patients (range, 0.5–11 years). The median OS was 36 months (range, 5–67 months; 95% CI: 25.314–46.686) among all patients. The median OS was higher for patients from group 1 compared to patients from group 2 (37 versus 23 months, resp.). According to the Kaplan-Meier analysis, the 1-, 3-, and 5-year estimated OS rates for the whole cohort were 71.7%, 47.3%, and 32.4%, respectively (Figure 1). Estimators for 1-year OS rates were similar between groups 1 and 2 (72.2% versus 70.3%, resp.). However, we observed significant differences for the 3- and 5-year OS rates between patients from groups 1 and 2 (53.1% versus 30.1% and 36.5% versus 20.1%, resp. (Figure 2)).

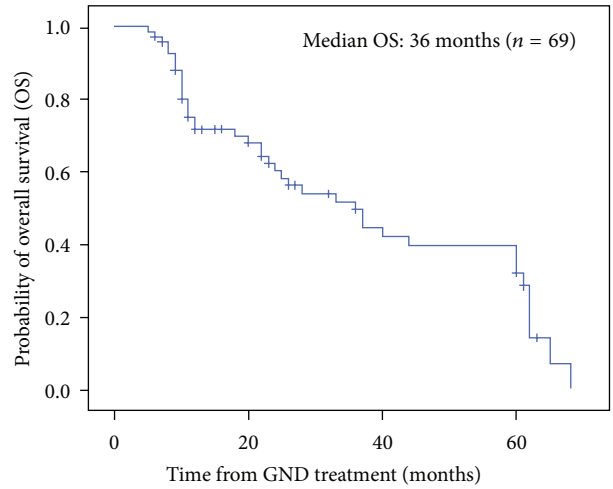

Figure 1: The Kaplan-Meier estimate of overall survival (OS) for all patients.

As shown in Table 1, univariate analysis identified 8 unfavorable prognostic factors for the 69 enrolled patients, including the time until recurrence (P = 0.021), B-symptoms (P = 0.014), bone marrow involvement (P = 0.000), splenomegaly (P = 0.010), disease stage (P = 0.004), lymphocyte counts (P = 0.005), β2-MG levels (P = 0.001), and LDH levels (P = 0.002). Moreover, multivariate Cox model analysis revealed that bone marrow involvement (P = 0.042; hazard ratio (HR): 3.816; 95% CI: 1.049–13.886), lymphocyte counts (P = 0.000; HR: 5.305; 95% CI: 2.100–13.403), and LDH levels (P = 0.018; HR: 2.538; 95% CI: 1.172–5.493) significantly influenced OS.

3.4. Treatment Toxicities. The GND regimen was well tolerated with grade 3 or greater treatment-emergent adverse events occurring in less than one-third of all responding patients. Unexpectedly, a significant difference in grade 3 to 4 toxicities was present between groups 1 and 2 (16.3% versus 40%, P = 0.035, by using χ^2-test). With regard to hematologic toxicities, which were more frequent relatively among all patients, grade 1 to 2 neutropenia or leukopenia was reported in 35 patients (50.7%), grade 1 to 2 anemia was noted in 23 patients (33.3%), and grade 1 to 2 thrombocytopenia was observed in 18 patients (26.1%). Grade 1 to 2 hematologic toxicities for group 2 patients were higher

Table 3: Treatment-emergent adverse events for the two groups.

Treatment toxicities	Number of patients (%)		
	Group 1 (n = 49)	Group 2 (n = 20)	Total (n = 69)
Grades 1-2			
Neutropenia or leukopenia	22 (44.9%)	13 (65%)	35 (50.7%)
Anemia	15 (30.6%)	8 (40%)	23 (33.3%)
Thrombocytopenia	11 (22.4%)	7 (35%)	18 (26.1%)
Infection	0	1 (5%)	1 (1.4%)
Nausea or emesis	25 (51.0%)	9 (45%)	34 (49.3%)
Fatigue	31 (63.3%)	13 (65%)	44 (63.8%)
Constipation	19 (38.8%)	10 (50%)	29 (42.2%)
Others	5 (10.2%)	2 (10%)	7 (10.1%)
Grades 3-4			
Hematologic toxicities	8 (16.3%)	7 (35%)	15 (21.7%)
Nonhematological toxicities	0	1 (5%)	1 (1.4%)

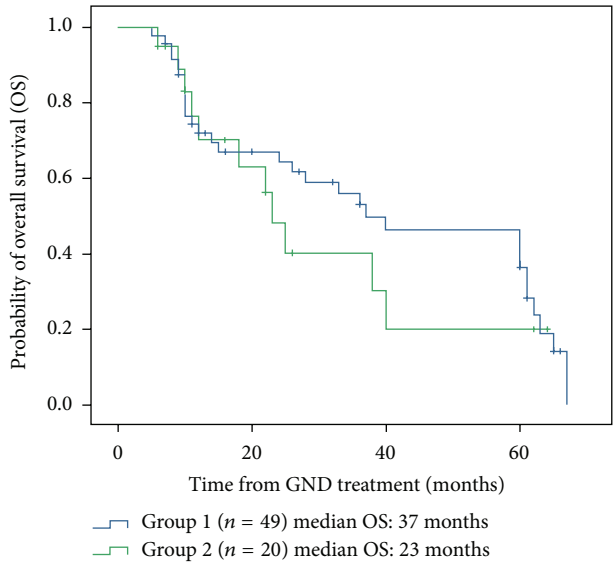

Figure 2: The Kaplan-Meier estimate of overall survival (OS) for groups 1 and 2.

than those for group 1 patients. Table 3 displays the specific proportions for the different groups. Although 21.7% of patients (group 1: 16.3%; group 2: 35.0%) developed grade 3 to 4 neutropenia or leukopenia, no grade 3 to 4 anemia or thrombocytopenia was observed. By using G-CSF and TPO, these hematological toxicities were easily manageable and mostly of short duration (≤1 week). Only 1 patient from group 2 had a neutropenia-associated pulmonary infection and recovered after anti-infective therapy. Nonhematological toxicities included nausea, emesis, fatigue, fever, headache, decreased appetite, constipation, and temporary dysfunction of the liver and kidney; most of these were mild and reversed spontaneously. No patients presented with severe pulmonary toxicity, catarrh, rash, dyspnea, anaphylaxis, edema, or peripheral nerve toxicity. Treatment related deaths did not occur. Other adverse effects included fever, headache, and temporary dysfunction of the liver and kidney.

4. Discussion

TCL encompasses a heterogeneous group of diseases, altogether accounting for less than 15% of all NHLs worldwide. It is known for its aggressive biological behavior, low response rate to initial treatment accompanied with a high recurrence rate, and poor prognosis even for stage I to II disease. Previously, many advances have been made in the treatment of TCL. Unfortunately, initiatives that just mirrored the therapies used for BCL have not achieved promising outcomes in TCL patients, especially in cases with relapsed or refractory disease. Because of the disappointing responses and serious toxicities, few options remain for therapeutic approaches incorporating novel agents such as alemtuzumab, bortezomib, or L-asparaginase containing regimes [7–9]. In addition, there is a paucity of data and consensus from phase III trials concerning the treatment of pretreated TCL patients.

Gemcitabine, a novel nucleoside analogue that is activated by deoxycytidine kinase (dCK), has shown promising results in solid tumors such as nonsmall cell lung cancer and in pancreatic and ovarian cancers [10–12]. Notably, recent studies showed that gemcitabine alone and/or gemcitabine containing chemotherapies were also efficient in the treatment of HL and NHL, including heavily pretreated lymphoma [1–3, 9]. In a phase II study of 44 pretreated patients with mycosis fungoides or cutaneous peripheral PTCL-U, this agent presented an attractive treatment option with a surprisingly high RR of 70.5% [13]. Furthermore, Marchi et al. reported RR of 75% with gemcitabine monotherapy in a phase II study of 32 previously untreated cutaneous TCL patients, with 22% of patients achieving CR [14]. Bergman et al. explored the possible mechanisms *in vitro* and found that gemcitabine acts against various human malignant cells with a multidrug resistance (MDR) phenotype by circumventing MDR [15]. MDR, associated with cross-resistance to some natural toxin-related compounds, is characterized by the overexpression of drug efflux pumps such as P-glycoprotein and MDR-associated proteins 1–3, which may be a result of increased dCK activity and reduced deoxycytidine deaminase activity [16]. Therefore, MDR cells often presented with

accumulated gemcitabine metabolism and sensitivity. This mechanism was related to the incorporation of gemcitabine into DNA and RNA, which in turn led to DNA damage [15].

According to previous studies, the effectiveness of gemcitabine is demonstrated with satisfactory response rates and acceptable toxicities. However, there are very limited data available describing the efficacy and safety of gemcitabine combined with navelbine and specifically about doxorubicin as treatment for patients with refractory or relapsed TCL. In this report, we retrospectively analyzed a cohort of 69 patients with a range of pretreated TCL histology, who had received the gemcitabine-containing regimen, GND.

The ORR was 65.2%, including 29.0% of patients who achieved CR and a significant survival benefit (median OS: 36 months). Our observations are encouraging and comparable to other published salvage regimens such as ICE [17] and DHAP [18]. Even though those intensive regimens could achieve an ORR of 60–70% [17, 18], significant toxicities, especially serious complications related to myelosuppression, affected patients' survival. In contrast, mild bone marrow toxicity with GND was another significant advantage over other regimens, as only 15 patients (21.7%) developed grade 3 to 4 neutropenia or leukopenia. The incidence of grade 3 or 4 nonhematological toxicity was low, and severe pulmonary toxicity associated with gemcitabine [19] was not observed. In addition, these promising results were observed in a cohort of refractory or relapsed patients, many of which were characterized according to poor prognostic features such as early relapse [6], stages III-IV disease, elevated LDH and β2-MG levels, and elevated lymphocyte counts [20, 21].

The different outcomes may be due to the schedule or dose intensity of our study compared to historical reports. Grade 3 to 4 myelosuppression related toxicity as documented in the Royal Marsden Hospital experience [22] for CALGB 59804 was common (grade 3 to 4 neutropenia, 62% and 63%, separately) [3]. In addition, it is well established that navelbine and doxorubicin, which act on different parts of the cell cycle, play an important role in the management of malignant lymphomas, especially in the first-line treatment. Thus, the GND regimen did not contain alkylating agents such as ifosfamide and cyclophosphamide, which could increase the risk of secondary malignancies in patients with NHL [23].

In the further subgroups, in which gemcitabine was given at different doses, the OS and treatment-associated adverse events, particularly grade 3 to 4 toxicities (16.3% versus 40% in groups 1 and 2, resp., $P = 0.035$), were significantly different despite similar ORRs (65.3% versus 65% in groups 1 and 2, resp., $P = 0.981$). The outcome of our study indicates that gemcitabine at 800 mg/m^2 on days 1 and 8 schedule repeated every 21 days was favorable for pretreated TCL patients.

5. Conclusion

In summary, our retrospective analysis showed that the GND treatment regimen was effective and well tolerated by patients with refractory or relapsed TCL. When interpreting the outcome of our study, the limited number of cases should be kept in mind. Therefore, further prospective investigations that involve a larger number of patients will be helpful to confirm the advantages of the GND regime and elucidate its clinical significance intensively.

Conflict of Interests

The authors declare that there is no conflict of interests regarding the publication of this paper.

References

[1] P. L. Zinzani, F. Venturini, V. Stefoni et al., "Gemcitabine as single agent in pretreated T-cell lymphoma patients: evaluation of the long-term outcome," *Annals of Oncology*, vol. 21, no. 4, pp. 860–863, 2009.

[2] B. Bai, H.-Q. Huang, Q.-Q. Cai et al., "Promising long-term outcome of gemcitabine, vinorelbine, liposomal doxorubicin (GVD) in 14-day schedule as salvage regimen for patients with previously heavily treated Hodgkin's lymphoma and aggressive non-Hodgkin's lymphoma," *Medical Oncology*, vol. 30, no. 1, p. 350, 2013.

[3] N. L. Bartlett, D. Niedzwiecki, J. L. Johnson et al., "Gemcitabine, vinorelbine, and pegylated liposomal doxorubicin (GVD), a salvage regimen in relapsed Hodgkin's lymphoma: CALGB 59804," *Annals of Oncology*, vol. 18, no. 6, pp. 1071–1079, 2007.

[4] S. A. Pileri, L. Leoncini, and B. Falini, "Revised European-American lymphoma classification," *Current Opinion in Oncology*, vol. 7, no. 5, pp. 401–407, 1995.

[5] B. D. Cheson, B. Pfistner, M. E. Juweid et al., "Revised response criteria for malignant lymphoma," *Journal of Clinical Oncology*, vol. 25, no. 5, pp. 579–586, 2007.

[6] C. Guglielmi, F. Gomez, T. Philip et al., "Time to relapse has prognostic value in patients with aggressive lymphoma enrolled onto the parma trial," *Journal of Clinical Oncology*, vol. 16, no. 10, pp. 3264–3269, 1998.

[7] S. J. Kim, K. Kim, Y. Park et al., "Dose modification of alemtuzumab in combination with dexamethasone, cytarabine, and cisplatin in patients with relapsed or refractory peripheral T-cell lymphoma: analysis of efficacy and toxicity," *Investigational New Drugs*, vol. 30, no. 1, pp. 368–375, 2012.

[8] J. Lee, C. Suh, H. J. Kang et al., "Phase I study of proteasome inhibitor bortezomib plus CHOP in patients with advanced, aggressive T-cell or NK/T-cell lymphoma," *Annals of Oncology*, vol. 19, no. 12, pp. 2079–2083, 2008.

[9] H. K. Ahn, S. J. Kim, D. W. Hwang et al., "Gemcitabine alone and/or containing chemotherapy is efficient in refractory or relapsed NK/T-cell lymphoma," *Investigational New Drugs*, vol. 31, no. 2, pp. 469–472, 2013.

[10] C. Manegold, B. Bergman, A. Chemaissani et al., "Single-agent gemeitabine versus cisplatln-etoposlde: early results of a randomised phase II study in locally advanced or metastatic non-small-cell lung cancer," *Annals of Oncology*, vol. 8, no. 6, pp. 525–529, 1997.

[11] H. A. Burris III, M. J. Moore, J. Andersen et al., "Improvements in survival and clinical benefit with gemcitabine as first-line therapy for patients with advanced pancreas cancer: a randomized trial," *Journal of Clinical Oncology*, vol. 15, no. 6, pp. 2403–2413, 1997.

[12] P. G. Rose, K. Mossbruger, N. Fusco, M. Smrekar, S. Eaton, and M. Rodriguez, "Gemcitabine reverses cisplatin resistance: demonstration of activity in platinum- and multidrug-resistant ovarian and peritoneal carcinoma," *Gynecologic Oncology*, vol. 88, no. 1, pp. 17–21, 2003.

[13] P. L. Zinzani, G. Baliva, M. Magagnoli et al., "Gemcitabine treatment in pretreated cutaneous T-cell lymphoma: experience in 44 patients," *Journal of Clinical Oncology*, vol. 18, no. 13, pp. 2603–2606, 2000.

[14] E. Marchi, L. Alinari, M. Tani et al., "Gemcitabine as frontline treatment for cutaneous T-cell lymphoma: phase II study of 32 patients," *Cancer*, vol. 104, no. 11, pp. 2437–2441, 2005.

[15] A. M. Bergman, H. M. Pinedo, I. Talianidis et al., "Increased sensitivity to gemcitabine of P-glycoprotein and multidrug resistance-associated protein-overexpressing human cancer cell lines," *British Journal of Cancer*, vol. 88, no. 12, pp. 1963–1970, 2003.

[16] A. M. Bergman, B. Munch-Petersen, P. B. Jensen et al., "Collateral sensitivity to gemcitabine (2′,2′-difluorodeoxycytidine) and cytosine arabinoside of daunorubicin- and VM-26-resistant variants of human small cell lung cancer cell lines," *Biochemical Pharmacology*, vol. 61, no. 11, pp. 1401–1408, 2001.

[17] C. H. Moskowitz, J. R. Bertino, J. R. Glassman et al., "Ifosfamide, carboplatin, and etoposide: a highly effective cytoreduction and peripheral-blood progenitor-cell mobilization regimen for transplant-eligible patients with non-Hodgkin's lymphoma," *Journal of Clinical Oncology*, vol. 17, no. 12, pp. 3776–3785, 1999.

[18] W. S. Velasquez, F. Cabanillas, P. Salvador et al., "Effective salvagae therapy for lymphoma with cisplatin in combination with high-dose ara-C and dexamethasone (DHAP)," *Blood*, vol. 71, no. 1, pp. 117–122, 1988.

[19] F. Barlési, C. Doddoli, C. Gimenez, L. Greillier, G. Lima, and J.-P. Kleisbauer, "Acute pulmonary toxicity due to gemcitabine: a role for asbestos exposure?" *Revue des Maladies Respiratoires*, vol. 20, no. 2, part 1, pp. 201–206, 2003.

[20] J. J. Castillo, D. Morales, P. Quinones, E. Cotrina, C. Desposorio, and B. Beltran, "Lymphopenia as a prognostic factor in patients with peripheral T-cell lymphoma, unspecified," *Leukemia and Lymphoma*, vol. 51, no. 10, pp. 1822–1828, 2010.

[21] M. P. Escalón, N. S. Liu, Y. Yang et al., "Prognostic factors and treatment of patients with T-cell non-Hodgkin lymphoma: the M. D. Anderson Cancer Center experience," *Cancer*, vol. 103, no. 10, pp. 2091–2098, 2005.

[22] H.-T. Arkenau, G. Chong, D. Cunningham et al., "Gemcitabine, cisplatin and methylprednisolone for the treatment of patients with peripheral T-cell lymphoma: the Royal Marsden Hospital experience," *Haematologica*, vol. 92, no. 2, pp. 271–272, 2007.

[23] Y. Xu, H. Wang, S. Zhou et al., "Risk of second malignant neoplasms after cyclophosphamide-based chemotherapy with or without radiotherapy for non-Hodgkin lymphoma," *Leukemia and Lymphoma*, vol. 54, no. 7, pp. 1396–1404, 2013.

Hindawi Publishing Corporation
BioMed Research International
Volume 2015, Article ID 195828, 9 pages
http://dx.doi.org/10.1155/2015/195828

Research Article

Construction of a CXCL12-KDEL Fusion Gene to Inhibit Head and Neck Squamous Cell Carcinoma Metastasis by Intracellular Sequestration of CXCR4

Wenchao Zhang, Xudong Wang, Kai Yue, Su Liu, and Xiaonan Liu

Department of Maxillofacial and ENT, National Cancer Clinical Research Center, Tianjin Medical University Cancer Institute & Hospital, Tianjin 300060, China

Correspondence should be addressed to Xudong Wang; zwbeyond_999@sina.com

Received 26 June 2014; Revised 18 August 2014; Accepted 19 August 2014

Academic Editor: Shiwu Zhang

The CXCL12-CXCR4 biological axis consisting of the chemotactic factor CXCL12 and its specific receptor CXCR4 plays an important role in oral cancer metastasis. High expression of CXCR4 may help oral squamous cancer cells invade local tissues and metastasize to lymph nodes. No obvious association was observed between CXCL12 expression and lymph node metastasis, suggesting that CXCL12 chemotaxis may only be related to CXCR4 expression on the tumor cell membrane. KDEL can be retained by receptors on the surface of the intracellular endoplasmic reticulum (ER) and also be called an ER retention signal sequence. So we adopted the KDEL sequence in this study to generate a CXCL12-KDEL fusion protein in combination with a traceable E-tag label. As such, CXCL12 was retained in the ER. Specific receptor CXCR4 binds to the CXCL12-KDEL, was also retained in the ER, and was thus prevented from reaching the oral squamous cancer cell surface. We reduced the cell surface level of CXCR4 and called the technique "intracellular sequestration." By this way, we have finished blocking of CXCL12-CXCR4 biological axis and inhibiting lymph node metastasis of oral carcinoma.

1. Introduction

Head and neck squamous cell carcinoma (HNSCC) is the most common malignant tumor of the oral cavity and throat, and subsequent neck lymph node metastases have important influence on prognosis [1–4]. The CXCL12-CXCR4 biological axis consisting of the chemotactic factor CXCL12 and its specific receptor CXCR4 plays an important role in cancer metastasis [5–7]. This axis facilitates tumor metastasis in breast cancer, non-small cell lung cancer, rhabdomyosarcoma, and other human malignant tumors, and the blocking of CXCL12-CXCR4 biological axis inhibits metastasis [8–11].

KDEL signal sequence is located in the carboxyl end of structural and functional proteins in the endoplasmic reticulum (ER). It represents a four-peptide sequence: Lys-Asp-Glu-Leu. Relevant receptors for the sequence in the Golgi membrane can recognize KDEL signals and combine with them, and then the combined ER proteins will be carried back to ER. KDEL can be retained by receptors on the surface of the intracellular ER and also be called an endoplasmic reticulum (ER) retention signal sequence.

Here we have made use of "intracellular sequestration" to reduce the cell surface level of CXCR4 by constructing CXCL12-KDEL fusion gene. Specific receptor CXCR4 binds to the CXCL12-KDEL, is also retained in the ER, and is thus prevented from reaching the Tb squamous cancer cell surface.

We aim to analyze the role of the CXCL12-CXCR4 biological axis on HNSCC lymph node metastasis. This will be achieved by constructing and utilizing a CXCL12-KDEL fusion gene expression vector (CXCL12-KDEL-pIRES2-EGFP) to block the CXCL12-CXCR4 biological axis and intracellularly sequester CXCR4, in order to inhibit HNSCC metastasis.

2. Materials and Methods

2.1. General Data. All the samples were collected from patients admitted to the Tianjin Medical University Cancer

Hospital between January 2005 and December 2006. Tissue samples surgically removed from 65 patients with HNSCC and 15 patients with benign lesions were included in this study, as the experimental and control groups, respectively. There were 43 men and 22 women, with an average age of 61 y (range: 19 to 83 y). Patients were staged according to the TNM staging criteria (2012) designed by the Union for International Cancer Control (UICC). In all, there were 26 cases in stages I-II and 39 cases in stages III-IV. Among the 65 patients of squamous cell carcinomas, 35 patients had ipsilateral and/or contralateral neck lymph node metastases, 30 patients had no lymph node metastases, and 2 patients had distant metastases. None of the patients received preoperative chemotherapy and radiotherapy. The carcinoma diagnosis was histopathologically confirmed with complete clinical and pathological data.

2.2. Experimental Materials. Competent *Escherichia coli* cells JM109, pMD19T plasmid, and DH5α cell were purchased from Takara Shuzo Co., Ltd. (Kyoto, Japan) and Promega (Madison, WI, USA), respectively. PIRES2-EGFP plasmid was prepared in our laboratory. Superscript II reverse transcription kit and PCR products extraction kit were purchased from Qiagen (Hilden, Germany) and Invitrogen Corporation (Maryland, USA), respectively. PCR purification and DNA connection kits were purchased from Takara Shuzo Co., Ltd. (Kyoto, Japan) and Roche Company (USA), respectively. RPMI-1640 culture medium was purchased from Invitrogen Company (USA) and fetal bovine serum (FBS) was purchased from Gibco Company (USA). Human tongue squamous cancer cell line Tb was provided by Shanghai Jiaotong University affiliated Ninth People's Hospital. Goat polyclonal antibody against CXCL12 was purchased from Santa Cruz Company (USA); horseradish peroxidase-labeled second antibody and mouse anti-β-actin antibody polyclonal antibody were purchased from Beijing Golden Bridge Biotechnology Company. RIPA lysis buffer was purchased from Millipore Company (USA).

2.3. Experimental Methods

2.3.1. Expression and Localization of CXCL12 and CXCR4 in Primary Tumors and Metastatic Lymph Nodes

(1) Expression and Localization of CXCL12 and CXCR4 in HNSCC and Lymph Nodes by Immunohistochemistry. CXCR4 and CXCL12 were detected using a rabbit anti-human polyclonal antibody (Boster Company, Wuhan, China) and rabbit anti-human monoclonal antibody (Santa Cruz, USA), respectively. Experiments were performed according to the manufacturer's instructions.

(2) CXCR4 mRNA Levels in HNSCC Metastasis Group, HNSCC Nonmetastasis Group, and Control Group and CXCL12 mRNA Levels in Metastatic Lymph Nodes and Nonmetastasis Group by RT-PCR. Total RNA was extracted using Trizol (Invitrogen, Carlsbad, CA, USA), following the manufacturer's protocol. RT reactions were performed in a final volume of 20 μL using M-MLT reverse transcriptase, according to the manufacturer instructions. The resulting cDNA products were stored at −20°C. The primers used in this study were as follows: endogenous control β-actin: 5′-CCTGGGCATGGAGTCCTGTG-3′ (forward), 5′-AGG–GGCCGGACTCGTCATAC-3′ (reverse); CXCL12: 5′-GCC–ATGAACGCCAAGGTC-3′ (forward), 5′-CGAGTGGGT–CTAGCGGAAAG-3′ (reverse), 312 bp; CXCR4; 5′-AGC–TGTTGGCTGAAAAGGTGGTCTATG-3′ (forward), 5′-GCGCTTCTGGTGGCCCTTGGAGTGTG-3′ (reverse), 254 bp. PCR amplification of CXCR4 was performed under the following conditions: 94°C for 5 min followed by 30 cycles of 94°C for 1 min, 56°C for 1 min, and 72°C for 1 min, with a final extension at 72°C for 10 min. PCR amplification of CXCL12 was performed under the following conditions: 94°C for 5 min, followed by 30 cycles of 94°C for 1 min, 55°C for 1 min, and 72°C for 1 min, with a final extension at 72°C for 10 min. RT-PCR products were detected by agarose gel electrophoresis.

2.3.2. Construction of the CXCL12-KDEL Fusion Gene

(1) CXCL12-KDEL Fusion Gene Primer Design and Fragments Amplification. CXCL12 coding gene sequences were retrieved from GenBank to determine the full amplification sequence. Once this was determined, cellular RNA was used as template, and the CXCL12-KDEL fragment was amplified by RT-PCR, resulting in an amplified fragment of 350 bp. The CXCL12-KDEL fusion gene primers used were as follows: 5′-TAGCAGATCTGCCATGGACGCCAAG-3′ (forward) and 5′-TAGCGTCGACTTACAGCTCGTCCTTCTCGCTTC-GCGGTTCCAGCGGATCCGGATACGGCACCGGCG-CACCCTTGTTTAAAGCTTTCTCCAGGTA-3′ (reverse); they were synthesized by SBS Genetech Co., Ltd. (Beijing, China). The ER retention sequence KDEL and the fusion gene's detecting marker genes sequence (E-tag) were added to reverse primers. The final PCR amplification reaction consisted of the following components: 5 μL of 10x PCR buffer, 4 μL of 4x dNTP (2.5 mM, each), 3 μL of $MgCl_2$ (25 mM), l μL each of P1 and P2 primers (both at 200 pmol), l μL of RNA template, 0.5 μL of Taq polymerase (2.5 U/μL), and 34.5 μL of double distilled water. The PCR reaction conditions were as follows: 94°C for 5 min, followed by 30 cycles of 94°C for 1 min, 62°C for 1 min, and 72°C for 1 min. The resulting 350-bp PCR product was separated and analyzed by electrophoresis on a 1% agarose gel, followed by purification and recovery.

(2) Amplification and Identification of Recombinant pMD19-T Vector. The purified CXCL12-KDEL gene was inserted into the pMD19-T vector to obtain a recombinant vector that was subsequently amplified and sequence verified.

(3) Construction of CXCL12-KDEL-pIRES2-EGFP Plasmid Eukaryotic Expression Vector. The amplified products were then subcloned into a pIRES2-EGFP plasmid, transformed into DH5α competent cells, and cultured overnight on a Luria broth agar plate containing kanamycin, in a 37°C constant temperature incubator. Single colonies were picked from the plate, following which plasmid DNA was extracted as per the

manufacturer's protocol. The resulting DNA was subjected to restriction digestion using two enzymes, *Bgl*II and *Sal*I, and 5 μL of the digested sample was separated by agarose gel electrophoresis. Positive clones identified by restriction enzyme digestion were then sequenced by Takara Company (Dalian, China). The resulting recombinant construct is referred to as CXCL12-KDEL-pIRES2-EGFP.

2.3.3. Recombinant Plasmid Transfection

(1) Tb Cell Culture and Gene Transfection. Tb cells were cultured in RPMI 1640 medium and supplemented with 10% FBS, 4 mM L-glutamine, 50 μ/mL penicillin, and 50 μg/mL streptomycin (Invitrogen, Carlsbad, CA, USA) at 37°C under 5% CO_2. Tb cells in logarithmic growth phase were seeded in 6-well plates, with 3×10^5 cells in each well. When the cells were 80% confluent, growth medium was removed, the cells were washed twice with PBS, and 2 mL of RPMI-1640 medium without serum was added back, and the cells were placed in an incubator at 37°C for 40 min. CXCL12-KDEL-pIRES2-EGFP plasmid (5 μL) was combined with Lipofectamine (10 μL) and added to the cell culture medium. The cells were then incubated at 37°C for 6 h, following which the medium was replaced with fresh complete medium and the cells were incubated for an additional 48 h until harvest.

(2) Assay for Transfection Efficiency. Tb3.l cells cultured for 48–72 h after transfection with CXCL12-KDEL-pIRES2-EGFP plasmid were evaluated for transfection efficiency by measuring levels of fluorescent protein expression using a DP70 fluorescence inverted phase contrast microscope. Fluorescent and bright field images were analyzed using the IPP5.1 software (Olympus Company, Japan).

2.3.4. Recombinant Fusion Gene Functional Experiment

(1) Determination of CXCL12-KDEL Protein Level by Western Blot. CXCL12-KDEL protein levels at 72 h after transfection were evaluated by measuring levels of the E-tag label using western blot. Cells were divided into six groups: CXCL12-KDEL-pIRES2-EGFP transfection group, empty vector pIRES2-EGFP transfection group, nontransfection group, and culture supernatants from each of the three groups.

(2) Analysis of Surface CXCR4 Expression in Transfected Cells. Transfected cells were harvested and incubated with CXCR4 antibody, following which they were analyzed by flow cytometry. Cells transfected with CXCL12-KDEL-pIRES2-EGFP were compared to cells transfected with the empty vector pIRES2-EGFP.

(3) Cell Chemotaxis Assay. For the chemotaxis assay, cancer cells were added to the upper layer of a chemotaxis chamber and recombinant CXCL12 was added to the bottom layer. Cells were counted and analyzed after incubation at 37°C for 2 h. Cells were divided into three groups: CXCL12-KDEL-pIRES2-EGFP transfection group, empty vector pIRES2-EGFP transfection group, and nontransfection group.

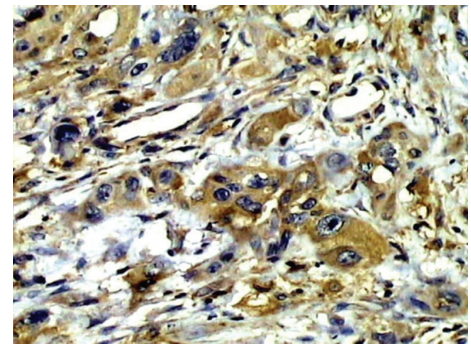

Figure 1: Strong positive expression of CXCR4 in metastatic squamous carcinoma tissues (200x).

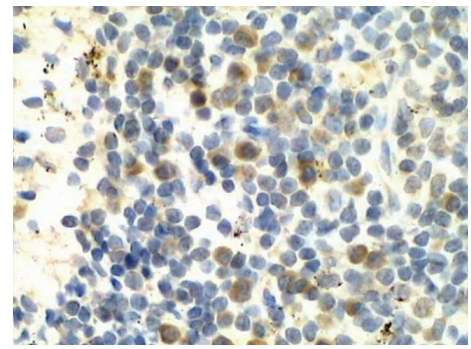

Figure 2: Positive expression of CXCL12 in lymph node tissues (200x).

2.4. Statistical Analysis. All the statistical analyses were performed using SPSS 16.0 (SPSS, Chicago, IL, USA). IHC results were estimated using χ^2 test or Fisher's exact test; RT-PCR results were estimated using ANOVA and two-sample t-test. A P value of <0.05 indicates a significant difference.

3. Results

3.1. Immunohistochemical Results. 65 patient's specimens were tested by IHC. CXCR4 was mostly expressed in squamous carcinoma tissues and localized mainly to the cytoplasm and partially to the cell membrane (Figure 1). CXCL12 was expressed in lymph node tissues, primarily in lymphocytes, and localized to the intercellular compartments (Figure 2).

Statistical analysis showed that the positive expression of CXCR4 in stages III-IV was significantly higher than that in stages I-II group ($P = 0.00$). Similarly, it was higher in G3 group than that in G1-G2 group ($P = 0.00$) and higher in metastatic group than that in the nonmetastatic group ($P = 0.017$) (Table 1).

There were no significant differences of CXCL12 positive expression in all compared groups ($P > 0.05$) (Table 1).

3.2. RT-PCR. Statistical analysis of integral optical density (IOD) showed that CXCR4 expression in metastatic group was higher than that in the nonmetastatic group and control

Table 1: The expression of CXCL12/CXCR4 by IHC in different groups of patients.

Clinicopathological parameter	n	Positive (%)		χ^2		P value	
		CXCR4	CXCL12	CXCR4	CXCL12	CXCR4	CXCL12
Gender				2.694	0.756	0.101	0.384
Male	43	23 (53.5)	12 (27.9)				
Female	22	12 (54.5)	6 (27.3)				
Age				1.234	0.618	0.267	0.432
<60 ys	31	16 (51.6)	8 (25.8)				
≥60 ys	34	19 (55.9)	10 (29.4)				
Stage				16.44	0.016	**0.000**	0.900
I-II	26	7 (26.9)	7 (26.9)				
III-IV	39	28 (71.8)	11 (28.2)				
Differentiation				27.41	1.025	**0.000**	0.311
G1-G2	47	20 (42.6)	13 (27.7)				
G3	18	15 (83.3)	5 (27.8)				
Metastasis of lymph node				5.704	0.296	**0.017**	0.587
No	30	10 (33.3)	8 (26.7)				
Yes	35	25 (71.4)	10 (28.6)				

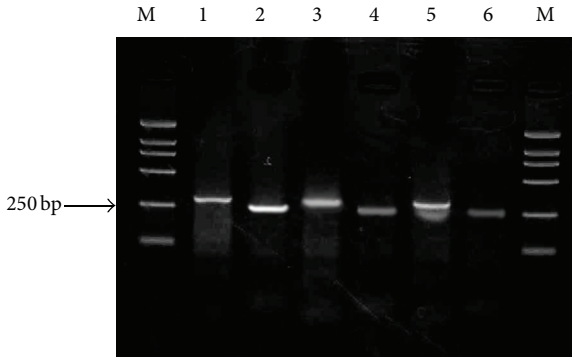

M: DL2000;1 ,3 , and 5: β-actin (305 bp); 2: CXCR4(254 bp) expression in HNSCC with lymph node metastasis; 4: CXCR4 expression in nonmetastatic HNSCC; 6: CXCR4 expression in benign tumor control group

Figure 3: CXCR4 expression in primary head and neck squamous carcinoma (HNSCC) tissues.

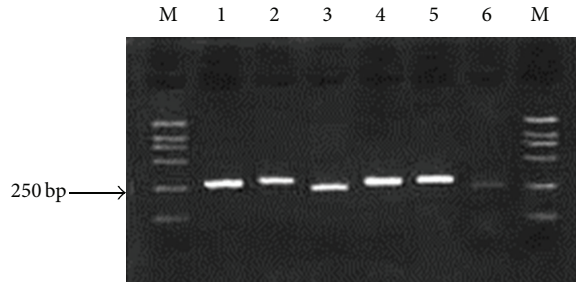

M: DL2000; 1, 4: β-actin (305 bp); 2: CXCL12 (312 bp) expression in metastatic lymph node; 3: CXCR4 (254 bp) expression in metastatic lymph node; 5: CXCL12 expression in nonmetastatic lymph node; 6: CXCR4 expression in nonmetastatic lymph node

Figure 4: CXCL12 and CXCR4 expression levels in neck lymph nodes.

Table 2: RT-PCR results of CXCR4 expression level in oral squamous cell carcinomas.

Group	n	CXCR4 IOD
Normal oral tissues and benign lesions	15	$0.406 \pm 0.044^{***}$
Nonmetastatic SCC	15	$0.464 \pm 0.068^{*}$
Lymph node metastatic SCC	15	$0.900 \pm 0.108^{**}$

SCC: squamous cell carcinomas and $^{*,**}P < 0.05$.
**VS $^{*}P < 0.05$, **VS $^{***}P < 0.05$, *VS $^{***}P < 0.05$.

group ($P < 0.05$); CXCR4 expression in the nonmetastatic group was significantly higher than that in the positive control group ($P < 0.05$) (as shown in Figure 3 and Table 2).

Statistical analysis showed that the expression of CXCR4 in lymph nodes with metastatic tumor was significantly higher than that of the nonmetastatic lymph nodes ($P < 0.05$), and there was no significant difference of CXCL12 expression in lymph nodes between the two groups ($P > 0.05$) (as shown in Figure 4 and Table 3).

3.3. Amplification of CXCL12-KDEL Gene. The expected and observed size of the amplified fragment were 350 bp (Figure 5).

3.4. Verification of Recombinant Plasmid by Enzyme Digestion and Sequencing. A *Bgl*II/*Sal*I restriction digest of CXCL12-KDEL-pIRES2-EGFP plasmid yields two predicted fragments of 350 bp and 5.3 kb. The length of the inserted product was confirmed to be of the same size as the predicted enzyme

Table 3: RT-PCR results of CXCL12 and CXCR4 expression level in neck lymph nodes (IOD).

Group	n	CXCL12*	CXCR4**
Metastatic lymph nodes	7	0.935 ± 0.087	0.947 ± 0.042
Nonmetastatic lymph nodes	7	0.861 ± 0.047	0.396 ± 0.071

* $P > 0.05$, ** $P < 0.05$.

Table 4: Chemotactic cells count and chemotactic index in each group ($\overline{x}$ ± s, $n = 3$).

Group	Cell count	CI value
Nontransfection group	825.67 ± 62.80	1
Empty vector (pIRES2-EGFP) transfection group	711.33 ± 49.54	0.86
CXCL12-KDEL transfection group	216.00 ± 84.12	0.26

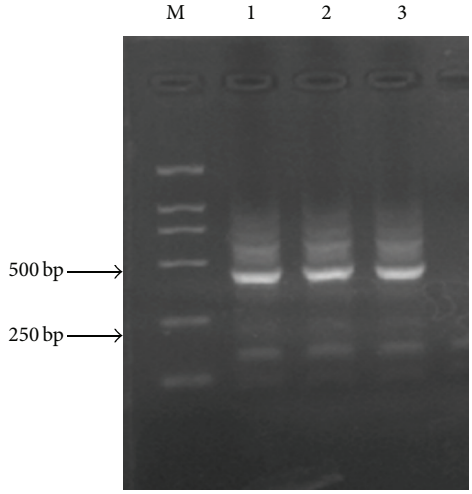

Figure 5: Agarose gel electrophoretogram of CXCL12-KDEL fusion gene PCR products. M: DL2000; 1–3: CXCL12-KDEL (350 bp).

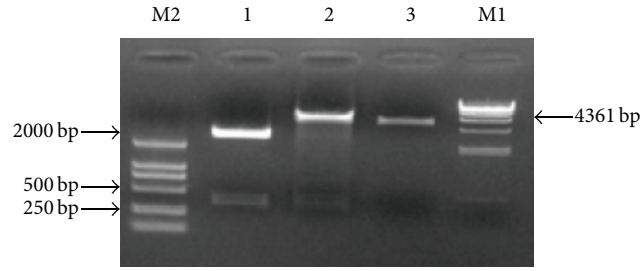

M1: λ-HindIII DNA Marker; 1: CXCL12-KDEL-19pMD-*Bgl*II/*Sal*I; 2: CXCL12-KDEL-pIRES2-EGFP-*Bgl*II/*Sal*I; 3: pIRES2-EGFP-*Bgl*II/*Sal*I; M2: DL 2, 000 DNA marker In the agarose gel electrophoretogram, CXCL12-KDEL gene bands (350 bp), and 19 pMD vector bands (2.7 kb) can be seen in Lane 1, CXCL12-KDEL gene bands (350 bp) and pIRES2-EGFP-vector bands (5.3 kb) can be seen in Lane 2, and pIRES2-EGFP-vector bands (5.3 kb) can be seen in Lane 3

Figure 6: Recombinant 19 pMD and pIRES2-EGFP-vector double digest gel electrophoretogram.

digestion product (Figure 6). The CXCL12-KDEL-pIRES2-EGFP plasmid was also sequence verified to be identical to the known gene sequence.

3.5. Determination of CXCL12-KDEL-pIRES2-EGFP Plasmid Transfection Efficiency. We observed that 48 h after recombinant plasmid transfection, 45% of the cells were positive for the expression of green fluorescent protein in Tb cells, and at 72 h after transfection this had increased to 50% (Figure 7).

3.6. Determination of CXCL12 Protein Levels by Western Blot. IOD was collected for each sample after transfection with recombinant CXCL12-KDEL-pIRES2-EGFP. Tb cells showed expression of E-tag protein, which is a surrogate label for CXCL12, whereas no protein expression was detected in the cells and the culture supernatant of the cells transfected with an empty plasmid or of those left untransfected (Figure 8).

3.7. CXCR4 Cell Surface Expression. Compared with the control group, CXCR4 expression on the cell surface in the experimental group is clearly reduced after transfection (Figure 9).

3.8. Chemotaxis Assay. Chemotaxis of cells in the experimental group was significantly less than that in the nontransfection group and the control group (transfected with empty vector) ($F = 70.14$, $P = 0.00$). However, there was no statistically significant difference between the nontransfection group and the empty vector transfection group (Table 4).

4. Discussion

Chemokines are a family of small proinflammatory chemoattractant cytokines that bind to leukocyte-expressed seven-transmembrane domain receptors and play a critical role in tumor angiogenesis and metastasis [12]. The chemokine CXCL12, also termed stromal cell derived factor-l (SDF-l), is a member of the CXC chemokine family, of which CXCR4 is a known CXCL12-specific receptor [13, 14]. CXCL12 is a small (8 kDa) chemokine that was originally regarded as an efficacious lymphocyte chemoattractant and was characterized as a modulator of several physiological processes. [15–18]. CXCR4 plays a key role in tumor cell dissemination and metastasis development in the majority of cancers and several types of leukemia [19–23].

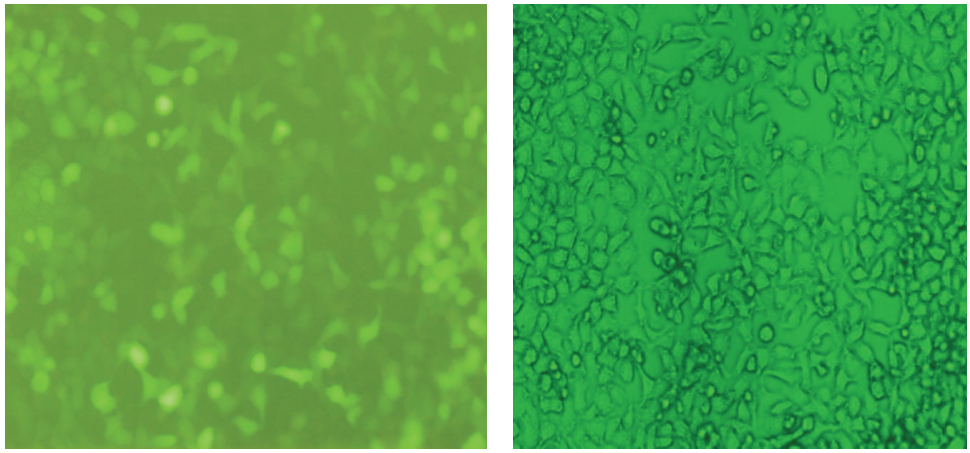

Figure 7: Analysis of Tb cells 72 h after transfection of recombinant CXCL12-KDEL-pIRES2-EGFP plasmid.

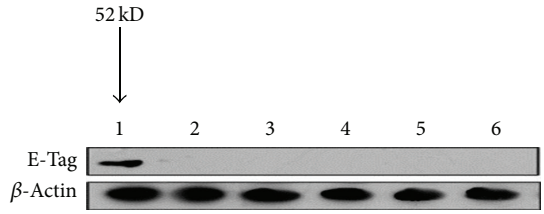

Figure 8: Western blot electrophoretogram of E-tag protein. 1: E-tag protein (52 kd) expression can be seen in Tb cells in the E-tag labeled CXCL12-KDEL transfection group, while no E-tag protein expression was observed in the remaining 5 groups; 2: red vector pIRES2 EGFP transfection group; 3: normal Tb nontransfection cells; 4–6: the culture supernatant of three kinds of cells.

Thus, the CXCL12-CXCR4 biological axis formed by CXCL12 and its specific receptor CXCR4 plays an important role in the process of metastasis of cancer cells [24]. The biological axis is related to the invasion, recurrence, and metastasis in many types of cancer including breast cancer [25], non-small cell lung cancer (NSCL) [26], colon cancer [27, 28], oral cavity squamous carcinoma [9], esophageal cancer [29], pancreatic carcinoma [30], renal cell carcinoma [31], and endometrial cancer [32].

In this study, our results show high CXCR4 expression in HNSCC, with higher expression in the metastatic group compared to the nonmetastatic group, which indicates that CXCR4 may play an important role in HNSCC metastasis. No obvious association was observed between CXCL12 expression and lymph node metastasis, suggesting that CXCL12 chemotaxis may only be related to CXCR4 expression on the tumor cell membrane. We speculate that tumor cells with high expression of CXCR4 have strong potential for local invasion, and CXCL12 expressed in lymph nodes has a chemotactic effect on their directional migration.

In vitro experiments confirmed that blocking the CXCL12-CXCR4 signal axis activity by different molecular biology methods such as RNAi, small molecule inhibitors in breast cancer cells, could effectively reverse the malignant phenotype of the tumor cells [33–35]. Animal experiments also show that CXCR4 monoclonal antibody can inhibit lymph node metastasis of human breast cancer cells in nude mice. The ER retention signal sequence KDEL represents a four-peptide sequence (Lys-Asp-Glu-Leu), which can be retained by receptors on the surface of the ER [36]. Based on this, we adopted the KDEL sequence in this study to generate a CXCL2-KDEL fusion protein in combination with a traceable E-tag label. As such, CXCL12 was retained in the endoplasmic reticulum allowing it to act as a sink for CXCR4, thus sequestering the latter within the intracellular space. The intracellular sequestration of CXCR4 provides a new strategy for blocking the CXCL12-CXCR4 biological axis. The validity of the CXCL12-KDEL-pIRES2-EGFP plasmid was confirmed by both restriction enzyme digestion and sequencing. At 48 and 72 h after Tb cells were transfected with the recombinant CXCL12-KDEL-pIRES2-EGFP plasmid, we were able to observe fluorescent gene expression from EGFP, confirming successful transfection. Vectors can be used to express EGFP protein alone or obtain stable transfection cell lines. The transfection efficiency can then be analyzed by the intensity of fluorescent protein expression [37]. As determined by western blot of the E-tag label protein, a surrogate marker for CXCL12 protein was successfully expressed following recombinant plasmid transfection, whereas CXCL12 protein expression was not detected in cells transfected with the empty plasmid or in those that were left untransfected.

In this study, we adopted a technique that used CXCL12-KDEL as an intrinsic factor for the intracellular sequestration of CXCR4. We inserted the KDEL sequence downstream of CXCL12 and through functional experiments were able to demonstrate the intracellular capture of CXCR4 surface expression and the blocking of the chemotaxis of cells via the CXCL12-CXCR4 biological axis [38]. This strategy of sequestering CXCR4 using another intracellular component is an example of technology using inactivated biomolecular molecules; other examples are the use of antisense nucleic acid, ribozymes-mediated negative mutation, and gene knockout technologies. These technologies are very similar to the "intracellular antibody" technology, ultimately aimed to form a phenotypic knockout model. In this study,

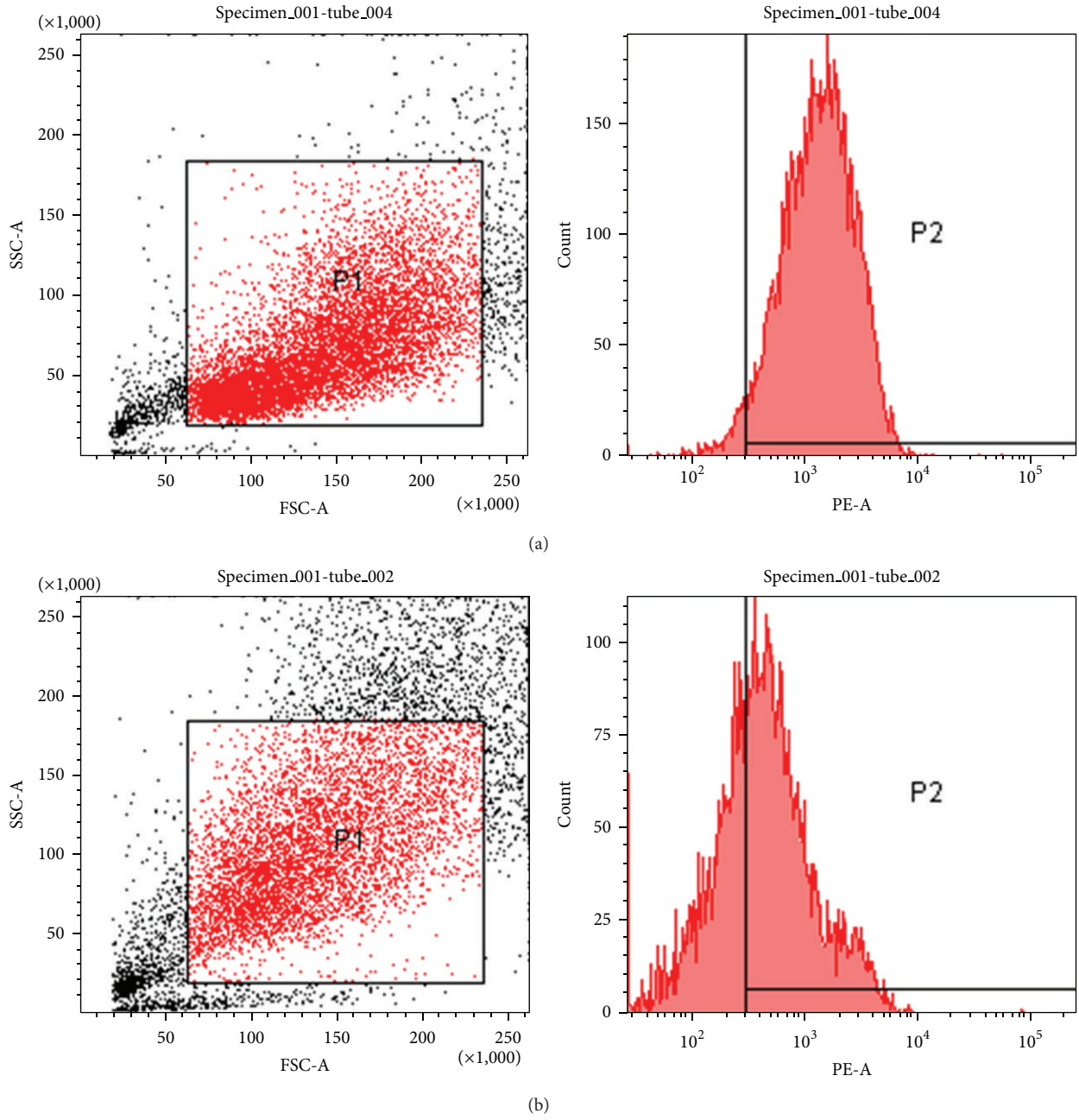

Figure 9: CXCR4 expression on the cell surface after transfection with empty vector (a) or target gene CXCL12-KDEL (b).

the transfection efficiency met the basic outcomes of the study; however, the specific transfection efficiency needs to be clarified by further screening. Meanwhile, application of this method in *in vitro* experiments can reduce cell surface expression of CXCR4 and the chemotaxis of tumor cells. As such, our results lay a foundation for further screening and animal experiments.

5. Conclusions

High expression of CXCR4 may help squamous cancer cells invade local tissues and metastasize to other tissues, and the intracellular sequestration of CXCR4 by transfection of the CXCL12-KDEL fusion gene may inhibit chemotaxis and metastasis in tongue squamous cancer cells.

Conflict of Interests

The authors declare that there is no conflict of interests regarding the publication of this paper.

References

[1] C. T. Liao, J. T. Chang, and H. M. Wang, "Analysis of risk factors of predictive local tumor control in oral cavity cancer," *Annals of Surgical Oncology*, vol. 15, no. 3, pp. 915–922, 2008.

[2] L. P. Kowalski, R. Bagietto, J. R. Lara, and et al, "Prognostic significance of the distribution of neck node metastasis from oral carcinoma," *Head & Neck*, vol. 22, no. 3, pp. 207–214, 2000.

[3] M. Noguchi, Y. Kido, H. Kubota, H. Kinjo, and G. Kohama, "Prognostic factors and relative risk for survival in N1-3 oral squamous cell carcinoma: a multivariate analysis using Cox's hazard model," *British Journal of Oral and Maxillofacial Surgery*, vol. 37, no. 6, pp. 433–437, 1999.

[4] J. A. Woolgar, S. Rogers, C. R. West, R. D. Errington, J. S. Brown, and E. D. Vaughan, "Survival and patterns of recurrence in 200 oral cancer patients treated by radical surgery and neck dissection," *Oral Oncology*, vol. 35, no. 3, pp. 257–265, 1999.

[5] M. P. Crump, J. H. Gong, P. Loetscher et al., "Solution structure and basis for functional activity of stromal cell-derived factor-1: dissociation of CXCR4 activation from binding and inhibition of HIV-1," *EMBO Journal*, vol. 16, no. 23, pp. 6996–7007, 1997.

[6] H. Kang, G. Watkims, A. Douglas-Jones, and et al, "The elevated level of CXCR4 is correlated with nodal metastasis of human breast cancer," *The Breast*, vol. 14, no. 5, pp. 360–367, 2005.

[7] J. J. Liang, S. Zhu, R. Bruggeman et al., "High levels of expression of human stromal cell-derived factor-1 are associated with worse prognosis in patients with stage II pancreatic ductal adenocarcinoma," *Cancer Epidemiology, Biomarkers & Prevention*, vol. 19, no. 10, pp. 2598–2604, 2010.

[8] M. Darash-Yahana, E. Pikarsky, R. Abramovitch et al., "Role of high expression levels of CXCR4 in tumor growth, vascularization, and metastasis," *The FASEB Journal*, vol. 18, no. 11, pp. 1240–1242, 2004.

[9] A. Almofti, D. Uchida, N. M. Begum et al., "The clinicopathological significance of the expression of CXCR4 protein in oral squamous cell carcinoma," *International Journal of Oncology*, vol. 25, no. 1, pp. 65–71, 2004.

[10] J. Libura, J. Drukala, M. Majka, and etal, "CXCR4-SDF-1 signaling is active in rhabdomyosarcoma cells and regulates locomotion, chemotaxis, and adhesion," *Blood*, vol. 100, no. 7, pp. 2597–2606, 2002.

[11] T. Kijima, G. Maulik, P. C. Ma et al., "Regulation of cellular proliferation, cytoskeletal function, and signal transduction through CXCR4 and c-Kit in small cell lung cancer cells," *Cancer Research*, vol. 62, no. 21, pp. 6304–6311, 2002.

[12] G. Lazennec and A. Richmond, "Chemokines and chemokine receptors: new insights into cancer-related inflammation," *Trends in Molecular Medicine*, vol. 16, no. 3, pp. 133–144, 2010.

[13] A. Orimo, P. B. Gupta, D. C. Sgroi et al., "Stromal fibroblasts present in invasive human breast carcinomas promote tumor growth and angiogenesis through elevated SDF-1/CXCL12 secretion," *Cell*, vol. 121, no. 3, pp. 335–348, 2005.

[14] R. M. Strieter, M. D. Burdick, J. Mestas, B. Gomperts, M. P. Keane, and J. A. Belperio, "Cancer CXC chemokine networks and tumour angiogenesis," *European Journal of Cancer*, vol. 42, no. 6, pp. 768–778, 2006.

[15] M. Kucia, K. Jankowski, R. Reca et al., "CXCR4-SDF-1 signalling, locomotion, chemotaxis and adhesion," *Journal of Molecular Histology*, vol. 35, no. 3, pp. 233–245, 2004.

[16] Y.-R. Zou, A. H. Kottman, M. Kuroda, I. Taniuchi, and D. R. Littman, "Function of the chemokine receptor CXCR4 in heaematopolesis and in cerebellar development," *Nature*, vol. 393, no. 6685, pp. 595–599, 1998.

[17] A. Aiuti, I. J. Webb, C. Bleul, T. Springer, and J. C. Gutierrez-Ramos, "The chemokine SDF-1 is a chemoattractant for human CD34+ hematopoietic progenitor cells and provides a new mechanism to explain the mobilization of CD34+ progenitors to peripheral blood," *Journal of Experimental Medicine*, vol. 185, no. 1, pp. 111–120, 1997.

[18] Q. Ma, D. Jones, P. R. Borghesani et al., "Impaired B-lymphopoiesis, myelopoiesis, and derailed cerebellar neuron migration in CXCR4- and SDF-1-deficient mice," *Proceedings of the National Academy of Sciences of the United States of America*, vol. 95, no. 16, pp. 9448–9453, 1998.

[19] A. Zlotnik, "New insights on the role of CXCR4 in cancer metastasis," *Journal of Pathology*, vol. 215, no. 3, pp. 211–213, 2008.

[20] F. Balkwill, "The significance of cancer cell expression of the chemokine receptor CXCR4," *Seminars in Cancer Biology*, vol. 14, no. 3, pp. 171–179, 2004.

[21] B. Furusato, A. Mohamed, M. Uhlén, and J. S. Rhim, "CXCR4 and cancer: review Article," *Pathology International*, vol. 60, no. 7, pp. 497–505, 2010.

[22] J. Vandercappellen, J. van Damme, and S. Struyf, "The role of CXC chemokines and their receptors in cancer," *Cancer Letters*, vol. 267, no. 2, pp. 226–244, 2008.

[23] M. Darash-Yahana, E. Pikarsky, R. Abramovitch et al., "Role of high expression levels of CXCR4 in tumor growth, vascularization, and metastasis," *FASEB Journal*, vol. 18, no. 11, pp. 1240–1242, 2004.

[24] R. K. Ganju, S. A. Brubaker, J. Meyer et al., "The α-chemokine, stromal cell-derived factor-1α, binds to the transmembrane G-protein-coupled CXCR-4 receptor and activates multiple signal transduction pathways," *The Journal of Biological Chemistry*, vol. 273, no. 36, pp. 23169–23175, 1998.

[25] A. Muller, B. Homey, H. Soto et al., "Involvementof chemokine receptors in breast cancermetastasi," *Nature*, vol. 410, pp. 50–56, 2001.

[26] L. Wang, Z. Wang, X. Liu, and et al, "High-level C-X-C chemokine receptor type 4 expression correlates with brain-specific metastasis following complete resection of non-small cell lung cancer," *Oncology Letters*, vol. 7, no. 6, pp. 1871–1876, 2014.

[27] J. Kim, H. Takeuchi, S. T. Lam et al., "Chemokine receptor CXCR4 expression in colorectal cancer patients increases the risk for recurrence and for poor survival," *Journal of Clinical Oncology*, vol. 23, no. 12, pp. 2744–2753, 2005.

[28] S. Saigusa, Y. Toiyama, K. Tanaka et al., "Stromal CXCR4 and CXCL12 expression is associated with distant recurrence and poor prognosis in rectal cancer after chemoradiotherapy," *Annals of Surgical Oncology*, vol. 17, no. 8, pp. 2051–2058, 2010.

[29] K. Koishi, R. Yoshikawa, T. Tsujimura et al., "Persistent CXCR4 expression after preoperative chemoradiotherapy predicts early recurrence and poor prognosis in esophageal cancer," *World Journal of Gastroenterology*, vol. 12, no. 47, pp. 7585–7590, 2006.

[30] W. C. Liao, H. P. Wang, H. Y. Huang et al., "CXCR4 expression predictsearly liver recurrence and poor survival after resection of pancreatic adenocarcinoma," *Clinical and Translational Gastroenterology*, vol. 3, article e22, 2012.

[31] L. Wang, W. Chen, L. Gao et al., "High expression of CXCR4, CXCR7 and SDF-1 predicts poor survival in renal cell carcinoma," *World Journal of Surgical Oncology*, vol. 10, article 212, 2012.

[32] A. S. Felix, R. A. Stone, M. Chivukula et al., "Survival outcomes in endometrial cancer patients are associated with CXCL12 and estrogen receptor expression," *International Journal of Cancer*, vol. 131, no. 2, pp. E114–E121, 2012.

[33] B. Guleng, K. Taleishi, M. Ohta, and et al, "Blockade of the stromal cell-derived factor-1/CXCR4 axis attenuates in vivo tumor groeth by inhibiting angiogenesis in a vascular endothelial groeth factor-independent manner," *Cancer Research*, vol. 65, no. 13, pp. 58–64, 2005.

[34] H. Tamamura, A. Hori, N. Kanzaki et al., "T140 analogs as CXCR4 antagonists identified as anti-metastatic agents in the treatment of breast cancer," *FEBS Letters*, vol. 550, no. 1–3, pp. 79–83, 2003.

[35] Z. Liang, Y. Yoon, J. Votaw et al., "Silencing of CXCR4 blocks breast cancer metastasis," *Cancer Research*, vol. 65, no. 3, pp. 967–971, 2005.

[36] I. S. Zeelenberg, L. Ruuls-Van Stalle, and E. Roos, "Retention of CXCR4 in the endoplasmic reticulum blocks dissemination of a T cell hybridoma," *Journal of Clinical Investigation*, vol. 108, no. 2, pp. 269–277, 2001.

[37] B. Dalby, S. Cates, A. Harris et al., "Advanced transfection with Lipofectamine 2000 reagent: primary neurons, siRNA, and high-throughput applications," *Methods*, vol. 33, no. 2, pp. 95–103, 2004.

[38] J. Kodama, Hasengaowa, T. Kusumoto, and et al, "Association receptor expression and lymph node metastasis in human cervical cancer," *Annals of Oncology*, vol. 18, no. 1, pp. 70–76, 2007.

Hindawi Publishing Corporation
BioMed Research International
Volume 2015, Article ID 809714, 7 pages
http://dx.doi.org/10.1155/2015/809714

Clinical Study

A Phase I Trial to Evaluate the Multiple-Dose Safety and Antitumor Activity of Ursolic Acid Liposomes in Subjects with Advanced Solid Tumors

Zhengzi Qian, Xianhuo Wang, Zheng Song, Huilai Zhang, Shiyong Zhou, Jing Zhao, and Huaqing Wang

Department of Lymphoma, Sino-US Center for Lymphoma and Leukemia, Tianjin Medical University Cancer Institute and Hospital, National Clinical Research Center of Cancer, Key Laboratory of Cancer Prevention and Therapy, Tiyuanbei, Huanhuxi Road, Hexi District, Tianjin 300060, China

Correspondence should be addressed to Huaqing Wang; huaqingw@163.com

Received 25 June 2014; Revised 9 October 2014; Accepted 12 October 2014

Academic Editor: Shiwu Zhang

Ursolic acid liposome (UAL), a new antitumor drug, has potential therapeutic value. However, limited clinical data exists regarding multiple-dose safety, antitumor activity, and the recommended dose (RD) of UAL for subjects with advanced solid tumors. All subjects were intravenously administered UAL for 14 consecutive days of a 21-day treatment cycle. Twenty-one subjects were enrolled in 1 of 3 sequential cohorts (56, 74, and 98 mg/m^2) to evaluate multiple-dose tolerability and efficacy. Eight additional subjects were treated with UAL (74 mg/m^2) to evaluate multiple-dose pharmacokinetics. No ≥grade 3 adverse events (NCI-CTC) were observed. Sixty percent subjects achieved stable disease after 2 treatment cycles. Multiple-dose pharmacokinetic analysis suggested UAL does not accumulate in the body. This trial demonstrates that UAL was tolerable, had manageable toxicity, and could potentially improve patient remission rates. A large phase II study is recommended to confirm these results (i.e., RD of 98 mg/m^2).

1. Introduction

Ursolic acid (UA) is a natural hydroxy pentacyclic triterpene compound (Figure 1) isolated from Chinese herbs including *Eriobotrya japonica*, *Rosmarinus officinalis*, and *Glechoma hederacea* [1, 2]. Previous studies have indicated that UA can induce apoptosis [3–5] and cell differentiation [6, 7], inhibit invasion and metastasis [8], and inhibit angiogenesis [9–11] in various tumors. UA treatment is also safe [12]. Thus, UA is a potentially valuable compound. However, the poor solubility of UA in hydrous solutions greatly limits its applications.

Liposomes have been utilized as a drug delivery system to overcome the poor solubility of UA, increase the therapeutic efficiency, reduce the side effects, and enhance the bioavailability of drugs that have been broadly applied [13–15]. Currently, ursolic acid liposomes (UALs) have been studied successfully and have been approved by the State Food and Drug Administration (SFDA) of China to enter clinical trials (number 2009L00634). We have previously published data regarding the maximum tolerated dose, dose-limiting toxicity (DLT), and pharmacokinetics of UAL in a single-dose administration study. The recommended doses in multiple-dose administration trials of UAL are 56, 74, and 98 mg/m^2 [16]. In actuality, multiple-dose administration is usually adopted for most of drugs in clinic. Therefore, it is more important to study the effects of UALs in a multiple-dose administration trial.

The primary objective of this study was to evaluate the tolerability of UAL treatment and the recommended dose (RD) in a multiple-dose administration phase II trial consisting of subjects with advanced solid tumors. The second objective was to perform a preliminary assessment of the antitumor activity of UALs.

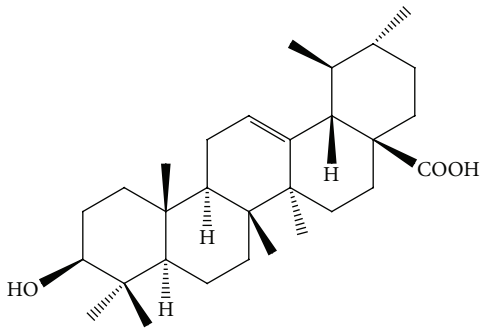

Figure 1: The chemical structure of ursolic acid.

2. Materials and Methods

We performed a phase I, open-label, single center trial in subjects with advanced solid tumors. The SFDA of China and the Hospital Medical Ethics Committees approved the trial and it was conducted in accordance with the Declaration of Helsinki and the applicable local regulatory requirements and laws. A signed, written informed consent of the legal representatives and the consent of each patient were obtained before any study procedure was performed. UALs were supplied by Wuhan Li Yuanheng Medicine Technology Co. Ltd (Wuhan, China) as a freeze-dried powder for infusion. Each glass vial contained 3 mg of active drug. It was uniformly dispersed in 250 mL of 5% glucose solution before administration.

2.1. Patient Eligibility. Eligible subjects were aged 18–75 years with cytologically or histologically confirmed advanced solid tumors; they either refused standard therapies or standard effective therapies did not exist; and they had an Eastern Cooperative Oncology Group (ECOG) performance status (PS) of 0–2, a Karnofsky score ≥ 60%, and a life expectancy ≥ 3 months; practiced adequate contraception; had adequate hematological function (white blood cell (WBC) ≥ 4.0×10^9/L, absolute neutrophil count (ANC) ≥ 2.0×10^9/L, platelet count ≥ 100×10^9/L, and hemoglobin ≥ 100 g/L); had adequate hepatic and renal function (alanine transaminase (ALT), aspartate transaminase (AST), and alkaline phosphatase (ALP) ≤ 2.5 the upper limit of normal (ULN) (or 5 × ULN for hepatic cancer/metastatic hepatic cancer), total bilirubin (TBIL) ≤ 1.5 × ULN, serum creatinine (CRE) levels of ≤ 1.5 × ULN, a creatinine clearance rate of ≤1.5 × ULN, and normal urea); and had normal pulmonary function.

2.2. Study Design and Treatment. Subjects were assigned to 1 of 3 sequential dose cohorts of UAL: 56, 74, or 98 mg/m^2, administered via a 14-day consecutive intravenous 4 h infusion and given a rest for 7-day per 21-day cycle. Each cohort consisted of at least 3 subjects. Once all enrolled subjects had been monitored for 2 weeks and had no higher than grade 3 nonhematological toxicity or grade 4 hematological toxicity, the next dose was administered. The trial was terminated when ≥1/3 of the subjects experienced DLT, a severe adverse event (AE), or tumor progression. The DLT was defined as grade 4 thrombocytopenia, grade 4 neutropenia lasting for ≥7 days, febrile neutropenia, grade 4 anemia, or grade 3/4 nonhematological toxicity. Evaluated subjects were required to complete at least 1 cycle of treatment. After that, if subjects needed to continue treatment because they could not gain any benefit from other treatments, additional cycles were administered until disease progression or unacceptable toxicity occurred, or if the patient refused further treatment. Additional subjects were recruited in order to evaluate the pharmacokinetics of UAL treatment. These subjects were administered a dose of 74 mg/m^2 of UAL via a consecutive, 14-day, intravenous 4 h infusion.

2.3. Tolerability and Toxicity. Tolerability and toxicity were evaluated in all subjects treated with at least 1 cycle of UAL therapy. Vital signs including body temperature, respiration, pulsation, and blood pressure were examined at screening and once a day thereafter. Hematological parameters (red blood cell, WBC, hemoglobin, ANC, and platelet), urine routines (urinary protein, glucose, erythrocyte, leukocyte, and urine bilirubin), and stool routines (fecal erythrocyte and fecal leukocyte) were tested, and an electrocardiogram was performed at screening and on the 14th day of the cycle. Blood biochemistries including ALT, AST, ALP, gamma-glutamyl transpeptidase (GGT), TBIL, direct-reacting bilirubin, total protein, GLU, lactate dehydrogenase, creatine kinase, bun urea nitrogen, CRE, UA, cholesterol, triglyceride (TG), high-density lipoprotein, low-density lipoprotein, K^+, Na^+, Ca^{2+}, and Cl^- were examined at screening and then once a week thereafter. Fibrinogen (Fbg) and prothrombin time (PT) were examined at screening and during the 3rd week. To further evaluate the immune functions of subjects after UAL administration, we measured CD4/CD8 and natural killer (NK) cell activity in the circulation both at screening and on the 14th day. AEs were evaluated according to the National Cancer Institute Common Terminology Criteria for AEs (NCI-CTCAE) version 3.0.

2.4. Response Evaluation. Serial randomly subjects treated with at least 2 cycles were selected to evaluate the therapeutic efficacy of UALs. The tumor response was examined by using computerized tomography, magnetic resonance imaging, chest radiography, or ultrasonography according to the response evaluation criteria in solid tumors (RECIST) at the scheduled times (baseline and 2 cycles later) either until the tumor progressed or until the final visit. Complete response (CR), partial response (PR), stable disease (SD), and progressive disease (PD) were defined according to RECIST.

2.5. Multiple-Dose Pharmacokinetics. Blood samples for pharmacokinetic analysis were collected into heparinized tubes on the 1st and 14th days of the study, at various time points including 0, 0.5, 1, 2, and 4 h during infusion and 5, 15, and 30 min and 1, 1.5, 2, 3, 4, 6, 8, and 12 h after the end of infusion. Plasma was separated using centrifugation and then stored at −20°C until analysis.

UAL concentrations were measured using validated ultra-performance liquid chromatography/tandem mass spectroscopy (UPLC/MS/MS) methods as described previously [17]. In brief, chromatography was performed using a Waters

Acquity UPLC BEH C_8 column (100 × 2.1 mm, 1.7 μm). The mobile phase consisted of acetonitrile and 10 mM ammonium formate (9 : 1, v/v) at a flow rate of 0.2 mL/min. The elution time was 3 m. Multiple-reaction monitoring was performed at $m/z455.1 \rightarrow 455.0$ and $m/z469.3 \rightarrow 425.2$ for UAL and glycyrrhetinic acid (internal standard), respectively, in negative ion mode with an electrospray ionization source. Estimates of pharmacokinetic parameters for UAL were derived from individual concentration-time data sets by noncompartmental analysis.

2.6. Statistical Considerations. Tolerability, toxicity, efficacy, and pharmacokinetic characteristics were explored and analyzed in detail. Noncompartmental pharmacokinetic parameters were determined from individual plasma concentration-time data using DAS version 2.1.1.

3. Results

3.1. Patient Characteristics. Twenty-one subjects (7 men and 14 women), aged 19–68 years (median age: 54 years), were enrolled in the study, and their characteristics at baseline are listed in Table 1. Twenty subjects (95%) had an ECOG performance status of 0-1. All subjects were treated with surgery (43%), radiotherapy (52%), chemotherapy (14%), and/or other therapies (67%). The study included 5 (24%) subjects with non-Hodgkin lymphoma, 5 (24%) subjects with Hodgkin lymphoma, 1 (5%) subject with renal carcinoma, 1 (5%) patient with hepatocellular carcinoma, 1 (5%) patient with gallbladder carcinoma, 2 (9%) subjects with breast cancer, 2 (9%) subjects with lung cancer, and 4 (19%) subjects with other cancers.

3.2. Tolerability and Toxicity. Tolerability and toxicity were evaluated for all subjects. The vital sign data showed that all values fluctuated within the normal range at every time point among the 3 cohorts (Figure 2). All hematological parameters (Fbg, PT) and results of electrocardiography and routine stool test were normal. Only 1 patient experienced grade 1 microscopic hematuria, while 2 subjects developed grade 1 proteinuria after 2 cycles of treatment with UAL (74 mg/m^2).

Immune function tests showed no significant differences in CD4/CD8 at screening and on the 14th day (0.60 ± 0.31 and 0.82 ± 0.24, $P > 0.05$, 56 mg/m^2; 0.82 ± 0.48 and 0.61 ± 0.24, $P > 0.05$, 74 mg/m^2; 1.39 ± 0.96 and 1.23 ± 0.23, $P > 0.05$, 98 mg/m^2). Significant differences in the NK cells were also not observed (18.40 ± 7.66 and 22.60 ± 5.97, $P > 0.05$, 56 mg/m^2; 17.52 ± 11.57 and 20.87 ± 8.58, $P > 0.05$, 74 mg/m^2; 17.91 ± 10.02 and 18.40 ± 7.50, $P > 0.05$, 98 mg/m^2). These results suggested that the UAL did not affect patient immune function.

In addition, 3 (14%) subjects treated with 56 mg/m^2 UAL developed a low-grade fever (grade 1) but then recovered after 2 h without any treatment (Table 2). Three (14%) subjects treated with 56, 74, and 98 mg/m^2 UAL experienced grade 2 GGT elevation. Two (10%) subjects treated with 56 and 74 mg/m^2 UAL experienced grade 1 abdominal distention. Finally, 1 (5%) patient had grade 2 ALT elevation. Other mild symptoms including AST and TG elevation, pruritus, arthralgia, and hypokalemia were also observed. However, no National Cancer Institute common toxicity criteria (NCI-CTC) ≥ grade 3 treatment-related AEs were observed. The most frequent AEs included pyrexia, GGT elevation, and abdominal distention. These results suggested that UAL was tolerable and safe among 3 dose cohorts after administration via a consecutive 14-day intravenous 4 h infusion every 21 days. Therefore, a UAL dose of 98 mg/m^2 was considered the RD for a phase II trial.

3.3. Efficacy. As only 5 of 21 (23.8%) subjects preferred to receive and finish at least 2 cycles of UAL treatment, the evaluation of preliminary antitumor efficacy was limited. Three (60%) subjects achieved stable disease. One of these subjects had advanced renal carcinoma and had no significant change in the lesion after 2 cycles of treatment with 56 mg/m^2 UAL. Another patient that had advanced hepatocellular carcinoma had no significant change in the lesion after 2 cycles of treatment with 74 mg/m^2 UAL. Finally, the third patient had advanced lung cancer in which the lesion shrunk from 9.6 to 7.5 cm after 2 cycles of treatment with 98 mg/m^2 UAL.

Two additional subjects, 1 with primary non-Hodgkin lymphoma and the other with breast cancer, showed PD after 2-cycle treatment with 74 mg/m^2 UAL. No CR or PR was observed, which could be because the subjects had advanced stage tumors and did not benefit from other prior treatment schemes. Another possible explanation is that the number of subjects that could be evaluated was too small. Regardless, UAL does have the potential to improve the patient remission rate. A phase II study of a large number of subjects is recommended to confirm this finding.

3.4. Multiple-Dose Pharmacokinetics. Eight additional subjects were enrolled in the trial in order to investigate the pharmacokinetics of UAL therapy. The pharmacokinetic data (Table 3) following multiple-dose administration showed that the values of the elimination half-life ($t_{1/2}$), maximum plasma concentration (C_{max}), area under the plasma concentration time curve ($AUC_{0\rightarrow t}$), and $AUC_{0\rightarrow\infty}$ during the 1st day were 4.58 ± 2.04 h, 1589 ± 635 ng/mL, 5172 ± 1136 ng·h/mL, and 5498 ± 1525 ng·h/mL, respectively. They were 4.00 ± 1.27 h, 1211 ± 204 ng/mL, 4705 ± 873 ng·h/mL, and 4834 ± 933 ng·h/mL, respectively, during the 14th day. There were no significant differences in the values of $t_{1/2}$, C_{max}, $AUC_{0\rightarrow t}$, and $AUC_{0\rightarrow\infty}$ ($P > 0.05$) between days 1 and 14, suggesting that the pharmacokinetics were unaltered with multiple-daily dosing and that the UAL did not accumulate in the body. In addition, we found that there was a close relationship between the values of C_{max} or AUC and AEs. The value of C_{max} or AUC increased as the AEs (including hepatotoxicity and abdominal distension) increased in seriousness.

4. Discussion

This study demonstrated that UAL treatment of subjects with advanced solid tumors via multiple-dose and consecutive 14-day intravenous infusion every 21 days at doses of 56, 74, and 98 mg/m^2 was safe. The results are consistent with

Table 1: Patient characteristics at baseline.

Characteristic	Subjects		
	56 mg/m^2 (n = 3)	74 mg/m^2 (n = 14)	98 mg/m^2 (n = 4)
Gender, *n*			
Male	1	4	2
Female	2	10	2
Median age (range)	57 (49–59)	40.5 (19–68)	53.5 (42–59)
ECOG PS, *n*			
0	2	9	1
1	1	4	3
2	—	1	—
Type of tumor, *n*			
Non-Hodgkin lymphoma	1	3	1
Hodgkin lymphoma	—	5	—
Renal carcinoma	1	—	—
Hepatocellular carcinoma	—	1	—
Gallbladder carcinoma	1	—	—
Breast cancer	—	1	1
Lung cancer	—	—	2
Other	—	4	—
Prior therapy, *n*			
Surgery	0	7	2
Radiotherapy	3	7	1
Chemotherapy	0	2	1
Other therapy	0	11	3

ECOG: Eastern Cooperative Oncology Group; PS: performance status.

Table 2: Incidence of treatment-related adverse events.

AE, *N*	Number of subjects											
	56 mg/m^2 (n = 3)			74 mg/m^2 (n = 14)			98 mg/m^2 (n = 4)			Total (n = 21)		
	G1	G2	≥G3	G1	G2	≥G3	G1	G2	≥G3	G1	G2	≥G3
Hepatotoxicity												
AST	—	—	—	1	—	—	—	—	—	1 (5%)	—	—
ALT	—	1	—	—	—	—	—	—	—	—	1 (5%)	—
GGT	—	1	—	—	1	—	—	1	—	—	3 (14%)	—
TG	—	—	—	1	—	—	—	—	—	1 (5%)	—	—
Abdominal distention	1	—	—	1	—	—	—	—	—	2 (10%)	—	—
Pruritus	—	—	—	1	—	—	—	—	—	1 (5%)	—	—
Arthralgia	—	—	—	1	—	—	—	—	—	1 (5%)	—	—
Low-grade fever	3	—	—	—	—	—	—	—	—	3 (14%)	—	—
Hypokalemia	—	—	—	1	—	—	—	—	—	1 (5%)	—	—

G1, G2, and G3 represent grade 1, grade 2, and grade 3, respectively, according to NCI-CTC grades.
AE: adverse event; —: no occurrence.

preclinical information [12]. In addition, multiple-dose pharmacokinetics showed that the value of C_{max} or AUC was associated with AEs. The value of C_{max} or AUC was greater when the risk of AEs occurring in subjects was elevated. The reasons for this might be the following: when the value of C_{max} is elevated, hepatocytes would be exposed to a high concentration of drug and would be stimulated to release serial enzymes including AST, ALT, and GGT. If the value of AUC was high simultaneously, the time of stimulation would be prolonged. Therefore, the risk of hepatotoxicity and gastrointestinal toxicity would become elevated. These results suggested that the manageable toxicity associated with UAL treatment could be further controlled via kinetic monitoring.

UA has been widely reported to have antitumor activities in preclinical studies [3–11, 18–21]. However, the clinical antitumor effects of UA or UAL have not been reported previously. In our study, the preliminary antitumor activity of UAL was evaluated for the first time in 5 subjects. Although

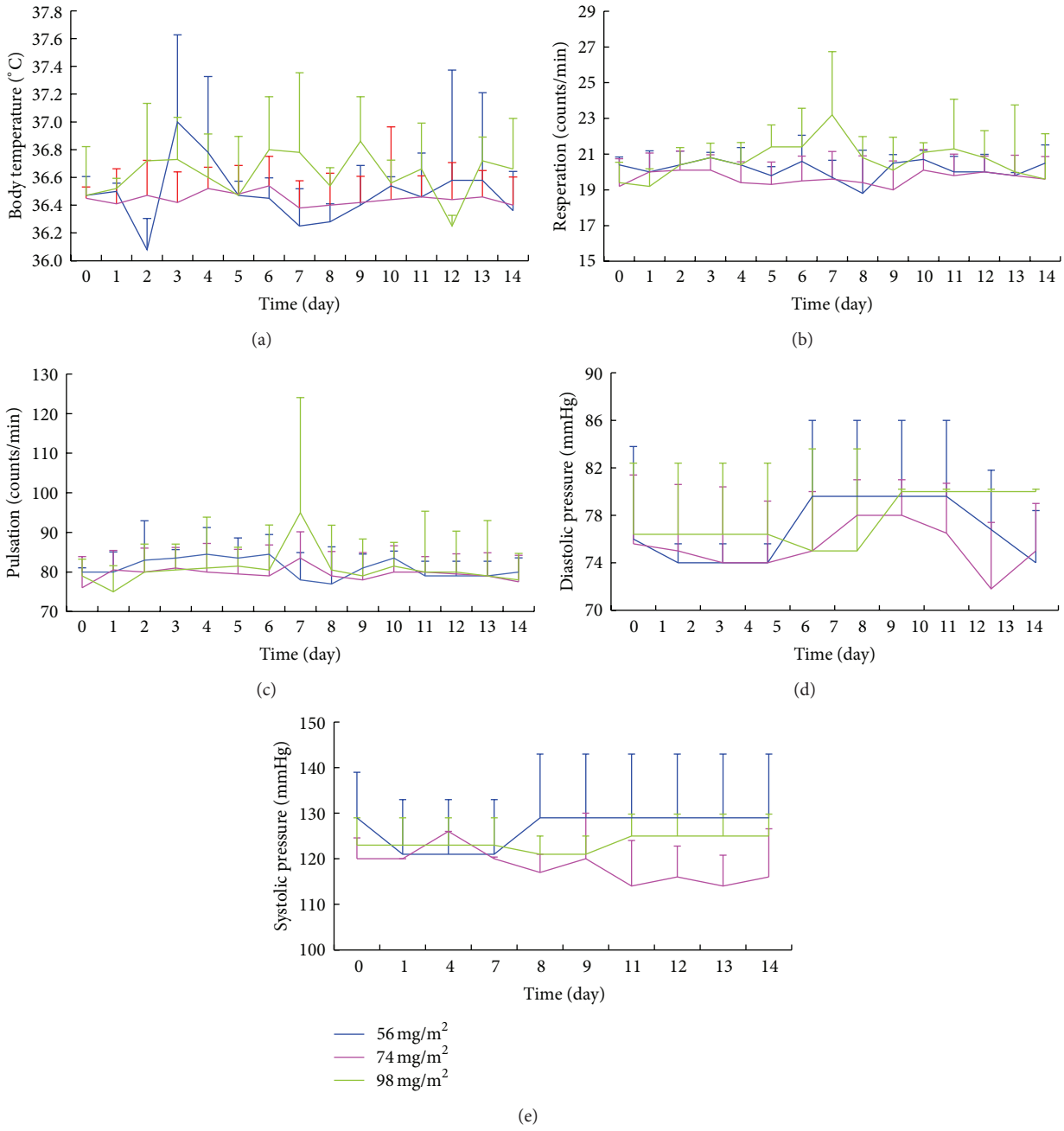

FIGURE 2: Vital sign data for the 3 cohorts at screening and throughout the infusion. (a) Body temperature, (b) respiration, (c) pulsation, (d) diastolic pressure, and (e) systolic pressure at the 3 different doses: 56 mg/m^2 (n = 3), 74 mg/m^2 (n = 14), and 98 mg/m^2 (n = 4).

no CR or PR occurred, SD was observed in 3 (60%) subjects with advanced solid tumors. Specifically, 1 lung cancer patient showed significant improvement and the lesion decreased in size (range, 9.6–7.5 cm) after 2 cycles of treatment with a UAL dose of 98 mg/m^2. These results indicate UAL can potentially improve patient remission.

The pharmacokinetic data of UA in animals showed that $T_{1/2}$ was about 4.3 h [22]. In this clinical trial, the mean $T_{1/2}$ of UAL was 4.00–4.58 h, suggesting the $T_{1/2}$ value was low so that it could rapidly be eliminated from blood. This phenomenon suggested that UAL did not accumulate in the body and that UAL must be infused repeatedly to keep the plasma-drug concentration steady and further enhance its antitumor effect.

5. Conclusions

In summary, the multiple-dose administration of UAL was tolerable with manageable toxicity. Further, the UAL did not accumulate in the body. We conclude that UAL has

Table 3: Ursolic acid liposome pharmacokinetic parameters for the 1st and 14th days (mean ± standard deviation, SD; $n = 8$).

Parameter	Unit	Day 1 Mean ± SD	Day 14 Mean ± SD
$t_{1/2}$	h	4.58 ± 2.04	4.00 ± 1.27
V_d	L/m^2	88.60 ± 31.80	89.90 ± 28.10
CL	L/(h·m^2)	14.40 ± 3.94	15.80 ± 3.05
$AUC_{(0-t)}$	ng·h/mL	5172 ± 1136	4705 ± 873
$AUC_{(0-\infty)}$	ng·h/mL	5498 ± 1525	4834 ± 933
$MRT_{(0-t)}$	h	3.34 ± 0.55	3.30 ± 0.31
$MRT_{(0-\infty)}$	h	4.31 ± 1.89	3.78 ± 0.70
T_{max}	h	3.00 ± 1.41	3.63 ± 1.06
C_{max}	ng/mL	1589 ± 635	1211 ± 204

the potential to improve the patient remission rates. The recommended dose of UAL for a phase II clinical trial is 98 mg/m^2.

Abbreviations

UA: Ursolic acid
UAL: Ursolic acid liposome
RD: Recommended dose
SFDA: State Food and Drug Administration
MTD: Maximum tolerated dose
DLT: Dose-limiting toxicity
ECOG: Eastern Cooperative Oncology Group
PS: Performance status
AEs: AEs
NCI-CTCAE: National Cancer Institute Common Terminology Criteria for AEs
CT: Computerized tomography
MRI: Scan or magnetic resonance imaging
CR: Complete response
PR: Partial response
SD: Stable disease
PD: Progressive disease
UPLC/MS/MS: Ultra-performance liquid chromatography/tandem mass spectroscopy
EIS: Electrospray ionization source
Fbg: Fibrinogen
PT: Prothrombin time
$t_{1/2}$: Elimination half-life
C_{max}: Maximum plasma concentration
AUC: Area under the plasma concentration time curve.

Conflict of Interests

The authors declare that there is no conflict of interests regarding the publication of this paper.

Authors' Contribution

The authors' contribution is as follows. Zhengzi Qian contributed with the design and implementation of the study protocol. Xianhuo Wang contributed with the analysis of the findings and writing of the paper. Zhao Yan had made contribution to acquisition of data. Zheng Song, Huilai Zhang, Shiyong Zhou, and Jing Zhao participated in patient recruitment. Huaqing Wang conceived the study and participated in its design and revised the paper. All authors read and approved the final paper.

Acknowledgments

The authors greatly appreciate financial support from the Tianjin Medical University Cancer Hospital Doctoral Fund and the Tianjin Medical University Science Fund at their institution. In addition, the authors thank Wuhan Li Yuanheng Medicine Technology Co. Ltd (Wuhan, China) for providing the UAL.

References

[1] J. Liu, "Oleanolic acid and ursolic acid: research perspectives," *Journal of Ethnopharmacology*, vol. 100, no. 1-2, pp. 92–94, 2005.

[2] S. B. Mahato, S. K. Sarkar, and G. Poddar, "Triterpenoid saponins," *Phytochemistry*, vol. 27, no. 10, pp. 3037–3067, 1988.

[3] Y. L. Hsu, P. L. Kuo, and C. C. Lin, "Proliferative inhibition, cell-cycle dysregulation, and induction of apoptosis by ursolic acid in human non-small cell lung cancer A549 cells," *Life Sciences*, vol. 75, no. 19, pp. 2303–2316, 2004.

[4] S. Prasad, V. R. Yadav, R. Kannappan, and B. B. Aggarwal, "Ursolic acid, a pentacyclin triterpene, potentiates trail-induced apoptosis through p53-independent up-regulation of death receptors: evidence for the role of reactive oxygen species and JNK," *The Journal of Biological Chemistry*, vol. 286, no. 7, pp. 5546–5557, 2011.

[5] Y. H. Choi, J. H. Baek, M. A. Yoo, H. Y. Chung, N. D. Kim, and K. W. Kim, "Induction of apoptosis by ursolic acid through activation of caspases and down-regulation of c-IAPs in human prostate epithelial cells," *International Journal of Oncology*, vol. 17, no. 3, pp. 565–571, 2000.

[6] H. Y. Lee, H. Y. Chung, K. H. Kim, J. J. Lee, and K. W. Kim, "Induction of differentiation in the cultured F9 teratocarcinoma stem cells by triterpene acids," *Journal of Cancer Research and Clinical Oncology*, vol. 120, no. 9, pp. 513–518, 1994.

[7] T. Zhang, Y. M. He, J. S. Wang, J. Shen, Y. Y. Xing, and T. Xi, "Ursolic acid induces HL60 monocytic differentiation and upregulates C/EBPβ expression by ERK pathway activation," *Anti-Cancer Drugs*, vol. 22, no. 2, pp. 158–165, 2011.

[8] H. J. Cha, S. K. Bae, H. Y. Lee et al., "Anti-invasive activity of ursolic acid correlates with the reduced expression of matrix metalloproteinase-9 (MMP-9) in HT1080 human fibrosarcoma cells," *Cancer Research*, vol. 56, no. 10, pp. 2281–2284, 1996.

[9] K.-H. Sohn, H.-Y. Lee, H.-Y. Chung, H.-S. Young, S.-Y. Yi, and K.-W. Kim, "Anti-angiogenic activity of triterpene acids," *Cancer Letters*, vol. 94, no. 2, pp. 213–218, 1995.

[10] M. S. Kiran, R. I. Viji, V. B. Sameer Kumar, and P. R. Sudhakaran, "Modulation of angiogenic factors by ursolic acid," *Biochemical and Biophysical Research Communications*, vol. 371, no. 3, pp. 556–560, 2008.

[11] C. Cárdenas, A. R. Quesada, and M. Á. Medina, "Effects of ursolic acid on different steps of the angiogenic process," *Biochemical and Biophysical Research Communications*, vol. 320, no. 2, pp. 402–408, 2004.

[12] D. da Silva Ferreira, V. R. Esperandim, M. P. A. Toldo, J. Saraiva, W. R. Cunha, and S. de Albuquerque, "Trypanocidal activity and acute toxicity assessment of triterpene acids," *Parasitology Research*, vol. 106, no. 4, pp. 985–989, 2010.

[13] D. Papahadjopoulos, T. M. Allen, A. Gabizon et al., "Sterically stabilized liposomes: improvements in pharmacokinetics and antitumor therapeutic efficacy," *Proceedings of the National Academy of Sciences of the United States of America*, vol. 88, no. 24, pp. 11460–11464, 1991.

[14] D. C. Drummond, O. Meyer, K. Hong, D. B. Kirpotin, and D. Papahadjopoulos, "Optimizing liposomes for delivery of chemotherapeutic agents to solid tumors," *Pharmacological Reviews*, vol. 51, no. 4, pp. 691–743, 1999.

[15] W. W. Zou, W. T. Sun, N. Zhang, and W. F. Xu, "Enhanced oral bioavailability and absorption mechanism study of N3-O-toluyl-fluorouracil-loaded liposomes," *Journal of Biomedical Nanotechnology*, vol. 4, no. 1, pp. 90–98, 2008.

[16] X.-H. Wang, S.-Y. Zhou, Z.-Z. Qian et al., "Evaluation of toxicity and single-dose pharmacokinetics of intravenous ursolic acid liposomes in healthy adult volunteers and patients with advanced solid tumors," *Expert Opinion on Drug Metabolism and Toxicology*, vol. 9, no. 2, pp. 117–125, 2013.

[17] Y. Xia, G. Wei, D. Si, and C. Liu, "Quantitation of ursolic acid in human plasma by ultra performance liquid chromatography tandem mass spectrometry and its pharmacokinetic study," *Journal of Chromatography B: Analytical Technologies in the Biomedical and Life Sciences*, vol. 879, no. 2, pp. 219–224, 2011.

[18] A. K. Pathak, M. Bhutani, A. S. Nair et al., "Ursolic acid inhibits STAT3 activation pathway leading to suppression of proliferation and chemosensitization of human multiple myeloma cells," *Molecular Cancer Research*, vol. 5, no. 9, pp. 943–955, 2007.

[19] P.-O. Harmand, R. Duval, C. Delage, and A. Simon, "Ursolic acid induces apoptosis through mitochondrial intrinsic pathway and caspase-3 activation in M4Beu melanoma cells," *International Journal of Cancer*, vol. 114, no. 1, pp. 1–11, 2005.

[20] N. Gao, S. Cheng, A. Budhraja et al., "Ursolic acid induces apoptosis in human leukaemia cells and exhibits anti-leukaemic activity in nude mice through the PKB pathway," *British Journal of Pharmacology*, vol. 165, no. 6, pp. 1813–1826, 2012.

[21] Y. Li, D. Xing, Q. Chen, and W. R. Chen, "Enhancement of chemotherapeutic agent-induced apoptosis by inhibition of NF-κB using ursolic acid," *International Journal of Cancer*, vol. 127, no. 2, pp. 462–473, 2010.

[22] Q. Liao, W. Yang, Y. Jia, X. Chen, Q. Gao, and K. Bi, "LC-MS determination and pharmacokinetic studies of ursolic acid in rat plasma after administration of the traditional Chinese medicinal preparation Lu-Ying extract," *Yakugaku Zasshi*, vol. 125, no. 6, pp. 509–515, 2005.

Hindawi Publishing Corporation
BioMed Research International
Volume 2014, Article ID 214727, 7 pages
http://dx.doi.org/10.1155/2014/214727

Clinical Study

Retrospective Comparative Study of the Effects of Dendritic Cell Vaccine and Cytokine-Induced Killer Cell Immunotherapy with that of Chemotherapy Alone and in Combination for Colorectal Cancer

Jingxiu Niu,[1] Yanjie Ren,[2] Tianyu Zhang,[2] Xuejing Yang,[2] Wei Zhu,[1] Hui Zhu,[1] Jing Li,[1] Jiali Li,[1] and Yan Pang[1]

[1] *Department of Oncology, Tianjin Union Medicine Center, No. 190 Jieyuan Road, Hongqiao District, Tianjin 300121, China*
[2] *Shanghai Claison Biotechnology Co. Ltd., Shanghai, China*

Correspondence should be addressed to Yan Pang; pangyancn@126.com

Received 8 May 2014; Revised 20 July 2014; Accepted 5 August 2014; Published 18 August 2014

Academic Editor: Shiwu Zhang

Purpose. This retrospective study determined the delayed-type hypersensitivity (DTH) skin test and safety of dendritic cell (DC) vaccine and cytokine-induced killer (CIK) cell immunotherapy and the survival compared to chemotherapy in 239 colorectal cancer (CRC) patients. *Methods.* DTH and safety of the immunotherapy were recorded. The overall survival (OS) and disease free survival curves were compared according to the immunotherapy and/or chemotherapy received with Kaplan-Meier estimates. *Results.* Of the 70 patients who received immunotherapy, 62.86% had a positive DTH skin test, 38.57% developed fever, 47.14% developed insomnia, 38.57% developed anorexia, 4.29% developed joint soreness, and 11.43% developed skin rash. For 204 resectable CRC patients, median survival time (MST) (198.00 days) was significantly longer in patients with immunotherapy plus chemotherapy than with chemotherapy alone (106.00 days) ($P = 0.02$). For 35 patients with unresectable or postsurgery relapsed CRC and who were confirmed to be dead, no statistical difference was observed in the MST between the patients treated with immunotherapy and with chemotherapy ($P = 0.41$). MST in the patients treated with chemotherapy plus immunotherapy was 154 days longer than that of patients treated with chemotherapy alone ($P = 0.41$). *Conclusions.* DC vaccination and CIK immunotherapy did not cause severe adverse effects, induce immune response against CRC, and prolong OS.

1. Introduction

Oxaliplatin and 5-FU-based chemotherapy are the standard treatment modalities for high-risk stage II, stage III, and stage IV CRC patients [1, 2]. Regimens of capecitabine, CapeOX, and FOLFOX 4 are also commonly used in clinical treatment, and they result in survival benefits. Oxaliplatin and/or 5-FU can kill both rapidly dividing CRC cells and normal cells [3, 4]. As a result, hair loss, diarrhea, nausea, and vomiting are commonly observed in CRC patients undergoing chemotherapy treatment. In addition to these adverse effects, severe adverse events including myelosuppression, immunosuppression, and permanent organ damage to the heart, lung, liver, and kidneys can occur during chemotherapy in CRC patients [5]. Because of their poor general condition, advanced CRC patients often cannot withstand the toxic effects of chemotherapy and, therefore, do not receive adequate therapy. In addition to its toxicity, chemotherapy sensitivity declines over time [6, 7]. CRC that recurs after an initial response to oxaliplatin and 5-FU tends to be resistant to subsequent chemotherapy with different drugs. Complete tumor eradication is rarely achieved in most advanced CRC patients treated with chemotherapy [7]. Because of the limited clinical benefit and toxicity of chemotherapy, immunotherapy may be a better option for improving OS in advanced CRC. Immunotherapy uses the body's immune system to attack cancer cells. Antigen-specific T cell dysfunction is common in cancer patients. As a result, tumor cells escape immune surveillance. Restoring the immune system may be a viable option to improve

cancer treatment. Immunotherapy may be a promising and safe approach for cancer eradication [8, 9]. Unlike routine therapies, immunotherapy may induce an effective antitumor immune response without adverse effects. Immunotherapy with dendritic cell (DC) and cytokine-induced killer (CIK) cells is targeted to kill residual cancer cells, which are the main cause of cancer recurrence and metastasis. DC and CIK immunotherapy has been shown to be well tolerated with excellent compliance in cancer patients [10, 11].

The purpose of this study was to compare the therapeutic efficacy in terms of survival prolongation of DC cells and CIK cells immunotherapy and chemotherapy alone and in combination in advanced CRC patients.

2. Patients and Methods

2.1. Patients. CRC patients who were treated at the Department of Oncology, Tianjin Union Medicine Center, from February 1, 2012 to September 30, 2013 were included in the study. Inclusion criteria consist of: (1) patients with histologically or cytologically diagnosed CRC and adequate kidney liver, coagulation, and bone marrow function; (2) resectable (stage II and stage III) CRC patients who accepted primary tumor resection and postoperative adjuvant chemotherapy and had an elevated serum carcinoembryonic antigen (CEA) level before surgery and a normal serum CEA level (5 ng/mL) within 1 month after surgery; and (3) advanced CRC patients (relapsed or metastatic CRC after surgery and unresectable CRC) who were confirmed to be dead of any cause.

The resectable CRC patients were divided into 2 groups according to the treatment they received. Patients who received routine adjuvant postsurgery chemotherapy alone were defined as group S + C (control group). Patients who received DC and CIK cells immunotherapy plus chemotherapy within 6 months after surgery were defined as group S + C + I (immunotherapy group). Advanced CRC patients were divided into 3 groups according to the treatment modalities they received: group I, DC cells and CIK cells immunotherapy; group C, chemotherapy; and group I + C, DC vaccine and CIK cell immunotherapy plus chemotherapy. The interval between immunotherapy and chemotherapy had to be less than 3 months; it is to ensure that the result of clinical efficacy is the result of immunotherapy and chemotherapy function together rather than unilateral.

2.2. Design of DC Cells and CIK Cells Therapy. The schedule of DC and CIK therapy was performed in accordance with the "Treatment with Autologous Immune Cells (T cells, NK cells)" class III medical techniques policy of the Ministry of Health of China. This study protocol was approved by ethical committees of the hospital. Written informed consent was obtained from each patient before treatment initiation. Adequate renal and coagulation function and peripheral lymphocyte and monocyte numbers greater than 1×10^9/L were required for patients to receive DC cells and CIK cells therapy.

2.3. Collection of Peripheral Blood Mononuclear Cells. On day 0, peripheral blood mononuclear cells (PBMCs) were collected by leukapheresis using a Fresenius KABI System (Germany) with an electrocardiogram monitoring system. PBMCs were cultured overnight and adherent cells (monocytes) and nonadherent cells (lymphocytes) were separated.

2.4. Preparation of DCs and CIK Cells. Tumor lysate was first prepared for pulsing DCs. A single cell suspension of SW480 colon cancer cell line was dissociated by ultrasound and centrifugation at 600 ×g for 30 min, and the supernatants were collected as tumor lysate. DCs were obtained by culturing the adherent cells through stimulating with tumor lysate, granulocyte macrophage colony-stimulating factor, interleukin (IL)-4, and tumor necrosis factor for 7 days [11, 12]. For preparation of CIK cells, SW480 cells CIK cells were obtained by culturing the nonadherent cells through stimulating with interferon γ, CD3 monoclonal antibody, and IL-2 for 10 days.

2.5. Quality Control of DCs and CIK Cells. The immune phenotypes of HLA2DR, CD80, and CD83 for DCs and CD3, CD8, and CD56 for CIK were analyzed by flow cytometry [13]. The bacteria, fungus, and endotoxin levels in cultured DC and CIK samples met the release criteria for infusion [10, 14, 15].

2.6. Schedule of DC Cells and CIK Cells Infusion. DCs (1×10^7) in 100 mL 0.9% normal saline (NS) were intravenously infused on days 8, 15, and 22 and injected intradermally on days 29, 36, and 43. CIK cells (1×10^9) in 100 mL NS were intravenously infused on days 11, 12, 13, and 14. An interval of 4–6 hours was needed to receive immunotherapy and chemotherapy within the same day [15].

2.7. Delayed-Type Hypersensitivity Testing of DC Vaccine and CIK Cell Infusion. For delayed-type hypersensitivity (DTH) tests, 4 μg of tumor lysate was intradermally injected 1 week after the last DC infusion and results were examined 48 hours later. An induration greater than 2 mm in diameter around the injection site was considered as a positive DTH response (Table 2).

2.8. Safety Evaluation of DC Cells and CIK Cells Immunotherapy. Adverse effects such as fever, insomnia, anorexia, joint soreness, and skin rash were evaluated during DC cells and CIK cells infusion. Several adverse effects occurred simultaneously in the same patient (Table 2).

2.9. Chemotherapy Schedules. Capecitabine was administered orally twice daily at a dose of 1000 mg/m^2 on day 1 to day 14. This regimen was repeated every 3 weeks [16, 17]. For the capecitabine plus oxaliplatin (CapeOX) regimen, oxaliplatin was intravenously infused at a dose of 130 mg/m^2 on day 1, and capecitabine was administered orally twice daily at a dose of 1000 mg/m^2 on day 1 to day 14. The regimen was repeated every 3 weeks. The FOLFOX 4 (oxaliplatin, leucovorin [LV], and 5-FU) regimen consisted of intravenous oxaliplatin infusion (85 mg/m^2) on day 1, intravenous LV

infusion (200 mg/m^2) on day 1 and day 2, and intravenous bolus injection (400 mg/m^2) and 22 h infusion (600 mg/m^2) of 5-FU on day 1 and day 2. This regimen was repeated every 2 weeks. To receive chemotherapy, patients were required to have adequate kidney, liver, and bone marrow function [17–20].

2.10. Follow-Up. Overall survival (OS) was recorded for the advanced CRC patients. For the resectable CRC patients, CEA levels were measured before operation and within 1 month after operation, and patients were followed up until November 14, 2013. The follow-up occurred 3 to 4 weeks postoperatively. Serum CEA levels were monitored every 3 weeks just before receiving adjuvant chemotherapy. Serum CEA levels were recorded every 3 months for the first 2 years of follow-up and thereafter every 6 months. Based on the restrictions presented below, the time from the date of surgery to the date of the first rise in serum CEA level above the normal upper limit reflected the duration of tumor-free status in patients, and, therefore, it was used to provide an estimate of disease-free survival (DFS). Patients with serum CEA levels more than 5 ng/mL before surgery, which was the reference cutoff in our hospital, were considered to have CEA-producing tumors, and, therefore, CEA could be used as an index for evaluation of tumor recurrence. Patients with serum CEA levels below 5 ng/mL within 1 month of surgery were considered as a radical surgery. Patients whose serum CEA level was above the normal upper limit 3 consecutive times during follow-up were considered to have tumor recurrence [21–24].

2.11. Data Collection and Statistical Analysis. The patients were followed up until November 14, 2013. In advanced CRC patients, OS was defined as the time from the date of study enrollment to the date of death from any cause. In resectable CRC patients, DFS was defined as the time from the date of the first rise in serum CEA level above the normal upper limit to the date of surgery.

Clinical data of the patients including diagnostic procedures and treatment were collected from the inpatients electronic medical records of our hospital and reanalyzed using EpiData database (version 3.02). Particular attention was paid to collecting data related to primary rumor resection, chemotherapy, and DC cells and CIK cells immunotherapy. Statistical analyses were carried out using the SPSS (version 19.0) statistical software package, which was docked with the EpiData database. DFS and OS curves were calculated using the Kaplan-Meier method. A P value less than 0.05 was considered statistically significant.

3. Results

3.1. Patient Characteristics. A total of 239 CRC patients (204 resectable CRC patients and 35 advanced CRC patients) were enrolled in the study during an 8-month period from February 1, 2012 to September 30, 2012 and followed up until November 14, 2013. Patient characteristics are shown in Table 1. Of the 239 patients, 133 male patients and 106 female patients were with a mean age of 64.2 ± 12.05 (range 28–86) years. The primary tumor was located in the colon and rectum in 92 patients and 147 patients, respectively. One patient, 188 patients, and 50 patients had well-differentiated, moderately differentiated, and poorly differentiated tumors, respectively. Of the unresectable CRC patients, 24 (20.8%) patients underwent primary tumor resection, 8 (8.3%) patients received radiotherapy, 28 patients received chemotherapy, and 24 patients received DC cells and CIK cells immunotherapy. Of the 28 patients who received chemotherapy, 5 patients received the capecitabine regimen, 6 patients received the CapeOX regimen, 12 patients received the FOLFOX 4 regimen, and 5 patients received other regimens.

Table 1: Characteristics of patients.

Characteristics	Number		
	Resectable	Advanced	Total
Number	204	35	239
Age (years)			
Range	28–83	40–86	28–86
Mean ± SD	61.74 ± 10.28	62.1 ± 8.10	64.2 ± 12.05
Gender			
Male	116	17	133
Female	88	18	106
Tumor location			
Colon	74	18	92
Rectum	130	17	147
Differentiation degrees			
High	1	0	1
Middle	161	27	188
Low	42	8	50
UICC stages			
I	0	0	0
II	85	0	85
III	119	0	119
IV + recurrence	0	35	35
Background of treatments			
Surgery	204	24	228
Radiology	0	8	8
Chemotherapy	204	28	232
DCs + CIK therapy	74	24	98

Table 2: Side effects in immunotherapy with DCs and CIK cells in immunotherapy group ($n = 70$).

Characteristics	Number of positives (%)	Number of negatives (%)
DTH	44 (62.86%)	26 (37.14%)
Fever	27 (38.57%)	43 (61.43%)
Insomnia	33 (47.14%)	37 (52.86%)
Anorexia	27 (38.57%)	43 (61.43%)
Joint soreness	3 (4.29%)	67 (95.71%)
Skin rash	8 (11.43%)	62 (88.57%)

Table 3: Serum CEA levels of presurgery, postsurgery, and tumor recurrence in both immunotherapy group and control group.

Group	Total	Immunotherapy group	Control group	*P* value
Presurgery				
Number	204	74	130	
Mean ± SD	15.88 ± 20.63	13.79 ± 11.99	17.05 ± 24.13	0.13
Range	10–48	10–48	10–48	
Postsurgery				
Number	204	74	130	
Mean ± SD	2.78 ± 1.11	2.91 ± 1.10	2.70 ± 1.12	0.81
Range	2–5	2–5	2–5	
Tumor recurrence				
Number/total number	48/204	17/74 (23.0%)	31/130 (23.8%)	0.89
Mean ± SD	8.21 ± 5.96	7.86 ± 6.05	8.40 ± 6.00	0.58
Range	5–10	5–10	5–10	

Of the 204 resectable CRC patients, 85 patients had stage II disease and 119 patients had stage III disease. These 204 patients were divided into 2 groups according to the treatment they received. The control group ($n = 130$) received primary tumor resection followed by adjuvant chemotherapy. The immunotherapy group ($n = 74$) received primary tumor resection followed by adjuvant chemotherapy plus adjuvant DC cells and CIK cells immunotherapy. The 35 advanced CRC patients were divided into 3 groups according to the treatment they received: group C ($n = 11$), chemotherapy alone; group I ($n = 7$), DC cells and CIK cells immunotherapy alone; and group I + C ($n = 17$), DC cells and CIK cells immunotherapy plus chemotherapy.

3.2. Immune Response and Safety of DC Cells and CIK Cells Therapy. Immune response and safety of DC cells and CIK cells therapy were recorded in 70 of the 74 patients in group I. These parameters were not evaluated in 4 patients because of incomplete follow-up data. Of the 70 group I patients, 44 (62.86%) patients had a positive immune response based on the DTH skin test. Twenty-seven (38.57%) patients developed fever, 33 (47.14%) patients developed insomnia, 27 (38.57%) patients developed anorexia, 3 (4.29%) patients developed joint soreness, and 8 (11.43%) patients developed skin rash (Table 2). Severe adverse events were not observed.

3.3. Serum CEA Levels in Resectable CRC Patients. Mean CEA level was significantly lower after operation compared with before operation in the 204 resectable CRC patients ($P = 0.81$). Mean serum CEA level before and after surgery was 15.88 ± 20.63 (range 5–48) ng/mL and 2.78 ± 1.11 (range 5–48) ng/mL, respectively.

At the end of follow-up, serum CEA levels significantly rose in 48 of the 204 resectable CRC patients including 17 of the 74 (23.0%) immunotherapy group patients and 31 of the 130 (23.8%) control group patients ($P = 0.58$). The mean serum CEA level of these patients was 8.21 ± 5.96 (range 5–48) ng/mL. Presurgery and postsurgery CEA levels and tumor recurrence were similar between the immunotherapy and control groups (Table 3).

Table 4: Comparison of MST in immunotherapy group and control group.

Group	Number	MST (days)	ΔMST (days)	χ^2	(*P* value)
Immunotherapy	17	198.00	92.00	5.109	0.02
Control	31	106.00			

3.4. DFS Based on Serum CEA Level. The 204 resectable CRC patients were followed up for 489.2 ± 160.4 (range 441–652) days. At the end of follow-up, serum CEA levels were increased in 48 of the 204 patients including 17 patients in the immunotherapy group and 31 patients in the control group. Median survival time (MST) was significantly longer in the immunotherapy group than in the control group ($P = 0.02$) (Table 4). MST was prolonged for 92 days in the immunotherapy group compared with the control group (198 days versus 106 days). The DFS curves for the immunotherapy and control groups are shown in Figure 1.

3.5. Comparison of OS and MST between Chemotherapy and Immunotherapy in Advanced CRC Patients. MSTs of the I, C, and I + C groups are shown in Table 5. MST was not significantly different between the I and C groups (249 days versus 110 days; $P = 0.41$). MST was significantly longer in the I + C group than in the C group ($P = 0.04$). MST was prolonged 154 days in the I + C group compared with the C group (264 versus 110 days). MST was not significantly different between the I and I + C groups (249 days versus 264 days; $P = 0.47$). The OS curves for the I, C, and I + C groups are shown in Figure 2.

4. Discussion

DTH as an indicator of immune response can serve as an efficacy end point for DC cells and CIK cells immunotherapy. OS is a powerful index to measure therapeutic efficacy in advanced CRC. Indices to evaluate therapeutic efficacy in early-stage CRC postsurgery are lacking. CEA is the most widely used tumor marker for the management of CRC

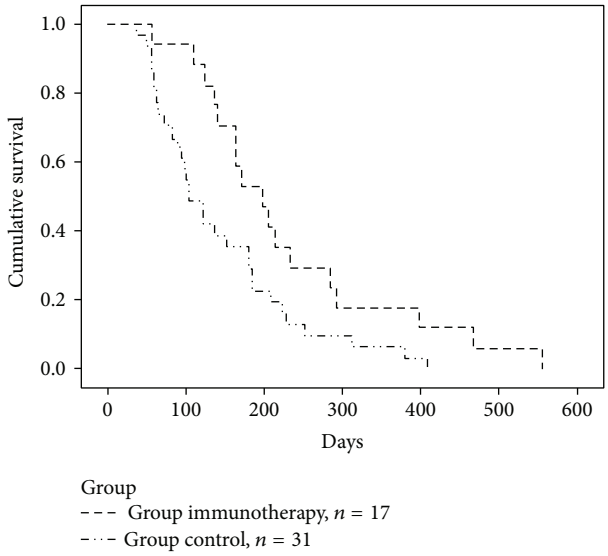

Figure 1: DFS curves by the Kaplan-Meier estimate in immunotherapy group and control group ($P = 0.024$).

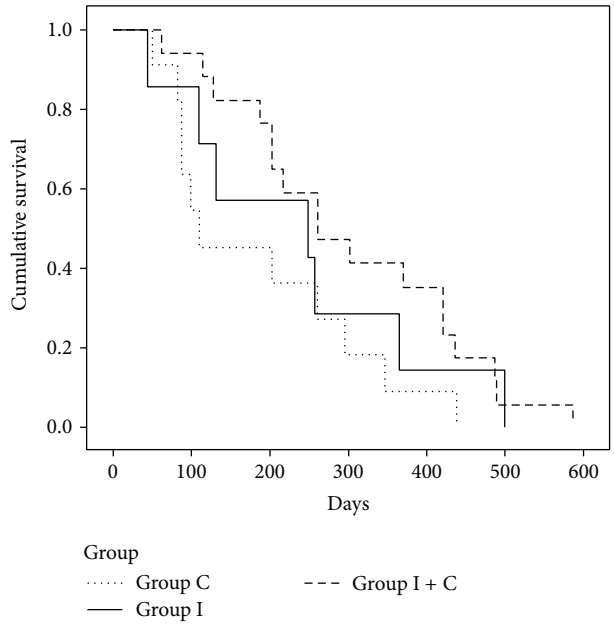

Figure 2: OS curves by the Kaplan-Meier estimate for patients with chemotherapy, immunotherapy alone, and immunotherapy plus chemotherapy of DC vaccine and CIK.

Table 5: Comparison of MST for patients with chemotherapy, immunotherapy alone, and immunotherapy plus chemotherapy of DC vaccine and CIK cells.

Group	Number	MST (day)	ΔMST	χ^2	(P value)
C versus I					
C	11	110	139	0.694	0.41
I	7	249			
C versus I + C					
C	11	110	154	4.127	0.04
I + C	17	264			
I versus I + C					
I	7	249	15	0.535	0.47
I + C	17	264			

[25, 26]. CEA is currently used to detect recurrent disease after curative resection and is believed to be effective indicator of postoperative mortality. Postoperative CEA level is an important indicator for both OS and DFS rates in CRC patients. CEA is an early marker for tumor recurrence. CEA level can detect tumor recurrence approximately 5 months earlier compared with clinical symptoms and imaging diagnosis. Quantitative measurement of serum CEA can be readily, easily, and inexpensively obtained. In this study, patients with serum CEA levels below 5 ng/mL before surgery were excluded because they were considered to have non-CEA-producing tumors and, therefore, CEA could not be used as an index for evaluation of tumor recurrence. The high false positive rate of CEA testing in CRC, which often results from incidental rises in CEA caused by benign gastrointestinal disorders, has been a main problem with its use. Serum CEA remains in the circulation for a period of time and requires several weeks to return to normal. It is believed that incidental rises in CEA can be filtered, and a higher specificity is expected by repetitive measurements of CEA at an interval of several weeks. In our study, a rise in the serum CEA level was defined as a CEA level above the normal upper limit for 3 consecutive follow-ups. Abnormal serum CEA levels in some patients persisted after surgery, which usually indicates the presence of residual microscopic disease. Patients with serum CEA levels above 5 ng/mL within 1 month after surgery were excluded from this study, because they were considered as nonradical surgery. If there is no residual disease after tumor resection, the serum CEA level should remain within normal range. If the CEA level rises, it is possible that a persistent source of CEA, such as a hidden metastasis or recurrent tumor is present. Based on these circumstances, the period from the date of surgery to that of the first rise in serum CEA level above the normal upper limit reflects the duration of tumor-free status, and this might provide another method to measure DFS [27, 28].

Based on the clinical observations of our study, 44 (62.86%) patients developed a positive immune response to DC cells and CIK cells immunotherapy based on the DTH skin test. Immunotherapy-related adverse effects including fever, insomnia, anorexia, joint soreness, and skin rash were observed. In general, these adverse effects were mild and resolved without the need for additional treatment. Severe adverse events were not observed. A rise in serum CEA level was detected in 17 of the 74 (23.0%) patients in the immunotherapy group and 31 of the 130 (23.8%) patients in the control group. Although the number of patients with an elevated CEA level during follow-up was not significantly different between the 2 groups, MST, defined as the time from the date of surgery to the date of the first rise in serum CEA level, was significantly longer (92 days) in the immunotherapy group than that in the control group. MST

was not significantly different between patients who received immunotherapy and those who received chemotherapy. MST was 154 days longer in the patients who received chemotherapy plus immunotherapy than in patients who received chemotherapy alone. This indicates that DC vaccine and CIK cell immunotherapy and chemotherapy may have a similar effect on survival in advanced CRC patients. Combined immunotherapy and chemotherapy may have a synergistic effect on survival compared with chemotherapy alone.

DC cells and CIK cells immunotherapy can induce an immune response against CRC and prolong OS and DFS. The therapy was safe and no severe adverse effects were observed. DC cells and CIK cells immunotherapy and chemotherapy had a similar survival benefit in CRC patients. Combined immunotherapy and chemotherapy had a synergistic effect on survival compared with chemotherapy alone. Immunotherapy represents a viable treatment option to benefit CRC patients.

5. Conclusion

DC vaccination and CIK cell therapy were safe and no severe adverse effects were observed. DC cells and CIK cells therapy were able to stimulate the patients to use their own immune system against cancer. As a result, DFS and OS were prolonged. Immunotherapy and chemotherapy had the same effect on survival in CRC patients. Combined immunotherapy and chemotherapy may have a synergistic effect on survival compared with chemotherapy alone [29–31].

Conflict of Interests

The authors declare that there is no conflict of interests regarding the publication of this paper.

Acknowledgment

The present study was supported in part by the Tianjin Municipal Science and Technology Commission (no. 12ZCDZSY17100).

References

[1] S. Loi, S. Y. K. Ngan, R. J. Hicks et al., "Oxaliplatin combined with infusional 5-fluorouracil and concomitant radiotherapy in inoperable and metastatic rectal cancer: a phase I trial," *British Journal of Cancer*, vol. 92, no. 4, pp. 655–661, 2005.

[2] A. Gunnlaugsson, P. Nilsson, E. Kjellén, and A. Johnsson, "The effect on the small bowel of 5-FU and oxaliplatin in combination with radiation using a microcolony survival assay," *Radiation Oncology*, vol. 4, no. 1, article 61, 2009.

[3] S. Tsuji, Y. Midorikawa, T. Takahashi et al., "Potential responders to FOLFOX therapy for colorectal cancer by Random Forests analysis," *British Journal of Cancer*, vol. 106, no. 1, pp. 126–132, 2012.

[4] S. Satram-Hoang, L. Lee, S. Yu et al., "Comparative effectiveness of chemotherapy in elderly patients with metastatic colorectal cancer," *Journal of Gastrointestinal Cancer*, vol. 44, no. 1, pp. 79–88, 2013.

[5] H. K. Sanoff, W. R. Carpenter, J. Freburger et al., "Comparison of adverse events during 5-fluorouracil versus 5-fluorouracil/oxaliplatin adjuvant chemotherapy for stage III colon cancer: a population-based analysis," *Cancer*, vol. 118, no. 17, pp. 4309–4320, 2012.

[6] K. Salem, C. O. Brown, J. Schibler, and A. Goel, "Combination chemotherapy increases cytotoxicity of multiple myeloma cells by modification of nuclear factor (NF)-κB activity," *Experimental Hematology*, vol. 41, no. 2, pp. 209–218, 2013.

[7] A. Dasgupta, J. E. Shields, and H. Trent Spencer, "Treatment of a solid tumor using engineered drug-resistant immunocompetent cells and cytotoxic chemotherapy," *Human Gene Therapy*, vol. 23, no. 7, pp. 711–721, 2012.

[8] B. A. Fox, D. J. Schendel, L. H. Butterfield et al., "Defining the critical hurdles in cancer immunotherapy," *Journal of Translational Medicine*, vol. 9, no. 1, article 214, 2011.

[9] A. Hoos, A. M. M. Eggermont, S. Janetzki et al., "Improved endpoints for cancer immunotherapy trials," *Journal of the National Cancer Institute*, vol. 102, no. 18, pp. 1388–1397, 2010.

[10] T. Yang, Y. Xiang, Y. Li, J. Shao, Q. Li, and H. Yu, "Clinical study of co-treatment with DC-CIK cells for advanced solid carcinomas," *The Chinese-German Journal of Clinical Oncology*, vol. 10, no. 6, pp. 354–359, 2011.

[11] R. Lubong-Sabado and N. Bhardwaj, "Directing dendritic cell immunotherapy towards successful cancer treatment," *Immunotherapy*, vol. 2, no. 1, pp. 37–56, 2010.

[12] N. Janikashvili, N. Laemonier, and E. Katsanis, "Personalized dendritic cell-based tumor immunotherapy," *Immunotherapy*, vol. 2, no. 1, pp. 57–68, 2010.

[13] X. Li, B. Xu, J. Wu et al., "Review of Chinese clinical trials on CIK cell treatment for malignancies," *Clinical and Translational Oncology*, vol. 14, no. 2, pp. 102–108, 2012.

[14] Y. Cui, X. Yang, W. Zhu, J. Li, X. Wu, and Y. Pang, "Immune response, clinical outcome and safety of dendritic cell vaccine in combination with cytokine-induced killer cell therapy in cancer patients," *Oncology Letters*, vol. 6, no. 2, pp. 537–541, 2013.

[15] Y. Liu, W. Zhang, B. Zhang, X. Yin, and Y. Pang, "DC vaccine therapy combined concurrently with oral capecitabine in metastatic colorectal cancer patients," *Hepato-Gastroenterology*, vol. 60, no. 122, pp. 23–27, 2013.

[16] W. Ling, J. Fan, Y. Ma, and H. Wang, "Capecitabine-based chemotherapy for metastatic colorectal cancer," *Journal of Cancer Research and Clinical Oncology*, vol. 137, no. 6, pp. 927–938, 2011.

[17] Y. Li, J. Li, M. Lu, X. Wang, and L. Shen, "Capecitabine maintenance therapy after first-line chemotherapy in patients with metastatic colorectal cancer," *Chinese Journal of Cancer Research*, vol. 22, no. 3, pp. 181–185, 2010.

[18] B. F. El-Rayes, M. M. Zalupski, S. G. Manza et al., "Phase-II study of dose attenuated schedule of irinotecan, capecitabine, and celecoxib in advanced colorectal cancer," *Cancer Chemotherapy and Pharmacology*, vol. 61, no. 2, pp. 283–289, 2008.

[19] M. Kochi, W. Ichikawa, E. Meguro et al., "Phase II study of FOLFOX4 with "wait and go" strategy as first-line treatment for metastatic colorectal cancer," *Cancer Chemotherapy and Pharmacology*, vol. 68, no. 5, pp. 1215–1222, 2011.

[20] C. Du, Z. Z. Liu, Z. Ding, F. Guo, D. Ma, and X. Xie, "Autologous cytokine-induced killer cells combined with chemotherapy in

the treatment of advanced colorectal cancer: a randomized control study," *The Chinese-German Journal of Clinical Oncology*, vol. 12, no. 10, pp. 487–491, 2013.

[21] X. Zhou, G. Xie, S. Wang et al., "Potent and specific antitumor effect for colorectal cancer by CEA and Rb double regulated oncolytic adenovirus harboring ST13 gene," *PLoS ONE*, vol. 7, no. 10, Article ID e47566, 2012.

[22] A. L. Small-Howard and H. Harris, "Advantages of the AMDL-ELISA DR-70 (FDP) assay over carcinoembryonic antigen (CEA) for monitoring colorectal cancer patients," *Journal of Immunoassay and Immunochemistry*, vol. 31, no. 2, pp. 131–147, 2010.

[23] H.-F. Qin, L.-L. Qu, H. Liu, S.-S. Wang, and H.-J. Gao, "Serum CEA level change and its significance before and after Gefitinib therapy on patients with advanced non-small cell lung cancer," *Asian Pacific Journal of Cancer Prevention*, vol. 14, no. 7, pp. 4205–4208, 2013.

[24] R. Petrioli, A. Licchetta, G. Roviello et al., "CEA and CA19.9 as early predictors of progression in advanced/metastatic colorectal cancer patients receiving oxaliplatin-based chemotherapy and bevacizumab," *Cancer Investigation*, vol. 30, no. 1, pp. 65–71, 2012.

[25] B. Su, H. Shi, and J. Wan, "Role of serum carcinoembryonic antigen in the detection of colorectal cancer before and after surgical resection," *World Journal of Gastroenterology*, vol. 18, no. 17, pp. 2121–2126, 2012.

[26] C. J. Verberne, C. H. Nijboer, G. H. de Bock, I. Grossmann, T. Wiggers, and K. Havenga, "Evaluation of the use of decision-support software in carcino-embryonic antigen (CEA)-based follow-up of patients with colorectal cancer," *BMC Medical Informatics and Decision Making*, vol. 12, no. 1, article 14, 2012.

[27] M. Li, J. Li, A. Zhao et al., "Comparison of carcinoembryonic antigen prognostic value in serum and tumour tissue of patients with colorectal cancer," *Colorectal Disease*, vol. 11, no. 3, pp. 276–281, 2009.

[28] S. Ito, H. Nakanishi, Y. Kodera, Y. Mochizuki, M. Tatematsu, and Y. Yamamura, "Prospective validation of quantitative CEA mRNA detection in peritoneal washes in gastric carcinoma patients," *British Journal of Cancer*, vol. 93, no. 9, pp. 986–992, 2005.

[29] X. Wei, X. Zhai, W. Zhao, D. Yang, and X. Han, "Research on the biological activity and anti-tumor effect against lymphoma cells of DC-CIK cells," *Chinese-German Journal of Clinical Oncology*, vol. 7, no. 11, pp. 666–669, 2008.

[30] S. Koido, T. Ohkusa, S. Homma et al., "Immunotherapy for colorectal cancer," *The World Journal of Gastroenterology*, vol. 19, no. 46, pp. 8531–8542, 2013.

[31] B. Rao, M. Han, L. Wang et al., "Clinical outcomes of active specific immunotherapy in advanced colorectal cancer and suspected minimal residual colorectal cancer: a meta-analysis and system review," *Journal of Translational Medicine*, vol. 9, article 17, 2011.

Hindawi Publishing Corporation
BioMed Research International
Volume 2014, Article ID 986768, 8 pages
http://dx.doi.org/10.1155/2014/986768

Review Article

From Sprouting Angiogenesis to Erythrocytes Generation by Cancer Stem Cells: Evolving Concepts in Tumor Microcirculation

Raafat S. Alameddine, Lana Hamieh, and Ali Shamseddine

Division of Hematology and Oncology, Faculty of Medicine, American University of Beirut, P.O. Box 11-0236, Riad El Solh, Beirut 1107-2020, Lebanon

Correspondence should be addressed to Ali Shamseddine; as04@aub.edu.lb

Received 9 May 2014; Revised 13 July 2014; Accepted 14 July 2014; Published 4 August 2014

Academic Editor: Shiwu Zhang

Angiogenesis is essential for tumor growth and metastasis. Over the last decades, a substantial progress has been achieved in defining different patterns of tumor microcirculation. Sprouting angiogenesis, the oldest model of microcirculation, is the de novo vessel formation from preexisting blood vessels. Vessel splitting and hijacking, also known, respectively, as intussusception and cooption, are alternative models that account for tumor resistance to antiangiogenic therapy. In addition to remodeling the microenvironment, the tumor cell can undergo intrinsic changes and survive hypoxic conditions by acquiring stem cell properties. In line with the concept of pluripotency, tumor cells can form vascular mimicry structures creating their own microcirculation despite a latent vessel growth. The recent identification of the polyploid giant cancer cells and tumor-derived erythrocytes is the most innovative survival mechanism in hypoxia and provides a potential target for more effective therapies.

1. Angiogenesis in Cancer

Angiogenesis is one of the oldest hallmarks of cancer. In the mid-twentieth century, the discovery of the highly vascular networks in solid tumors allowed a better understanding of tumor microcirculation. Over the last decades this fascinating feature has satisfied the pressing need for the oncology community in defining novel targets. More selective therapies were developed based on the better understood biologic features of the tumor. The class of antiangiogenic agents, the largest among targeted therapies, has been constantly growing as well as its approved indications (Table 1). In this review, we survey the earliest models of angiogenesis in the light of clinical experience with antiangiogenic agents. We explore the role of hypoxia in inducing an aggressive pattern in the tumor cell and acquisition of stem cell features. Finally we shed light on the recent findings of vascular mimicry structures and erythrocytes generation by pluripotent cancer stem cells.

2. Sprouting Angiogenesis: The Classical Model of Angiogenesis

In 1977, Folkman and Ausprunk proposed a model for sprouting of new vessels from preexisting vasculature. In sprouting angiogenesis, endothelial cells redefine their role and assume a new configuration to maintain the perfusion of the growing tumor. Factors released by tumor cells, such as vascular endothelial growth factor (VEGF), follicular growth factor (FGF), platelet derived growth factor (PDGF), stimulate a cascade of endothelial changes leading to de novo vessel formation [1]. The whole process starts by the disintegration of the basement membrane followed by the loosening of the intercellular junctions that link endothelial cells [2]. Once free, the endothelial cells rearrange and polarize to invade the surrounding extracellular matrix and finally seal gaps and produce a basement membrane lining the growing vessel. Angiogenesis is regulated by a wide array of receptors and ligands participating all together in an organized crosstalk

Table 1: List of FDA approved antiangiogenic agents.

Antiangiogenic agent	Pharmacological class	FDA approvals
Bevacizumab	Monoclonal antibody	(i) Metastatic colorectal cancer (ii) Metastatic non-small nonsquamous cell lung carcinoma (iii) Renal cell carcinoma (in combination with interferon-alpha immunotherapy) (iv) Glioblastoma
Pazopanib	Multireceptor tyrosine kinase inhibitor	(i) Renal cell carcinoma (ii) Soft tissue sarcoma
Sunitinib	Multireceptor tyrosine kinase inhibitor	(i) Second line in gastrointestinal stromal tumor after imatinib exposure (ii) Advanced renal cell carcinoma (iii) Progressive pancreatic neuroendocrine tumors
Vandetanib	Multireceptor tyrosine kinase inhibitor	Medullary thyroid carcinoma
Sorafenib	Multireceptor tyrosine kinase inhibitor	(i) Renal cell carcinoma (ii) Hepatocellular carcinoma
Ziv-aflibercept	Monoclonal antibody	Second line in metastatic colorectal cancer
Ramucirumab	Monoclonal antibody	Metastatic esophageal, gastric, or gastroesophageal junction carcinoma

[1, 3]. The family of VEGF and its receptors VEGFRs has been recognized as the power horse driving de novo vessel formation [1]. VEGF-A and its receptor VEGFR-2 are of particular importance [4–7]. The activation of the VEGFR is translated by the dimerization of the tyrosine kinase domains and the triggering of intracellular signaling cascades ending by endothelial proliferation and budding of new vessels [8].

3. Alternative Models of Endothelium-Dependent Microcirculation

Clinical experience with VEGF targeting therapies unveiled the caveats in the conventional model of angiogenesis in cancer. A telltale story is the short-term improvement in the progression free survival with the use of bevacizumab, a monoclonal antibody blocking VEGF-A, in breast cancer followed by rebound aggressiveness and metastasis shortening the overall survival [9, 10]. Poor clinical response with antiangiogenic therapy invited a reconsideration of alternative models of tumor microcirculation. In mice inoculated with cancer cells, short-term treatment with a multireceptor tryosine kinase inhibitor resulted in metastatic conditioning with accelerated metastasis and death of the mice [11]. In glioblastoma and pancreatic neuroendocrine tumor models, Pàez-Ribes et al. observed that pharmacological or genetic silencing of VEGF-A surprisingly translated into a higher invasion and distant metastasis [12]. Interestingly enough, the relapsing tumor was hypoxic and devoid of vasculature. This association between hypoxia and a more aggressive behavior corroborates a series of clinical and experimental studies [13–16]. Hypoxia involves a cascade of molecular and phenotypic changes in the tumor cell enhancing its ability to grow, invade, and metastasize. These changes can evoke endothelium dependent models such as vessel cooption and intussusception.

3.1. Vessel Cooption. Vessel cooption is one the earliest mechanisms giving tumor cells access to nutrients and oxygen from the intravascular space. Driven by low oxygen tension, tumor cells abut the walls of existing vessels as preliminary step before forming a new full-blown vasculature [17]. Densely vascularized organs such as lung, liver, and brain provide an excellent niche for tumor cells to hijack preexisting vessels and form solitary metastases [18, 19]. Vessel cooption is one of the mechanisms of acquired resistance to antiangiogenic therapy. Treatment of brain metastases with ZD6474, an antiangiogenic agent, was shown to induce a marked rise in vessel cooption [20]. In patients with renal cell carcinoma, treatment with Sunitinib was associated with extensive necrosis at the tumor center in contrast to the rim highly rich with viable tumor cells [21, 22]. Deregulation in cellular energetic is essential feature of the coopting tumor cells [23]. In vessel cooption, tumor cells highly depend on an active mitochondrial metabolism, protein synthesis, and cell cycle. On the opposite side, angiogenic tumors are highly dependent on remodeling of the microenvironment as reflected by the elevated expression of membrane vesicles, integrins, and growth factors [23]. Vessel cooption can also account for the differential response to antiangiogenic therapy among different tumors. Liver metastases from breast cancer origin have been shown to depend more on cooption of the liver vasculature than those from colorectal origin [24]. The latter finding can account for the higher efficacy of VEGF targeting therapy in metastatic colorectal cancer compared to metastatic breast cancer.

3.2. Intussusception. Intussusception is another adaptive response of the tumor cells to stress and hypoxia. First observed in neonatal rat lungs in 1986, and in colon cancer in 1996, intussusceptive vessel growth results from change in shear stress and remodeling of the vascular network [25, 26]. Switch from sprouting angiogenesis to intussusceptive

angiogenesis is an escape strategy from radiation induced damage to the tumor vasculature [27]. Despite exposure to antiangiogenic therapy and subsequent significant decrease in microvascular density, mammary carcinoma had a rapid recovery post treatment cessation, in virtue of intussusceptive pruning. Intussusceptive vessel growth involves bilateral centripetal protrusion of opposite endothelial cells lining the vessel wall [28]. Once in contact, the opposite vessel walls fuse and tiny apertures in endothelial lining of the vessel walls form, ultimately leading to the splitting of the two newly formed vessels [28, 29]. In contrast to sprouting angiogenesis, splitting angiogenesis is an energy conserving mechanism as it does not dependent on a high rate of proliferation or on basement membrane degradation and invasion, therefore saving energy and permitting survival of the tumor despite hypoxia and stress [25, 28, 30, 31].

4. Epithelial Mesenchymal Transition and Underlying Molecular Pathways

Besides the remodeling in vascular network, the tumor cell can undergo radical morphological and functional changes to survive hypoxia and stress. The epithelial mesenchymal transition (EMT) is a biological model that accounts for tumor cell adaptation to hypoxia in an endothelium-independent manner [32]. EMT involves a cascade of changes at different levels including rearrangement of markers from cell surface to nucleus, cytoskeleton remodeling, and acquisition of mesenchymal identity [33]. The cell gradually loses the epithelial tags. [34]. The intracellular scaffold undergoes also a radical transformation as its constituents change from actin microfilaments to vimentin and its polarity from well-defined apicobasal to a new flexible geometry more commensurate with the new invasive identity. Also, the production of matrix metalloproteinases (MMPs) is increased, and the extracellular matrix (ECM) production line shifts from the basement membrane towards interstitial filaments [35, 36]. EMT changes ultimately lead to the cell acquisition of stem cell properties conferring survival advantage to the transforming cell. EMT depends on a range of molecular pathways involved in early morphogenesis and accounts for resistance to chemotherapy including NF-κB, PI3 K/Akt/mTOR, Notch, Wnt/β-catenin, and Hedgehog signaling [33].

4.1. Nuclear Factor Kappa B (NF-κB). The NF-κB pathway is one of the pathways most intimately linked to the tumorigenesis and survival in hypoxia [37]. The NF-κB is located the cytoplasm as an inactive heterodimeric protein that gets activated and releases its subunits to the nuclear compartments where they upregulate the expression of many oncogenic proteins [38]. Hypoxia promotes the phosphorylation and degradation of the inhibitor of kappa B (IκBa), thus leading to activation of NF-κB and subsequent transition to a mesenchymal phenotype [39, 40]. In pancreatic cancer cell lines, hypoxia was shown to induce the acquisition of mesenchymal properties by epithelial cells through the production of HIF-alpha [41]. Upon inhibition of NF-κB, a regression was observed in the aggression induced by hypoxia exposure. Even under normoxic conditions, the same pattern was reproduced indicating a critical role for NF-κB in translating of HIF overexpression into phenotypical changes [41].

4.2. The PI3K mTOR Pathway. The PI3K/Akt/mTOR axis also regulates hypoxia induced EMT. Blockade of PI3K pathway in hepatocellular carcinoma (HCC) abrogated all the EMT changes induced by hypoxia [42]. The same pattern was reproduced in prostate and ovarian cancer cell lines where the addition of PI3K inhibitor abolished the HIF-1 α activation of Smad2/3 and Akt/GSK-3β, decreased the expression of Snail of transcription and translation, and prevented the decrease in E-cadherin expression and increased cell motility [43].

4.3. The Notch Family of Ligands. Notch signaling is implicated in the cellular response to hypoxia. The Notch family is composed of four receptors and five membrane ligands. Interplay among all of these molecules results in intercellular communication through direct cell-cell contact [44]. Notch signaling is triggered by the binding of Notch ligand to the Notch receptor in the counterpart cell. In oral squamous cell carcinoma, Ishida, Hijioka noted the upregulation of Notch receptors, ligands, and target genes in hypoxia, the fact that translated in increased invasion and cellular motility. The expression of the epithelial marker E-cadherin, a key event in EMT, was decreased in hypoxia. Addition of Notch-specific inhibitor abrogated all the hypoxia induced cellular changes [45, 46]. In breast cancer cell lines, blockade of Notch pathway repressed the expression of Snail and Slug and decreased acquisition of mesenchymal features under hypoxia conditions [46].

4.4. The Wnt/β-Catenin Pathway. The Wnt/β-catenin signalling system is one of the main mediators of hypoxia induced EMT changes [47]. The Wnt/β-catenin is a highly conserved signaling pathway and operates through three different pathways: the canonical pathway involved in the regulation of gene transcription and the noncanonical pathways involved in regulation of intracellular calcium and cytoskeleton [48, 49]. Overexpression of HIF-alpha in prostate cancer cell lines correlated with increased beta catenin protein expression and resulted in enhanced typical EMT changes [50]. In colorectal cancer, hypoxia activated β-catenin and Nur77 with a subsequent increase in cell invasion and migration [51]. In HCC, beta catenin expression was shown to be a key mediator of hypoxia induced EMT, the latter correlated in both in vitro and in vivo models [52]. On microarray analysis of HCC samples, beta catenin and HIF alpha were coexpressed and significantly associated with a shorter survival.

4.5. The Hedgehog Signaling Pathway. The Hedgehog (Hh) pathway also promotes EMT in response to hypoxia. Three ligands compose the family of Hh signals: the Sonic Hedgehog (Shh), the Indian Hedgehog (Ihh), and the Desert Hedgehog (Dhh) [53]. Pretreatment of gastric cancer cells with Shh upregulates EMT, decreases E-cadherin, and induces tumor

invasiveness in vitro [54]. Analysis of gastric cancer tissues revealed significant correlation between Shh expression, EMT, and lymphangiogenesis [54]. Hypoxia effect on cell invasion was negated by antagonism of Smoothened (SMO), the cell surface receptor in Hh pathway. Lei et al. investigated the effect of inhibition of the noncanonical Hh axis on hypoxia induced EMT. The authors found that hypoxia effect on GLI1, a key transcription factor in the Hh pathway, is not restricted to SMO and involves other factors [55]. In a separate experiment on pancreatic ductal adenocarcinoma, Onishi et al. found that increase in cell invasiveness is affected by hypoxia stimulation of Hh axis in a process involving SMO, Gli1 [56].

5. Vascular Mimicry: Insight into Tumor Plasticity

In 1999, the landmark work of Maniotis et al. paved the way for a novel understanding of an endothelium-independent tumor microcirculation [57]. Uveal melanoma cells were found to align in the form of channels gaining access to the systemic circulation by expressing the embryonic genetic repertoire. In contrast to the classical erratic growth of vessels in sprouting angiogenesis, these vascular structures are part of a highly organized network of vessels devoid of any endothelial lining [57]. Vasculogenic mimicry involves several signaling pathways contributing to embryonic vasculogenesis and reflecting an acquired pluripotency in melanoma cells [58]. Additionally, it highly depends on the elevated expression of VEGFR-2. Francescone et al. examined the knock-down of VEGFR-2 or the selective blockade of this receptor in two glioblastoma cell lines U87 and GSDC and reported the detrimental effects of these manipulations on vascular formation [59]. The intracellular cascades mediating proliferation and migration were also significantly affected. The same results were not replicated when using the monoclonal antibody to VEGF-A Indicating that VEGF-A independent mechanisms account for vascular formation in the glioblastoma models [59, 60]. Moreover in another study on glioblastoma cell lines done by Scully et al., vascular channels were found to selectively express platelet derived growth factor receptor (PDGFR) β, smooth muscle markers, and VEGFR-2 with a striking lack of expression of CD31 and VE-cadherin [60]. Another feature of vascular mimicry structures is the unique crosstalk exhibited with the microenvironment through upregulation of proteases such as matrix metalloproteinases (MMPs) 1, 2, 9 and MT1-MMP (MMP-14) or basement membrane proteins such as laminin 5 (Ln-5, gamma 2 chain) [61]. Additionally, the activation of antiapoptotic proteins was found to be essential for generation of VM structures in response to hypoxia. Indeed, Bcl-2 silencing by means of si-RNA depressed the VM response to hypoxia [62]. Central to the vascular mimicry formation as well is the interaction between the cell surface marker VE-cadherin and its receptor the Ephrin type-A receptor 2. The former is known as CD144 is an adhesion molecule playing a vital role for maintaining interendothelial cell contact. The latter is a transmembrane protein kinase closely related to the MAP/ERK kinase cascade. The colocalization between these two molecules on the cell surface is crucial for conductance of proper intracellular signaling in the endothelium mimicking tumor cell with all the ensuing alteration in protein synthesis necessary for fulfillment of this new task [63]. Ewing sarcoma cells also formed VM structures allowing perfusion of tumor cells. And hypoxia is essential in giving these tumor cells plasticity. Given the high prevalence of vascular mimicry structures in Ewing sarcoma, this disease is a prototype for studying of formation of such unique tumor based conduits and defining potential targets for therapy [64]. In prostate cancer, high grade tumors exhibit abundance of vascular mimicry structures, and these cells might be located even in the close vicinity of conventional endothelium-lined blood vessels [65]. In gliomas, the presence of vascular mimicry correlated with a worse prognosis. In fact, vascular mimicry structures allowed a better tumor perfusion even in areas with lower vessel microdensity [66]. In colon cancer, the presence of vasculogenic mimicry was associated with poor anatomical risk factors and a shorter survival [67].

6. Polyploid Giant Cancer Cells (PGCCs) and Erythrocytes Generation

An effective tumor microcirculation rests on a sustainable access to the systemic circulation and a continuous supply with red blood cells to meet the tumor needs. In contrast to tumor angiogenesis, little is known about tumor erythropoiesis. Until recently, the bone marrow has been considered the sole source for erythrocytes circulating in the tumor microenvironment. However, the immunohistochemical detection of fetal forms of hemoglobin in various solid tumors suggested the presence of an alternative origin for high affinity hemoglobin [68]. The tumor stroma was proposed to a potential source of erythrocytes [69]. The recent finding of erythrocytes generation by cancer cells under conditions of hypoxia stirred a lot of interest. In the absence of angiogenesis, cancer cells can produce erythrocytes with embryonic and fetal forms of hemoglobin that carry oxygen with high affinity [70]. The work of Zhang et al. has substantially contributed to the delineation of the steps underlying formation of erythrocytes from cancer cells [70]. Zhang et al. reported the presence of polyploid giant cancer cells (PGCCs) in cells exposed to hypoxia and stress conditions. In virtue of their pluripotency, these cells represent a salvage pathway to survive genotoxic insults [71].

PGCCs are a special population of human tumor cells characterized by a large cytoplasm, aneuploidy, and multiple nuclei [72]. PGCCs are survivors from mitotic catastrophe, whereby failure of induction of programmed cell death results in the formation of aneuploid cells [73]. In states of hypoxia and stress, cancer cells fuse by means of endoreduplication typical of lower eukaryotes and form giant cells with multiple copies of the genome [74].

The presence of aneuploid cells and PGCCs is associated with an increased risk for malignant transformation [73]. In different malignancies, PGCCs are a marker of increased

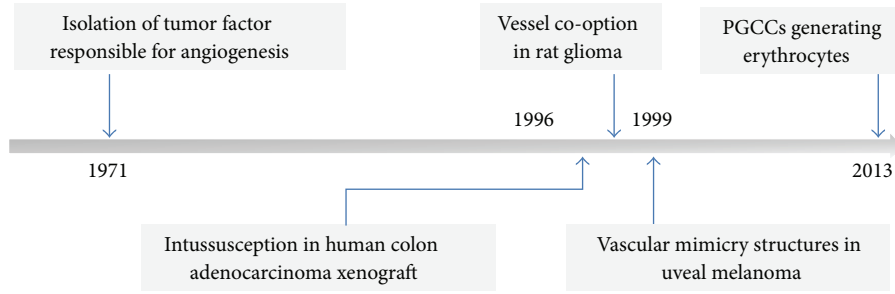

Figure 1: Historical overview of evolution of models of angiogenesis.

stem cell properties, EMT, and a more aggressive biology [75–78].

The novel feature of erythrocytes production by PGCCs was validated in different experiments. Treatment of breast cancer cells with CoCl2, a hypoxia-mimicking agent, resulted in the selective survival of giant cancer cells similar in size to PGCCs [70]. After multiple rounds of exposure to hypoxia, PGCCs gave rise to spheroids expressing cancer stem cell markers. On histological examination, the newly formed spheroids shared with erythrocytes morphological features in terms of size, biconcavity, and absence of nuclei. Spheroids were positively stained for fetal and embryonic forms of hemoglobin, all consistent with a highly efficient oxygen delivery system to the growing tumor. Similarly ovarian fibroblasts cancer cell lines exposed to hypoxia produced erythrocytes with a predominance of the embryonic and fetal forms of hemoglobin. In a separate experiment, breast cancer cell lines treated with a microtubule stabilizer "paclitaxel" went into a mitotic arrest [71]. Subsequently, they formed PGCCs that used peculiar modes of replication to develop into a variety of stromal cells including erythroid cells, all conferring resistance to treatment with paclitaxel [71]. In human glioma PGCCs identified by morphological features in the tumor tissue bank were inoculated into chicken embryonating eggs. Immunohistochemical staining was performed for $\beta/\gamma/\varepsilon/\delta$ chain on red cells bodies inside PGCCs, and red cell bodies turned out to be erythrocytes [76]. All this evidence suggests that cancer cells can be endowed with marvelous features such as erythrocytes generation when challenged with hypoxia.

7. Future Directions

The ability of cancer cells to form new blood vessels was a groundbreaking finding in the early seventies (Figure 1). The alternative models of angiogenesis provided explanation for the failure of antiangiogenic therapy. Subsequently, the demonstration of VM structures was another major leap in understanding the growth and survival of tumor cells in the absence of neo-vessel formation. It illustrates the tumor cell plasticity through the induction of molecular pathways involved in embryogenesis and early morphogenesis, also found in cancer stem cell formation. The most recent finding of tumor microcirculation is the erythrocytes generation by PGCCs. Erythrocytes generation by cancer stem cells will invite a lot of future research to better understand the molecular pathways underlying the genesis of tumor-derived erythrocytes and to potentially develop novel therapies targeting them.

Conflict of Interests

Dr. Shamseddine reports receiving research grants from Roche, Sanofi Aventis, and GlaxoSmithKline in addition to honoraria from Roche, Sanofi Aventis, and Merck. He is also on the advisory board of Roche, Sanofi Aventis, GlaxoSmithKline, Pfizer, and Amgen. Dr. Alameddine and Dr. Hamieh have no potential conflict of interests to declare.

References

[1] Z. K. Otrock, R. A. R. Mahfouz, J. A. Makarem, and A. I. Shamseddine, "Understanding the biology of angiogenesis: review of the most important molecular mechanisms," *Blood Cells, Molecules, and Diseases*, vol. 39, no. 2, pp. 212–220, 2007.

[2] P. Carmeliet, "Mechanisms of angiogenesis and arteriogenesis," *Nature Medicine*, vol. 6, no. 4, pp. 389–395, 2000.

[3] R. S. Alameddine, Z. K. Otrock, A. Awada, and A. Shamseddine, "Crosstalk between HER2 signaling and angiogenesis in breast cancer: molecular basis, clinical applications and challenges," *Current Opinion in Oncology*, vol. 25, no. 3, pp. 313–324, 2013.

[4] L. B. Jakeman, M. Armanini, H. S. Phillips, and N. Ferrara, "Developmental expression of binding sites and messenger ribonucleic acid for vascular endothelial growth factor suggests a role for this protein in vasculogenesis and angiogenesis," *Endocrinology*, vol. 133, no. 2, pp. 848–859, 1993.

[5] N. Ferrara, H. Gerber, and J. LeCouter, "The biology of VEGF and its receptors," *Nature Medicine*, vol. 9, no. 6, pp. 669–676, 2003.

[6] M. J. Cross, J. Dixelius, T. Matsumoto, and L. Claesson-Welsh, "VEGF-receptor signal transduction," *Trends in Biochemical Sciences*, vol. 28, no. 9, pp. 488–494, 2003.

[7] G. Neufeld, S. Tessler, H. Gitay-Goren, T. Cohen, and B. Z. Levi, "Vascular endothelial growth factor and its receptors," *Progress in Growth Factor Research*, vol. 5, no. 1, pp. 89–97, 1994.

[8] J. D. Hood, C. J. Meininger, M. Ziche, and H. J. Granger, "VEGF upregulates ecNOS message, protein, and NO production in human endothelial cells," *American Journal of Physiology—Heart and Circulatory Physiology*, vol. 274, no. 3, part 2, pp. H1054–H1058, 1998.

[9] K. Miller, M. Wang, J. Gralow et al., "Paclitaxel plus bevacizumab versus paclitaxel alone for metastatic breast cancer,"

The New England Journal of Medicine, vol. 357, no. 26, pp. 2666–2676, 2007.

[10] R. S. Kerbel, "Tumor angiogenesis," *The New England Journal of Medicine*, vol. 358, no. 19, pp. 2039–2049, 2008.

[11] J. M. L. Ebos, C. R. Lee, W. Cruz-Munoz, G. A. Bjarnason, J. G. Christensen, and R. S. Kerbel, "Accelerated metastasis after short-term treatment with a potent inhibitor of tumor angiogenesis," *Cancer Cell*, vol. 15, no. 3, pp. 232–239, 2009.

[12] M. Pàez-Ribes, E. Allen, J. Hudock et al., "Antiangiogenic therapy elicits malignant progression of tumors to increased local invasion and distant metastasis," *Cancer Cell*, vol. 15, no. 3, pp. 220–231, 2009.

[13] D. M. Brizel, G. S. Sibley, L. R. Prosnitz, R. L. Scher, and M. W. Dewhirst, "Tumor hypoxia adversely affects the prognosis of carcinoma of the head and neck," *International Journal of Radiation Oncology Biology Physics*, vol. 38, no. 2, pp. 285–289, 1997.

[14] M. Höckel, K. Schlenger, B. Aral, M. Mitze, U. Schäffer, and P. Vaupel, "Association between tumor hypoxia and malignant progression in advanced cancer of the uterine cervix," *Cancer Research*, vol. 56, no. 19, pp. 4509–4515, 1996.

[15] S. Walenta, A. Salameh, H. Lyng et al., "Correlation of high lactate levels in head and neck tumors with incidence of metastasis," *The American Journal of Pathology*, vol. 150, no. 2, pp. 409–415, 1997.

[16] G. Pitson, A. Fyles, M. Milosevic, J. Wylie, M. Pintilie, and R. Hill, "Tumor size and oxygenation are independent predictors of nodal diseases in patients with cervix cancer," *International Journal of Radiation Oncology Biology Physics*, vol. 51, no. 3, pp. 699–703, 2001.

[17] J. Holash, P. C. Maisonpierre, D. Compton et al., "Vessel cooption, regression, and growth in tumors mediated by angiopoietins and VEGF," *Science*, vol. 284, no. 5422, pp. 1994–1998, 1999.

[18] T. Donnem, J. Hu, M. Ferguson et al., "Vessel co-option in primary human tumors and metastases: an obstacle to effective anti-angiogenic treatment?" *Cancer Medicine*, vol. 2, no. 4, pp. 427–436, 2013.

[19] P. B. Vermeulen, C. Colpaert, R. Salgado et al., "Liver metastases from colorectal adenocarcinomas grow in three patterns with different angiogenesis and desmoplasia," *Journal of Pathology*, vol. 195, no. 3, pp. 336–342, 2001.

[20] W. P. J. Leenders, B. Küsters, K. Verrijp et al., "Antiangiogenic therapy of cerebral melanoma metastases results in sustained tumor progression via vessel co-option," *Clinical Cancer Research*, vol. 10, no. 18 I, pp. 6222–6230, 2004.

[21] A. D. Smith, S. N. Shah, B. I. Rini, M. L. Lieber, and E. M. Remer, "Morphology, Attenuation, Size, and Structure (MASS) criteria: assessing response and predicting clinical outcome in metastatic renal cell carcinoma on antiangiogenic targeted therapy," *American Journal of Roentgenology*, vol. 194, no. 6, pp. 1470–1478, 2010.

[22] J. C. Welti, T. Powles, S. Foo et al., "Contrasting effects of sunitinib within in vivo models of metastasis," *Angiogenesis*, vol. 15, no. 4, pp. 623–641, 2012.

[23] J. Hu, F. Bianchi, M. Ferguson et al., "Gene expression signature for angiogenic and nonangiogenic non-small-cell lung cancer," *Oncogene*, vol. 24, no. 7, pp. 1212–1219, 2005.

[24] F. Stessels, G. van den Eynden, I. van der Auwera et al., "Breast adenocarcinoma liver metastases, in contrast to colorectal cancer liver metastases, display a non-angiogenic growth pattern that preserves the stroma and lacks hypoxia," *British Journal of Cancer*, vol. 90, no. 7, pp. 1429–1436, 2004.

[25] J. H. Caduff, L. C. Fischer, and P. H. Burri, "Scanning electron microscope study of the developing microvasculature in the postnatal rat lung," *Anatomical Record*, vol. 216, no. 2, pp. 154–164, 1986.

[26] S. Patan, L. L. Munn, and R. K. Jain, "Intussusceptive microvascular growth in a human colon adenocarcinoma xenograft: a novel mechanism of tumor angiogenesis," *Microvascular Research*, vol. 51, no. 2, pp. 260–272, 1996.

[27] R. Hlushchuk, O. Riesterer, O. Baum et al., "Tumor recovery by angiogenic switch from sprouting to intussusceptive angiogenesis after treatment with PTK787/ZK222584 or ionizing radiation," *American Journal of Pathology*, vol. 173, no. 4, pp. 1173–1185, 2008.

[28] V. Djonov, O. Baum, and P. H. Burri, "Vascular remodeling by intussusceptive angiogenesis," *Cell and Tissue Research*, vol. 314, no. 1, pp. 107–117, 2003.

[29] V. Djonov, M. Schmid, S. A. Tschanz, and P. H. Burri, "Intussusceptive angiogenesis: its role in embryonic vascular network formation," *Circulation Research*, vol. 86, no. 3, pp. 286–292, 2000.

[30] A. Collen, R. Hanemaaijer, F. Lupu et al., "Membrane-type matrix metalloproteinase-mediated angiogenesis in a fibrin-collagen matrix," *Blood*, vol. 101, no. 5, pp. 1810–1817, 2003.

[31] G. W. Prager, J. M. Breuss, S. Steurer, J. Mihaly, and B. R. Binder, "Vascular endothelial growth factor (VEGF) induces rapid prourokinase (pro-uPA) activation on the surface of endothelial cells," *Blood*, vol. 103, no. 3, pp. 955–962, 2004.

[32] M. C. Brahimi-Horn, J. Chiche, and J. Pouysségur, "Hypoxia and cancer," *Journal of Molecular Medicine*, vol. 85, no. 12, pp. 1301–1307, 2007.

[33] B. Bao, A. S. Azmi, S. Ali et al., "The biological kinship of hypoxia with CSC and EMT and their relationship with deregulated expression of miRNAs and tumor aggressiveness," *Biochimica et Biophysica Acta*, vol. 1826, no. 2, pp. 272–296, 2012.

[34] M. K. Asiedu, J. N. Ingle, M. D. Behrens, D. C. Radisky, and K. L. Knutson, "TGFβ/TNFα-mediated epithelial-mesenchymal transition generates breast cancer stem cells with a claudin-low phenotype," *Cancer Research*, vol. 71, no. 13, pp. 4707–4719, 2011.

[35] E. D. Hay, "An overview of epithelio-mesenchymal transformation," *Acta Anatomica*, vol. 154, no. 1, pp. 8–20, 1995.

[36] H. Hugo, M. L. Ackland, T. Blick et al., "Epithelial—mesenchymal and mesenchymal—epithelial transitions in carcinoma progression," *Journal of Cellular Physiology*, vol. 213, no. 2, pp. 374–383, 2007.

[37] A. M. Shannon, D. J. Bouchier-Hayes, C. M. Condron, and D. Toomey, "Tumour hypoxia, chemotherapeutic resistance and hypoxia-related therapies," *Cancer Treatment Reviews*, vol. 29, no. 4, pp. 297–307, 2003.

[38] R. Schreck, K. Albermann, and P. A. Baeuerle, "Nuclear factor $\kappa\beta$: an oxidative stress-responsive transcription factor of eukaryotic cells (a review)," *Free Radical Research Communications*, vol. 17, no. 4, pp. 221–237, 1992.

[39] A. C. Koong, E. Y. Chen, and A. J. Giaccia, "Hypoxia causes the activation of nuclear factor κB through the phosphorylation of IκBα on tyrosine residues," *Cancer Research*, vol. 54, no. 6, pp. 1425–1430, 1994.

[40] M. A. Huber, N. Azoitei, B. Baumann et al., "NF-κB is essential for epithelial-mesenchymal transition and metastasis in a model of breast cancer progression," *Journal of Clinical Investigation*, vol. 114, no. 4, pp. 569–581, 2004.

[41] Z. Cheng, B. Sun, S. Wang et al., "Nuclear factor-κB-dependent epithelial to mesenchymal transition induced by HIF-1α activation in pancreatic cancer cells under hypoxic conditions," *PLoS ONE*, vol. 6, no. 8, Article ID e23752, 2011.

[42] W. Yan, Y. Fu, D. Tian et al., "PI3 kinase/Akt signaling mediates epithelial-mesenchymal transition in hypoxic hepatocellular carcinoma cells," *Biochemical and Biophysical Research Communications*, vol. 382, no. 3, pp. 631–636, 2009.

[43] G. Lin, R. Gai, Z. Chen et al., "The dual PI3K/mTOR inhibitor NVP-BEZ235 prevents epithelial-mesenchymal transition induced by hypoxia and TGF-beta1," *European Journal of Pharmacology*, vol. 729, pp. 45–53, 2014.

[44] L. Miele, "Notch signaling," *Clinical Cancer Research*, vol. 12, no. 4, pp. 1074–1079, 2006.

[45] T. Ishida, H. Hijioka, K. Kume, A. Miyawaki, and N. Nakamura, "Notch signaling induces EMT in OSCC cell lines in a hypoxic environment," *Oncology Letters*, vol. 6, no. 5, pp. 1201–1206, 2013.

[46] J. Chen, N. Imanaka, and J. D. Griffin, "Hypoxia potentiates Notch signaling in breast cancer leading to decreased E-cadherin expression and increased cell migration and invasion," *British Journal of Cancer*, vol. 102, no. 2, pp. 351–360, 2010.

[47] R. Fodde and T. Brabletz, "Wnt/β-catenin signaling in cancer stemness and malignant behavior," *Current Opinion in Cell Biology*, vol. 19, no. 2, pp. 150–158, 2007.

[48] R. Nusse and H. E. Varmus, "Wnt genes," *Cell*, vol. 69, no. 7, pp. 1073–1087, 1992.

[49] C. Y. Logan and R. Nusse, "The Wnt signaling pathway in development and disease," *Annual Review of Cell and Developmental Biology*, vol. 20, pp. 781–810, 2004.

[50] Y. G. Jiang, Y. Luo, D. L. He et al., "Role of Wnt/β-catenin signaling pathway in epithelial-mesenchymal transition of human prostate cancer induced by hypoxia-inducible factor-1α," *International Journal of Urology*, vol. 14, no. 11, pp. 1034–1039, 2007.

[51] S. K. To, W. J. Zeng, J. Z. Zeng, and A. S. Wong, "Hypoxia triggers a Nur77-beta-catenin feed-forward loop to promote the invasive growth of colon cancer cells," *The British Journal of Cancer*, vol. 110, no. 4, pp. 935–945, 2014.

[52] L. Liu, X. Zhu, W. Wang et al., "Activation of β-catenin by hypoxia in hepatocellular carcinoma contributes to enhanced metastatic potential and poor prognosis," *Clinical Cancer Research*, vol. 16, no. 10, pp. 2740–2750, 2010.

[53] M. P. Di Magliano and M. Hebrok, "Hedgehog signalling in cancer formation and maintenance," *Nature Reviews Cancer*, vol. 3, no. 12, pp. 903–911, 2003.

[54] Y. A. Yoo, M. H. Kang, H. J. Lee et al., "Sonic hedgehog pathway promotes metastasis and lymphangiogenesis via activation of Akt, EMT, and MMP-9 pathway in gastric cancer," *Cancer Research*, vol. 71, no. 22, pp. 7061–7070, 2011.

[55] J. Lei, J. Ma, Q. Ma et al., "Hedgehog signaling regulates hypoxia induced epithelial to mesenchymal transition and invasion in pancreatic cancer cells via a ligand-independent manner," *Molecular Cancer*, vol. 12, no. 1, article 66, 2013.

[56] H. Onishi, M. Kai, S. Odate et al., "Hypoxia activates the hedgehog signaling pathway in a ligand-independent manner by upregulation of Smo transcription in pancreatic cancer," *Cancer Science*, vol. 102, no. 6, pp. 1144–1150, 2011.

[57] A. J. Maniotis, R. Folberg, A. Hess et al., "Vascular channel formation by human melanoma cells *in vivo* and *in vitro*: vasculogenic mimicry," *The American Journal of Pathology*, vol. 155, no. 3, pp. 739–752, 1999.

[58] M. J. C. Hendrix, E. A. Seftor, A. R. Hess, and R. E. B. Seftor, "Vasculogenic mimicry and tumour-cell plasticity: lessons from melanoma," *Nature Reviews Cancer*, vol. 3, no. 6, pp. 411–421, 2003.

[59] R. Francescone, S. Scully, B. Bentley et al., "Glioblastoma-derived tumor cells induce vasculogenic mimicry through Flk-1 protein activation," *The Journal of Biological Chemistry*, vol. 287, no. 29, pp. 24821–24831, 2012.

[60] S. Scully, R. Francescone, M. Faibish et al., "Transdifferentiation of glioblastoma stem-like cells into mural cells drives vasculogenic mimicry in glioblastomas," *Journal of Neuroscience*, vol. 32, no. 37, pp. 12950–12960, 2012.

[61] R. E. B. Seftor, E. A. Seftor, N. Koshikawa et al., "Cooperative interactions of laminin 5 γ2 chain, matrix metalloproteinase-2, and membrane type-1-matrix/metalloproteinase are required for mimicry of embryonic vasculogenesis by aggressive melanoma," *Cancer Research*, vol. 61, no. 17, pp. 6322–6327, 2001.

[62] N. Zhao, B. C. Sun, T. Sun et al., "Hypoxia-induced vasculogenic mimicry formation via VE-cadherin regulation by Bcl-2," *Medical Oncology*, vol. 29, no. 5, pp. 3599–3607, 2012.

[63] A. R. Hess, E. A. Seftor, L. M. Gruman, M. S. Kinch, R. E. B. Seftor, and M. J. C. Hendrix, "VE-cadherin regulates EphA2 in aggressive melanoma cells through a novel signaling pathway: implications for vasculogenic mimicry," *Cancer Biology and Therapy*, vol. 5, no. 2, pp. 228–233, 2006.

[64] D. W. J. van der Schaft, F. Hillen, P. Pauwels et al., "Tumor cell plasticity in Ewing sarcoma, an alternative circulatory system stimulated by hypoxia," *Cancer Research*, vol. 65, no. 24, pp. 11520–11528, 2005.

[65] N. Sharma, R. E. B. Seftor, E. A. Seftor et al., "Prostatic tumor cell plasticity involves cooperative interactions of distinct phenotypic subpopulations: role in vasculogenic mimicry," *Prostate*, vol. 50, no. 3, pp. 189–201, 2002.

[66] Y. S. Chen and Z. P. Chen, "Vasculogenic mimicry: a novel target for glioma therapy," *Chinese Journal of Cancer*, vol. 33, no. 2, pp. 74–79, 2014.

[67] C. I. M. Baeten, F. Hillen, P. Pauwels, A. P. de Bruine, and C. G. M. I. Baeten, "Prognostic role of vasculogenic mimicry in colorectal cancer," *Diseases of the Colon and Rectum*, vol. 52, no. 12, pp. 2028–2035, 2009.

[68] M. Wolk, "Considerations on the possible origins of fetal hemoglobin cells produced in developing tumors," *Stem Cells and Development*, vol. 23, no. 8, pp. 791–795, 2014.

[69] E. Szabo, S. Rampalli, R. M. Risueño et al., "Direct conversion of human fibroblasts to multilineage blood progenitors," *Nature*, vol. 468, no. 7323, pp. 521–526, 2010.

[70] S. Zhang, I. Mercado-Uribe, and J. Liu, "Generation of erythroid cells from fibroblasts and cancer cells in vitro and in vivo," *Cancer Letters*, vol. 333, no. 2, pp. 205–212, 2013.

[71] S. Zhang, I. Mercado-Uribe, and J. Liu, "Tumor stroma and differentiated cancer cells can be originated directly from polyploid giant cancer cells induced by paclitaxel," *International Journal of Cancer*, vol. 134, no. 3, pp. 508–518, 2014.

[72] T. Yang, K. Rycaj, Z. Liu, and D. G. Tang, "Cancer stem cells: constantly evolving and functionally heterogeneous therapeutic targets," *Cancer Research*, vol. 74, no. 11, pp. 2922–2927, 2014.

[73] M. Castedo, J. Perfettini, T. Roumier, K. Andreau, R. Medema, and G. Kroemer, "Cell death by mitotic catastrophe: a molecular definition," *Oncogene*, vol. 23, no. 16, pp. 2825–2837, 2004.

[74] D. Zhang, Y. Wang, and S. Zhang, "Asymmetric cell division in polyploid giant cancer cells and low eukaryotic cells," *BioMed*

Research International, vol. 2014, Article ID 432652, 8 pages, 2014.

[75] J. Erenpreisa and M. S. Cragg, "Three steps to the immortality of cancer cells: senescence, polyploidy and self-renewal," *Cancer Cell International*, vol. 13, no. 1, article 92, 2013.

[76] Y. Qu, L. Zhang, Z. Rong, T. He, and S. Zhang, "Number of glioma polyploid giant cancer cells (PGCCs) associated with vasculogenic mimicry formation and tumor grade in human glioma," *Journal of Experimental & Clinical Cancer Research*, vol. 32, no. 1, p. 75, 2013.

[77] T. M. Illidge, M. S. Cragg, B. Fringes, P. Olive, and J. A. Erenpreisa, "Polyploid giant cells provide a survival mechanism for p53 mutant cells after DNA damage," *Cell Biology International*, vol. 24, no. 9, pp. 621–633, 2000.

[78] S. Zhang, I. Mercado-Uribe, Z. Xing, B. Sun, J. Kuang, and J. Liu, "Generation of cancer stem-like cells through the formation of polyploid giant cancer cells," *Oncogene*, vol. 33, no. 1, pp. 116–128, 2014.

Hindawi Publishing Corporation
BioMed Research International
Volume 2014, Article ID 603871, 5 pages
http://dx.doi.org/10.1155/2014/603871

Clinical Study

Immune Response, Safety, and Survival and Quality of Life Outcomes for Advanced Colorectal Cancer Patients Treated with Dendritic Cell Vaccine and Cytokine-Induced Killer Cell Therapy

Hui Zhu,[1] Xuejing Yang,[2] Jiali Li,[1] Yanjie Ren,[2] Tianyu Zhang,[2] Chunze Zhang,[3] Jintai Zhang,[4] Jing Li,[1] and Yan Pang[1]

[1] *Department of Oncology, Tianjin Union Medicine Centre, 190 Jieyuan Road, Hongqiao District, Tianjin 300121, China*
[2] *Shanghai Claison Biotechnology Co. Ltd, Shanghai, China*
[3] *Department of Colorectal Surgery, Tianjin Union Medicine Centre, Tianjin 300121, China*
[4] *Department of General Surgery, Tianjin Union Medicine Centre, Tianjin 300121, China*

Correspondence should be addressed to Yan Pang; pangyancn@126.com

Received 25 April 2014; Revised 8 June 2014; Accepted 8 June 2014; Published 17 July 2014

Academic Editor: Shiwu Zhang

Purpose. To determine the immune response after dendritic cell (DC) vaccine and cytokine-induced killer cells (CIK) therapy and assess its associated toxicity, survival benefit, and changes in the quality of life (QOL) of advanced colorectal cancer (CRC) patients. *Methods.* We recruited 100 patients with unresectable CRC orrelapsed CRC after surgery who received DC vaccine and CIK cells (group immunotherapy, group I), and, as a control, 251 patients who had similar characteristics and underwent similar treatments, except for this immunotherapy (group nonimmunotherapy, group NI). After a follow-up period of 489.2 ± 160.4 days, overall survival (OS) of the two groups was compared using the Kaplan-Meier method. *Results.* In group I, 62% of patients developed a positive delayed type hypersensitivity response, and most patients showed an improvement in physical strength (75.2%), appetite (74.2%), sleeping (72.1%), and body weight (70.1%). Adverse events were fever (29.5%), insomnia (19.2%), anorexia (9.1%), sore joints (5.4%), and skin rash (1.0%). No toxicity was observed in patients treated with DC vaccine and CIK therapy. OS was significantly longer in group I than in group NI ($P = 0.043$). *Conclusion.* DC vaccine and CIK therapy were safe and could induce an immune response against CRC, thereby improving QOL and prolonging OS.

1. Introduction

Colorectal cancer (CRC) is one of the most common cancers worldwide, and more than half of the patients with this malignancy will die from their disease [1–3]. Surgery, chemotherapy, and radiotherapy are the standard treatment modalities for CRC, which have provided significant benefits for patients [4–6]. For early-stage CRC patients, resection followed by adjuvant chemotherapy and radiotherapy is the preferred treatment strategy, resulting in a 5-year survival rate of 70% to 80% [7]. However, early-stage CRC is asymptomatic, and consequently this malignancy is often not diagnosed until it has reached an advanced stage. Furthermore, most patients with early-stage CRC will relapse and eventually develop advanced CRC, which has a poor prognosis, with a 5-year survival rate of 5% or less [7]. In this situation, chemotherapy is regarded as the first-line treatment.

The adverse effects of these routine therapies are a major problem, and severe treatment-related toxicity may result in discontinuation. Further, the poor general health of patients with advanced CRC can prevent the use of standard therapies [8, 9]. In addition to the problem of severe adverse effects, routine therapies often do not lead to complete tumor eradication in advanced CRC patients [10].

New strategies are needed in order to improve the clinical outcomes for these patients. Many patients are in an immunosuppressed state after surgery, radiotherapy, and chemotherapy, and dysfunction of antigen-specific T cells is common. As a result, tumor cells escape from immune surveillance. Recovering anticancer immunity is one possible approach to cancer treatment and is referred to as immunotherapy. Unlike other therapies, immunotherapy may help build an effective and specific immune response, killing tumor cells whilst minimizing toxicity. Dendritic cell (DC) and cytokine-induced killer (CIK) cell-based immunotherapy is one of the most effective means for killing residual cancer cells, which are a leading cause of recurrence and metastasis, and is well tolerated and associated with excellent compliance [11–15].

The purpose of this study was to evaluate the cellular immune response in terms of delayed type hypersensitivity (DTH), improvement in quality of life (QOL), and the safety and survival benefit of DC vaccine and CIK cell therapy in patients with advanced CRC.

Table 1: Patient characteristics.

Characteristics	No. (%)			P
	Total	Group I	Group NI	
No.	351	100	251	
Age (years)				
Range	19–92	25–85	19–92	0.47
Mean ± SD	65.9 ± 13.2	62.1 ± 12.4	67.4 ± 13.2	
Gender				
Male	229 (65.2)	71 (71.0)	158 (62.9)	0.15
Female	122 (34.8)	29 (29.0)	93 (37.1)	
Tumor location				
Colon	108 (30.8)	29 (29.0)	79 (31.5)	0.65
Rectum	243 (69.2)	71 (71.0)	172 (68.5)	
Treatment baseline				
Surgery	73 (20.8)	28 (28.0)	45 (17.9)	0.04
Radiotherapy	29 (8.3)	8 (8.0)	21 (8.4)	0.91
Chemotherapy	55 (15.7)	18 (18.0)	37 (14.7)	0.45

2. Patients and Methods

2.1. Patients. The study was performed at the Department of Oncology, Tianjin Union Medicine Center, Tianjin, China. Patients with advanced CRC were advised to undergo immunotherapy consisting of an autologous DC vaccine and CIK cell treatment (group I) and were asked to provide informed consent. The inclusion criteria were (1) a histological or cytological diagnosis of advanced CRC; (2) hospitalization between February 1, 2012, and August 30, 2012; (3) an unresectable tumor at the first diagnosis and relapsed or metastatic CRC after surgery; (4) adequate kidney, bone marrow, and liver function and normal coagulation.

Patients who met these inclusion criteria but who did not receive immunotherapy consisting of DC vaccine and CIK cell treatment (group NI) were selected as a control group. All patients were followed up until November 14, 2013. Overall survival (OS) was compared between the two groups and the benefit of the DC vaccine and CIK cell-based immunotherapy regimen were evaluated on this basis (Table 1).

2.2. Study Design. This was an open-label, single-institution, parallel-group, nonrandomized, retrospective study performed at the Department of Oncology, Tianjin Union Medicine Center, Tianjin China, between February 1, 2012, and August 30, 2012. The study complied with the class III medical techniques described in "Treatment with autologous immune cells (T cells, NK cells)" that was published by the Chinese Ministry of Health. The protocol was approved by the hospital's ethics committee. All patients provided written informed consent before treatment.

2.3. Treatment Schedules. For DC vaccine and CIK cell therapy, peripheral blood mononuclear cells (PBMCs) were collected on day 0. Subsequently, 1×10^7 DCs were infused intravenously for the first three weeks and intradermally for the last three weeks from day 8, and 1×10^9 CIK cells were infused intravenously once a day for 4 days from day 11.

2.4. Preparation of DCs and CIK Cells. DCs and CIK cells were prepared as described previously [16–19]. The cancer cells were well separated from the cultured colon cancer cell line Sw480. These cells were disrupted by ultrasound and then centrifuged at 600 g for 30 min. The supernatants (tumor lysate) were collected and used for pulsing DCs and testing for DTH. PBMCs were collected by leukapheresis using the Fresenius KABI System (Germany) and subsequently cultured in serum-free medium overnight. Adherent and nonadherent cells were separated, and DC vaccine was prepared by culturing the adherent cells in the presence of granulocyte-macrophage colony-stimulating factor, interleukin-4, tumor lysate, and tumor necrosis factor for 7 days. CIK cells were prepared by culturing the nonadherent cells in the presence of interferon-γ, CD3 monoclonal antibody, and interleukin-2 for 10 days.

2.5. Criteria for Allowing the Clinical Use of DC Vaccine and CIK Cells. After analysis of the immune phenotype markers HLA2DR, CD80, and CD83 for DCs and CD3, CD8, and CD56 for CIK cells by flow cytometry, the cultured samples were checked for contamination by bacteria and fungi, and endotoxin levels were less than 5 EU/kg. A total of 1×10^7 DCs were drawn into a syringe for intradermal vaccination or were mixed with 100 mL normal saline (NS) for intravenous vaccination, and 1×10^9 CIK cells were mixed with 100 mL NS for intravenous infusion.

2.6. DTH. DTH tests were performed 1 week after the last DC vaccination by the intradermal injection of 4 μg tumor lysate. Tests were read 48 h later. According to the diameter of induration, the results were classified as strongly positive (>10 mm), positive (5–10 mm), weakly positive (2–5 mm), and negative (<2 mm) (Table 2).

2.7. QOL. QOL was evaluated by a general improvement in physical strength, appetite, sleeping, and body weight using

Table 2: DTH skin test results in the DC vaccine and CIK cell therapy group ($N = 100$).

Results of the DTH skin test	Definition (mm)	No. (%)
Strongly positive	>10	24 (24.0)
Positive	5–10	26 (26.0)
Weakly positive	2–5	12 (12.0)
Negative	<2	38 (38.0)

a standardized questionnaire. Changes in QOL were classified as major changes, minor changes, no change, and a worsening of the symptom. Major and minor changes were considered as to be an improvement in the general status (Table 3).

3. Safety

Adverse events including fever, insomnia, anorexia, joint soreness, and skin rash were monitored during DC vaccine and CIK cell therapy. Several of these events might occur simultaneously in the same patient (Table 4).

3.1. OS. The patients were followed up until November 14, 2013. OS was defined as the survival of patients from the date of enrollment to the date of death due to CRC. Patients who were lost to followup, who died due to an uncertain cause, or whose date of death could not be confirmed were excluded from the OS analysis (Figure 1).

3.2. Data Collection and Statistical Analysis. The primary efficacy endpoint for this study was OS. The secondary endpoints were DTH, QOL, and safety. Clinical data were collected from the inpatients electronic medical records of our hospital and reanalyzed and documented for use in this analysis by using Epidata Data Base software (version 3.02, Denmark). Statistical analyses were performed using SPSS (version 19.0) statistical software package, which interfaced with the Epidata Data Base. OS curves were calculated using the Kaplan-Meier method. A P value less than 0.05 was considered to be statistically significant.

4. Results

4.1. Patient Characteristics. A total of 351 CRC patients (229 men and 122 women) were enrolled in this study, with a mean age of 65.9 ± 13.2 years (range, 19–92 years). Patients either received routine treatment alone (251 patients, group NI) or routine treatment plus DC vaccine and CIK cell therapy (100 patients, group I). The characteristics of the patients were well balanced between the two groups, except that more patients in group I underwent surgery (28.0% versus 17.9%, $P = 0.04$). The primary tumor was located in the colon in 108 (30.8%) patients and in the rectum in the other 243 (69.2%) patients. Of the 351 patients, 73 (20.8%) underwent primary tumor resection, 29 (8.3%) received radiotherapy, and 55 (15.7%) received chemotherapy (Table 1).

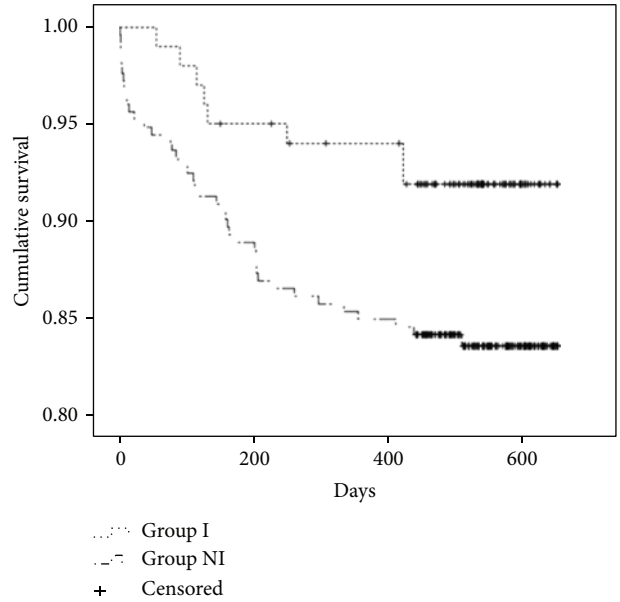

Figure 1: Overall survival curves by the Kaplan-Meier method for patients in group I and group NI. There were a total of 100 patients in group I, 8 of whom died, and a total of 251 patients in group NI, 41 of whom died ($P = 0.04$).

4.2. DTH Skin Test. The DTH skin test was used to assess the immune response to DC vaccine and CIK cell therapy for all patients in group I. Of these 100 patients, 24 patients (24%) had a strongly positive response, 26 patients (26%) had a positive response, and 12 patients (12%) had a weakly positive response. In total, 62% of patients (62 of 100) had a positive immune response and the other 38% of patients (38 of 100) failed to show an immune response (Table 2).

4.3. QOL. QOL was recorded as an improvement in the general health of patients, although in group I, this data were only available for 97 out of the 100 patients. Out of these 97 patients, 73 (75.2%) showed a positive improvement in their physical strength, 72 (74.2%) had improved appetite, 70 (72.1%) were able to sleep better, and 68 (70.1%) had an increase in body weight (Table 3).

4.4. Adverse Effects. Adverse effects were assessed in 97 out of the 100 patients in group I; no data were available for the remaining 3 patients. Of the 97 patients, 29 (29.5%) developed fever, 11 (19.2%) developed insomnia, 9 (9.1%) developed anorexia, 5 (5.4%) developed joint soreness, and 1 (1.0%) developed skin rash. No toxicity resulted from DC vaccine and CIK cell therapy (Table 4).

4.5. OS. The mean follow-up period for patients in this study was 489.2 ± 160.4 days (range, 441–652 days). On the last day of the follow-up period (November 14, 2013), 8 out of the 100 patients in group I had died of CRC and 41 out of the 251 patients in group NI had died of CRC. OS was significantly longer in group I than in group NI ($P = 0.04$; Figure 1).

Table 3: QOL in the DC vaccine and CIK cell therapy group ($N = 100$, censored data in 3 cases).

	Improvement in general status, number of patients (%)			
	Major (%)	Minor (%)	No change (%)	Worse (%)
Physical strength	50 (51.5)	23 (23.7)	19 (19.6)	5 (5.2)
Appetite	49 (50.5)	23 (23.7)	16 (19.6)	9 (5.2)
Sleeping status	53 (54.6)	17 (17.5)	16 (16.5)	11 (11.4)
Weight	49 (50.5)	19 (19.6)	23 (23.7)	6 (6.2)

Table 4: Adverse events resulting from DC vaccine and CIK cell therapy ($N = 100$, censored data in 3 cases).

Event	No. (%)
Fever	29 (29.5)
Insomnia	11 (19.2)
Anorexia	9 (9.1)
Joint soreness	5 (5.4)
Skin rash	1 (1.0)

5. Discussion

DCs can prime both a primary and secondary immune response against cancer and function as antigen-presenting cells, and DC vaccine can both initiate and amplify tumor antigen-specific responses through the activation of both T helper cells and cytotoxic T lymphocytes [20–24]. CIK cells are a heterogeneous population with both T cell- and natural killer cell-like characteristics. They have cytotoxic activity and can kill tumor cells both directly and indirectly through stimulation of the host immune system. CIK cells thus have the potential to eradicate residual cancer cells, thereby preventing recurrence after tumor resection. These properties have led to CIK cells being included in immunotherapy strategies against cancer [25–29]. Immunotherapy with DCs and/or CIK cells have been shown to be a potential therapeutic approach against cancers and are now widely used in the clinic for several types of malignancy [30–32].

In this study, we found that 62% of patients (62 of 100) treated with DC vaccine and CIK cells developed a positive cell-mediated cytotoxicity response (Table 2). Subsequently, 75.2%, 74.2%, 72.1%, and 70.1% of 97 patients for whom data were available showed improved physical strength, appetite, sleep, and body weight, respectively (Table 3). In general, the adverse effects resulting from the administration of DC vaccine and CIK cells were mild and self-resolving without special treatments, and no toxicity was observed. Furthermore, our results show that DC vaccine and CIK cell treatment significantly improved the OS of advanced CRC patients compared to those treated with conventional therapies alone.

Our findings suggest that DC vaccine and CIK cell therapy could induce an immune response against CRC, improve QOL, and prolong OS. The therapy was safe with no severe adverse effects and could therefore be tolerated by patients in poor health. It is therefore a potentially beneficial option for patients with advanced CRC.

6. Conclusion

Our findings indicate that DC vaccine and CIK cell therapy is an effective and safe treatment for advanced CRC that can potentially overcome the severe adverse effects associated with conventional cytotoxic therapy. This immunotherapy regimen improved both the QOL and OS of these patients and may confer a significant clinical benefit in many cases.

Conflict of Interests

The authors declare that there is no conflict of interests regarding the publication of this paper.

Acknowledgment

The present study was partially supported by the Tianjin Municipal Science and Technology Commission (no. 12ZCDZSY17100).

References

[1] P. Boyle and M. E. Leon, "Epidemiology of colorectal cancer," *The British Medical Bulletin*, vol. 64, pp. 1–25, 2002.

[2] E. T. Hawk, P. J. Limburg, and J. L. Viner, "Epidemiology and prevention of colorectal cancer," *Surgical Clinics of North America*, vol. 82, no. 5, pp. 905–941, 2002.

[3] A. Shin, K. Z. Kim, K. W. Jung et al., "Increasing trend of colorectal cancer incidence in Korea, 1999–2009," *Cancer Research and Treatment*, vol. 44, no. 4, pp. 219–226, 2012.

[4] D. C. Damin and R. A. Lazzaron, "Evolving treatment strategies for colorectal cancer: a critical review of current therapeutic options," *World Journal of Gastroenterology*, vol. 20, no. 4, pp. 877–887, 2014.

[5] T.-W. Ke, Y.-M. Liao, H.-C. Chiang et al., "Effectiveness of neoadjuvant concurrent chemoradiotherapy versus up-front proctectomy in clinical stage II-III rectal cancer: a population-based study," *Asia-Pacific Journal of Clinical Oncology*, 2014.

[6] M. Laurent, E. Paillaud, C. Tournigand et al., "Assessment of solid cancer treatment feasibility in older patients: a prospective cohort study," *Oncologist*, vol. 19, no. 3, pp. 275–282, 2014.

[7] M. Z. Ratajczak, T. Jadczyk, G. Schneider, S. S. Kakar, and M. Kucia, "Induction of a tumor-metastasis-receptive microenvironment as an unwanted and underestimated side effect of treatment by chemotherapy or radiotherapy," *Journal of Ovarian Research*, vol. 6, no. 1, article 95, 2013.

[8] P. C. Kurniali, L. G. Luo, and A. B. Weitberg, "Role of calcium/magnesium infusion in oxaliplatin-based chemotherapy for colorectal cancer patients," *Oncology*, vol. 24, no. 3, pp. 289–292, 2010.

[9] D. J. Gallagher and N. Kemeny, "Metastatic colorectal cancer: from improved survival to potential cure," *Oncology*, vol. 78, no. 3-4, pp. 237–248, 2010.

[10] S. Koido, T. Ohkusa, S. Homma et al., "Immunotherapy for colorectal cancer," *World Journal of Gastroenterology*, vol. 19, no. 46, pp. 8531–8542, 2013.

[11] E. Ellebaek, M. H. Andersen, I. M. Svane, and P. T. Straten, "Immunotherapy for metastatic colorectal cancer: present status and new options," *Scandinavian Journal of Gastroenterology*, vol. 47, no. 3, pp. 315–324, 2012.

[12] B. Xiang, A. E. Snook, M. S. Magee, and S. A. Waldman, "Colorectal cancer immunotherapy," *Discovery Medicine*, vol. 15, no. 84, pp. 301–308, 2013.

[13] P. G. Toomey, N. A. Vohra, T. Ghansah, A. A. Sarnaik, and S. A. Pilon-Thomas, "Immunotherapy for gastrointestinal malignancies," *Cancer Control*, vol. 20, no. 1, pp. 32–42, 2013.

[14] A. Amedei, E. Niccolai, and M. M. D'Elios, "T cells and adoptive immunotherapy: recent developments and future prospects in gastrointestinal oncology," *Clinical and Developmental Immunology*, vol. 2011, Article ID 320571, 17 pages, 2011.

[15] Y. Cui, X. Yang, W. Zhu, J. Li, X. Wu, and Y. Pang, "Immune response, clinical outcome and safety of dendritic cell vaccine in combination with cytokine-induced killer cell therapy in cancer patients," *Oncology Letters*, vol. 6, no. 2, pp. 537–541, 2013.

[16] M. N. López, C. Pereda, G. Segal et al., "Prolonged survival of dendritic cell-vaccinated melanoma patients correlates with tumor-specific delayed type IV hypersensitivity response and reduction of tumor growth factor β-expressing T cells," *Journal of Clinical Oncology*, vol. 27, no. 6, pp. 945–952, 2009.

[17] P. A. Burch, J. K. Breen, J. C. Buckner et al., "Priming tissue-specific cellular immunity in a phase I trial of autologous dendritic cells for prostate cancer," *Clinical Cancer Research*, vol. 6, no. 6, pp. 2175–2182, 2000.

[18] Y. Liu, W. Zhang, B. Zhang, X. Yin, and Y. Pang, "DC vaccine therapy combined concurrently with oral capecitabine in metastatic colorectal cancer patients," *Hepato-Gastroenterology*, vol. 60, no. 122, pp. 23–27, 2013.

[19] A. D. Garg, A. M. Dudek, and P. Agostinis, "utophagy-dependent suppression of cancer immunogenicity and effector mechanisms of innate and adaptive immunity," *Oncoimmunology*, vol. 2, no. 10, Article ID e26260, 2013.

[20] L. Galluzzi, L. Senovilla, E. Vacchelli et al., "Trial watch: dendritic cell-based interventions for cancer therapy," *Oncoimmunology*, vol. 1, no. 7, pp. 1111–1134, 2012.

[21] H. Ragde, W. A. Cavanagh, and B. A. Tjoa, "Dendritic cell based vaccines: progress in immunotherapy studies for prostate cancer," *Journal of Urology*, vol. 172, no. 6, pp. 2532–2538, 2004.

[22] K. F. Bol, J. Tel, I. J. de Vries, and C. G. Figdor, "Naturally circulating dendritic cells to vaccinate cancer patients," *Oncoimmunology*, vol. 2, no. 3, Article ID e23431, 2013.

[23] J. Tel, E. L. Smits, S. Anguille, R. N. Joshi, C. G. Figdor, and I. J. M. de Vries, "Human plasmacytoid dendritic cells are equipped with antigen-presenting and tumoricidal capacities," *Blood*, vol. 120, no. 19, pp. 3936–3944, 2012.

[24] X. Wang, W. H. Yu, J. Li et al., "Can the dual-functional capability of CIK cells be used to improve antitumor effects?" *Cellular Immunology*, vol. 287, no. 1, pp. 18–22, 2014.

[25] C. E. Jäkel, S. Hauser, S. Rogenhofer, S. C. Müller, P. Brossart, and I. G. H. Schmidt-Wolf, "Clinical studies applying cytokine-induced killer cells for the treatment of renal cell carcinoma," *Clinical and Developmental Immunology*, vol. 2012, Article ID 473245, 7 pages, 2012.

[26] J. Yu, X. Ren, H. Li et al., "Synergistic effect of CH-296 and interferon gamma on cytokine-induced killer cells expansion for patients with advanced-stage malignant solid tumors," *Cancer Biotherapy & Radiopharmaceuticals*, vol. 26, no. 4, pp. 485–494, 2011.

[27] G. Mesiano, M. Todorovic, L. Gammaitoni et al., "Cytokine-induced killer (CIK) cells as feasible and effective adoptive immunotherapy for the treatment of solid tumors," *Expert Opinion on Biological Therapy*, vol. 12, no. 6, pp. 673–684, 2012.

[28] S. Shi, R. Wang, Y. Chen, H. Song, L. Chen, and G. Huang, "Combining antiangiogenic therapy with adoptive cell immunotherapy exerts better antitumor effects in non-small cell lung cancer models," *PLoS ONE*, vol. 8, no. 6, Article ID e65757, 2013.

[29] K. Hasumi, Y. Aoki, R. Wantanabe, and D. L. Mann, "Clinical response of advanced cancer patients to cellular immunotherapy and intensity-modulated radiation therapy," *Oncoimmunology*, vol. 2, no. 10, Article ID e26381, 2013.

[30] R. Zhong, J. Teng, B. Han, and H. Zhong, "Dendritic cells combining with cytokine-induced killer cells synergize chemotherapy in patients with late-stage non-small cell lung cancer," *Cancer Immunology, Immunotherapy*, vol. 60, no. 10, pp. 1497–1502, 2011.

[31] H. Zhan, X. Gao, X. Pu et al., "A randomized controlled trial of postoperative tumor lysate-pulsed dendritic cells and cytokine-induced killer cells immunotherapy in patients with localized and locally advanced renal cell carcinoma," *Chinese Medical Journal*, vol. 125, no. 21, pp. 3771–3777, 2012.

[32] L. Yin, S. Wang, L. Zhang et al., "Efficacy of dendritic cells/cytokine induced killer cells adoptive immunotherapy combined with chemotherapy in treatment of metastatic colorectal cancer," *Chinese Journal of Cancer Biotherapy*, vol. 20, no. 2, pp. 217–224, 2013.

Hindawi Publishing Corporation
BioMed Research International
Volume 2014, Article ID 282657, 9 pages
http://dx.doi.org/10.1155/2014/282657

Research Article

Administration of the Resveratrol Analogues Isorhapontigenin and Heyneanol-A Protects Mice Hematopoietic Cells against Irradiation Injuries

Hui Wang,[1] Yi-ling Yang,[2] Heng Zhang,[1,3] Hao Yan,[1] Xiao-jing Wu,[1] and Chun-ze Zhang[4]

[1] *Department of Radiation Oncology, Tianjin Union Medical Center, Tianjin 300121, China*
[2] *Department of Breast Cancer Pathology and Research Laboratory, Key Laboratory of Breast Cancer Prevention and Therapy (Ministry of Education), Key Laboratory of Cancer Prevention and Therapy (Tianjin), National Clinical Research Center for Cancer, Tianjin Medical University Cancer Institute and Hospital, Tianjin 300060, China*
[3] *Institute of Radiation Medicine, Peking Union Medical College (PUMC), Tianjin 300192, China*
[4] *Department of Anorectal Surgery, Tianjin Union Medical Center, Tianjin 300121, China*

Correspondence should be addressed to Heng Zhang; zh_tj@sina.com

Received 16 April 2014; Revised 27 May 2014; Accepted 8 June 2014; Published 24 June 2014

Academic Editor: Shiwu Zhang

Ionizing radiation (IR) is known not only to cause acute bone marrow (BM) suppression but also to lead to long-term residual hematopoietic injury. These effects have been attributed to IR inducing the generation of reactive oxygen species (ROS) in hematopoietic cells. In this study, we examined if isorhapontigenin and heyneanol-A, two analogues of resveratrol, could mitigate IR-induced BM suppression. The results of cell viability assays, clonogenic assays, and competitive repopulation assays revealed that treatment with these compounds could protect mice BM mononuclear cells (BMMNC), hematopoietic progenitor cells, and hematopoietic stem cells from IR-induced BM suppression. Moreover, the expression of genes related to the endogenous cellular antioxidant system in hematopoietic cells was analyzed. The expression and activity of SOD2 and GPX1 were found to be decreased in irradiated BMMNC, and the application of the resveratrol analogues could ameliorate this damage. Our results suggest that in comparison with resveratrol and isorhapontigenin, treatment with heyneanol-A can protect hematopoietic cells from IR-induced damage to a greater degree; the protective effects of these compounds are probably the result of their antioxidant properties.

1. Introduction

Radiation therapy is a common and effective tool in the management of a wide variety of tumors; in some cases, it may be the single best treatment for cancer. Bone marrow (BM) suppression is the most common dose-limiting side effect during radiation therapy [1, 2]; BM suppression is also the primary cause of death following accidental exposure of a patient to a high dose of total body irradiation. Myelosuppression, which can occur as a result of high total body irradiation, not only worsens the outcome of cancer treatment but also adversely affects the quality of life of cancer patients [2, 3]. However, the mechanisms by which ionizing radiation (IR) induces BM injury remain poorly understood, and no effective treatment has been developed to ameliorate this type of injury.

Injuries due to IR occur as a result of the ionization of water resulting in the formation of reactive oxygen species (ROS), notably hydroxyl radicals, increasing oxidative stress [4, 5]. Several studies have demonstrated that the induction of oxidative stress in hematopoietic cells is associated with sustained oxidative DNA damage; this results in a persistent loss of proliferative capacity in hematopoietic progenitor cells (HPCs) and hematopoietic stem cells (HSCs) [4, 6, 7]. Our recent studies have indicated that a persistent IR-induced increase in the production of reactive oxygen species (ROS) can be achieved in hematopoietic cells, in part, via the down-regulation of superoxide dismutase (SOD) and glutathione

peroxidase (GPX) and the upregulation of NADPH oxidase 4 (NOX4) [8, 9]. Several recent studies have also demonstrated that the induction of oxidative stress is primarily responsible for the loss of HSC self-renewal as well as the premature exhaustion of HSCs in mice that have mutations in the ATM [10] and deletion of FoxO3(s) [11]. These findings suggest that it may be possible to ameliorate IR-induced BM injury through treatment with a potent antioxidant.

Resveratrol (trans-3,5,4′-trihydroxystilbene, REV), a polyphenolic compound primarily found in grapes, is a potent antioxidant [12]. Accumulating reports have shown that REV can prevent or slow a wide variety of diseases related to oxidative stress, including cancer, cardiovascular diseases, and Alzheimer's disease [13]. It has been demonstrated that REV can act as a scavenger of hydroxyl, superoxide, and metal-induced radicals [12]. It is likely that the protective effects of REV against oxidative injury can be attributed to REV upregulating endogenous cellular antioxidant systems, such as SOD and GPX, rather than through directly scavenging ROS [9, 12]. Although the effects of REV in ameliorating IR-induced hematopoietic cell injuries have been investigated [9], little is known of the effects of oligomers of REV, such as isorhapontigenin (ISOR), a derivative of stilbene that can be isolated from *Belamcanda chinensis*, and heyneanol-A (HEY-A), a tetramer of REV that can be isolated from *Vitis heyneana*. Previous studies have revealed that these compounds possess anti-inflammatory, anti-apoptotic, and anti-oxidative activity [14, 15], but the biological activity of these compounds against irradiation injuries has not been investigated.

Owing to the remarkable therapeutic potential of REV's oligomers ISOR and HEY-A, we examined their effects on IR-induced BM suppression in our well-established and well-characterized mouse model. The results indicated that the two oligomers of REV could ameliorate IR-induced BM injury and that this occurred, at least partly, via the upregulation of the expression of SOD2 and GPX1 in hematopoietic cells.

2. Materials and Methods

2.1. Reagents. Anti-mouse-CD45.1-FITC (clone A20, Ly5.1), anti-mouse-CD45.2-PE (clone104, Ly5.2), anti-mouse-Ly6G/Gr-1-PE/Cy7 (cloneRB6-8C5), anti-mouse-CD45R/B220-PerCP (cloneRA3-6B2), anti-mouse-CD11b-PE/Cy7 (cloneM1/70), and anti-mouse-CD3-APC (clone145-2C11) antibodies were obtained from eBioscience (San Diego, CA, USA). REV and ISOR were purchased from Sigma (St. Louis, MO, USA). HEY-A was kindly provided by Dr. Qi Hou from the Institute of Materia Medica at Peking Union Medical College (PUMC, Beijing, China).

2.2. Mice. Male C57BL/6 mice were purchased from the Institute of Laboratory Animal Sciences (PUMC, Beijing, China) and were bred at the certified animal care facility in the Institute of Radiation Medicine of PUMC. All of the mice used in the study were aged approximately 8–10 weeks. The Institutional Animal Care and Use Committee of PUMC approved all the experimental procedures used in this study.

2.3. Treatment of IR-Exposed BM Mononuclear Cells with REV, ISOR, and HEY-A. The mice were euthanized using CO_2; immediately following this, the femora and the tibiae were harvested from the mice. BM mononuclear cells (BMMNC) were isolated from the mice according to a previously described method [9, 17]; the BMMNC were incubated (1×10^6/mL in complete medium) with REV, ISOR, HEY-A (0.01–100 μM), or 0.2% dimethyl sulfoxide (DMSO; used as a vehicle control) at 37°C for 60 min. The cells were then exposed to 1, 2, or 4 Gy IR generated in an Exposure Instrument Cammacell-40 ^{137}Cesium irradiator (Atomic Energy, Lin, CA) at a rate of 0.76 Gy/min and sham-irradiation cells were set. Cells were incubated at 37°C, 5% CO_2, and 100% humidity for various durations, as indicated in the individual experiments.

2.4. Cell Viability Assays. The cells were plated into a 96-well plate (1×10^5 cells/well in 100 μL of medium) and were cultured for 18 h. Cell viability was monitored using the luminescent-based CellTiter-Glo system (Promega Corporation, Madison, WI, USA) according to the manufacturer's recommended protocols [16]. The luminescence of each well was read using an Infinite M200 multimode microplate reader (TECAN, Switzerland). Cell viability was normalized and expressed as a percentage of the untreated cells [17].

2.5. Colony-Forming Cells Assay. The colony-forming cells (CFC) assay was performed by culturing BMMNC in MethoCult M3534 methylcellulose medium (StemCell Technologies, Vancouver, BC, Canada) according to the manufacturer's instructions. BMMNC, incubated with REV, ISOR, or HEY-A (0.01–1 μM), and irradiated as described above, were suspended in MethoCult M3534 medium at 2×10^4 or 1×10^5 viable cells/mL; the cells were then seeded in the wells of 24-well plates. The plates were incubated for 7 days. Colonies of ≥50 cells were scored under an inverted microscope [2, 17] and the results were expressed as the number of CFU-GM per 10^5 cells.

2.6. Competitive Repopulation Assays. Competitive repopulation assays were performed using the Ly5 congenic mouse system according to a previously described method [8, 9, 17]. After incubation with REV, ISOR, and HEY-A (1 μM) or exposure to irradiation (2 Gy) as described above, the donor cells (C57BL/6-Ly-5.1 mice, 1×10^5 BMMNC) were mixed with 1×10^5 competitive BMMNC that was pooled from three Ly5.1/Ly5.2 hybrid mice. The cells were then transplanted by lateral canthus-vein injection into C57BL/6-Ly-5.2 mice (seven recipients/groups) that had received a lethal IR dose (9.0 Gy total body irradiation). To analyze the engraftment, peripheral blood was collected 2 months after transplantation, using heparin-coated micropipettes (Drummond Scientific, Broomall, PA, USA), from the medial canthus of all the recipients. Following this, the red blood cells were lysed in 0.15 M NH_4Cl solution and the blood samples were stained using FITC-conjugated anti-CD45.1, PE-conjugated anti-CD45.2, PerCP-conjugated anti-B220, APC-conjugated anti-CD3, PE/Cy7-conjugated Anti-Gr-1,

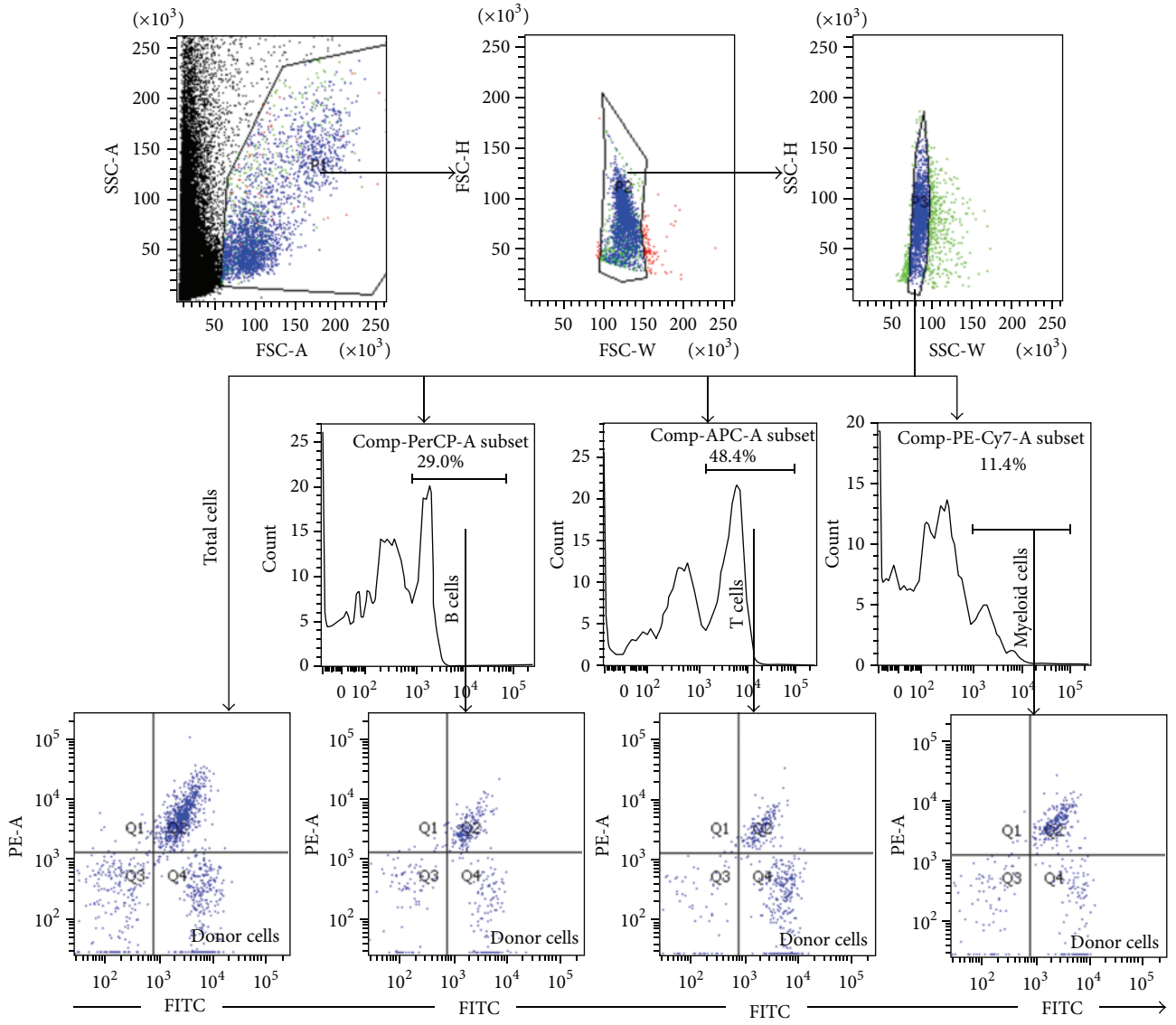

Figure 1: A representative gating strategy of the multilineage cell analysis performed by flow cytometry. After the red blood cells had been lysed in 0.15 M NH_4Cl solution, the blood samples were stained with FITC-conjugated anti-CD45.1, PE-conjugated anti-CD45.2, PerCP-conjugated anti-B220, APC-conjugated anti-CD3, and PE/Cy7-conjugated anti-Gr-1 and CD11b. The samples were then analyzed using an LSR II flow cytometer.

and CD11b antibodies and were analyzed by an LSR II flow cytometer (BD Bioscience, San Jose, CA, USA), as illustrated in Figure 1.

2.7. Quantitative Real-Time PCR Assays. BMMNC were incubated with REV, ISOR, and HEY-A or exposed to irradiation (2 Gy) as described above and the cells were incubated for 24 h. Total RNA was extracted from the BMMNC using TRIzol reagent (ABI Co., USA) following the manufacturer's protocol. First-strand cDNA was synthesized from total RNA using an RNA PCR Kit (AWV) Ver3.0 (TAKARA Co., Japan) according to the manufacturer's protocol. PCR primers for the SOD2, GPX1, and the housekeeping gene GAPDH were obtained from Sangon Biotech (Shanghai, China). The sequences of the primers used in this study were: SOD2, 5′-ATT AAC GCG CAG ATC ATG CA-3′ (forward) and 5′-TGT CCC CCA CCA TTG AAC TT-3′ (reverse); GPX1, 5′-TGC TCA TTG AGA ATG TCG CGT CTC-3′ (forward) and 5′-AGG CAT TCC GCA GGA AGG TAA AGA-3′ (reverse); GAPDH, 5′-TGA AGG TCG GTG TGA ACG GAT TTG GC-3′ (forward); and 5′-CAT GTA GGC CAT GAG GTC CAC CAC-3′ (reverse) [9]. cDNA samples were mixed with primers and SYBR Master Mix (ABI Co.) to a total volume of 25 μL. All the samples were analyzed in triplicate using an ABI Prism 7500 Sequence Detection System (Applied Biosystems-Life Technologies). The thermal cycling conditions used in the protocol were 2 min at 50°C and 10 min at 95°C, followed with 40 cycles at 95°C for 15 s, and finally 60°C for 1 min. The threshold cycle (CT)

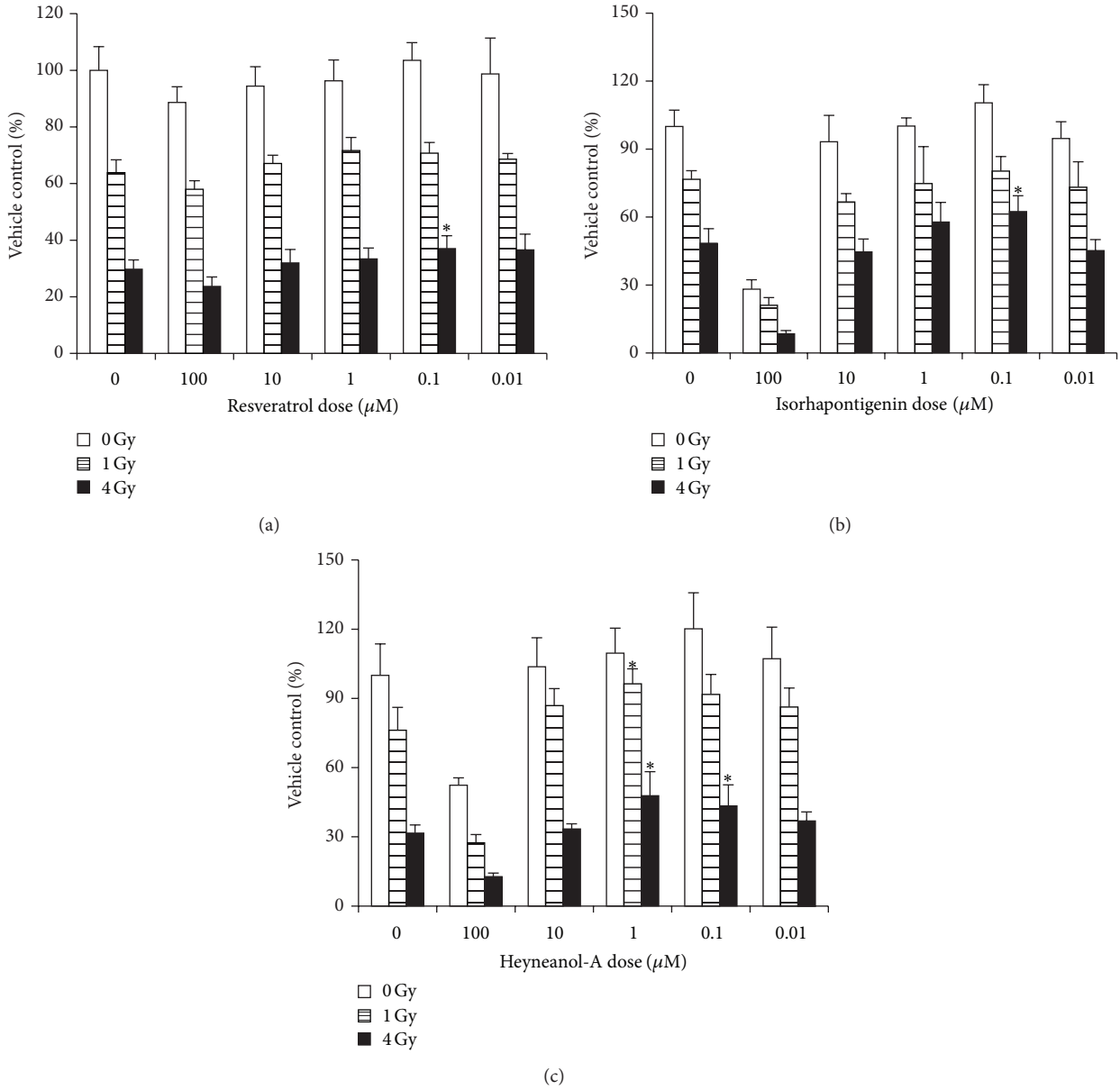

Figure 2: REV (a), ISOR (b), and HEY-A (c) reduce IR-induced suppression of the viability of BMMNC. Cells received treatment with control, REV, ISOR, or HEY-A before being sham-irradiated as a control or irradiated with 1–4 Gy IR; following this, the cells were cultured for 18 h. Cell viability was monitored as described in the paper text. Data are expressed as the relative mean viability ± SE. $^{*}P < 0.05$ versus control, $n = 6$. REV: resveratrol; ISOR: isorhapontigenin; HEY-A: heyneanol-A; IR: ionizing radiation; BMMNC: bone marrow mononuclear cells.

values for each reaction were determined and the average CT value was calculated using TaqMan SDS analysis software (Applied Biosystems-Life Technologies). The changes in the level of expression of the target genes were calculated using the comparative CT method (fold changes = $2^{[-\Delta\Delta CT]}$) as described previously [18].

2.8. Analysis of the Enzymatic Activity of SOD2 and GPX1. The enzymatic activities of SOD2 and GPX1 in BMMNC were analyzed using a SOD2 assay kit and a Cellular Glutathione Peroxidase 1 assay kit (Beyotime Institute of Biotechnology, Jiangsu, China); these assays were performed following the manufacturer's instruction, as described previously [9].

2.9. Statistical Analysis. The data were analyzed using an analysis of variance (ANOVA) test. In the event that the ANOVA test justified post hoc comparisons between the means of the group, these comparisons were made using the Student-Newman-Keuls test for multiple comparisons. Differences were considered significant at $P < 0.05$. The statistical analysis was performed using SPSS 16.0 software (SPSS Inc., Chicago, IL, USA).

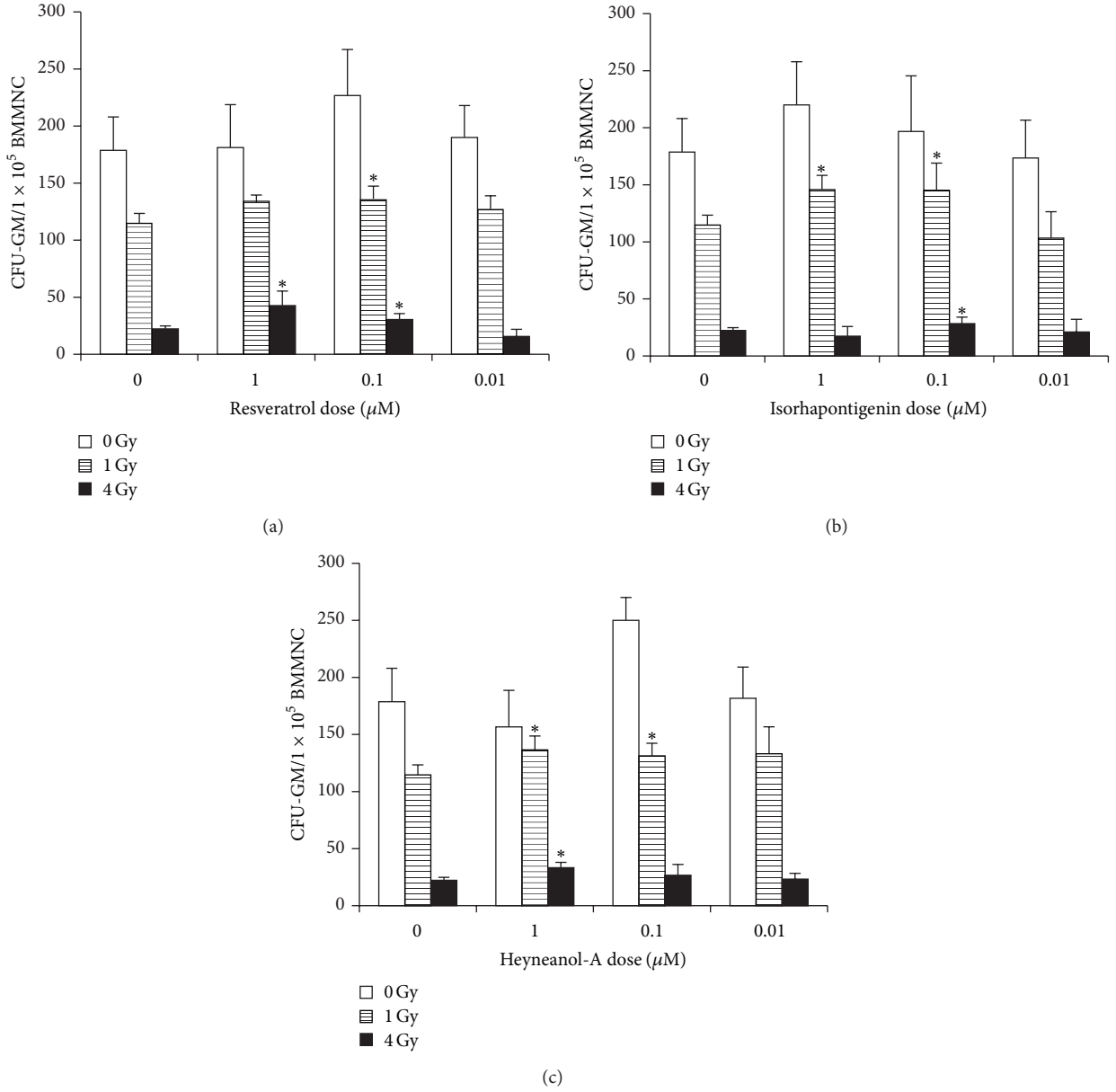

Figure 3: REV (a), ISOR (b), and HEY-A (c) reduce IR-induced suppression of HPC clonogenic function. Mice BMMNC received treatment with control, REV, ISOR, or HEY-A before being sham-irradiated as a control or sublethally irradiated with 1–4 Gy IR. The clonogenic function of HPCs and BMMNC was analyzed using a CFC assay. Colonies of ≥50 cells were scored under an inverted microscope on day 7 and the results are expressed as the number of CFU-GM per 10^5 cells. Data are presented as the mean ± SE. $^*P < 0.05$ versus control, $n = 6$. REV: resveratrol; ISOR: isorhapontigenin; HEY-A: heyneanol-A; IR: ionizing radiation; HPC: hematopoietic progenitor cell; BMMNC: bone marrow mononuclear cells; CFC: colony-forming cells.

3. Results

3.1. REV, ISOR, and HEY-A Protect BMMNC from Irradiation Injury In Vitro. Luminescence assays were performed to evaluate cell viability, as described in our previous work [17]. As shown in Figure 2, the viability of BMMNC decreased significantly after IR exposure. In comparison with the control group, the viability of irradiated (4 Gy) BMMNC increased by 24.6, 28.9, and 37.3–51.3% after being incubated with REV (0.1 μM, $P < 0.05$), ISOR (0.1 μM, $P < 0.05$), and HEY-A (0.01–0.1 μM, $P < 0.05$), respectively. These data suggest that treatment with REV, ISOR, or HEY-A may be able to ameliorate IR-induced injuries in mice BMMNC and that, of the three, HEY-A has the most significant protective effect.

3.2. REV, ISOR, and HEY-A Increase the Ability of HPCs to Form Colonies of CFU-GM. The CFC assay was performed to evaluate the viability of HPCs affected by IR after treatment with REV, ISOR, and HEY-A [2, 8, 17]. The ability of BMMNC that had been treated with sham-irradiation or vehicles to form CFU-GM is shown in Figure 3. The cells

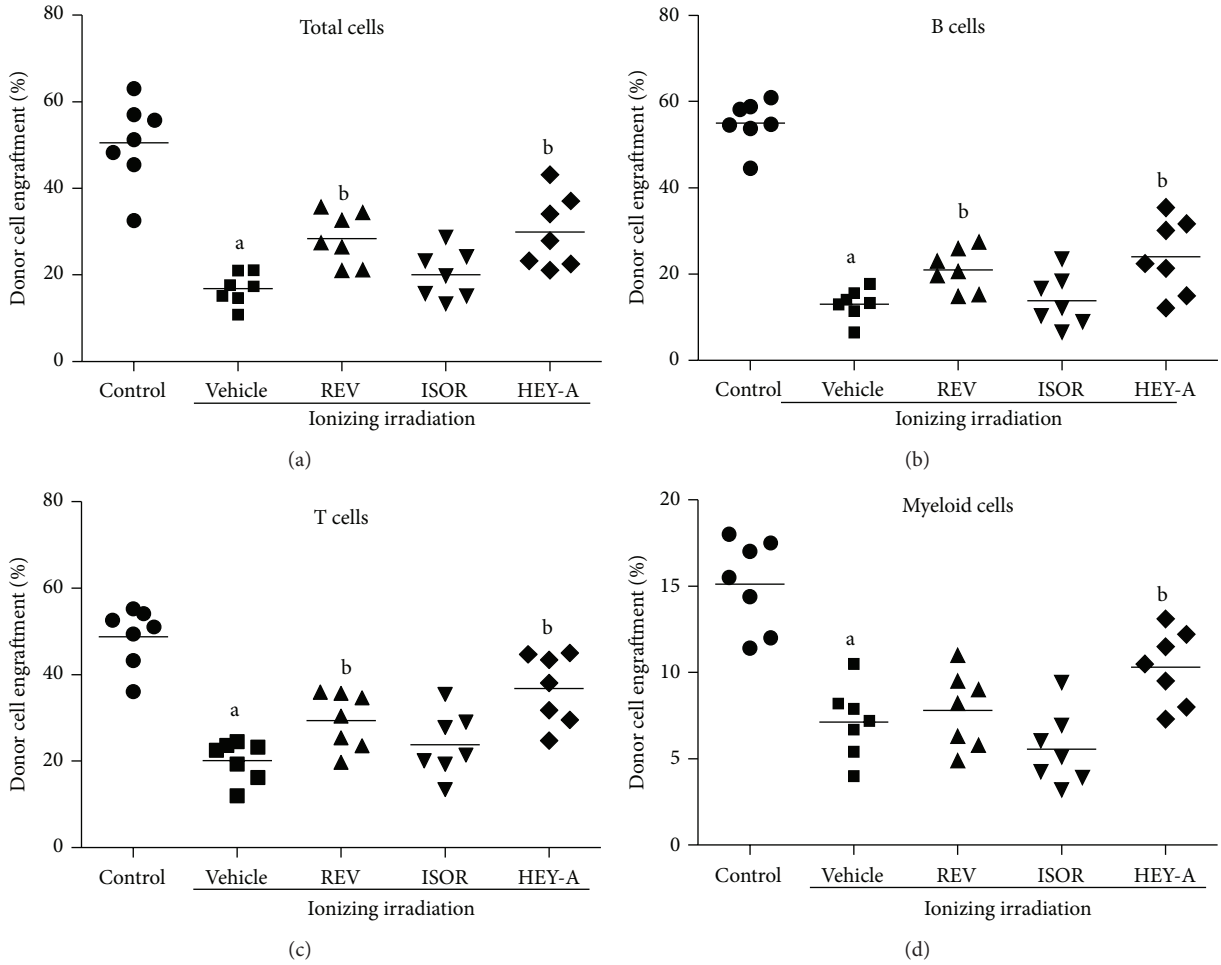

Figure 4: REV, ISOR, and HEY-A reduce IR-induced suppression of posttransplantation long-term engraftment of HSCs. Donor BMMNC received treatment with control, REV, ISOR, or HEY-A (1 μM) before being treated with IR (2 Gy); the BMMNC were then mixed with competitive cells. Cells were transplanted into receptor mice as described in the paper text, and donor cell engraftment was analyzed 2 months after transplantation. The data are expressed as means ± SE of the percentage of donor-derived cells in the peripheral blood. (a) donor-derived leukocytes (CD45.1 + CD45.2 − cells), (b) donor-derived B cells (CD45.1 + CD45.2 − B220 + cells), (c) donor-derived T cells (CD45.1 + CD45.2 − CD3 + cells), and (d) donor-derived myeloid cells (CD45.1 + CD45.2 − CD11b + and/or Gr-1 + granulocyte-monocyte-macrophage). $^{a}P < 0.05$ versus control; $^{b}P < 0.05$ versus vehicle, ($n = 7$ recipient mice/group). REV: resveratrol; ISOR: isorhapontigenin; HEY-A: heyneanol-A; IR: ionizing radiation; HSC: hematopoietic stem cell; BMMNC: bone marrow mononuclear cells.

that were exposed to different doses of IR (1–4 Gy) exhibited a diminished ability (35.8–87.5%) to form CFU-GM ($P < 0.01$), while treatment with the three compounds caused a moderate, but still significant, recovery in colony-forming abilities. In comparison with one of the IR groups (4 Gy), the number of colonies of CFU-GM increased by 91.5, 49.3 ($P < 0.01$), and 26.46% ($P < 0.01$) after treatment with REV (1 μM), HEY-A (1 μM), and ISOR (0.1 μM), respectively. These results suggest REV, HEY-A, and ISOR could ameliorate IR-induced injuries in mice HPCs.

3.3. REV and HEY-A Enhance Long-Term and Multilineage Engraftment of Irradiated HSCs. We performed long-term and multilineage engraftment assays, a gold standard in measuring HSC function, to validate whether treatment with these three compounds could ameliorate IR-induced functional declines in HSCs. As can be seen in Figure 4, at 2 months after transplantation, the mice that received donor cells that had been exposed to irradiation with vehicle treatment exhibited a substantial decrease in donor cell engraftment in all lineages. When treated with REV (1 μM), the donor cell engraftment increased by 11.58% at 2 months, with increases of 7.86% in B cells, 9.16% in T cells, and 0.68% in myeloid cells derived from the donor cells. When treated with HEY-A (1 μM), the donor cell engraftment increased by 13.07% at 2 months, with increases of 10.92% in B cells, 16.59% in T cells, and 3.17% in myeloid cells derived from donor cells. These findings suggest that treatment with REV and HEY-A can indeed preserve the functions of HSCs after IR exposure, resulting in enhanced long-term and multilineage engraftment after BM transplantation, in which HEY-A demonstrates a greater protective effect than REV.

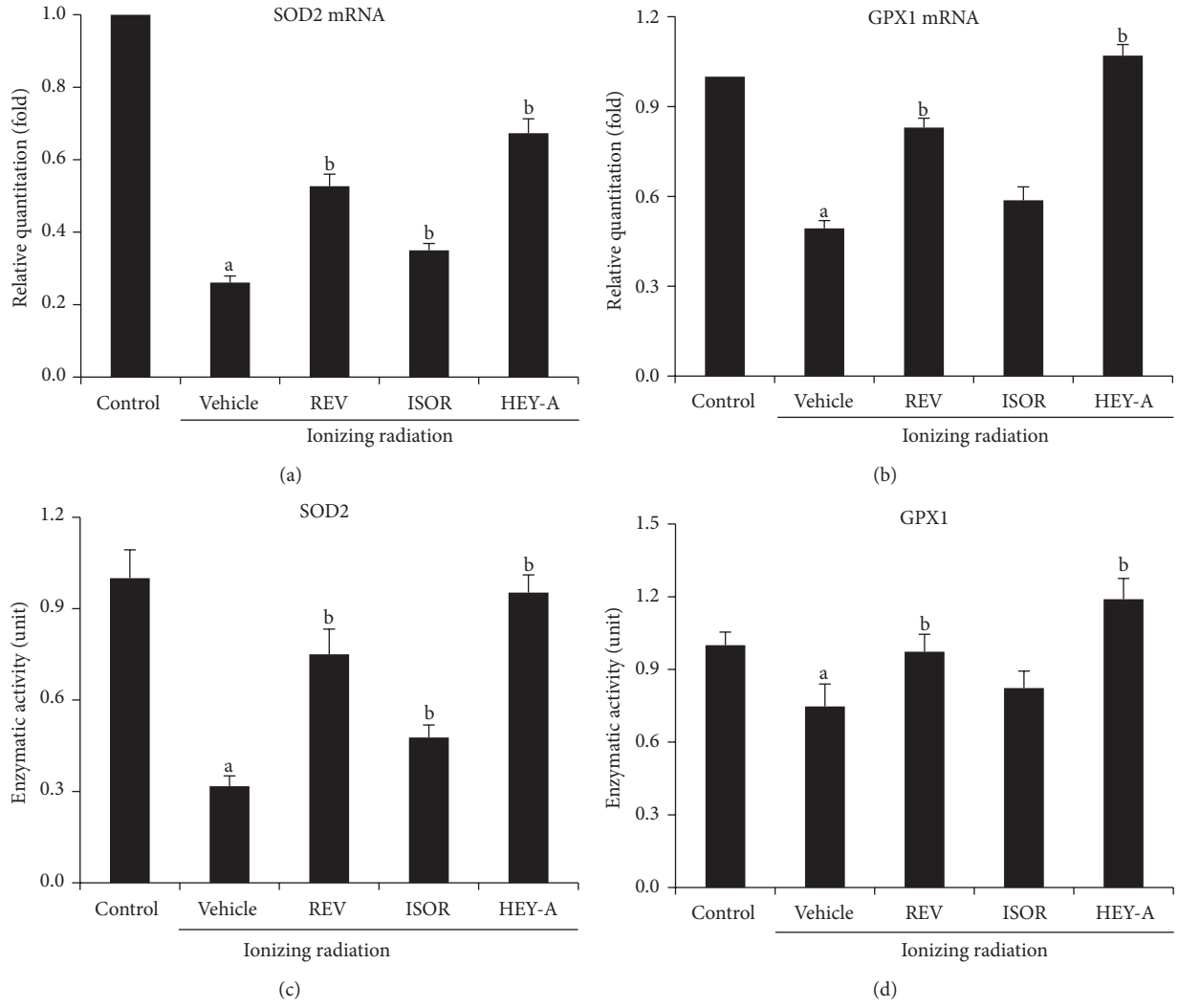

Figure 5: REV, ISOR, and HEY-A increase the enzymatic activity of SOD2 and GPX1 in BMMNC. The cells received treatment with control, REV, ISOR, or HEY-A (1 μM) before being sham-irradiated as a control or irradiated with 2.0 Gy IR. The cells were incubated for 24 h before being analyzed. The expression of SOD2 and GPX1 mRNA was analyzed using qRT-PCR, and the enzymatic activities of SOD2 and GPX1 were analyzed using a SOD2 assay kit and a cellular GPX1 assay kit, respectively. ((a), (b)) Expression levels of SOD2 and GPX1 mRNA; ((c), (d)) enzymatic activity of SOD2 and GPX1 in BMMNC. Results of the mRNA-expression analysis and the enzymatic-activity analysis are expressed as means ± SE of changes in expression/activity in comparison with those of the control. $^{a}P < 0.01$ versus control, $^{b}P < 0.01$ versus vehicle, $n = 3$. REV: resveratrol; ISOR: isorhapontigenin; HEY-A: heyneanol-A; BMMNC: bone marrow mononuclear cells; IR: ionizing radiation.

3.4. REV, ISOR, and HEY-A Ameliorate IR-Induced Reductions in SOD2 and GPX1 Activity. In a recent study, we demonstrated that IR-induced ROS stress contributes to IR-induced BM failure in hematopoietic cells partly via downregulating the activity of the proteins SOD2 and GPX1 [9]. In this study, the expression of SOD2 and GPX1 in BMMNC that had been exposed to IR and treated with the therapeutic compounds was investigated. As indicated in Figures 5(a) and 5(b), IR exposure significantly downregulated the expression of SOD2 and GPX1. The expression of SOD2 and GPX1 decreased by 73.9 ($P < 0.01$) and 50.7% ($P < 0.01$), respectively, at 24 h. Following treatment with REV, ISO, and HEY-A, the expression of SOD2 was upregulated 1.02-, 0.35-, and 1.58-fold, respectively, and the expression of GPX1 was upregulated 0.68-, 0.19-, and 1.17-fold, respectively. The modulation of SOD2 and GPX1 expression by IR and the three compounds in BM cells was also confirmed by performing enzymatic assays, which are shown in Figures 5(c) and 5(d). These data suggest that radiation exposure could downregulate the expression of SOD2 and GPX1 in BMMNC and that REV's analogues, ISOR, and HEY-A could neutralize this IR-induced downregulation in SOD2 and GPX1 expression and activity.

4. Discussion

In this study, we examined whether the REV oligomers ISOR and HEY-A could inhibit IR-induced BM injury in mice. Our results demonstrate that treatment with HEY-A could protect hematopoietic cells from IR-induced injury much

better than REV. Moreover, it was demonstrated that ISOR has a protective effect on BMMNC and HPCs, but not on HSCs, following IR-induced injury. The effects of REV and its oligomers on IR-induced BM injury are likely the result of their antioxidant properties.

REV and its oligomers are not conventional antioxidants that inhibit oxidative stress by scavenging free radicals directly. As demonstrated in our study, we found that REV and its oligomers may effectively upregulate the expression of SOD2 and GPX1 in hematopoietic cells. Consequently, the oligomers of REV may be more efficacious than other antioxidants that are commonly used as a medical countermeasure to IR-induced injury. In particular, considering that these compounds are natural products, inexpensive, and low in toxicity and that they have been used widely as food supplements, they may be very suitable for medical applications. However, at present, the results of this study do not allow us to determine whether these compounds function as a radiation protectant, a radiation mitigator, or both. Further studies, where cells are treated either before or after IR exposure, will be needed to clarify this.

Furthermore, the mechanisms by which REV and its oligomers differentially regulate the expression of SOD2 and GPX1 in hematopoietic cells have yet to be investigated. REV is a putative activator of SIRT1, a NAD(+)-dependent histone deacetylase that can regulate gene expression by modulating the structure of chromatin [19]. In addition, multiple nonhistone targets have also been described for SIRT1, including some transcription factors or cofactors such as Forkhead box class O (FOXO) transcription factors, nuclear factor kB, and peroxisome proliferator-activated receptor-coactivator 1a [20, 21]. However, which of these mechanisms is involved in the regulation of GPX1 and SOD2 expression in hematopoietic cells has not yet been identified.

In addition, exposure to IR not only induces BM injury but also causes tissue damage including fibrosis, inflammation, and apoptosis [22–24]; IR also plays a major role in many side effects of radiotherapy in cancer patients. In addition to having an adverse effect on the quality of life of cancer patients, IR-induced injuries can also worsens the outcome of cancer treatment. It has been shown that oxidative stress is also an underlying cause of the types of tissue damage (fibrosis, inflammation, and apoptosis) that can arise from IR exposure. Therefore, it will be also interesting to examine whether REV and its oligomers have the potential to be useful as therapeutic agents for the treatment of other types of IR-induced tissue damage. Interestingly, it has been reported that a variety of cancer cells, including gastric, colorectal, lung, breast, prostate, esophageal, and thyroid carcinomas, can be inhibited by REV and its oligomers [25, 26]. Therefore, REV and its oligomers have the potential to increase the therapeutic efficacy of radiotherapy, not only by reducing tissue injury but also by inhibiting tumor growth.

Conflict of Interests

The authors declare that there is no conflict of interests regarding the publication of this paper.

Authors' Contribution

Experimental conception and design was done by Heng Zhang. Execution of experimental protocols was done by Hui Wang, Yi-ling Yang, and Hao Yan. Analysis of the experimental data was done Yi-ling Yang and Chun-ze Zhang. Contribution of reagents/materials/analytical tools was done by Hui Wang and Xiao-jing Wu. Preparation of the paper was done by Heng Zhang, Yi-ling Yang, and Hui Wang. Hui Wang and Yi-ling Yang contributed equally to this paper.

Acknowledgment

The authors are grateful for the excellent work of Zhibin Zhai.

References

[1] Y. Wang, B. A. Schulte, A. C. LaRue, M. Ogawa, and D. Zhou, "Total body irradiation selectively induces murine hematopoietic stem cell senescence," *Blood*, vol. 107, no. 1, pp. 358–366, 2006.

[2] A. Meng, Y. Wang, G. Van Zant, and D. Zhou, "Ionizing radiation and busulfan induce premature senescence in murine bone marrow hematopoietic cells," *Cancer Research*, vol. 63, no. 17, pp. 5414–5419, 2003.

[3] N. Dainiak, "Hematologic consequences of exposure to ionizing radiation," *Experimental Hematology*, vol. 30, no. 6, pp. 513–528, 2002.

[4] W. W. Kam and R. B. Banati, "Effects of ionizing radiation on mitochondria," *Free Radical Biology & Medicine*, vol. 65, pp. 607–619, 2013.

[5] S. S. Puthran, K. Sudha, G. M. Rao, and B. V. Shetty, "Oxidative stress and low dose ionizing radiation," *Indian Journal of Physiology and Pharmacology*, vol. 53, no. 2, pp. 181–184, 2009.

[6] L. Shao, Y. Lou, and D. Zhou, "Hematopoietic stem cell injury induced by ionizing radiation," *Antioxidants & Redox Signaling*, vol. 20, no. 9, pp. 1447–1462, 2013.

[7] H. Li, Y. Wang, S. K. Pazhanisamy et al., "Mn(III) meso-tetrakis-(N-ethylpyridinium-2-yl) porphyrin mitigates total body irradiation-induced long-term bone marrow suppression," *Free Radical Biology and Medicine*, vol. 51, no. 1, pp. 30–37, 2011.

[8] Y. Wang, L. Liu, S. K. Pazhanisamy, H. Li, A. Meng, and D. Zhou, "Total body irradiation causes residual bone marrow injury by induction of persistent oxidative stress in murine hematopoietic stem cells," *Free Radical Biology and Medicine*, vol. 48, no. 2, pp. 348–356, 2010.

[9] H. Zhang, Z. Zhai, Y. Wang et al., "Resveratrol ameliorates ionizing irradiation-induced long-term hematopoietic stem cell injury in mice," *Free Radical Biology and Medicine*, vol. 54, pp. 40–50, 2013.

[10] K. Ito, A. Hirao, F. Arai et al., "Regulation of oxidative stress by ATM is required for self-renewal of haematopoietic stem cells," *Nature*, vol. 431, no. 7011, pp. 997–1002, 2004.

[11] K. Miyamoto, K. Y. Araki, K. Naka et al., "Foxo3a is essential for maintenance of the hematopoietic stem cell pool," *Cell Stem Cell*, vol. 1, no. 1, pp. 101–112, 2007.

[12] S. Pervaiz and A. L. Holme, "Resveratrol: its biologic targets and functional activity," *Antioxidants & Redox Signaling*, vol. 11, no. 11, pp. 2851–2897, 2009.

[13] J. A. Baur and D. A. Sinclair, "Therapeutic potential of resveratrol: the *in vivo* evidence," *Nature Reviews Drug Discovery*, vol. 5, no. 6, pp. 493–506, 2006.

[14] H. Li, A. Wang, Y. Huang et al., "Isorhapontigenin, a new resveratrol analog, attenuates cardiac hypertrophy via blocking signaling transduction pathways," *Free Radical Biology and Medicine*, vol. 38, no. 2, pp. 243–257, 2005.

[15] M. H. Jang, X. L. Piao, H. Y. Kim et al., "Resveratrol oligomers from Vitis amurensis attenuate β-amyloid-induced oxidative stress in PC12 cells," *Biological and Pharmaceutical Bulletin*, vol. 30, no. 6, pp. 1130–1134, 2007.

[16] J. W. Noah, W. Severson, D. L. Noah, L. Rasmussen, E. L. White, and C. B. Jonsson, "A cell-based luminescence assay is effective for high-throughput screening of potential influenza antivirals," *Antiviral Research*, vol. 73, no. 1, pp. 50–59, 2007.

[17] H. Zhang, Y. A. Wang, A. Meng et al., "Inhibiting TGFβ1 has a protective effect on mouse bone marrow suppression following ionizing radiation exposure in vitro," *Journal of Radiation Research*, vol. 54, pp. 630–636, 2013.

[18] H. Zhang, J. Li, Y. Wang et al., "Retinoblastoma 94 enhances radiation treatment of esophageal squamous cell carcinoma in vitro and in vivo," *Journal of Radiation Research*, vol. 53, no. 1, pp. 117–124, 2012.

[19] J. D. Lambeth, "Nox enzymes, ROS, and chronic disease: an example of antagonistic pleiotropy," *Free Radical Biology and Medicine*, vol. 43, no. 3, pp. 332–347, 2007.

[20] J. Landry, A. Sutton, S. T. Tafrov et al., "The silencing protein SIR2 and its homologs are NAD-dependent protein deacetylases," *Proceedings of the National Academy of Sciences of the United States of America*, vol. 97, no. 11, pp. 5807–5811, 2000.

[21] A. D. Napper, J. Hixon, T. McDonagh et al., "Discovery of indoles as potent and selective inhibitors of the deacetylase SIRT1," *Journal of Medicinal Chemistry*, vol. 48, no. 25, pp. 8045–8054, 2005.

[22] M. Kitada, S. Kume, N. Imaizumi, and D. Koya, "Resveratrol improves oxidative stress and protects against diabetic nephropathy through normalization of Mn-SOD dysfunction in AMPK/SIRT1- independent pathway," *Diabetes*, vol. 60, no. 2, pp. 634–643, 2011.

[23] R. E. Carsten, A. M. Bachand, S. M. Baileya, and R. L. Ullrich, "Resveratrol reduces radiation-induced chromosome aberration frequencies in mouse bone marrow cells," *Radiation Research*, vol. 169, no. 6, pp. 633–638, 2008.

[24] Y. Yang, J. H. Paik, D. Cho, J. Cho, and C. Kim, "Resveratrol induces the suppression of tumor-derived $CD4^+CD25^+$ regulatory T cells," *International Immunopharmacology*, vol. 8, no. 4, pp. 542–547, 2008.

[25] M. Athar, J. H. Back, X. Tang et al., "Resveratrol: a review of preclinical studies for human cancer prevention," *Toxicology and Applied Pharmacology*, vol. 224, no. 3, pp. 274–283, 2007.

[26] E. O. Lee, H. J. Lee, H. S. Hwang et al., "Potent inhibition of Lewis lung cancer growth by heyneanol A from the roots of Vitis amurensis through apoptotic and anti-angiogenic activities," *Carcinogenesis*, vol. 27, no. 10, pp. 2059–2069, 2006.

Hindawi Publishing Corporation
BioMed Research International
Volume 2014, Article ID 260859, 7 pages
http://dx.doi.org/10.1155/2014/260859

Clinical Study

The Diagnostic Value of Cervical Lymph Node Metastasis in Head and Neck Squamous Carcinoma by Using Diffusion-Weighted Magnetic Resonance Imaging and Computed Tomography Perfusion

Jin Zhong, Zonghong Lu, Liang Xu, Longchun Dong, Hui Qiao, Rui Hua, Yi Gong, Zhenxing Liu, Caixian Hao, Xuehuan Liu, Changqing Zong, Li He, and Jun Liu

Department of Imaging, Tianjin Union Medicine Centre, Tianjin 300121, China

Correspondence should be addressed to Jun Liu; cjr.liujun@vip.163.com

Received 9 May 2014; Revised 30 May 2014; Accepted 1 June 2014; Published 24 June 2014

Academic Editor: Shiwu Zhang

Purpose. The aim of this study was to compare diffusion-weighted magnetic resonance imaging (DWI) with computed tomography perfusion (CTP) for preoperative detection of metastases to lymph nodes (LNs) in head and neck squamous cell carcinoma (SCC). *Methods.* Between May 2010 and April 2012, 30 patients with head and neck SCC underwent preoperative DWI and CTP. Two radiologists measured apparent diffusion coefficient (ADC) values and CTP parameters independently. Surgery and histopathologic examinations were performed on all patients. *Results.* On DWI, 65 LNs were detected in 30 patients. The mean ADC value of metastatic nodes was lower than benign nodes and the difference was statistically significant ($P < 0.05$). On CTP images, the mean value in metastatic nodes of blood flow (BF) and blood volume (BV) was higher than that in benign nodes, and mean transit time (MTT) in metastatic nodes was lower than that in benign nodes. There were significant differences in BF and MTT values between metastatic and benign LNs ($P < 0.05$). There were significant differences between the AUCs of DWI and CTP ($Z = 4.612$, $P < 0.001$). *Conclusion.* DWI with ADC value measurements may be more accurate than CTP for the preoperative diagnosis of cervical LN metastases.

1. Introduction

Squamous cell carcinoma (SCC) is the most common malignancy of the head and neck region. It accounts for 5% of all malignant tumours worldwide [1]. A meta-analysis by Dünne et al. [2] showed a 5-year survival rate between 17% and 55.8% for SCC with cervical node metastases and 44.6–76% for SCC patients without cervical node metastases. The presence of multiple metastatic lymph nodes (LNs) is presumed to be a worse prognostic sign [3]. The detection of cervical node metastases provides very important prognostic information and often helps decide the treatment of head and neck SCC. Node sampling is the definitive method of differentiating benign LNs from metastatic LNs, but biopsy methods are invasive and operator-dependent, with a high incidence of false-negative results [4, 5]. With advancements in imaging methods, several noninvasive imaging techniques have arisen, with the potential for identifying benign and metastatic LNs in head and neck SCC, thus avoiding the complications due to biopsy sampling [6].

Although ultrasound, routine contrast-enhanced computed tomography (CT) and magnetic resonance imaging (MRI) allow the detection of enlarged cervical LNs, none of these methods can distinguish between benign and malignant causes of enlargement with any accuracy [7], as they use standard parameters (shape, size, internal architecture, extranodal invasion, and vascular features) that are nonspecific for malignancy [8, 9].

Single photon emission computed tomography (SPECT) and positron-emission tomography (PET) are imaging techniques that supply functional information, but they involve

radiation exposure and are expensive with low availability and are hampered by relatively low spatial resolution [10–13].

Recently, other functional imaging techniques such as MRI diffusion-weighted imaging (DWI) and CT perfusion imaging (CTP) have shown promise in detecting metastatic cervical LNs, and there is increasing experience in head and neck SCC. DWI is an MR technique that depicts molecular diffusion, which is the Brownian motion of water protons in biologic tissues. Examination of molecular diffusion using DWI performs with an EPI (echo planar imaging) sequence and a linear regression after a logarithmic transformation of the signal intensity was used to calculate the ADC values [14]. To date, the diagnosis of LN metastases has been based mainly on size criteria; however, nonenlarged nodes may harbour malignancy, whereas benign reactive nodes may be enlarged. Promising results with DWI to help detect cervical LN metastases (especially in normal-sized nodes) and to differentiate between benign and malignant enlarged nodes have been reported. The general consensus is that ADCs of malignant nodes are significantly lower than those of benign nodes [15].

Unlike conventional contrast-enhanced CT, which is normally assessed visually, perfusion imaging requires quantification of the enhancement in tissue and blood at certain time points following intravenous injection. These enhancement data are used to calculate blood flow (BF), blood volume (BV), and mean transit time (MTT) for each voxel, depicted in a color-coded display. Data processing methods are based on the robust physiological principles of compartmental analysis or linear systems theory. In the compartmental modeling technique, analysis can be done by one compartment method which assumes the intravascular and extravascular compartment as a single compartment and allows measurement of tissue perfusion during the first pass of contrast [15, 16].

Although DWI and CTP are increasingly used to detect LN metastases in head and neck SCC, comparison of the diagnostic value of the two imaging modalities has been rarely performed. The aim of this study was to compare the value of DWI and CTP for detecting metastatic LNs which were confirmed by pathologic diagnosis in patients with head and neck SCC.

2. Materials and Methods

2.1. Ethics Statement. The study was approved by the local ethics committee and all patients signed review board-approved consent before participation.

2.2. Patients. Sixty-five cervical LNs from 30 treatment-naïve patients with head and neck SCC were excised during surgery from May 01, 2010, to April 30, 2012. All LNs underwent pathological analysis. Among the 30 patients, 21 were men and 9 were women; their age ranged from 38 to 70 years, with a mean age of 53.6 years. The primary cancers were of the larynx ($n = 9$), tongue ($n = 3$), nasopharynx ($n = 6$), floor of mouth ($n = 3$), nasal cavity ($n = 4$), oropharynx ($n = 4$), and gingiva ($n = 1$). All patients underwent DWI and CTP before surgery.

2.3. Imaging Protocols

2.3.1. MRI/DWI. All MRI examinations were performed using a 1.5 T MRI unit (Philips Intera Achieva, Philips Medical Systems, Best, The Netherlands) with a head and neck coil. Thirty patients underwent conventional MRI and DWI to include nodes from the base of the skull to the suprasternal notch. Before scanning, all patients were trained to avoid swallowing during the MRI examination.

In all patients the following protocol was performed:

(i) fast spin-echo (FSE) T2-weighted images (TR, 4600 ms; TE, 80 ms; slice thickness, 3 mm) in the axial plane;

(ii) fast spin-echo (FSE) T2-weighted images (TR, 3850 ms; TE, 75 ms; slice thickness, 3 mm), in the coronal plane;

(iii) fast spin-echo (FSE) T1-weighted images, with fat suppression (TR, 480 ms; TE, 15 ms; slice thickness, 3 mm) in the axial plane;

(iv) diffusion-weighted imaging with background body signal suppression (DWIBS) images (TR, 17131 ms; TE, 60 ms; TI, 165 ms; Matrix 132 × 98; SENSE factor 2; NSA, 6; b, 600 s/mm^2) in the axial and coronal planes. Image of black and white reverse image was constructed.

2.4. MRI Data Analysis. The ADC values were automatically measured by standard software (Philips Extended MR Workspace, Philips Medical Systems, Best, The Netherlands). The ADC values were obtained by drawing regions of interest (ROIs) around the solid portions of nodes, avoiding necrotic-appearing areas. Two experienced radiologists analysed the results independently. Disagreements (controversy about positive nodes) regarding image findings were resolved with mutual accord.

2.5. CT Perfusion. The thirty patients underwent preoperative routine CT and perfusion CT scans using a multidetector 16-slice CT scanner (Philips MX 8000, Philips Medical Systems, Andover MA, USA). Selection of the nodal targets was based on a plain CT scan; nonionic iodinated contrast agent (Ultravist 370, Bayer, Germany) (45 mL, 350 mg I/mL) was injected at a flow rate of 5 mL/s via the antecubital vein with an injector (Liebel-Flarsheim, Cincinnati, OH, USA) for dynamic perfusion CT scanning. The perfusion CT parameters were as follows: 120 kVp, 150 mAs, 16 × 1.5 detector collimation, 3 mm slice thickness, and a scanning speed of 1 s/rotation. Thus, we could evaluate flow perfusion in eight slices, including 24 mm from top to bottom.

2.6. CT Perfusion Data Analysis. Choosing the common carotid or internal carotid artery as the input artery and internal jugular vein as the output vein, we obtained time density curves and calculated BF, BV, and MTT of the ROIs with perfusion software (deconvolution arithmetic) from the workstation (Extended Brilliance, Philips Medical Systems, Best, The Netherlands). ROIs again were placed in solid areas

of the LNs, avoiding calcified or necrotic-appearing areas. Two experienced radiologists carried out this procedure and the mean values were calculated.

2.7. Statistical Analysis. ADC values and BF, BV, and MTT of the LNs were compared using Student's t-test. The two imaging techniques were compared using receiver operating characteristic curves (ROC curves). $P < 0.05$ was considered statistically significant. All statistical analyses were performed with the SPSS 17.0 software package.

3. Results

3.1. DWI and ADC Values. Of the 65 LNs, 48 nodes were proven to be histologically malignant, and 17 nodes were benign. On DWI, 43/48 metastatic LNs showed high signal intensity ($b = 600\,s/mm^2$), whereas on the black and white flip images they presented low signal (Figure 1(a)). Thirteen of the 17 benign nodes were low in signal intensity ($b = 600\,s/mm^2$) on DWI images (Figure 1(b)). The mean ADC value of metastatic nodes was approximately $0.849 \times 10^{-3}\,mm^2/s$ (range: 0.738×10^{-3}–$0.960 \times 10^{-3}\,mm^2/s$), lower than the mean value of the benign nodes ($1.443 \times 10^{-3}\,mm^2/s$, range: $1.037 \times 10^{-3}\,mm^2/s$–$1.849 \times 10^{-3}\,mm^2/s$); this difference was statistically significant ($P < 0.05$) with $t = 2.629$ (Table 1). In this study, the best threshold value for diagnosing metastatic nodes was $0.960 \times 10^{-3}\,mm^2/s$, yielding a sensitivity of 89.58%, specificity of 76.47%, accuracy of 86.15%, PPV of 91.48%, and NPV of 72.22%.

3.2. CT Perfusion. On CTP images, 33/48 metastatic LNs showed increased perfusion. On conventional enhanced CT, images demonstrated enhancement (Figure 2(a) (A-B)). Nine of 17 benign LNs displayed low blood perfusion and mild-to-moderate enhancement (Figure 2(a) (C-D)) on CTAP and conventional CT images, respectively.

The mean BF, BV, and MTT values for metastatic nodes were $114.62 \pm 14.26\,mL/100\,g/min$, $32.15 \pm 13.21\,mL/100\,g$, and $5.56 \pm 0.39\,s$, respectively. The mean values for BF, BV, and MTT in benign nodes were $67.82 \pm 13.84\,mL/100\,g/min$, $19.36 \pm 7.34\,mL/100\,g$, and $9.46 \pm 3.23\,s$, respectively. There were significant differences in BF and MTT values between metastatic and benign LNs ($P < 0.05$) (Table 1). The optimum threshold BF value for differentiating malignant from benign nodes was $100.36\,mL/100\,g/min$, yielding a sensitivity of 68.18%, specificity of 52.94%, accuracy of 64.46%, PPV of 80.48%, and NPV of 37.50%.

Figure 2(b) shows the ROC curves of the ADC and BF values used for differentiating benign from metastatic LNs. The areas under the curve (AUC) were 0.830 and 0.605. There were significant differences between the AUCs of DWI and CTP ($Z = 4.612$, $P < 0.001$) (Table 2) for diagnosing metastatic LNs in head and neck SCC.

4. Discussion

4.1. DWI and ADC Values. DWI is an MR imaging-based technique whereby diffusion properties of water can be quantified using the ADC. Hypercellular tissue, such as solid tumour, is characterized by a low ADC, while more hypocellular tissue, such as normal tissue, is typically characterized by a higher ADC. As several studies reported, metastatic nodes showed a reduction of diffusivity, which can be attributed to hypercellularity, to an increased nuclear-to-cytoplasmic ratio, and to perfusion [17, 18]. King et al. [19] reported that DWI could improve the accuracy in the distinction between benign and malignant nodes.

Pathological states, such as malignant tumor cell, strongly affect water diffusion more than benign tumor cell and so influence DWI, and hence the technique has attracted considerable research attention for both benign and malignant disease processes.

One of the DWI investigations performed in the head and neck [20] showed the potential of this technique for differentiating benign from malignant lesions. Srinivasan et al. [21] and Abdel Razek et al. [22] reported that there was a significant difference in ADCs between benign and malignant lesions. In one of these investigations [21], the authors found a lack of overlap between the higher ADCs of benign and the lower ADCs of malignant head and neck lesions. Using an ADC obtained with two b values (0 and $800\,s/mm^2$) and a 3 T MR unit, they established an optimal ADC threshold of $1.3 \times 10^{-3}\,mm^2/s$ for diagnosis. The authors of the other DWI investigation [22] confirmed the difference in ADCs between benign and malignant lesions. In that study, b values of 0, 500, and $1000\,s/mm^2$ at 1.5 T yielded a significant difference between benign and malignant lesions ($P < 0.001$). Also, an optimal ADC threshold of $1.25 \times 10^{-3}\,mm^2/s$ to help differentiate benign from malignant lesions was established, consistent with that of the previous study [21], and yielded an accuracy of 92.8%, sensitivity of 94.4%, and specificity of 91.2%. Although these results showed the advantage of DWI for diagnosis of head and neck lesions, there will be exceptions and overlap in ADC results. Therefore, a single ADC threshold cannot be used in all conditions, and combining it with specific sites and morphological findings will be necessary.

In our series, the evaluation with DWI showed that metastatic nodes appeared hyperintense ($b = 600\,mm^2/s$); conversely, benign nodes were hypointense ($b = 600\,mm^2/s$). We chose $0.960 \times 10^{-3}\,mm^2/s$ as the optimal ADC threshold value for distinguishing benign from metastatic nodes, with a sensitivity of 89.58%, a specificity of 76.47%, an accuracy of 86.15%, a PPV of 91.48%, and an NPV of 72.22%. Our data are not in agreement with those of Kato et al. [23] who found, for SCC LNs, the mean ADC value ($1.45 \pm 0.48 \times 10^{-3}\,mm^2/s$) to be higher than that in benign lymphadenopathies ($0.89 \pm 0.21 \times 10^{-3}\,mm^2/s$).

Differences among these studies can be attributed to several causes. One is the choice of the b values: a lower b value increases signal-to-noise ratio but lowers the sensitivity to diffusion. Other factors are the size of the ROI (solid portion, necrotic portion, or whole area) and the use of sequences that reduce the artefacts in order to make the measurement of the ROI more precise [24].

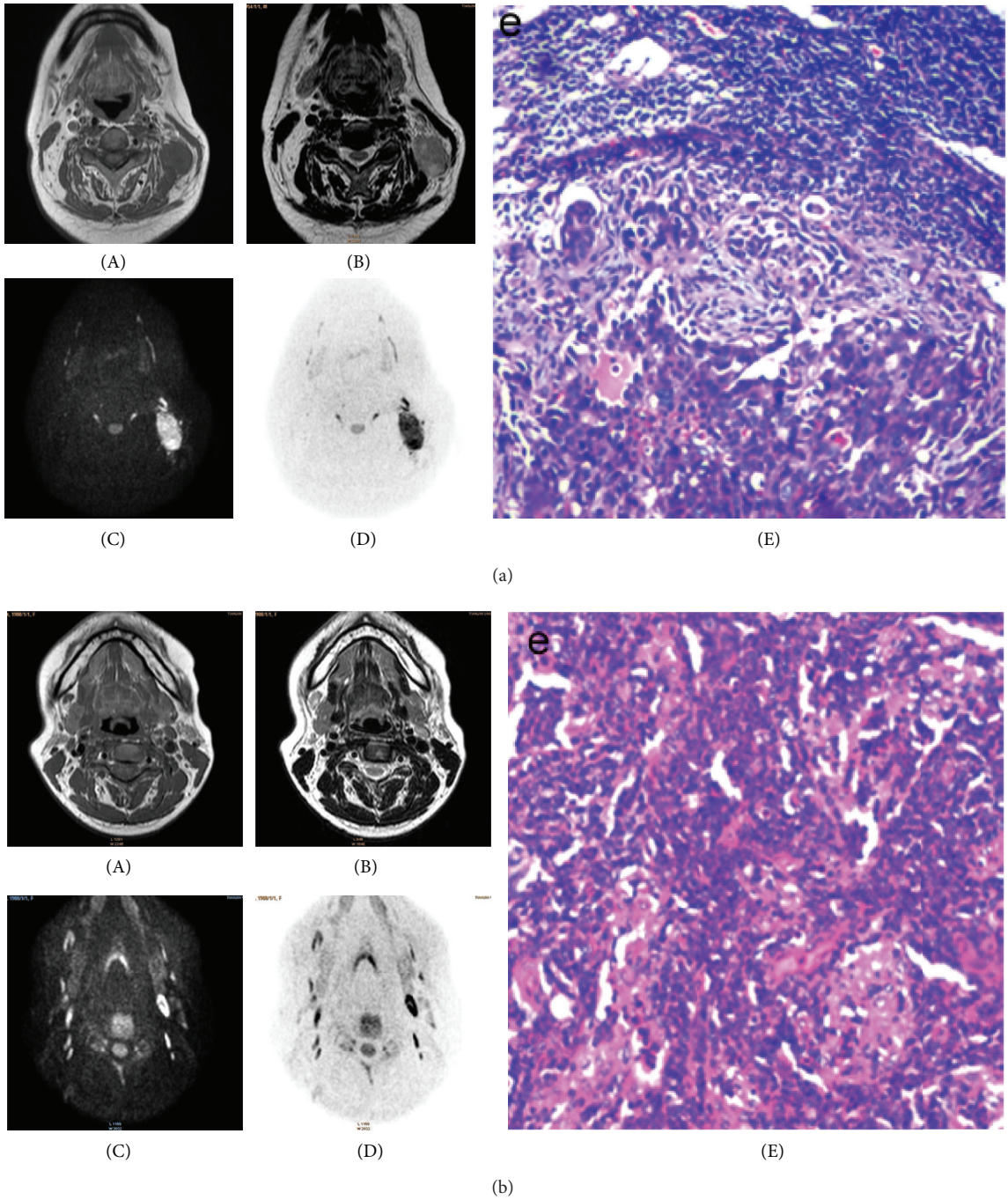

Figure 1: (a): Patient with rhinal cancer. (A) Axial T1-weighted and (B) fast spin-echo-T2-weighted images showing a rounded, enlarged neck node on the left side, showing T1 and T2 signal isointensity. (C) Diffusion-weighted image (DWI) at $b = 600\,\text{s/mm}^2$ showed that the node has high signal intensity. (D) On DWI inversion image, the same node exhibits low signal intensity. Mean apparent diffusion coefficient (ADC) value of the lymph node is $0.85 \times 10^{-3}\,\text{mm}^2/\text{s}$. (E) Lymph node with metastatic squamous cell carcinoma confirmed by pathologic diagnosis (H&E staining, ×200). (b) Hyperplastic benign lymph node in a case of nasopharyngeal carcinoma. (A) Axial T1-weighted and (B) fast spin-echo-T2-weighted images showing an oval node on the left side, which demonstrates T1 and T2 signal isointensity. (C) Diffusion-weighted image (DWI) at $b = 600\,\text{s/mm}^2$ shows that the node has slightly elevated signal intensity. (D) On DWI inversion image, the same node exhibits low signal intensity. The mean apparent diffusion coefficient (ADC) value of the node is $0.85 \times 10^{-3}\,\text{mm}^2/\text{s}$. (E) Hyperplastic benign lymph node confirmed by pathologic diagnosis (H&E staining, ×200).

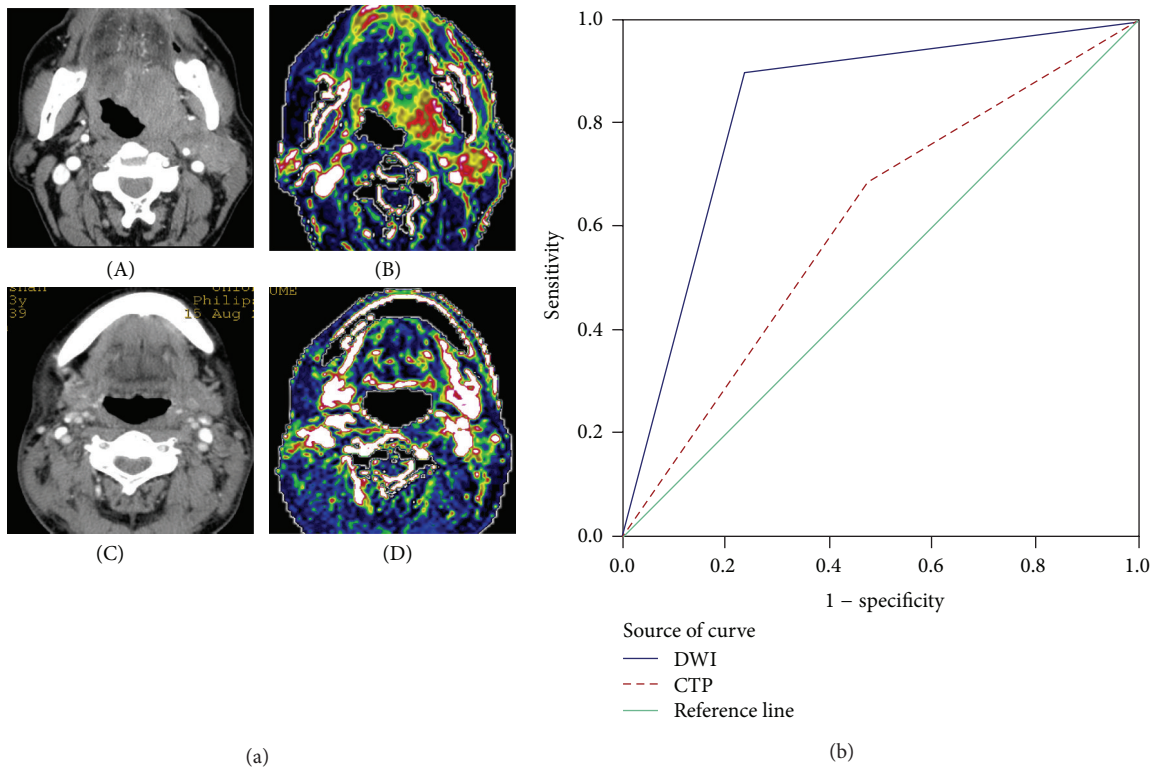

Figure 2: (a) (A-B) Patient with floor of mouth cancer. (A) On contrast-enhanced CT, an intensely enhancing mass is visible in the left base of tongue and left cervical area, with involvement of the sternocleidomastoid. (B) The lesions have high blood flow (BF) values. The mean BF value of the lymph node (LN) is 113.45 mL/100 g/min, (C-D) lymphadenitis with laryngeal carcinoma, (C) enhanced CT showing a nodule in the left cervical area with heterogeneous enhancement. (D) Marginal BF of 86.95 mL/100 g/min. (b) Receiver operating characteristic (ROC) curve for diffusion-weighted imaging (DWI) and CT perfusion (CTP). Areas under the curves (AUCs) are 0.830 and 0.605, respectively. There is a significant difference between the AUC of DWI and the AUC of CTP ($Z = 4.612$, $P < 0.001$).

Table 1: Quantitative measurements of benign and metastatic LNs.

	Benign $n = 17$	Metastatic $n = 48$	t	P
ADC ($\times 10^{-3}$ mm^2/s)	1.443 ± 0.406	0.849 ± 0.111	2.629	0.011
BF (mL/100 g/min)	67.82 ± 13.84	114.62 ± 14.26	3.336	0.002
BV (mL/100 g)	19.36 ± 7.34	32.15 ± 13.21	1.006	0.209
MTT (s)	9.46 ± 3.23	5.56 ± 0.39	2.346	0.002

ADC = apparent diffusion coefficient, BF = blood flow, BV = blood volume, and MTT = mean transit time.

4.2. CT Perfusion. CTP is a technique that allows quick qualitative and quantitative evaluation of tissue blood perfusion by generating maps of BF, BV, and MTT. Gandhi et al. [25] reported that CT perfusion parameters may provide valid information on angiogenic activity induced by neoplastic cells invading LNs. Tumour vessels in malignant LNs have certain characteristics, including short artery and vein circuits and a lack of smooth muscle around the vessel walls, which can result in increased blood perfusion [26].

In our study, 13/17 metastatic LNs showed high BF and BV and short MTT. There were significant differences between metastatic LNs and benign LNs in BF and MTT. In metastatic nodes, BF is increased by newly developed vessels, while MTT is usually decreased by the presence of pathological arteriovenous shunts. Changes in vascular endothelium and in the function of vessels are induced by neoangiogenesis [27, 28].

In our study, 15/48 metastatic LNs also had lower BF, reflecting the necrotic tumour elements (although any macroscopic nonviable areas were excluded from the analysis), a quite common phenomenon in malignant tumours [29, 30]. This type of inter- or intralesional heterogeneity sometimes resulted in high standard deviations of the perfusion values. This heterogeneity could be a pitfall of measuring perfusion values in ROIs (variable in size and location) scattered through the LNs [26]. It may have been the factor behind the significant differences in BF values, and not in BV values, between benign and metastatic nodes. The

Table 2: Accuracy of diffusion-weighted imaging (DWI) and perfusion CT (CTP).

	Sensitivity	Specificity	PPV	NPV	Accuracy	AUC
DWI	43/48 (89.58%)	13/17 (76.47%)	43/47 (91.49%)	13/18 (72.22%)	56/65 (86.15%)	0.830
CTP	33/48 (68.75%)	9/17 (52.94%)	33/41 (80.48%)	9/24 (37.50%)	42/65 (64.61%)	0.605

$Z = 4.612$, $P < 0.001$.
PPV = positive predictive value, NPV = negative predictive value, and AUC = area under the ROC curve.

best threshold BF value for differentiating malignant from benign nodes was 100.36 mL/100 g/min, yielding a sensitivity of 68.18%, specificity of 52.94%, accuracy of 64.46%, PPV of 80.48%, and NPV of 37.50%.

4.3. Comparison between DWI and CT Perfusion. DWI has been reported to be able to distinguish between malignant and benign LNs with sensitivities ranging from 52% to 98% and specificities ranging from 88% to 97% [31, 32]. ADC values played an important role in differentiating between benign and metastatic LNs. Some authors reported similar threshold ADC values such as $0.94 \times 10^{-3}\,mm^2/s$. Our data was in agreement with the results mentioned above and obtained a sensitivity of 89.58%, a specificity of 76.47%, and an accuracy of 86.15%.

In CTP, there were general differences between benign and metastatic LNs, but with some overlap [33]. We obtained a sensitivity of 68.18%, specificity of 52.94%, and accuracy of 64.46% with BF 100.36 mL/100 g/min as the threshold value. The ROC curve was used to evaluate the two imaging techniques, with an AUC of 0.830 (DWI) and 0.605 for CTP ($P < 0.001$). In addition, the patients undergoing CTP were injected with an iodinated contrast agent that has been confirmed to have some nephrotoxicity; meanwhile, patients inevitably suffer from radiation injury.

5. Conclusion

In conclusion, DWI exhibited better sensitivity and specificity than CTP. DWI may be the preferred technique for the preoperative assessment of LNs in head and neck SCC.

Abbreviations

DWI: Diffusion-weighted magnetic resonance imaging
CTP: Computed tomography perfusion
LN: Lymph node
SCC: Squamous cell carcinoma
ADC: Apparent diffusion coefficient
PPV: Positive predictive value
NPV: Negative predictive value.

Conflict of Interests

The authors declare that they have no conflict of interests.

Authors' Contributions

Jin Zhong, Zonghong Lu, and Liang Xu participated in collection and/or assembly of data. Longchun Dong, Hui Qiao, Rui Hua, and Yi Gong participated in data analysis and interpretation. Caixian Hao, Xuehuan Liu, and Li He participated in paper writing. Changqing Zong participated in statistical analysis. Jun Liu participated in conception and design, financial support, and final approval of the paper. All authors read and approved the paper.

Acknowledgment

This work was supported in part by the Key Foundation of Tianjin Health Bureau (2010KY13, 2011KY19).

References

[1] S. Nakamatsu, E. Matsusue, H. Miyoshi, S. Kakite, T. Kaminou, and T. Ogawa, "Correlation of apparent diffusion coefficients measured by diffusion-weighted MR imaging and standardized uptake values from FDG PET/CT in metastatic neck lymph nodes of head and neck squamous cell carcinomas," *Clinical Imaging*, vol. 36, no. 2, pp. 90–97, 2012.

[2] A. A. Dünne, H. H. Müller, D. W. Eisele, K. Keßel, R. Moll, and J. A. Werner, "Meta-analysis of the prognostic significance of perinodal spread in head and neck squamous cell carcinomas (HNSCC) patients," *European Journal of Cancer*, vol. 42, no. 12, pp. 1863–1868, 2006.

[3] J. A. Langendijk, B. J. Slotman, I. van der Waal, P. Doornaert, J. Berkof, and C. R. Leemans, "Risk-group definition by recursive partitioning analysis of patients with squamous cell head and neck carcinoma treated with surgery and postoperative radiotherapy," *Cancer*, vol. 104, no. 7, pp. 1408–1417, 2005.

[4] M. W. M. van den Brekel, J. A. Castelijns, H. V. Stel et al., "Occult metastatic neck disease: detection with US and US-guided fine-needle aspiration cytology," *Radiology*, vol. 180, no. 2, pp. 457–461, 1991.

[5] M. W. M. van den Brekel, J. A. Castelijns, H. V. Stel, R. P. Golding, C. J. L. Meyer, and G. B. Snow, "Modern imaging techniques and ultrasound-guided aspiration cytology for the assessment of neck node metastases: a prospective comparative study," *European Archives of Oto-Rhino-Laryngology*, vol. 250, no. 1, pp. 11–17, 1993.

[6] S. L. Focht, "Lymphatic mapping and sentinel lymph node biopsy," *AORN journal*, vol. 69, no. 4, pp. 802–809, 1999.

[7] H. D. Curtin, H. Ishwaran, A. A. Mancouso et al., "Comparison of CT and MR imagingin staging of neck metastsis," *Radiology*, vol. 207, pp. 123–130, 1998.

[8] M. W. M. van den Brekel, J. A. Castelijns, and G. B. Snow, "The size of lymph nodes in the neck on sonograms as a radiologic criterion for metastasis: how reliable is it?" *American Journal of Neuroradiology*, vol. 19, no. 4, pp. 695–700, 1998.

[9] M. W. M. van den Brekel, J. A. Castelijns, and G. B. Snow, "Detection of lymph node metastases in the neck: radiologic criteria," *Radiology*, vol. 192, no. 3, pp. 617–618, 1994.

[10] J. Kotani, J. Kawabe, S. Higashiyama et al., "Evaluation of diagnostic abilities of Ga-SPECT for head and neck lesions," *Annals of Nuclear Medicine*, vol. 22, no. 4, pp. 297–300, 2008.

[11] Y. Yamazaki, M. Saitoh, K. I. Notani et al., "Assessment of cervical lymph node metastases using FDG-PET in patients with head and neck cancer," *Annals of Nuclear Medicine*, vol. 22, no. 3, pp. 177–184, 2008.

[12] H. S. Jeong, C. H. Baek, Y. I. Son et al., "Use of integrated 18F-FDG PET/CT to improve the accuracy of initial cervical nodal evaluation in patients with head and neck squamous cell carcinoma," *Head and Neck*, vol. 29, no. 3, pp. 203–210, 2007.

[13] S. H. Ng, T. C. Yen, C. T. Liao et al., "18F-FDG PET and CT/MRI in oral cavity squamous cell carcinoma: a prospective study of 124 patients with histologic correlation," *Journal of Nuclear Medicine*, vol. 46, no. 7, pp. 1136–1143, 2005.

[14] D. Le Bihan, E. Breton, D. Lallemand, M.-L. Aubin, J. Vignaud, and M. Laval-Jeantet, "Separation of diffusion and perfusion in intravoxel incoherent motion MR imaging," *Radiology*, vol. 168, no. 2, pp. 497–505, 1988.

[15] H. C. Thoeny, F. De Keyzer, and A. D. King, "Diffusion-weighted MR imaging in the head and neck," *Radiology*, vol. 263, no. 1, pp. 19–32, 2012.

[16] K. A. Miles and M. R. Griffiths, "Perfusion CT: a worthwhile enhancement?" *British Journal of Radiology*, vol. 76, no. 904, pp. 220–231, 2003.

[17] V. Vandecaveye, F. de Keyzer, V. Vander Poorten et al., "Head and neck squamous cell carcinoma: value of diffusion-weighted MR imaging for nodal staging," *Radiology*, vol. 251, no. 1, pp. 134–146, 2009.

[18] M. Maeda, H. Kato, H. Sakuma, S. E. Maier, and K. Takeda, "Usefulness of the apparent diffusion coefficient in line scan diffusion-weighted imaging for distinguishing between squamous cell carcinomas and malignant lymphomas of the head and neck," *American Journal of Neuroradiology*, vol. 26, no. 5, pp. 1186–1192, 2005.

[19] A. D. King, A. T. Ahuja, D. K. W. Yeung et al., "Malignant cervical lymphadenopathy: diagnostic accuracy of diffusion-weighted MR imaging," *Radiology*, vol. 245, no. 3, pp. 806–813, 2007.

[20] J. Wang, S. Takashima, F. Takayama et al., "Head and neck lesions: characterization with diffusion-weighted echo-planar MR imaging," *Radiology*, vol. 220, no. 3, pp. 621–630, 2001.

[21] A. Srinivasan, R. Dvorak, K. Perni, S. Rohrer, and S. K. Mukherji, "Differentiation of benign and malignant pathology in the head and neck using 3T apparent diffusion coefficient values: early experience," *The American Journal of Neuroradiology*, vol. 29, no. 1, pp. 40–44, 2008.

[22] A. A. K. Abdel Razek, G. Gaballa, G. Elhawarey, A. S. Megahed, M. Hafez, and N. Nada, "Characterization of pediatric head and neck masses with diffusion-weighted MR imaging," *European Radiology*, vol. 19, no. 1, pp. 201–208, 2009.

[23] H. Kato, M. Kanematsu, Z. Kato et al., "Necrotic cervical nodes: usefulness of diffusion-weighted MR imaging in the differentiation of suppurative lymphadenitis from malignancy," *European Journal of Radiology*, vol. 82, no. 1, pp. e28–e35, 2013.

[24] A. Perrone, P. Guerrisi, L. Izzo et al., "Diffusion-weighted MRI in cervical lymph nodes: differentiation between benign and malignant lesions," *European Journal of Radiology*, vol. 77, no. 2, pp. 281–286, 2011.

[25] D. Gandhi, D. B. Chepeha, T. Miller et al., "Correlation between initial and early follow-up CT perfusion parameters with endoscopic tumor response in patients with advanced squamous cell carcinomas of the oropharynx treated with organ-preservation therapy," *The American Journal of Neuroradiology*, vol. 27, no. 1, pp. 101–106, 2006.

[26] S. Bisdas, M. Baghi, J. Wagenblast et al., "Differentiation of benign and malignant parotid tumors using deconvolution-based perfusion CT imaging: feasibility of the method and initial results," *European Journal of Radiology*, vol. 64, no. 2, pp. 258–265, 2007.

[27] S. Bisdas, K. Spicer, and Z. Rumboldt, "Whole-tumor perfusion CT parameters and glucose metabolism measurements in head and neck squamous cell carcinomas: a pilot study using combined positron-emission tomography/CT imaging," *The American Journal of Neuroradiology*, vol. 29, no. 7, pp. 1376–1381, 2008.

[28] A. Trojanowska, P. Trojanowski, S. Bisdas et al., "Squamous cell cancer of hypopharynx and larynx—evaluation of metastatic nodal disease based on computed tomography perfusion studies," *European Journal of Radiology*, vol. 81, no. 5, pp. 1034–1039, 2012.

[29] P. Trojanowski, J. Klatka, A. Trojanowska, T. Jargiełło, and A. Drop, "Evaluation of cervical lymph nodes with CT perfusion in patients with hypopharyngeal and laryngeal squamous cell cancer," *Polish Journal of Radiology*, vol. 76, no. 1, pp. 7–13, 2011.

[30] Z. Y. Yang, Q. F. Meng, Q. L. Xu et al., "CT perfusion imaging of cervical lymph nodes," *Clinical Radiology*, vol. 26, pp. 865–868, 2007.

[31] M. Sumi, N. Sakihama, T. Sumi et al., "Discrimination of metastatic cervical lymph nodes with diffusion-weighted MR imaging in patients with head and neck cancer," *The American Journal of Neuroradiology*, vol. 24, no. 8, pp. 1627–1634, 2003.

[32] A. A. K. Abdel Razek, N. Y. Soliman, S. Elkhamary, M. K. Alsharaway, and A. Tawfik, "Role of diffusion-weighted MR imaging in cervical lymphadenopathy," *European Radiology*, vol. 16, no. 7, pp. 1468–1477, 2006.

[33] Z. Rumboldt, R. Al-Okaili, and J. P. Deveikis, "Perfusion CT for head and neck tumors: pilot study," *The American Journal of Neuroradiology*, vol. 26, no. 5, pp. 1178–1185, 2005.

Hindawi Publishing Corporation
BioMed Research International
Volume 2014, Article ID 432652, 8 pages
http://dx.doi.org/10.1155/2014/432652

Review Article

Asymmetric Cell Division in Polyploid Giant Cancer Cells and Low Eukaryotic Cells

Dan Zhang,[1] Yijia Wang,[2] and Shiwu Zhang[1,2]

[1] *Department of Pathology, Tianjin Union Medicine Center (Nankai University Affiliated Hospital), Tianjin 300121, China*
[2] *Clinical and Translation Medicine Lab, Tianjin Union Medicine Center, Tianjin 300121, China*

Correspondence should be addressed to Shiwu Zhang; zhangshiwu666@aliyun.com

Received 9 May 2014; Accepted 8 June 2014; Published 22 June 2014

Academic Editor: Jun Liu

Asymmetric cell division is critical for generating cell diversity in low eukaryotic organisms. We previously have reported that polyploid giant cancer cells (PGCCs) induced by cobalt chloride demonstrate the ability to use an evolutionarily conserved process for renewal and fast reproduction, which is normally confined to simpler organisms. The budding yeast, *Saccharomyces cerevisiae*, which reproduces by asymmetric cell division, has long been a model for asymmetric cell division studies. PGCCs produce daughter cells asymmetrically in a manner similar to yeast, in that both use budding for cell polarization and cytokinesis. Here, we review the results of recent studies and discuss the similarities in the budding process between yeast and PGCCs.

1. Introduction

Asymmetric cell division is essential for generating cell diversity during development in low-level eukaryotes, including yeast. The budding yeast, *Saccharomyces cerevisiae*, has served as an excellent model for studying this process [1]. In animals, stem cells have the ability to undergo an asymmetrical, self-renewing cell division, resulting in one stem cell and one more differentiated progenitor cell [2].

Polyploid giant cancer cells (PGCCs) are key contributors to the cellular heterogeneity observed in human solid tumors. We have successfully purified and cultured PGCCs from 22 kinds of cancer and immortalized cell lines. PGCCs meet the definitions of cancer stem cells and play a fundamental role in regulating heterogeneity, stemness, and chemoresistance among human solid tumor cells. Single PGCCs formed cancer spheroids *in vitro* and generated tumors in immunodeficient mice, demonstrating that PGCCs have cancer stem cell-like properties. The PGCCs were slow-cycling in nature and stained positively for both normal stem cell and cancer stem cell markers. They were prone to differentiate into other tissue types, including adipose, cartilage, and bone, and were found to generate regular cancer cells through the budding, splitting or burst-like mechanisms common in the replication of low-level eukaryotes, including yeast [3–5]. In this review, we review the possible molecular mechanism of asymmetric cell division in lower eukaryotic cells and PGCCs.

2. Polyploid Giant Cells

Polyploidy refers to a karyotypic state where the chromosome number is a multiple of the chromosome number of the gamete [6]. It gives rise to chromosomal instability, as seen in a high rate of chromosomal division errors. Polyploidy is an important cause of human reproductive diseases, such as infertility, spontaneous abortions, and congenital birth defects, with data showing that about 20% of spontaneous abortions are caused by polyploidy [7]. Polyploidy are considered as being on the verge of mitotic catastrophe and subsequent apoptosis [8].

3. Polyploid Giant Cells and Cancer

As long as a century ago, it was found that some tumor cells often have extra chromosomes. Normal human cells contain 46 chromosomes but tumors cells contain abnormal numbers (usually between 60 and 90), with cell-to-cell variability.

Structural abnormalities such as inversions, deletions, duplications, and translocations are commonly observed in these chromosomes but are rare in normal cells, and PGCCs are key contributors to the heterogeneity of human solid tumors. By and large, however, PGCCs have not attracted the attention they deserve from the cancer research community because of their poorly understood biological role in cancer. Studies have reported a close relationship between the proportion of PGCCs in tumors and tumor deterioration, risk of metastasis [9], treatment effectiveness, and recurrence rate [10, 11]. The relationship between polyploidy and cancer has long been known, but it is not clear if polyploidy is a contributing factor to tumorigenesis or only a consequence of malignant transformation [12, 13].

Clinical evidence is accumulating in support of the idea that polyploidy positively contributes to tumorigenesis. First, polyploidy occurs before transformation. *In vivo*, polyploid cells exist in many precancerous tissues, such as the cervix [14], head and neck [15], colon [16], esophagus, and bone marrow [17]. Polyploid cells are also observed in breast [18] and skin tissues of experimental animals [19]. Second, polyploidy disturbs the overall transcription level, upregulating genes promoting cell growth and downregulating cytostatic genes. Tumorigenesis and transformation caused by polyploidy need many rearrangements to build the complex karyotype of tumor cells. Expression errors in tumor cell genes contribute to unrestricted growth, which is similar to the upward trend in the tumorigenesis rate that occurs with increasing age [20]. Polyploidy, rather than a cellular genetic phenomenon, is necessary for tumorigenesis [21, 22]. Tetraploidy might enhance tumorigenesis by the buffering effects of additional normal chromosomes. Extra chromosome sets might mask the effects of deleterious mutations if these mutations are recessive or partially recessive, thereby allowing cells with DNA damage to survive longer until a crucial growth-enhancing or transforming mutation occurs. This effect of increased ploidy has been best studied in yeast evolution experiments [23]. Diploid budding yeast mutator strains defective in mismatch repair have a significant advantage over haploid mutators in long-term evolution experiments [23]. Besides increasing tumorigenesis, polyploidy is also a contributing factor to or an incidental product of cell malignant transformation [24].

4. PGCCs and Cancer Stem Cells

In cancer, multiple stresses, including antimitotic chemotherapy drugs, radiotherapy, hypoxia, or poor microenvironment, can increase the formation of PGCCs. PGCCs with slow-cycling nature stain positively for normal and cancer stem cell markers. These cells are prone to differentiation into other tissues and cell types, including adipose, cartilage, erythrocytes, fibroblasts, and bone [3–5, 25]. Single PGCCs form cancer spheroids *in vitro* and generate tumors in immunodeficient mice, whereas large numbers (hundreds) of regular cancer cells do not, demonstrating that PGCCs have cancer stem cell-like properties. Proteomic analysis of PGCCs reveals a distinct signature, involving proteins related to hypoxia, invasion, chromatin-remodeling, and cell cycle regulation [3]. Thus, PGCCs may exhibit an evolutionarily conserved mechanism that cancer cells use to achieve malignant growth through increased cell size and highly efficient replication. PGCCs play a fundamental role in regulating heterogeneity, stemness, and chemoresistance in solid human cancers [5].

Cancer stem cells are a small subset of cancer cells that are capable of generating entire tumors [26, 27]. To date, stem cell-like populations have been characterized using cell-surface protein markers in tumors [28]. The nature of such so-called stem cells remains disputed, however [29, 30]. The American Association for Cancer Research consensus conference workshop broadly defined a cancer stem cell as "a cell within a tumor that possesses the capacity to self-renew and to cause the heterogeneous lineages of cancer cells that comprise the tumor [2]." Single cells in mice that generate tumors represent the gold standard for cancer stem cells. Cancer stem cells also have slow cycles, exhibit asymmetric division, and have the unique potential to divide asymmetrically to generate daughter cells with different fates, one of which remains a stem cell and the other turns into a cell committed to tumor formation [31]. By dividing asymmetrically, cancer stem cells maintain the stem cell pool and simultaneously generate committed cells that form tumor mass [32]. Many secrets of the cell cycle have been resolved by studying the asymmetric division of cancer stem cells in which cytoplasmic structures like the midbody are often inherited by only one of the two daughters.

5. Asymmetric Cell Division of PGCCs in Cancer

In multicellular eukaryotes, mitosis is the recognized process for somatic cell division, ensuring the accurate separation of duplicated genetic material to progeny cells. As a result, eukaryotes have well-regulated and orderly growth, with a low mutation frequency. In contrast, prokaryotes and unicellular eukaryotes divide by amitotic processes, including binary fission and budding. Although mitosis predominates in complex eukaryotes, it is well documented that depending on the organism or cell type, variations can occur in the mitotic cell cycle to replicate cells and meet growth and developmental needs [33, 34]. Among these variations is the endocycle (or endoreduplication), a variation of the normal mitotic cell cycle involving multiple rounds of DNA replication. This process is commonly employed in certain forms of growth in plants, insects [33, 35–37], and trophoblasts and in the generation of platelets from megakaryocytes in mammals [34, 37]. David von Hansemann proposed that abnormal mitosis occurs in polyploid tumor cells. He found dividing cells with chromosomes of abnormal configuration and size by observing various tumor tissue sections [38]. Two chromosome configurations were mentioned by Hansemann as follows: late bridges and multipole splitting. Both of these can result in abnormal chromosome numbers and the phenomenon of heterozygosity loss caused by missing unstable chromosomes [39]. After Hansemann, Theodor Boveri, a German cell biologist and zoologist, found multipolar

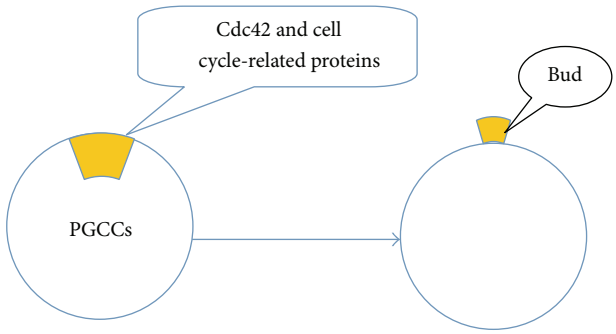

Figure 1: Asymmetric cell division in PGCCs. Cdc42 and cell cycle-related proteins involved in the process of PGCCs generating daughter cells.

spindles and aneuploid daughter cells. In 1902 and 1914, he propounded the hypothesis that the generation of polyploidy leads to tumorigenesis and malignancy and is unrelated to the origins of abnormal chromosome constitution [40].

We previously reported that PGCCs can be induced and purified by $CoCl_2$. These cells were found to be in a dynamic equilibrium with regular cancer cells and could be formed through endoreduplication or cell fusion [5]. They reverted to regular cancer cells via asymmetric cell divisions, including the splitting, budding, or burst-like mechanisms commonly used in the replication of low-level eukaryotes, plants, and viruses [5]. In fact, these giant cells revert to regular-sized cancer cells through a process of reductive division named depolyploidization [37, 41]. Asymmetric cell division of giant cancer cells by meiosis-like depolyploidization had been previously proposed to explain the unexpected life cycle of these cells [35, 36]. This mechanism by which PGCCs generate daughter cells has also been reported in the normal growth of skeletal muscle, osteoclasts, viral infection, and even tissue culture.

Asymmetric cell division is a fundamental process, whereby the asymmetric inheritance of cellular components defines distinct fates for each daughter cell. In a typical outcome, the stem or progenitor cell generates a copy of itself and a second daughter cell programmed to differentiate into a nonstem cell type [42]. Thus, by balancing self-renewal with differentiation, asymmetric divisions maintain the stem and progenitor cell pool while allowing the generation of diverse functional cells. Asymmetric division is a key mechanism ensuring tissue homeostasis. In normal stem and progenitor cells, asymmetric cell division balances proliferation and self-renewal with cell-cycle exit and differentiation. Disruption of asymmetric cell division leads to aberrant self-renewal and impairs differentiation. In normal, nontumor stem cells, a number of genes like *Bmi-1*, *Wnt*, and *Notch* have been described, which are responsible for self-renewal capacity. These genes have also been discovered in cancer stem cells, and their aberrant expression has been demonstrated to be essential for the formation of tumor cell mass [43]. Asymmetric cell division plays an important role in producing cell diversity during normal tissue development [44]. In principle, there are two mechanisms involved in asymmetric cell divisions. One is extrinsic asymmetric cell division, in which the daughter cells are initially equivalent, but a difference is induced by surrounding cells—the microenvironment—and the precursor cell; the second is intrinsic asymmetric cell division, in which the daughter cells are inherently different at the time of division of the mother cell [45]. Intrinsic asymmetric cell division does not depend on interactions between the daughter cells and the surrounding cells, relying instead on the different locations of proteins, RNA transcripts, and macromolecules in the daughter cells that cause each cell to assume a separate fate from that of its sibling.

6. Cell Cycle-Related Proteins and Asymmetric Division

Cyclins are regulatory subunits of cyclin-dependent kinases. The abnormal expression of cyclin-related proteins is important in the formation of stem cells. De Luca et al. confirmed that cyclin D3, a member of the mitogen-activated D-type cyclin family, is critically required for proper developmental progression in skeletal muscle stem cells [46]. Cyclin A, the first cyclin to be cloned, is thought to be a component of the cell-cycle engine whose function is essential for cell-cycle progression in hematopoietic and embryonic stem cells [47]. Our previous results also showed that cell cycle-related proteins are involved in PGCC formation [5]. These proteins, including FOXM1, Chk1, Chk2, cyclin A2, cyclin E, cyclin B1, and CDK6, play important roles in regulating the asymmetric division of PGCCs generating daughter cells (Figure 1). Expression levels of cyclin E and cyclin D1 were markedly elevated in purified PGCCs compared with that in diploid cancer cells. In particular, cyclin B1 was expressed only in the cytoplasm of PGCCs from human high-grade serous carcinomas and metastatic ovarian cancers, but had scant nuclear expression in low-grade serous ovarian cancers and no expression in benign ovarian serous cystadenomas, demonstrating that PGCC formation is regulated by recompartmentalization of cell cycle regulatory proteins normally involved in the regulation of asymmetric division [5].

7. Asymmetric Cell Division in Yeast

Yeast has both asexual and sexual modes of reproduction. Budding is one of the asexual modes that has long been a model in studies of cellular asymmetry aiming to discover the general principles of eukaryotic cell polarization and cytokinesis, both of which occur in yeast. Budding is a special kind of cell polarization adopted by yeast in order to undergo asymmetric cell division [48].

Cell polarity has been observed in almost all cells, with different cell types employing it in different ways. The mother cell divides asymmetrically by producing buds that can grow into daughter cells when they detach after cytokinesis. Polarity relies on the active determinants that localize to the plasma membrane and are associated with cell shape, cell adhesion and migration, cell division, and the uptake and release of molecules. In the polarized cell system, yeast exhibits asymmetry both in signaling molecule distribution

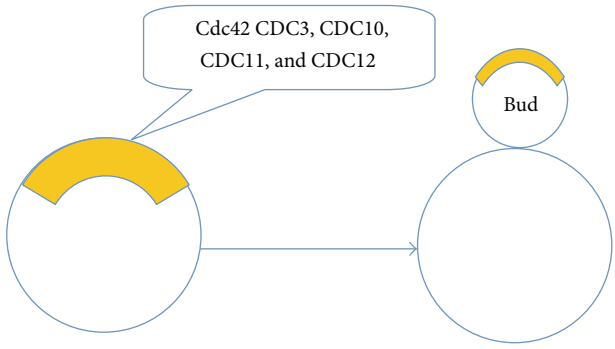

Figure 2: Asymmetric cell division in yeast. Cdc42 and other molecules including CDC3, CDC10, CDC11, and CDC12 locate in the special sites that will generate bud growth.

and cytoskeleton organization. Before budding, the yeast cytoskeleton and membrane trafficking machinery become polarized to deliver cargo to the buds and then promote their growth into daughter cells [49]. The master regulator of cell polarity in budding yeast is the small GTPase, Cdc42 (cell division control protein 42). This plays a central role in cell polarization from yeasts to humans [50, 51]. It was first discovered in the yeast *Saccharomyces cerevisiae* [52]. There are six types of Rho-type GTPases in yeast, namely Rho1–Rho5 and Cdc42. They locate to the cell membrane, where they establish and maintain cell polarity. Cdc42 is critical for budding and polarization growth [52, 53]; this was initially recognized in a temperature-sensitive mutant for polarized actin organization and cell growth [54, 55]. Homologs from other species share 80–85% identity in amino acid sequence and functionally complement yeast *cdc42* mutants [55]. Cdc42 is a master regulator of cell polarization. The protein contains a C-terminal CAAX-linked geranylgeranyl membrane anchor and is uniformly distributed around the plasma membrane in symmetric interphase cells, as well as being present in the cytoplasm [48]. Loss of Cdc42 activity causes cells to grow without budding. Isotropic and polarized distribution of Cdc42 in yeast is required for polarized organization of the cytoskeleton and membrane trafficking system. In recent years, it has been shown that the cytoskeleton and membrane trafficking system are in turn able to impact Cdc42 distribution [56–58]. Actin redistribution in yeast is a dynamic process that is also regulated by Cdc42 [59]. Polarized morphogenesis is a critical process for determining the specialized functions and physiologies of cells and organs. During these processes, Cdc42 localizes to a small cortical domain that can become the bud or Shamoo site (Figure 2) [60, 61]. Here, it can impact morphological development by controlling oriented actin cables that direct both transportation of membrane vesicles and organelles and the assembly of septin. Members of the septin family, such as CDC3, CDC10, CDC11, and CDC12, are distributed to the special sites that will generate bud growth and are involved in the selection of budding sites [51, 62].

Cytokinesis is another component of the process of asymmetric cell division and plays an important role in increasing cell numbers and cell diversity during development [63–65]. It is carried out by contraction of the contractile actomyosin ring (AMR), followed by centripetal growth of the primary septum (PS) [66]. At the end of PS formation, two secondary septa (SS) are synthesized on either side of the PS. The PS and a portion of SS are then degraded by endochitinase and glucanases from the daughter side, resulting in cell separation [66]. The AMR generates contractile power that is thought to be involved in guiding membrane deposition and formation of the primary septum [66, 67]. The functions of the AMR and the PS are interdependent [68], in that the disruption of the AMR causes severely misoriented PS formation [67], and disruption of PS formation results in abnormal AMR contraction [68]. In *S. cerevisiae*, there are six families of proteins involved in AMR assembly: septins, Myo1, Mlc1, Iqg1, Bni1, and actin. Septins are the first to arrive at the division site, and their presence ensures that the other cytokinesis proteins also localize there. The members of the septin family are distributed to special sites that will generate bud growth. Septins form polymers [52, 68]. In temperature-sensitive mutants of any member of the septin family, polymerization does not occur, cytokinesis is blocked, and mitosis may proceed with the formation of multinucleated cells, a process that is similar to that forming some PGCCs. Septin1 is one of the important regulators that in mammals localizes to the mitotic contractile ring and participates in cytokinesis [52].

8. Asymmetric Cell Division in *Drosophila melanogaster* and *Caenorhabditis elegans*

In addition to work on asymmetric cell division in yeast, there have been other studies, mostly in invertebrates (*D. melanogaster* and *C. elegans*). In 1994, an asymmetrically segregating cell-fate determinant was found in *D. melanogaster* and named Numb [69]. This endocytic protein (which inhibits Notch-Delta signaling) was found localized at cell margins during mitosis and segregated to only one of the two daughter cells [70]. This work also implied that high levels of Numb can cause one of the daughter cells to divide asymmetrically. Most studies on asymmetric cell division in *D. melanogaster* were done with neuroblasts [30, 71–73]. Numb and the translation inhibitor brain tumor (BRAT) transiently accumulate at the basal plasma membrane in the late prometaphase [70, 74, 75]. Before mitosis, proteins of another type, including the PDZ domain-containing proteins PAR3 and PAR6 (PAR3 and PAR6 are mutants of which are partitioning defective) and the atypical protein kinase, PKC, are required to accumulate at the apical cell cortex (Figure 3). These are involved in the asymmetric localization of basal determinants, for which asymmetric phosphorylation is the key mechanism behind the asymmetric segregation of cell fate determinants [76]. Establishing and maintaining apicobasal polarity requires apical localization of PAR proteins. It was shown that PAR3, PAR6, PKC, and their homologs play a central role in almost all known cell polarity events, including epithelial polarity, axon outgrowth, synapse formation, and specification of the anteroposterior body axis [77, 78].

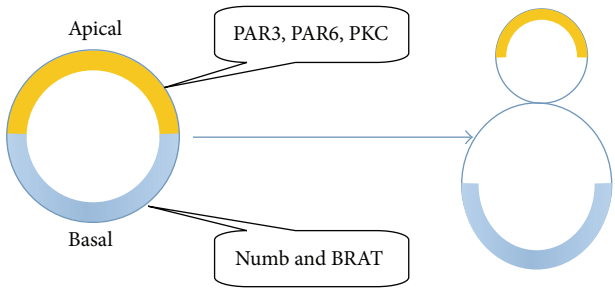

Figure 3: In *D. melanogaster* cells, Numb and BRAT transiently accumulate at the basal plasma membrane in the late prometaphase. Before mitosis, PAR3, PAR6, and PKC accumulate at the apical cell cortex and regulate the process of asymmetric cell division.

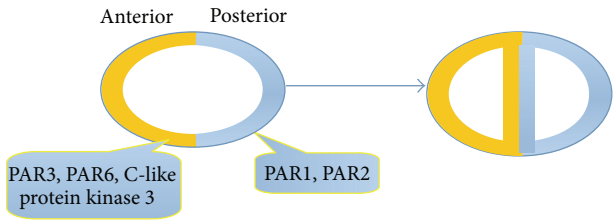

Figure 4: PAR protein complexes including PAR-3, PAR-6, and C-like protein kinase 3 were asymmetrically located and involve asymmetric cell division in *C. elegans*.

In *C. elegans*, PAR proteins were similarly asymmetrically located. PAR-3, PAR-6, and C-like protein kinase 3 accumulate at the anterior cell cortex of the *C. elegans* zygote when the first division occurs, whereas PAR-1 and PAR-2 accumulate posteriorly [76, 77, 79]. PAR protein complexes are also needed in *C. elegans* for other aspects of asymmetric cell division, such as the orientation and position of the mitotic spindle. The two daughter cells have different sizes and fates, but the mechanisms generating asymmetry are similar to those in neuroblasts. PAR-3, PAR-6, and PKC-3 are initially located on the cortical side and then concentrate on the anterior side after fertilization [80]. PAR-1 and PAR-2 become enriched in the posterior, noncontracting cell cortex, and inhibitory interactions between the anterior and posterior PAR proteins ensure that the groups maintain their localization to opposite cortical domains. PAR-2 prevents the cortical localization of PKC-3 [81], and PKC-3 phosphorylates PAR-2. PAR proteins in *C. elegans* are involved in regulating both asymmetric cell division and the symmetry-breaking events that establish the anteroposterior axis in the zygote [81], which is different from their functions in *D. melanogaster* (Figure 4).

9. Future Perspectives

Eukaryotes have a well-regulated and orderly growth with a low frequency of mutation via mitosis [82]. Conversely, in prokaryotes and unicellular eukaryotes, cells divide by amitotic processes, including budding. Although mitosis prevails in complex eukaryotes, endocycle involving multiple rounds of DNA replication without intervening mitosis step is an evolutionarily conserved means of generating multinucleated cells [33, 36, 37]. The process of PGCCs generating daughter cells through budding is very different from the traditional mitotic growth of eukaryotic diploid cells [5], which is regulated by many kinds of cell-cycle related proteins and Cdc42 [3]. PGCCs thus use budding from simple organisms and may demonstrate the ability to use an evolutionarily conserved process for renewal and fast reproduction.

In recent years, many of the key questions in asymmetric cell division have been answered. Despite these major advances, we still lack a molecular understanding of many of the processes involved. Furthermore, we still have no real clue as to how asymmetric cell division is regulated in mammalian adult stem cell lineages. Researchers have found that there is a link between the dysregulated asymmetric cell division of stem cells and tumorigenesis in mammals. Neuroblasts fail to differentiate in *D. melanogaster* embryos, leading to tumor-like overproliferation. After they have been transplanted into the abdomen of another fly, the tumors continue to grow, metastasize, and become aneuploid. The detailed mechanism of PGCCs generating daughter cells via budding is still unclear. Budding in yeast, *D. melanogaster*, and *C. elegans* may be served as the model to understand the potential mechanism of asymmetric division in PGCCs. In future, more studies of understanding the contribution of asymmetric cell division of PGCCs to mammalian development and tumorigenesis will be the primary goal.

Conflict of Interests

The authors declare that they have no conflict of interests.

Acknowledgments

This work was supported by the Key Foundation of Tianjin Health Bureau (2013KR14) and the Foundation of Committee on Science and Technology of Tianjin (13JCYBJC42700).

References

[1] E. Bi and H.-O. Park, "Cell polarization and cytokinesis in budding yeast," *Genetics*, vol. 191, no. 2, pp. 347–387, 2012.

[2] M. F. Clarke, J. E. Dick, P. B. Dirks et al., "Cancer stem cells—perspectives on current status and future directions: AACR workshop on cancer stem cells," *Cancer Research*, vol. 66, no. 19, pp. 9339–9344, 2006.

[3] S. Zhang, I. Mercado-Uribe, S. Hanash, and S. Liu, "iTRAQ-based proteomic analysis of polyploid giant cancer cells and budding progeny cells reveals several distinct pathways for ovarian cancer development," *PloS ONE*, vol. 8, no. 11, Article ID e80120, 2013.

[4] S. Zhang, I. Mercado-Uribe, and J. Liu, "Tumor stroma and differentiated cancer cells can be originated directly from polyploid giant cancer cells induced by paclitaxel," *International Journal of Cancer*, vol. 134, no. 3, pp. 508–518, 2014.

[5] S. Zhang, I. Mercado-Uribe, Z. Xing, B. Sun, J. Kuang, and J. Liu, "Generation of cancer stem-like cells through the formation

of polyploid giant cancer cells," *Oncogene*, vol. 33, pp. 116–128, 2014.

[6] N. J. Ganem, Z. Storchova, and D. Pellman, "Tetraploidy, aneuploidy and cancer," *Current Opinion in Genetics and Development*, vol. 17, no. 2, pp. 157–162, 2007.

[7] D. J. Bond, "Mechanisms of aneuploid induction," *Mutation Research*, vol. 181, no. 2, pp. 257–266, 1987.

[8] H. Vakifahmetoglu, M. Olsson, and B. Zhivotovsky, "Death through a tragedy: mitotic catastrophe," *Cell Death and Differentiation*, vol. 15, no. 7, pp. 1153–1162, 2008.

[9] F. Mitelman, B. Johansson, N. Mandahl, and F. Mertens, "Clinical significance of cytogenetic findings in solid tumors," *Cancer Genetics and Cytogenetics*, vol. 95, no. 1, pp. 1–8, 1997.

[10] M. Tingjie, W. Ze, S. Nianli, X. Rucheng, and C. Shilong, "Clinical significance of flow cytometric deoxyribonucleic acid measurements of deparaffinized specimens in bladder tumors," *European Urology*, vol. 21, no. 2, pp. 98–102, 1992.

[11] W.-J. Zeng, G.-Y. Liu, J. Xu, X.-D. Zhou, Y.-E. Zhang, and N. Zhang, "Pathological characteristics, PCNA labeling index and DNA index in prognostic evaluation of patients with moderately differentiated hepatocellular carcinoma," *World Journal of Gastroenterology*, vol. 8, no. 6, pp. 1040–1044, 2002.

[12] M. A. Matzke, M. F. Mette, T. Kanno, and A. J. M. Matzke, "Does the intrinsic instability of aneuploid genomes have a causal role in cancer?" *Trends in Genetics*, vol. 19, no. 5, pp. 253–256, 2003.

[13] E. A. Nigg, "Centrosome aberrations: cause or consequence of cancer progression?" *Nature Reviews Cancer*, vol. 2, no. 11, pp. 815–825, 2002.

[14] S. Duensing and K. Münger, "Mechanisms of genomic instability in human cancer: insights from studies with human papillomavirus oncoproteins," *International Journal of Cancer*, vol. 109, no. 2, pp. 157–162, 2004.

[15] H. Ai, J. E. Barrera, A. D. Meyers, K. R. Shroyer, and M. Varella-Garcia, "Chromosomal aneuploidy precedes morphological changes and supports multifocality in head and neck lesions," *Laryngoscope*, vol. 111, no. 10, pp. 1853–1858, 2001.

[16] J. Cardoso, L. Molenaar, R. X. De Menezes et al., "Chromosomal instability in MYH- and APC-mutant adenomatous polyps," *Cancer Research*, vol. 66, no. 5, pp. 2514–2519, 2006.

[17] A. Amiel, N. Gronich, M. Yukla et al., "Random aneuploidy in neoplastic and pre-neoplastic diseases, multiple myeloma, and monoclonal gammopathy," *Cancer Genetics and Cytogenetics*, vol. 162, no. 1, pp. 78–81, 2005.

[18] D. Medina, "Biological and molecular characteristics of the premalignant mouse mammary gland," *Biochimica et Biophysica Acta*, vol. 1603, no. 1, pp. 1–9, 2002.

[19] T. P. Dooley, V. L. Mattern, C. M. Moore, P. A. Porter, E. S. Robinson, and J. L. VandeBerg, "Cell lines derived from ultraviolet radiation-induced benign melanocytic nevi in *Monodelphis domestica* exhibit cytogenetic aneuploidy," *Cancer Genetics and Cytogenetics*, vol. 71, no. 1, pp. 55–66, 1993.

[20] D. Rasnick and P. H. Duesberg, "How aneuploidy affects metabolic control and causes cancer," *Biochemical Journal*, vol. 340, no. 3, pp. 621–630, 1999.

[21] P. Duesberg, D. Rasnick, R. Li, L. Winters, C. Rausch, and R. Hehlmann, "How aneuploidy may cause cancer and genetic instability," *Anticancer Research*, vol. 19, no. 6A, pp. 4887–4906, 1999.

[22] C. Lengauer, K. W. Kinzler, and B. Vogelstein, "Genetic instabilities in human cancers," *Nature*, vol. 396, no. 6712, pp. 643–649, 1998.

[23] C. Zeyl, "Experimental studies of ploidy evolution in yeast," *FEMS Microbiology Letters*, vol. 233, no. 2, pp. 187–192, 2004.

[24] W. C. Hahn and R. A. Weinberg, "Rules for making human tumor cells," *The New England Journal of Medicine*, vol. 347, no. 20, pp. 1593–1603, 2002.

[25] S. Zhang, I. Mercado-Uribe, and J. Liu, "Generation of erythroid cells from fibroblasts and cancer cells in vitro and in vivo," *Cancer Letters*, vol. 333, no. 2, pp. 205–212, 2013.

[26] D. Bonnet and J. E. Dick, "Human acute myeloid leukemia is organized as a hierarchy that originates from a primitive hematopoietic cell," *Nature Medicine*, vol. 3, no. 7, pp. 730–737, 1997.

[27] U. Silván, A. Díez-Torre, J. Arluzea, R. Andrade, M. Silió, and J. Aréchaga, "Hypoxia and pluripotency in embryonic and embryonal carcinoma stem cell biology," *Differentiation*, vol. 78, no. 2-3, pp. 159–168, 2009.

[28] J. E. Visvader and G. J. Lindeman, "Cancer stem cells in solid tumours: accumulating evidence and unresolved questions," *Nature Reviews Cancer*, vol. 8, no. 10, pp. 755–768, 2008.

[29] H. Clevers, "The cancer stem cell: premises, promises and challenges," *Nature Medicine*, vol. 17, no. 3, pp. 313–319, 2011.

[30] L. L. C. Marotta and K. Polyak, "Cancer stem cells: a model in the making," *Current Opinion in Genetics and Development*, vol. 19, no. 1, pp. 44–50, 2009.

[31] R. A. Neumüller and J. A. Knoblich, "Dividing cellular asymmetry: asymmetric cell division and its implications for stem cells and cancer," *Genes and Development*, vol. 23, no. 23, pp. 2675–2699, 2009.

[32] A. Gromley, C. Yeaman, J. Rosa et al., "Centriolin anchoring of exocyst and SNARE complexes at the midbody is required for secretory-vesicle-mediated abscission," *Cell*, vol. 123, no. 1, pp. 75–87, 2005.

[33] B. A. Edgar and T. L. Orr-Weaver, "Endoreplication cell cycles: more for less," *Cell*, vol. 105, no. 3, pp. 297–306, 2001.

[34] H. O. Lee, J. M. Davidson, and R. J. Duronio, "Endoreplication: polyploidy with purpose," *Genes and Development*, vol. 23, no. 21, pp. 2461–2477, 2009.

[35] J. Erenpreisa, M. S. Cragg, K. Salmina, M. Hausmann, and H. Scherthan, "The role of meiotic cohesin REC8 in chromosome segregation in γ irradiation-induced endopolyploid tumour cells," *Experimental Cell Research*, vol. 315, no. 15, pp. 2593–2603, 2009.

[36] J. Erenpreisa, A. Ivanov, M. Cragg, G. Selivanova, and T. Illidge, "Nuclear envelope-limited chromatin sheets are part of mitotic death," *Histochemistry and Cell Biology*, vol. 117, no. 3, pp. 243–255, 2002.

[37] J. Erenpreisa, K. Salmina, A. Huna et al., "Polyploid tumour cells elicit paradiploid progeny through depolyploidizing divisions and regulated autophagic degradation," *Cell Biology International*, vol. 35, no. 7, pp. 687–695, 2011.

[38] L. P. Bignold, B. L. D. Coghlan, and H. P. A. Jersmann, "Hansemann, Boveri, chromosomes and the gametogenesis-related theories of tumours," *Cell Biology International*, vol. 30, no. 7, pp. 640–644, 2006.

[39] G. A. Pihan, "Centrosome dysfunction contributes to chromosome instability, chromoanagenesis, and genome reprograming in cancer," *Frontiers in Oncology*, vol. 3, article 277, 2013.

[40] I. P. de Castro and M. Malumbres, "Mitotic stress and chromosomal instability in cancer: the case for TPX2," *Genes and Cancer*, vol. 3, no. 11-12, pp. 721–730, 2012.

[41] I. Vitale, L. Senovilla, M. Jema et al., "Multipolar mitosis of tetraploid cells: inhibition by p53 and dependency on Mos," *The EMBO Journal*, vol. 29, no. 7, pp. 1272–1284, 2010.

[42] S. J. Morrison and J. Kimble, "Asymmetric and symmetric stem-cell divisions in development and cancer," *Nature*, vol. 441, no. 7097, pp. 1068–1074, 2006.

[43] S. Gómez-López, R. G. Lerner, and C. Petritsch, "Asymmetric cell division of stem and progenitor cells during homeostasis and cancer," *Cellular and Molecular Life Sciences*, vol. 71, no. 4, pp. 575–597, 2014.

[44] H. R. Horvitz and I. Herskowitz, "Mechanisms of asymmetric cell division: two Bs or not two Bs, that is the question," *Cell*, vol. 68, no. 2, pp. 237–255, 1992.

[45] N. Hawkins and G. Garriga, "Asymmetric cell division: from A to Z," *Genes and Development*, vol. 12, no. 23, pp. 3625–3638, 1998.

[46] G. De Luca, R. Ferretti, M. Bruschi, E. Mezzaroma, and M. Caruso, "Cyclin d3 critically regulates the balance between self-renewal and differentiation in skeletal muscle stem cells," *Stem Cells*, vol. 31, no. 11, pp. 2478–2491, 2013.

[47] I. Kalaszczynska, Y. Geng, T. Iino et al., "Cyclin A is redundant in fibroblasts but essential in hematopoietic and embryonic stem cells," *Cell*, vol. 138, no. 2, pp. 352–365, 2009.

[48] B. D. Slaughter, S. E. Smith, and R. Li, "Symmetry breaking in the life cycle of the budding yeast," *Cold Spring Harbor Perspectives in Biology*, vol. 1, no. 3, 2009.

[49] B. J. Thompson, "Cell polarity: models and mechanisms from yeast, worms and flies," *Development*, vol. 140, no. 1, pp. 13–21, 2013.

[50] S. Etienne-Manneville, "Cdc42: the centre of polarity," *Journal of Cell Science*, vol. 117, no. 8, pp. 1291–1300, 2004.

[51] H.-O. Park and E. Bi, "Central roles of small GTPases in the development of cell polarity in yeast and beyond," *Microbiology and Molecular Biology Reviews*, vol. 71, no. 1, pp. 48–96, 2007.

[52] E. S. Johnson and G. Blobel, "Cell cycle-regulated attachment of the ubiquitin-related protein SUMO to the yeast septins," *The Journal of Cell Biology*, vol. 147, no. 5, pp. 981–994, 1999.

[53] D. I. Johnson and J. R. Pringle, "Molecular characterization of CDC42, a *Saccharomyces cerevisiae* gene involved in the development of cell polarity," *The Journal of Cell Biology*, vol. 111, no. 1, pp. 143–152, 1990.

[54] S. Munemitsu, M. A. Innis, R. Clark, F. McCormick, A. Ullrich, and P. Polakis, "Molecular cloning and expression of a G25K cDNA, the human homolog of the yeast cell cycle gene CDC42," *Molecular and Cellular Biology*, vol. 10, no. 11, pp. 5977–5982, 1990.

[55] K. Shinjo, J. G. Koland, M. J. Hart et al., "Molecular cloning of the gene for the human placental GTP-binding protein Gp (G25K): Identification of this GTP-binding protein as the human homolog of the yeast cell-division-cycle protein CDC42," *Proceedings of the National Academy of Sciences of the United States of America*, vol. 87, no. 24, pp. 9853–9857, 1990.

[56] J. E. Irazoqui, A. S. Howell, C. L. Theesfeld, and D. J. Lew, "Opposing roles for actin in Cdc42p polarization," *Molecular Biology of the Cell*, vol. 16, no. 3, pp. 1296–1304, 2005.

[57] T. S. Karpova, S. L. Reck-Peterson, N. B. Elkind, M. S. Mooseker, P. J. Novick, and J. A. Cooper, "Role of actin and Myo2p in polarized secretion and growth of *Saccharomyces cerevisiae*," *Molecular Biology of the Cell*, vol. 11, no. 5, pp. 1727–1737, 2000.

[58] R. Wedlich-Soldner, S. Altschuter, L. Wu, and R. Li, "Spontaneous cell polarization through actomyosin-based delivery of the Cdc42 GTPase," *Science*, vol. 299, no. 5610, pp. 1231–1235, 2003.

[59] Y. Mao, A. L. Tournier, P. A. Bates, J. E. Gale, N. Tapon, and B. J. Thompson, "Planar polarization of the atypical myosin Dachs orients cell divisions in Drosophila," *Genes and Development*, vol. 25, no. 2, pp. 131–136, 2011.

[60] T. J. Richman, M. M. Sawyer, and D. I. Johnson, "*Saccharomyces cerevisiae* Cdc42p localizes to cellular membranes and clusters at sites of polarized growth," *Eukaryotic Cell*, vol. 1, no. 3, pp. 458–468, 2002.

[61] M. Ziman, D. Preuss, J. Mulholland, J. M. O'Brien, D. Botstein, and D. I. Johnson, "Subcellular localization of Cdc42p, a *Saccharomyces cerevisiae* GTP- binding protein involved in the control of cell polarity," *Molecular Biology of the Cell*, vol. 4, no. 12, pp. 1307–1316, 1993.

[62] R. Wedlich-Soldner, S. C. Wai, T. Schmidt, and R. Li, "Robust cell polarity is a dynamic state established by coupling transport and GTPase signaling," *The Journal of Cell Biology*, vol. 166, no. 6, pp. 889–900, 2004.

[63] M. K. Balasubramanian, E. Bi, and M. Glotzer, "Comparative analysis of cytokinesis in budding yeast, fission yeast and animal cells," *Current Biology*, vol. 14, no. 18, pp. R806–R818, 2004.

[64] F. A. Barr and U. Gruneberg, "Cytokinesis: placing and making the final cut," *Cell*, vol. 131, no. 5, pp. 847–860, 2007.

[65] T. D. Pollard, "Mechanics of cytokinesis in eukaryotes," *Current Opinion in Cell Biology*, vol. 22, no. 1, pp. 50–56, 2010.

[66] G. Lesage and H. Bussey, "Cell wall assembly in *Saccharomyces cerevisiae*," *Microbiology and Molecular Biology Reviews*, vol. 70, no. 2, pp. 317–343, 2006.

[67] X. Fang, J. Luo, R. Nishihama et al., "Biphasic targeting and cleavage furrow ingression directed by the tail of a myosin II," *The Journal of Cell Biology*, vol. 191, no. 7, pp. 1333–1350, 2010.

[68] L. VerPlank and R. Li, "Cell cycle-regulated trafficking of Chs2 controls actomyosin ring stability during cytokinesis," *Molecular Biology of the Cell*, vol. 16, no. 5, pp. 2529–2543, 2005.

[69] M. S. Rhyu, L. Y. Jan, and Y. N. Jan, "Asymmetric distribution of numb protein during division of the sensory organ precursor cell confers distinct fates to daughter cells," *Cell*, vol. 76, no. 3, pp. 477–491, 1994.

[70] E. P. Spana, C. Kopczynski, C. S. Goodman, and C. Q. Doe, "Asymmetric localization of numb autonomously determines sibling neuron identity in the Drosophila CNS," *Development*, vol. 121, no. 11, pp. 3489–3494, 1995.

[71] C. Q. Doe, "Neural stem cells: balancing self-renewal with differentiation," *Development*, vol. 135, no. 9, pp. 1575–1587, 2008.

[72] J. A. Knoblich, "Mechanisms of asymmetric stem cell division," *Cell*, vol. 132, no. 4, pp. 583–597, 2008.

[73] P.-S. Wu, B. Egger, and A. H. Brand, "Asymmetric stem cell division: lessons from Drosophila," *Seminars in Cell and Developmental Biology*, vol. 19, no. 3, pp. 283–293, 2008.

[74] B. Bello, H. Reichert, and F. Hirth, "The brain tumor gene negatively regulates neural progenitor cell proliferation in the larval central brain of Drosophila," *Development*, vol. 133, no. 14, pp. 2639–2648, 2006.

[75] C.-Y. Lee, B. D. Wilkinson, S. E. Siegrist, R. P. Wharton, and C. Q. Doe, "Brat is a Miranda cargo protein that promotes neuronal differentiation and inhibits neuroblast self-renewal," *Developmental Cell*, vol. 10, no. 4, pp. 441–449, 2006.

[76] J. A. Knoblich, "Asymmetric cell division: recent developments and their implications for tumour biology," *Nature Reviews Molecular Cell Biology*, vol. 11, no. 12, pp. 849–860, 2010.

[77] S. Ohno, "Intercellular junctions and cellular polarity: the PAR-aPKC complex, a conserved core cassette playing fundamental roles in cell polarity," *Current Opinion in Cell Biology*, vol. 13, no. 5, pp. 641–648, 2001.

[78] A. Suzuki and S. Ohno, "The PAR-aPKC system: lessons in polarity," *Journal of Cell Science*, vol. 119, no. 6, pp. 979–987, 2006.

[79] K. J. Kemphues, J. R. Priess, D. G. Morton, and N. Cheng, "Identification of genes required for cytoplasmic localization in early *C. elegans* embryos," *Cell*, vol. 52, no. 3, pp. 311–320, 1988.

[80] E. Munro, J. Nance, and J. R. Priess, "Cortical flows powered by asymmetrical contraction transport PAR proteins to establish and maintain anterior-posterior polarity in the early *C. elegans* embryo," *Developmental Cell*, vol. 7, no. 3, pp. 413–424, 2004.

[81] Y. Hao, L. Boyd, and G. Seydoux, "Stabilization of cell polarity by the *C. elegans* RING protein PAR-2," *Developmental Cell*, vol. 10, no. 2, pp. 199–208, 2006.

[82] B. Alberts JA, J. Lewis, M. Raff, K. Roberts, and P. Walter, *Molecular Biology of the Cell*, Garland Science, New York, NY, USA, 4th edition, 2002.

Hindawi Publishing Corporation
BioMed Research International
Volume 2014, Article ID 832562, 8 pages
http://dx.doi.org/10.1155/2014/832562

Research Article

Overexpression of Wnt5a Promotes Angiogenesis in NSCLC

Lingli Yao,[1,2] Baocun Sun,[1,3,4] Xiulan Zhao,[1,4] Xueming Zhao,[1] Qiang Gu,[1,4] Xueyi Dong,[1] Yanjun Zheng,[1] Junying Sun,[1] Runfen Cheng,[3] Hong Qi,[1] and Jindan An[3]

[1] *Department of Pathology, Tianjin Medical University, Tianjin 300070, China*
[2] *Department of Pathology, Affiliated Anhui Provincial Hospital, Anhui Medical University, Hefei, Anhui 230001, China*
[3] *Department of Pathology, Tianjin Cancer Hospital, Tianjin Medical University, Tianjin 300060, China*
[4] *Department of Pathology, Tianjin General Hospital, Tianjin Medical University, Tianjin 300052, China*

Correspondence should be addressed to Baocun Sun; baocunsun@gmail.com

Received 5 May 2014; Accepted 13 May 2014; Published 5 June 2014

Academic Editor: Shiwu Zhang

To evaluate Wnt5a expression and its role in angiogenesis of non-small-cell lung cancer (NSCLC), immunohistochemistry and CD31/PAS double staining were performed to examine the Wnt5a expression and we analyze the relationships between Wnt5a and microvessel density (MVD), vasculogenic mimicry (VM), and some related proteins. About 61.95% of cases of 205 NSCLC specimens exhibited high expression of Wnt5a. Wnt5a expression level was upregulated in the majority of NSCLC tissues, especially in squamous cell carcinoma, while its expression level in adenocarcinoma was the lowest. Wnt5a was also found more frequently expressed in male patients than in female patients. Except for histological classification and gender, little association was found between Wnt5a and clinicopathological features. Moreover, Wnt5a was significantly correlated with prognosis. Overall, Wnt5a-positive expression in patients with NSCLC indicated shorter survival time. As for vascularization in NSCLC, Wnt5a showed close association with VM and MVD. In addition, Wnt5a was positively related with β-catenin-nu, VE-cadherin, MMP2, and MMP9. The results demonstrated that overexpression of Wnt5a may play an important role in NSCLC angiogenesis and it may function via canonical Wnt signal pathway. This study will provide evidence for further research on NSCLC and also will provide new possible target for NSCLC diagnosis and therapeutic strategies.

1. Introduction

In recent years, primary lung cancer occupies the leading cause of cancer mortality in the world [1]. Among primary lung cancer cases, approximately 80% of the cases are non-small-cell lung cancer [1, 2]. Although recent advancements have improved the survival rate of NSCLC patients [3–5], the high mortality related to NSCLC remains a daunting challenge [6]. Therefore, it is important to pay more attention to clarifying the mechanism of tumor biology in order to improve the prognosis of NSCLC patients. Indeed, angiogenesis theory has contributed significantly to tumor research.

Angiogenesis theory believes that tumor angiogenesis is essential for tumor growth and metastasis. When solid tumor grows to more than 2 mm in diameter, it needs to induce the generation new blood vessels to obtain a continuous supply of oxygen and nutrition to maintain its growth; otherwise, it would result in necrosis due to ischemia and anoxia [7, 8]. Thus, antiangiogenesis has become hot topic on tumor research. In fact, Wnt signaling pathway has been proven to be involved in this theory [9, 10].

Wnt5a is an important regulator of Wnt signaling pathway and has been demonstrated to play an important role in lung development and tumorigenesis [11, 12]. However, the biologics of Wnt5a in human cancers are still unclear. On the one hand, Wnt5a was found frequently upregulated in various cancers, including breast cancer, pancreatic cancer, prostate cancer, and gastric cancer [13–16]. On the other hand, Wnt5a was reported as a tumor suppressor gene in several cancers [12, 17, 18]. In addition, Wnt5a was proven to contribute to vascularization of embryonic stem cells [19]. Although Wnt5a was considered as an oncogene in lung cancer [20], its role in angiogenesis of lung cancer is still ambiguous.

Herein, the present study would investigate the expression of Wnt5a and its role in angiogenesis of human NSCLC.

First, immunohistochemistry was performed to examine the Wnt5a expression in 205 NSCLC tissues. Then, the relationship between Wnt5a and microvessel density (MVD) was detected. In addition, the relationship between Wnt5a and vasculogenic mimicry (VM), a special blood supply mode, was also detected. Finally, correlations between Wnt5a and expressions of some angiogenesis-related proteins and β-catenin were analyzed.

2. Materials and Methods

2.1. Patients. Tissue specimens were obtained from 205 patients who had undergone surgical resection for lung cancer in Tianjin Medical University Cancer Institute and Hospital from October 1990 to November 2010. The 205 NSCLC samples were composed of 79 cases of squamous cell carcinoma, 75 cases of adenocarcinoma, and 51 cases of large cell lung cancer. The diagnoses of these samples were independently verified by two pathologists according to the standards of classification [2, 21]. The average age of the patients at the time of diagnosis was 59.1 years (30 years to 88 years). The data of clinicopathological parameters were harvested from the patients' clinical records and pathological reports. Time to death, final follow-up examination, and diagnosis of metastasis were recorded from the date of surgery. This study was approved by the Ethical Committee of Tianjin Medical University prior to its initiation.

2.2. Immunohistochemistry and CD31/Periodic Acid Schiff (PAS) Double Staining. This assay was performed as described by Zhang et al. [22] and Sun et al. [23, 24]. The tissues were 10% formalin-fixed, paraffin-embedded, and cut into 4 μm thickness. All slides were then deparaffinized in xylene and dehydrated with descending-grade alcohol. Endogenous peroxidase activity was quenched by brooding in methanol containing 3% hydrogen peroxide for 30 min at room temperature. After blocking with recommended serum for 20 min at room temperature, the slides were incubated with a primary antibody overnight at 4°C and a homologous secondary antibody for 1 h at room temperature in a humidified box. Then the sections were stained with freshly dispensed diaminobenzidine solution (DAB) for observation under a microscope. In the process, the slides were all rinsed three times in phosphate-buffered saline (PBS) (pH 7.2) before each step, except for the procedure of serum blocking to incubation with the primary antibody. The slides were then counterstained with hematoxylin, dehydrated with ascending-grade ethanol, air-dried, cleared with xylene, and mounted. For CD31/periodic acid Schiff (PAS) double staining, the sections were still incubated with 1% periodic acid for 15 min and Schiff reagent for observation under a microscope at 37°C between DAB staining and hematoxylin counterstaining. In this process, distilled water instead of PBS was used for washing.

In the current study, the primary antibodies to Wnt5a and VE-cadherin were purchased from Abcam (Cambridge, UK). Antibodies to CD31, CD34, β-catenin, and MMP2 were from Invitrogen Zymed Laboratories (San Diego, USA). Antibody to MMP9 was from Santa Cruz Biotechnology (Santa Cruz, CA, USA). Positive control and negative control were performed for each batch. For the negative control, PBS was used instead of the primary antibody. For the positive control, a foregone positively expressed tissue section was used.

The results were evaluated following the method described by Bittner et al. [25]. The percentage and the intensity of the positive cells were both measured. The percentage was stratified as follows: 0 for less than 5% positive cells, 1 for less than 30% positive cells, 2 for less than 60% positive cells, and 3 for more than 60% positive cells. The intensity was also classified as follows: 0 (negative), 1 (weak), 2 (moderate), and 3 (strong). The sum of positive cell and staining intensity scores, which was more than 3 for the final result, was considered as the positive sample for each slide. Positive sample of β-catenin nuclear expression was deemed as those tissues which lost consecutive membrane location and acquired nuclear location more than 10% cells. MVD was determined from CD34-stained sections at the hot spot through light microscopy examination. The fields with the greatest neovascularization were examined by scanning tumor sections at low power (×100). The average vessel count of the five fields (×200) was regarded as the MVD.

2.3. Statistical Analysis. All data in the study were evaluated with SPSS17.0 software (SPSS, Chicago, IL, USA). Survival data were analyzed according to Kaplan-Meier test. Differences in survival curves were assessed by the log rank test. Crosstabs, Pearson χ^2 test, and Spearman correlation analysis were used as needed. All P values were two-sided, and $P < 0.05$ was considered statistically significant.

3. Results

3.1. Association of Wnt5a with Clinicopathological Features in Human NSCLC. Wnt5a positive expression appeared as brown granules staining in the cytoplasms of the tumor cells. Among 205 NSCLC specimens, Wnt5a was detected in 127 cases (Figure 1). Approximately 61.95% of NSCLC exhibited high expression of Wnt5a. According to Wnt5a presence, all samples were divided into two groups: Wnt5a-positive group ($n = 127$) and Wnt5a-negative group ($n = 78$). Then, the relationship between Wnt5a and clinicopathological features was analyzed separately. Statistical data in Table 1 showed that Wnt5a was significantly associated with histological classification and gender ($P = 0.016$ and 0.012, resp.). Among the three histological types, Wnt5a was frequently expressed in squamous cell carcinoma (70.89%, 56/79), while Wnt5a-positive expression in adenocarcinoma was the lowest (49.33%, 37/75). In male samples, Wnt5a was found expressed more than in female patients (67.59%, 98/145 *versus* 48.33%, 29/60). However, little correlation was found between Wnt5a-positive expression and other clinicopathological characteristics, such as age, tumor size, location, histological differentiation, pleura invasion, stage, metastasis, lymph node status, and therapy before surgery ($P > 0.05$, Table 1).

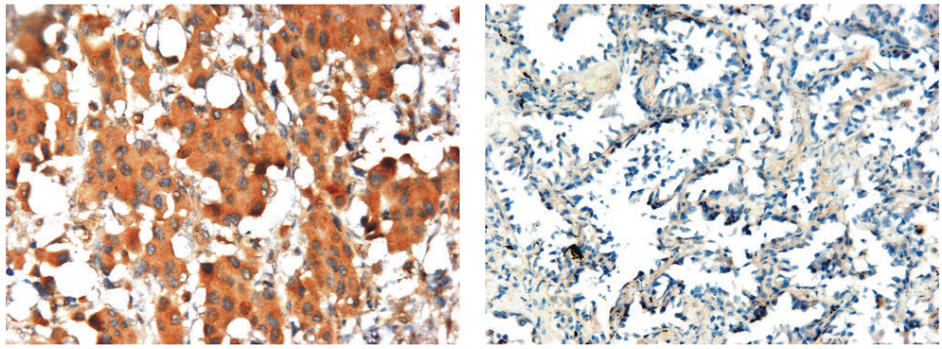

Figure 1: The expression of Wnt5a in NSCLC tissues (immunohistochemical staining, ×200). Left photo showed that Wnt5a was positively expressed in the cytoplasm of tumor cells while Wnt5a was negatively expressed in the tumor cells at the right picture.

To verify the clinical significance of Wnt5a, all 205 NSCLC patients were followed up and the relationship between their outcomes and Wnt5a expression was examined. Statistical analysis showed that the overall survival period of Wnt5a-positive patients was enormously shorter than that of Wnt5a-negative patients ($P = 0.026$). The mean survival period of Wnt5a-negative group was 52.31 months, whereas that of Wnt5a-positive group was only 33.64 months (Figure 2).

3.2. Association of Wnt5a with Angiogenesis in Human NSCLC. To evaluate the role of Wnt5a in angiogenesis of NSCLC, relationships between MVD, VM, and Wnt5a were examined. CD34 was stained to calculate the MVD and CD31/PAS double staining was recruited to identify the VM (Figure 3). According to the median value of MVD or the presence of VM, all 205 NSCLC cases were classified as high CD34-MVD ($\geq 28, n = 113$) or low CD34-MVD ($<28, n = 92$) and divided into VM group ($n = 28$) or non-VM group ($n = 177$). As shown in Table 2, significant correlation was found between Wnt5a and VM ($P = 0.021$, $r = 0.165$), as well as Wnt5a and CD34-MVD ($P = 0.026$, $r = 0.157$).

3.3. Association of Wnt5a with Angiogenesis Related Proteins in Human NSCLC. To further investigate the angiogenesis of NSCLC, some related proteins (VE-cadherin, MMP2, and MMP9) were also examined in this study. Positive expressions of these proteins were all located in the cytoplasm of tumor cells (Figure 4). Among 205 NSCLC tissues, VE-cadherin was positively expressed in 101 specimens (49.27%, 101/205), while MMP2 and MMP9 were found positively expressed in 67 cases (32.68%, 67/205) and 80 samples (39.02%, 80/205), respectively. Moreover, the relationships between Wnt5a and these related proteins were also studied. VE-cadherin was found closely related with Wnt5a ($P = 0.004$, $r = 0.210$) (Table 2). VE-cadherin-positive and Wnt5a-positive samples included 73 cases, and both negative samples included 50 cases. Similar to VE-cadherin, MMP2 and MMP9 both showed the remarkable relevance with Wnt5a ($P < 0.001$, $r = 0.268$; $P = 0.003$, $r = 0.215$, resp.) (Table 2).

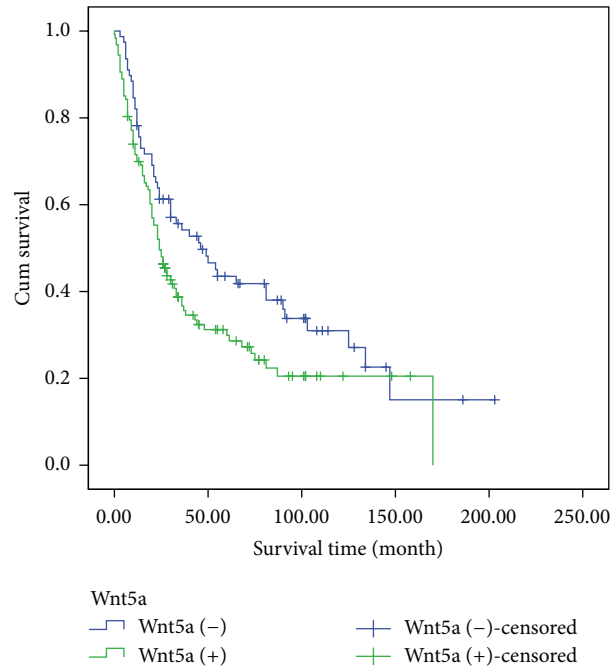

Figure 2: Result of the Kaplan-Meier survival analysis. Kaplan-Meier survival analysis showed that Wnt5a-positive patients have shorter survival periods than Wnt5a-negative patients ($P = 0.026$).

3.4. Association of Wnt5a with β-Catenin Nuclear Expression in Human NSCLC. To elucidate the possible mechanism of Wnt5a in angiogenesis of human NSCLC, β-catenin nuclear expression was detected and its relationship with Wnt5a was analyzed (Figure 5). In the current study, positive β-catenin nuclear expression appeared in 32 cases of 205 NSCLC tissues (15.61%, 32/205). Wnt5a was shown to be closely associated with β-catenin nuclear location ($P = 0.017$, $r = 0.171$). Both Wnt5a and β-catenin nuclear locations were detected positively in 26 cases, while Wnt5a and β-catenin nuclear locations were both negatively expressed in 72 samples. Wnt5a-positive expression but β-catenin-nu

Table 1: Correlation between Wnt5a and clinicopathological features in NSCLC.

Variant	Total	Wnt5a		x^2	P value
	n	Negative (%)	Positive (%)		
Gender					
Male	145	47 (32.41)	98 (67.59)	6.674	0.012
Female	60	31 (51.67)	29 (48.33)		
Age (yr)					
<60	101	37 (36.63)	64 (63.37)	0.169	0.774
≥60	104	41 (39.42)	63 (60.58)		
Size (cm)					
<3	29	11 (37.93)	18 (62.07)	0.000	1.000
≥3	176	67 (38.07)	109 (61.93)		
Location					
Center	106	38 (35.85)	68 (64.15)	0.451	0.565
Peripheral	99	40 (40.40)	59 (59.60)		
Histological classification					
SCC	79	23 (29.11)	56 (70.89)	8.222	0.016
AC	75	38 (50.67)	37 (49.33)		
LCC	51	17 (33.33)	34 (66.67)		
Differentiation					
Well	35	17 (48.57)	18 (51.43)	2.044	0.360
Moderate	87	32 (36.78)	55 (63.22)		
Poor	83	29 (34.94)	54 (65.06)		
Pleura invasion					
No	113	39 (34.51)	74 (65.49)	1.335	0.252
Yes	92	39 (42.39)	53 (57.61)		
Lymph node metastasis					
No	117	45 (38.46)	72 (61.54)	0.020	1.000
Yes	88	33 (37.50)	55 (62.50)		
T stage					
T1 + T2	149	56 (37.58)	93 (62.42)	0.050	0.872
T3 + T4	56	22 (39.29)	34 (60.71)		
Clinical stage					
I + II	158	62 (39.24)	96 (60.76)	0.415	0.609
III + IV	47	16 (34.04)	31 (65.96)		
Distant metastasis					
No	147	57 (38.78)	90 (61.22)	0.116	0.752
Yes	58	21 (36.21)	37 (63.79)		
Therapy before surgery					
No	186	69 (37.10)	117 (62.90)	0.772	0.458
Yes	19	9 (47.37)	10 (52.63)		

$P < 0.05$ means statistical significance.

negative location was found in 101 tissues, whereas β-catenin-nu positive and Wnt5a-negative samples included 6 cases (Table 2).

Table 2: Relationship between Wnt5a and angiogenesis, expression of related proteins, and β-catenin nuclear expression in NSCLC.

Variant	Total	Wnt5a		P value	r
	n	Negative (%)	Positive (%)		
CD34-MVD					
<28	92	52 (56.52)	40 (43.48)	0.026	0.157
≥28	113	46 (40.71)	67 (59.29)		
VM					
Negative	177	73 (41.24)	104 (58.76)	0.021	0.165
Positive	28	5 (17.86)	23 (82.14)		
VE-cadherin					
Negative	104	50 (48.08)	54 (51.92)	0.004	0.210
Positive	101	28 (27.72)	73 (72.28)		
MMP2					
Negative	138	65 (47.10)	73 (52.90)	<0.001	0.268
Positive	67	13 (19.40)	54 (80.60)		
MMP9					
Negative	125	58 (46.40)	67 (53.60)	0.003	0.215
Positive	80	20 (25.00)	60 (75.00)		
β-Catenin nuclear expression					
Negative	173	72 (41.62)	101 (58.38)	0.017	0.171
Positive	32	6 (18.75)	26 (81.25)		

$P < 0.05$ means statistical significance.

4. Discussion

The Wnt proteins family includes at least 19 secreted cysteine-rich glycoproteins that are involved in the regulation of a wide variety of normal and pathologic processes, including embryogenesis, differentiation, and tumorigenesis [26–30]. As one of the important members in the large Wnt family, Wnt5a has been shown to have close correlation with various cancers [13–15, 18].

In this study, expression of Wnt5a was investigated by immunohistochemistry in a large cohort of 205 human NSCLC tissues. The results showed that Wnt5a was upexpressed in the majority of cases. Except for histological classification and gender, Wnt5a-positive expression was found to exhibit little correlation with clinicopathological parameters. Wnt5a was more frequently expressed in squamous cell carcinoma. Our result was in accordance with the previous report. Huang and his colleagues examined Wnt5a expression in 123 NSCLC cases and found a similar result [20]. We also found that Wnt5a was more often expressed in male NSCLC patients, although none of the previous studies examined the relation between Wnt5a and gender in NSCLC [20, 31]. However, two studies strongly supported our result. Heikkila et al. reported that deficiency of Wnt5a could result in sex reversal, infertility, and/or malformation of the internal and external genitals [32]. In addition, Kovalchuk et al. concluded that Wnt signaling pathway, including Wnt5a, was differently induced between male and female mice after

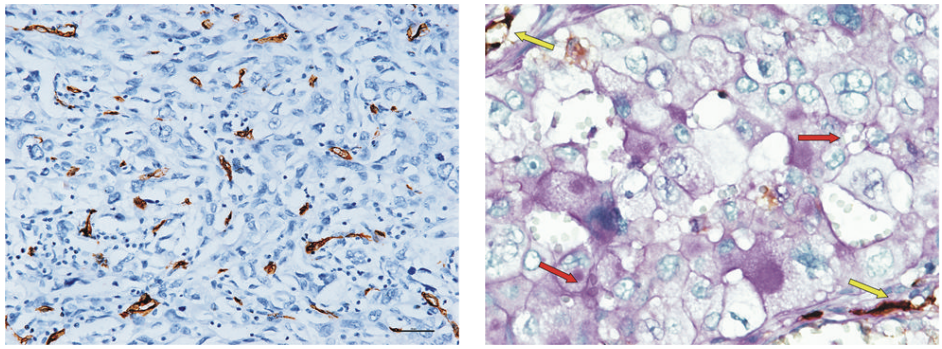

(a) (b)

Figure 3: The angiogenesis status in NSCLC. (a) MVD staining for CD34 in NSCLC (immunohistochemical staining, ×200). A hotspot with high MVD was positively stained. (b) CD31/PAS double staining for VM (×400). The VM channel showed a positive expression for PAS but a negative expression for CD31 (red arrow). The endothelial channel showed positive expressions for both CD31 and PAS (yellow arrow).

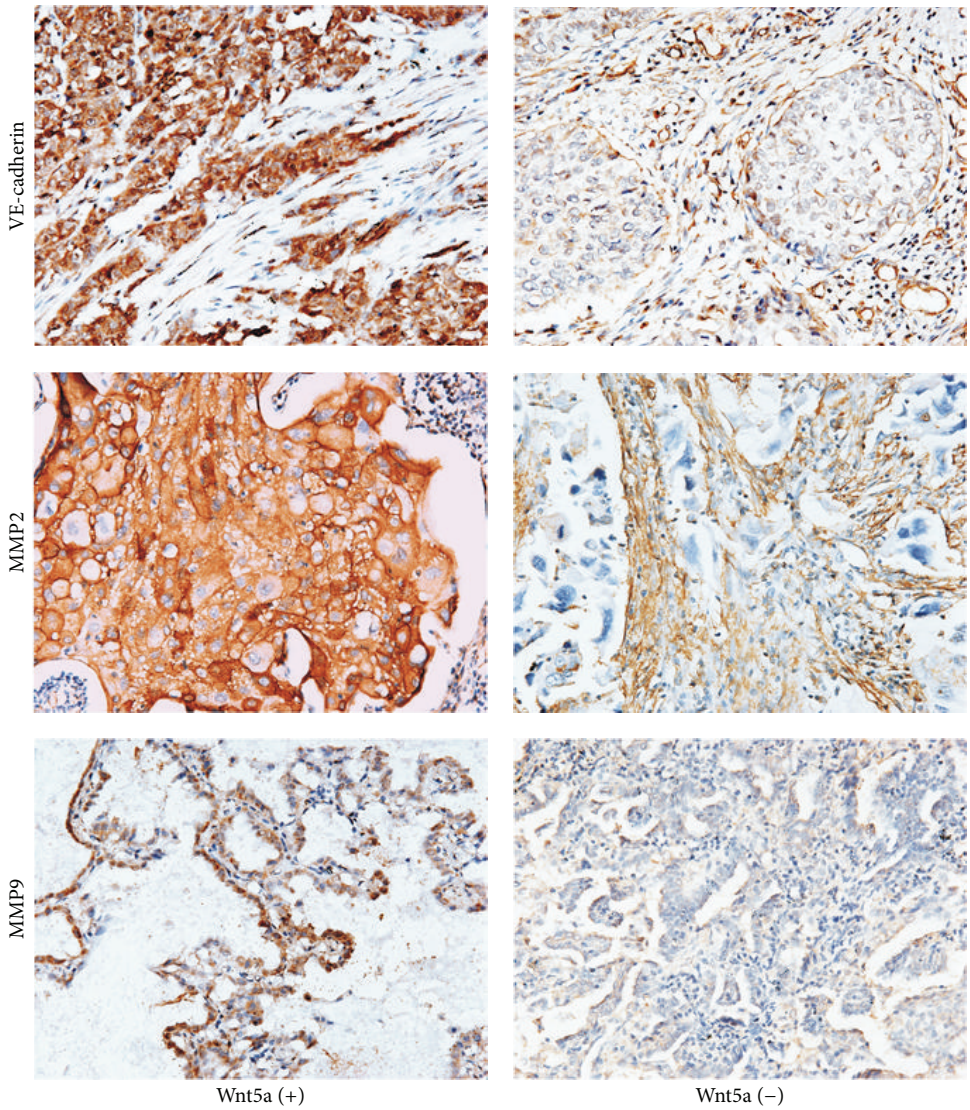

Figure 4: The expressions of some related proteins in NSCLC (immunohistochemical staining, ×200). In Wnt5a-positive group, positive expressions of VE-cadherin, MMP2, and MMP9 were all located in the cytoplasm of tumor cells. However, these proteins were negatively expressed in NSCLC tissues of Wnt5a-negative group. VE-cadherin positive expression in endothelial cells or MMPs positive expression in stromal cells could provide an internal positive control for both, respectively.

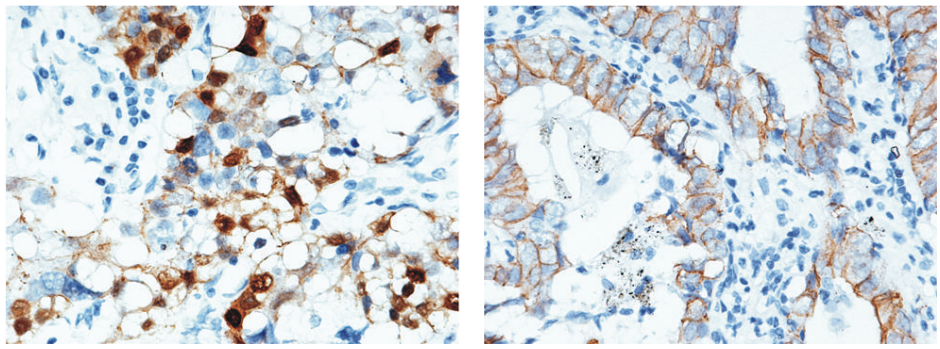

Figure 5: The expression of β-catenin in NSCLC (immunohistochemical staining, ×400). In Wnt5a-negative tissues, β-catenin exhibited the continuous expression in membrane, while in Wnt5a-positive group, β-catenin lost its continuous membrane expression and translocated to nucleus.

chronic radiation exposure [33]. Thus, we supposed that it may be related with sex hormone. Moreover, our data showed that overall survival time of those NSCLC patients with Wnt5a-positive expression was shorter than that of Wnt5a negative-expressed patients, which supported the results of Huang et al. and Nakashima et al. [20, 31]. Therefore, it may provide a good marker for clinical diagnosis and prognosis of NSCLC.

It is well known that a continuous supply of oxygen and nutrition is crucial for indefinite growth of solid tumors. Angiogenesis plays a vital role in development of tumor. Huang et al. investigated the relationship between Wnt5a and angiogenesis in 123 NSCLCs which included 67 cases of adenocarcinoma (AC), 50 cases of squamous cell carcinoma (SCC), and 6 cases of large cell carcinoma (LCC). They reported that the intratumoral Wnt5a expression was significantly correlated with the stromal expression of VEGF-A but insignificantly correlated with intratumoral microvessel density [20]. In this study, we also examined the relationship between Wnt5a and angiogenesis in NSCLC. Firstly, we evaluated the relation between Wnt5a and MVD, which is a classic marker of tumor angiogenesis. However, contrary to previous results [20], we found that there was significant correlation between Wnt5a and MVD in the present study. We supposed that it is due to the difference of object. Our study contained more samples including 205 NSCLC specimens. Moreover, the ratio for LCC was larger than Huang's study. As we know, LCC is a more progressive tumor in NSCLC. In addition, they only reported the relationship between Wnt5a and MVD, which only reflected the endothelial dependent vessel in the tumor. However, besides endothelial dependent vessel, Maniotis detected a novel blood supply mode, named vasculogenic mimicry (VM), in highly aggressive uveal melanomas [34]. Subsequently, many researchers have found VM in several malignant tumors [22, 35–40]. Thus, we also analyzed the correlation between Wnt5a and VM, which could reflect the blood supply of tumor at some degree. Statistical analysis showed that Wnt5a was positively correlated with VM. Wnt5a may play an important role in angiogenesis of NSCLC.

To further investigate the relationship between Wnt5a and angiogenesis, we conducted immunohistochemistry to examine expressions of some related proteins and analyzed their associations with Wnt5a. VE-cadherin, MMP2, and MMP9 have been proven to participate and represent partially VM [35, 39, 41]. Our data showed that Wnt5a was also positively associated with all the above proteins. The results further demonstrated that Wnt5a play an active role in angiogenesis of NSCLC.

We also detected β-catenin nuclear expression in NSCLC tissues and found it was positively correlated with Wnt5a. β-Catenin is a vital molecule of canonical Wnt signal pathway. Normally, β-catenin shows continuous membrane location, and while canonical Wnt pathway is activated, β-catenin shows translocation to nucleus. Thus, β-catenin nuclear expression is considered as an important marker for activated canonical Wnt pathway. Therefore, our data indicated that Wnt5a may function through canonical Wnt pathway. Though it was a member of noncanonical Wnt pathway, Wnt5a was reported to play a role in the canonical Wnt/β-catenin signaling pathway. The Wnt5a protein can act via Frz-5 receptor to initiate an intracellular pathway leading to the accumulation of β-catenin [20, 42].

5. Conclusions

Taken together, the current study demonstrated that Wnt5a was overexpressed in human NSCLC tissues and closely associated with tumor angiogenesis. Enhanced expression of Wnt5a may induce the nuclear accumulation of β-catenin and activate the canonical Wnt signaling pathway, thus leading to the upexpression of VE-cadherin, MMP2, and MMP9, then resulting in angiogenesis, and ultimately promoting the growth and metastasis of NSCLC. Therefore, this study may contribute to the mechanism of NSCLC research and provide new hope for NSCLC diagnosis and therapeutic strategies.

Conflict of Interests

The authors declare that there is no conflict of interests regarding the publication of this paper.

Authors' Contribution

The conception and design of the study, acquisition of data, most of immunohistochemical staining, analysis and interpretation of data, and drafting of the paper were performed by Lingli Yao. Baocun Sun and Xiulan Zhao made the decision of the conception and design of the study. Professor Sun is also responsible for this paper. All 4 μm slides, H&E staining, and CD31/PAS staining were performed by Xueming Zhao, Qiang Gu, and Xueyi Dong. Some supporting works, such as followup and collecting patients' records, were accomplished by Yanjun Zheng, Junying Sun, and Jindan An. A small part of immunohistochemical staining was performed by Runfen Cheng and Hong Qi. Lingli Yao, Baocun Sun, and Xiulan Zhao equally contributed to this study.

Acknowledgments

This work was supported by Grants from the Key project of the National Natural Science Foundation of China (no. 81230050), the National Natural Science Foundation of China (nos. 81172046 and 81173091), and the Key Project of the Tianjin Natural Science Foundation (no. 12JCZDJC23600).

References

[1] R. Siegel, J. Ma, Z. Zou, and A. Jemal, "Cancer statistics, 2014," *CA: A Cancer Journal for Clinicians*, vol. 64, pp. 9–29, 2014.

[2] M. B. Beasley, E. Brambilla, and W. D. Travis, "The 2004 World Health Organization classification of lung tumors," *Seminars in Roentgenology*, vol. 40, no. 2, pp. 90–97, 2005.

[3] L. Tao, G. Huang, S. Shi, and L. Chen, "Bevacizumab improves the antitumor efficacy of adoptive cytokine-induced killer cells therapy in non-small cell lung cancer models," *Medical Oncology*, vol. 31, p. 777, 2014.

[4] A. Pircher, I. K. Wasle, M. Mian et al., "Docetaxel in the treatment of non-small cell lung cancer (NSCLC)—an observational study focusing on symptom improvement," *Anticancer Research*, vol. 33, pp. 3831–3836, 2013.

[5] M. Christodoulou, N. Bayman, P. McCloskey, C. Rowbottom, and C. Faivre-Finn, "New radiotherapy approaches in locally advanced non-small cell lung cancer," *European Journal of Cancer*, vol. 50, pp. 525–534, 2014.

[6] V. L. Keedy, S. Temin, M. R. Somerfield et al., "American Society of clinical oncology provisional clinical opinion: epidermal growth factor receptor (EGFR) mutation testing for patients with advanced non-small-cell lung cancer considering first-line EGFR tyrosine kinase inhibitor therapy," *Journal of Clinical Oncology*, vol. 29, no. 15, pp. 2121–2127, 2011.

[7] J. Folkman, "Tumor angiogenesis: therapeutic implications," *The New England Journal of Medicine*, vol. 285, no. 21, pp. 1182–1186, 1971.

[8] J. Folkman, "Angiogenesis in cancer, vascular, rheumatoid and other disease," *Nature Medicine*, vol. 1, no. 1, pp. 27–31, 1995.

[9] H. Park, H. Y. Jung, H. J. Choi et al., "Distinct roles of DKK1 and DKK2 in tumor angiogenesis," *Angiogenesis*, vol. 17, pp. 221–234, 2014.

[10] J. A. Stefater III, I. Lewkowich, S. Rao et al., "Regulation of angiogenesis by a non-canonical Wnt-Flt1 pathway in myeloid cells," *Nature*, vol. 474, no. 7352, pp. 511–516, 2011.

[11] T. N. H. Masckauchán, D. Agalliu, M. Vorontchikhina et al., "Wnt5a signaling induces proliferation and survival of endothelial cells in vitro and expression of MMP-1 and Tie-2," *Molecular Biology of the Cell*, vol. 17, no. 12, pp. 5163–5172, 2006.

[12] R. Cheng, B. Sun, Z. Liu et al., "Wnt5a suppresses colon cancer by inhibiting cell proliferation and epithelial-mesenchymal transition," *Journal of Cellular Physiology*, 2014.

[13] M. Fernandez-Cobo, F. Zammarchi, J. Mandeli, J. F. Holland, and B. G. T. Pogo, "Expression of Wnt5A and Wnt10B in non-immortalized breast cancer cells," *Oncology Reports*, vol. 17, no. 4, pp. 903–907, 2007.

[14] H. Bo, S. Zhang, L. Gao et al., "Upregulation of Wnt5a promotes epithelial-to-mesenchymal transition and metastasis of pancreatic cancer cells," *BMC Cancer*, vol. 13, article 496, 2013.

[15] G. T. Lee, D. I. Kang, Y. S. Ha et al., "Prostate cancer bone metastases acquire resistance to androgen deprivation via WNT5A-mediated BMP-6 induction," *The British Journal of Cancer*, vol. 110, pp. 1634–1644, 2014.

[16] M. Kanzawa, S. Semba, S. Hara, T. Itoh, and H. Yokozaki, "WNT5A is a key regulator of the epithelial-mesenchymal transition and cancer stem cell properties in human gastric carcinoma cells," *Pathobiology*, vol. 80, no. 5, pp. 235–244, 2013.

[17] W. Jiang, D. K. Crossman, E. H. Mitchell, P. Sohn, M. R. Crowley, and R. Serra, "WNT5A inhibits metastasis and alters splicing of Cd44 in breast cancer cells," *PLoS ONE*, vol. 8, no. 3, Article ID e58329, 2013.

[18] L. Bi, X. Liu, C. Wang et al., "Wnt5a involved in regulation of the biological behavior of hepatocellular carcinoma," *International Journal of Clinical and Experimental Pathology*, vol. 7, pp. 987–995, 2014.

[19] D.-H. Yang, J.-Y. Yoon, S.-H. Lee et al., "Wnt5a is required for endothelial differentiation of embryonic stem cells and vascularization via pathways involving both Wnt/β-Catenin and protein kinase Cα," *Circulation Research*, vol. 104, no. 3, pp. 372–379, 2009.

[20] C.-L. Huang, D. Liu, J. Nakano et al., "Wnt5a expression is associated with the tumor proliferation and the stromal vascular endothelial growth factor—an expression in non-small-cell lung cancer," *Journal of Clinical Oncology*, vol. 23, no. 34, pp. 8765–8773, 2005.

[21] W. D. Travis, E. Brambilla, M. Noguchi et al., "International association for the study of lung cancer/American Thoracic Society/European Respiratory Society international multidisciplinary classification of lung adenocarcinoma," *Journal of Thoracic Oncology*, vol. 6, no. 2, pp. 244–285, 2011.

[22] Y. Zhang, B. Sun, X. Zhao et al., "Clinical significances and prognostic value of cancer stem-like cells markers and vasculogenic mimicry in renal cell carcinoma," *Journal of Surgical Oncology*, vol. 108, no. 6, pp. 414–419, 2013.

[23] T. Sun, N. Zhao, X.-L. Zhao et al., "Expression and functional significance of Twist1 in hepatocellular carcinoma: its role in vasculogenic mimicry," *Hepatology*, vol. 51, no. 2, pp. 545–556, 2010.

[24] T. Sun, B.-C. Sun, X.-L. Zhao et al., "Promotion of tumor cell metastasis and vasculogenic mimicry by way of transcription coactivation by Bcl-2 and Twist1: a study of hepatocellular carcinoma," *Hepatology*, vol. 54, no. 5, pp. 1690–1706, 2011.

[25] M. Bittner, P. Meltzer, Y. Chen et al., "Molecular classification of cutaneous malignant melanoma by gene expression profiling," *Nature*, vol. 406, no. 6795, pp. 536–540, 2000.

[26] C. Lange, E. Mix, K. Rateitschak, and A. Rolfs, "Wnt signal pathways and neural stem cell differentiation," *Neurodegenerative Diseases*, vol. 3, no. 1-2, pp. 76–86, 2006.

[27] D. Herzlinger, J. Qiao, D. Cohen, N. Ramakrishna, and A. M. C. Brown, "Induction of kidney epithelial morphogenesis by cells expressing Wnt-1," *Developmental Biology*, vol. 166, no. 2, pp. 815–818, 1994.

[28] T. C. Dale, "Signal transduction by the Wnt family of ligands," *Biochemical Journal*, vol. 329, no. 2, pp. 209–223, 1998.

[29] Z. You, D. Saims, S. Chen et al., "Wnt signaling promotes oncogenic transformation by inhibiting c-Myc-induced apoptosis," *Journal of Cell Biology*, vol. 157, no. 3, pp. 429–440, 2002.

[30] T. Reya and H. Clevers, "Wnt signalling in stem cells and cancer," *Nature*, vol. 434, no. 7035, pp. 843–850, 2005.

[31] N. Nakashima, C.-L. Huang, D. Liu, M. Ueno, and H. Yokomise, "Intratumoral Wnt1 expression affects survivin gene expression in non-small cell lung cancer," *International Journal of Oncology*, vol. 37, no. 3, pp. 687–694, 2010.

[32] M. Heikkil, H. Peltoketo, and S. Vainio, "Wnts and the female reproductive system," *Journal of Experimental Zoology*, vol. 290, no. 6, pp. 616–623, 2001.

[33] O. Kovalchuk, A. Ponton, J. Filkowski, and I. Kovalchuk, "Dissimilar genome response to acute and chronic low-dose radiation in male and female mice," *Mutation Research*, vol. 550, no. 1-2, pp. 59–72, 2004.

[34] A. J. Maniotis, R. Folberg, A. Hess et al., "Vascular channel formation by human melanoma cells in vivo and in vitro: vasculogenic mimicry," *The American Journal of Pathology*, vol. 155, no. 3, pp. 739–752, 1999.

[35] J. Du, B. Sun, X. Zhao et al., "Hypoxia promotes vasculogenic mimicry formation by inducing epithelial-mesenchymal transition in ovarian carcinoma," *Gynecologic Oncology*, 2014.

[36] H. J. Chung and M. Mahalingam, "Angiogenesis, vasculogenic mimicry and vascular invasion in cutaneous malignant melanoma—implications for therapeutic strategies and targeted therapies," *Expert Review of Anticancer Therapy*, vol. 14, no. 5, pp. 621–639, 2014.

[37] J. T. Zhang, W. Sun, W. Z. Zhang et al., "Norcantharidin inhibits tumor growth and vasculogenic mimicry of human gallbladder carcinomas by suppression of the PI3-K/MMPs/Ln-5gamma2 signaling pathway," *BMC Cancer*, vol. 14, article 193, 2014.

[38] F. Luo, K. Yang, R. L. Liu, C. Meng, R. F. Dang, and Y. Xu, "Formation of vasculogenic mimicry in bone metastasis of prostate cancer: correlation with cell apoptosis and senescence regulation pathways," *Pathology: Research and Practice*, vol. 210, pp. 291–295, 2014.

[39] K. Chiablaem, K. Lirdprapamongkol, S. Keeratichamroen, R. Surarit, and J. Svasti, "Curcumin suppresses vasculogenic mimicry capacity of hepatocellular carcinoma cells through STAT3 and PI3K/AKT inhibition," *Anticancer Research*, vol. 34, pp. 1857–1864, 2014.

[40] Y. S. Chen and Z. P. Chen, "Vasculogenic mimicry: a novel target for glioma therapy," *Chinese Journal of Cancer*, vol. 33, pp. 74–79, 2014.

[41] W.-B. Liu, G.-L. Xu, W.-D. Jia et al., "Prognostic significance and mechanisms of patterned matrix vasculogenic mimicry in hepatocellular carcinoma," *Medical Oncology*, vol. 28, supplement 1, pp. S228–S238, 2011.

[42] X. He, J.-P. Saint-Jeannet, Y. Wang, J. Nathans, I. Dawid, and H. Varmus, "A member of the frizzled protein family mediating axis induction by Wnt-5A," *Science*, vol. 275, no. 5306, pp. 1652–1654, 1997.

Hindawi Publishing Corporation
BioMed Research International
Volume 2014, Article ID 981261, 7 pages
http://dx.doi.org/10.1155/2014/981261

Research Article

Stem Cell-Like Circulating Tumor Cells Indicate Poor Prognosis in Gastric Cancer

Man Li,[1] Baogang Zhang,[2] Zhiguang Zhang,[1] Xia Liu,[1] Xiangjuan Qi,[1] Jianqiu Zhao,[1] Yong Jiang,[1] Haoyu Zhai,[1] Yinglan Ji,[1] and Dan Luo[1]

[1] *Department of Digestive, The Second Hospital of Tianjin Medical University, Tianjin 300211, China*
[2] *Tianjin Children Hospital, Tianjin 300074, China*

Correspondence should be addressed to Zhiguang Zhang; zhiguang_zh@sina.com

Received 22 April 2014; Revised 11 May 2014; Accepted 12 May 2014; Published 22 May 2014

Academic Editor: Shiwu Zhang

Circulating tumor cells (CTCs), which have stem cell-like characteristics, might play a crucial role in cancer metastasis. CD44 has been identified as gastric cancer (GC) stem cell (CSC) marker. Here, the prognostic significance of CD44-positive CTCs in GC patients was investigated. CTCs were detected in 27 of 45 GC patients. The presence of CTCs was significantly associated with lymph node metastasis, distant metastasis, and recurrence ($P = 0.007$, $P = 0.035$, and $P = 0.035$, resp.). Nineteen of the 27 CTC-positive patients had CD44-positive CTCs. These patients were more likely to develop metastasis and recurrence than patients with CD44-negative CTCs. CD44-positive CTC counts were higher in recurrent patients than in the nonrecurrent ones (means 4.8 and 1.9, resp.; $P = 0.010$). Furthermore, 13 of 19 patients with CD44-positive CTCs developed recurrent disease, and the mean time to recurrence was shorter than that in patients with CD44-negative CTCs (10.54 ± 5.55 and 19.13 ± 9.72 months, resp.; $P = 0.04$). COX proportional hazards model indicated that the presence of CD44-positive CTCs and TNM stage were independent predictors of recurrence for GC ($P = 0.030$ and 0.008). So identifying the stem cell-like CTC subset may provide more clinically useful prognostic information than only detecting CTCs.

1. Introduction

Gastric cancer (GC) is the second leading cause of cancer-related deaths in the world [1]. Despite advances in diagnostic tools and therapeutic methods, the 5-year relative survival rate is still less than 30% [2]. Common causes of death in GC patients are recurrent and metastatic disease.

Recently, many studies in medical science have focused on disseminated tumor cells present in patients' blood, known as circulating tumor cells (CTCs), which correlate with the risk of recurrence and metastasis in cancer patients. CTCs could be detected in cancer patients with no clinically detectable metastasis and the presence of CTCs is associated with poor patient prognosis [3, 4]. However, not all CTCs have the potency to develop into metastasis. Only the small population of CTCs with stem cell-like properties can survive and migrate to distant sites to establish secondary tumors. These cells are called circulating tumor stem cells (CTSC) and have the ability to self-renew, proliferate, and initiate tumors similar to cancer stem cells (CSCs) [5].

Recent advances in technology have allowed the detection and characterization of CTCs in GC. It has been shown that presence of CTCs is an independent predictive marker of poor prognosis in GC patients [6]. However, no studies investigating the prognostic and biological relevance of CTSC in GC patients have been reported. In previously published work, CD44-positive GC cells were highly invasive and exhibited the stem cell property of self-renewal [7]. Thus, CD44 might be served as a biomarker for tumor-initiating cells in GC.

Here, we identified GC patients with CD44-positive CTCs and evaluated their clinical characteristics to test the

hypothesis that these represent more aggressive stem cell-like subpopulation of CTCs in GC.

2. Materials and Methods

2.1. Tissue Specimens. Blood samples from 45 GC patients being treated at the 2nd Hospital of Tianjin Medical University from March 2010 to December 2012 were obtained before the initiation of treatment. Detailed clinicopathological data, including age, gender, tumor location, TNM stage, and distant and lymph node metastasis, were collected by reviewing medical charts and pathological records for all of the patients. Clinical outcome was followed from the date of diagnosis until December 2013. The diagnoses of recurrence and metastasis were based on the computed tomography scans, with or without histological confirmation. Blood samples from 20 healthy volunteers acted as controls. The study was approved by the local ethics committee. Informed consent was obtained from both GC patients and cancer-free volunteers before obtaining samples.

2.2. Sample Preparation. Approximately 10 mL blood was collected in EDTA vacutainer tubes after discarding the first 2 mL of blood to avoid contamination of the blood sample with epithelial cells of skin. Peripheral blood mononuclear cells (PBMCs) were isolated by density gradient centrifugation using Lymphocyte Separation Medium (Tianjin Chuanye Biochemical Co., Ltd.). The mononuclear cells then were washed twice with 1 × phosphate buffered saline (PBS) and centrifuged at 1800 rpm for 10 min. The cells were resuspended in 100 μL 1 × PBS and spread onto glass slides using a cytocentrifuge, prior to being fixed with 4% methanol. Fixed slides were stored at −80°C until use. Two slides from each patient were used for staining experiments.

The human gastric cancer cell line BGC-823 was obtained from the Tianjin Cancer Research Institute. To determine assay sensitivity, 10 BGC-823 cells were added to 10 mL of blood from healthy volunteersprior to being processed as described above for patients' samples.

2.3. Double Immunofluorescent Staining to Detect CK19 and CD44. Cytospin preparations were washed in 1 × PBS at room temperature for 15 min and permeabilized with Triton X-100. Following blocking with undiluted normal goat serum for 1 h, the samples were incubated with CK19 rabbit polyclonal antibody (dilution 1 : 100, BA2266-1, Boster, China) and Leukocyte Common Antigen (LCA/CD45, mouse monoclonal antibody, dilution 1 : 100, ZM-0183, Zhongshan, China) for 1 h and washed for 10 min with blocking buffer, followed by incubation with CD44 mouse monoclonal antibody (sc-65265, Santa Cruz) diluted 1 : 100 in a dark, humid chamber to stay overnight. After at least 20 hours, cytospin preparations were washed in 1 × PBS at room temperature for 15 min again. The samples were incubated with FITC-conjugated rabbit anti-human IgG (dilution 1 : 100, ZF0306, Zhongshan, China) and Rhodamine (TRITC)-conjugated AffiniPure Goat Anti-mouse IgG (dilution 1 : 100, ZF0313, Zhongshan, China) for 60 min. Cells were postfixed with methanol for 5 min at −20°C, washed twice with 1 × PBS, and DNA stained with 4,6-diamino-2-phenylindole (DAPI). The samples were washed twice with PBS and mounted with coverslips.

The cytomorphological criteria proposed by Meng and colleagues [8] (e.g., high nuclear/cytoplasmic ratio and cells larger than white blood cells) were used to characterize a CK19-positive cell as a CTC. CTC-positive case was defined by the presence of at least 1 CTC per 10 mL sample.

CK19 and/or CD44 expression was analyzed by a computerized fluorescence microscope (Imager 090–135.001, Leica, Germany). Samples were visualized by light microscopy to identify CK19-positive-cells (green staining). After detection of CK19-positive cells, samples were analyzed by fluorescence microscopy to identify CD44-positive cells (red staining).

Five fields with the greatest number of CK19-positive CTCs or CD44/CK19 double positive CTCs were chosen to quantify the number of CTCs in the sample. The average count of five fields at 400x magnification was recorded as the mean count of CTCs (CK19-positive only) or CD44-positive CTCs (double CK19/CD44-positive cells).

2.4. Statistical Methods. Statistical analysis was conducted using the SPSS 16.0 software (SPSS, Chicago, IL, USA). Data are expressed either as mean ± standard deviation or as percentages. The χ^2 test, the Student's t-test, and Mann Whitney test were used to establish significance. Two-tailed $P < 0.05$ values were considered statistically significant. Kaplan-Meier survival analysis and log-rank test were performed to analyze the time to recurrence for the CTCs and CD44-positive CTCs groups. Multivariate recurrence analysis was performed using the COX proportional hazards model.

3. Results

3.1. Patient Characteristics. 45 GC patients, comprising 27 males and 18 females, with a mean age of 62.18 ± 10.57 years were included in the present study. The time to recurrence ranged from 1 to 45 months (mean 15.12 ± 9.03 months). Of the 45 patients, 25 had TNM stage I/II and 20 had TNM stage III/IV.

3.2. Definition of CTCs and CD44-Positive CTCs in GC Patients. A methodology that would permit specific double staining for CK19 and CD44, as well as DNA, in the same sample was established. Prior to this, we added 10 BGC-823 human gastric cancer cells into 10 mL blood obtained from healthy volunteers. In these spike-recovery experiments, the recovery rate of BCG-823 cells was approximately between 65% and 75%. CTCs were defined as nucleated intact cells that were positive for CK19 and negative for Leukocyte Common Antigen (LCA/CD45) (Figure 1). CK19-positive cells, defined here as CTCs, were further evaluated for the expression of CD44. Cells with CK19/CD44 both staining were defined as CD44-positive CTCs (Figure 2).

3.3. Relationships between CTCs and Clinicopathological Features of GC Patients. Detailed clinicopathological data and

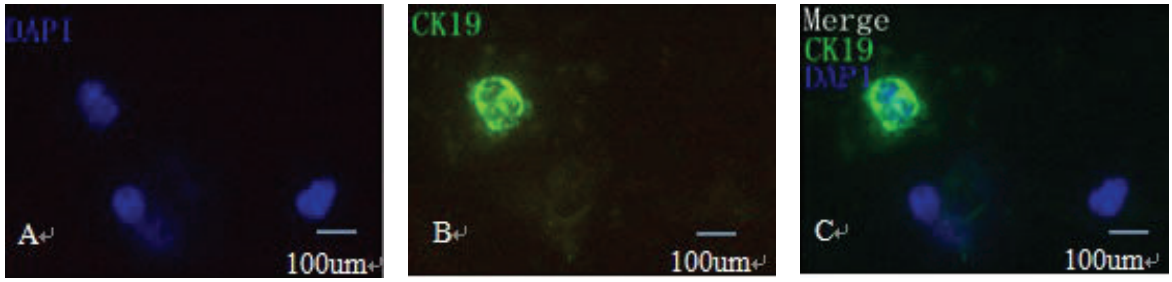

(a) (b) (c)

Figure 1: Detection of CTCs using immunofluorescent staining (×400). (a) Chromatin was decorated by the DNA-binding dye DAPI (blue staining). (b) CK19 was green staining. (c) A CTC was identified by CK19-positive staining with high nuclear/cytoplasmic ratio and cells larger than white blood cells.

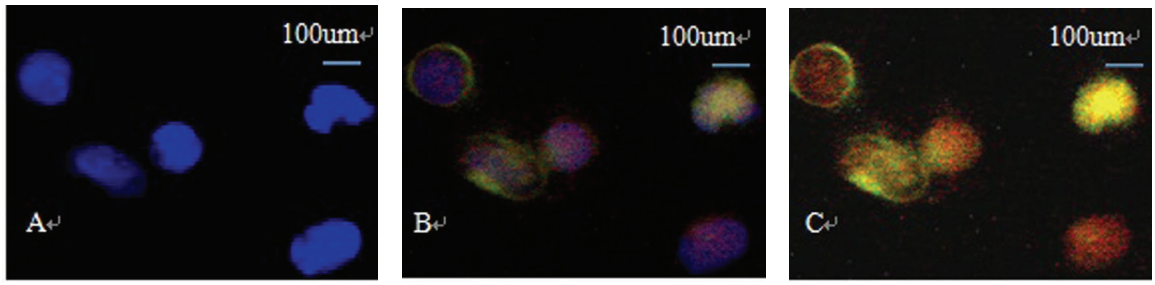

(a) (b) (c)

Figure 2: Detection of CD44-positive CTCs using double-immunofluorescent staining (×400). (a) Chromatin was decorated by the DNA-binding dye DAPI (blue staining). (b) CK19 was green staining. (c) CD44 (red) and CK19 (green) were costained.

CTC status in the GC patients included in this study are summarized in Table 1. The presence of CTCs was significantly associated with lymph node metastasis, distant metastasis, and recurrence of GC ($P = 0.007$, $P = 0.035$, and $P = 0.035$, resp.). Of the 45 GC patients analyzed, 27 (60.0%) were identified as CTC positive. Among the 27 CTC-positive patients, 19 patients (70.4%) and 15 patients (55.6%) developed lymph node and distant metastasis, respectively. Recurrence was observed in 15 of the 27 (55.6%) CTC-positive patients. No statistically significant difference was detected between the CTC-positive patients and the CTC-negative patients with respect to age, gender, tumor location, and TNM stage.

3.4. Relationships between CD44-Positive CTCs and Clinicopathological Features of GC Patients. Clinicopathological data and CD44-positive CTC status in the GC patients included in this study are summarized in Table 2. The incidence of CD44-positive CTCs was significantly associated with tumor location, lymph node metastasis, distant metastasis, and recurrence of GC ($P = 0.027$, $P = 0.033$, $P = 0.033$ and $P = 0.011$, resp.). CD44-positive CTCs were detected in 19 (70.4%) of the 27 CTC-positive patients (Table 1). Among the 19 patients with CD44-positive CTCs, 14 patients (73.7%) and 12 patients (63.2%) developed lymph node and distant metastasis, respectively. Of 27 patients with recurrent disease, 14 were positive for CTCs and 13 of the CTC-positive patients were also positive for CD44-positive CTCs. The number of CD44-positive CTCs was significantly higher in patients with recurrent disease than in disease free patients (mean number of CD44-positive CTC 4.8 and 1.9, resp.; $P = 0.010$). Furthermore, of the 19 patients that had CD44-positive CTCs, 13 patients (68.4%) developed recurrent disease (mean time to recurrence 10.54± 5.55 months) which was significantly shorter than the time to recurrence in the CTC-positive patients (mean time to recurrence 19.13 ± 9.72 months; $P = 0.04$; Figure 3). Finally, patients with gastric cardia cancer were more likely to have CD44-positive CTCs than gastric noncardia cancer patients (16 out of 19 patients and 3 out of 8 patients, resp.; $P = 0.027$). Cox proportional hazards model analysis was performed and showed that the presence of CD44-positive CTCs and the TNM stage were independent indicators of recurrence for GC ($P = 0.030$ and 0.008).

4. Discussion

Recently, circulating tumor cells (CTCs) have emerged as an important field of study in biomedical research. Detection of CTCs is an early marker of tumor recurrence occurring before clinical symptoms present. CTCs quantitation could serve as a "liquid biopsy" to predict poor prognosis in a number of epithelial-derived cancers [9–11].

Most recent studies investigating CTCs have been carried out in breast cancer. There have been fewer studies focusing

Table 1: The relation between CTCs and clinicopathological data of GC patients.

Characteristic	Total	CTC		χ^2	P
		Positive	Negative		
Gender					
Male	27	19	8	3.025	0.122
Female	18	8	10		
Age					
≥60	29	20	9	2.732	0.122
<60	16	7	9		
Tumor location					
Proximal	32	21	11	1.46	0.317
Distant	13	6	7		
Histologic grade					
Poorly differentiated	23	13	10	0.237	0.763
Well differentiated	22	14	8		
Lymph node metastasis					
Positive	24	19	5	7.872	0.007
Negative	21	8	13		
Distant metastasis					
Positive	19	15	4	4.919	0.035
Negative	26	12	14		
TNM stage					
I-II	25	18	7	3.375	0.125
III-IV	20	9	11		
Recurrence					
Positive	19	15	4	4.919	0.035
Negative	26	12	14		

Table 2: The relation between CD44-positive CTCs and clinicopathological data of GC patients.

Characteristic	Total	CD44 + CTCs		χ^2	P
		Positive	Negative		
Gender					
Male	18	13	5	0.089	1
Female	9	6	3		
Age					
≥60	18	12	6	0.355	0.676
<60	9	7	2		
Tumor location					
Proximal	19	16	3	5.891	0.027
Distant	8	3	5		
Histologic grade					
Poorly differentiated	15	12	3	1.501	0.398
Well differentiated	12	7	5		
Lymph node metastasis					
Positive	16	14	2	5.527	0.033
Negative	11	5	6		
Distant metastasis					
Positive	13	12	1	5.787	0.033
Negative	14	7	7		
Recurrence					
Positive	14	13	1	7.052	0.011
Negative	13	6	7		

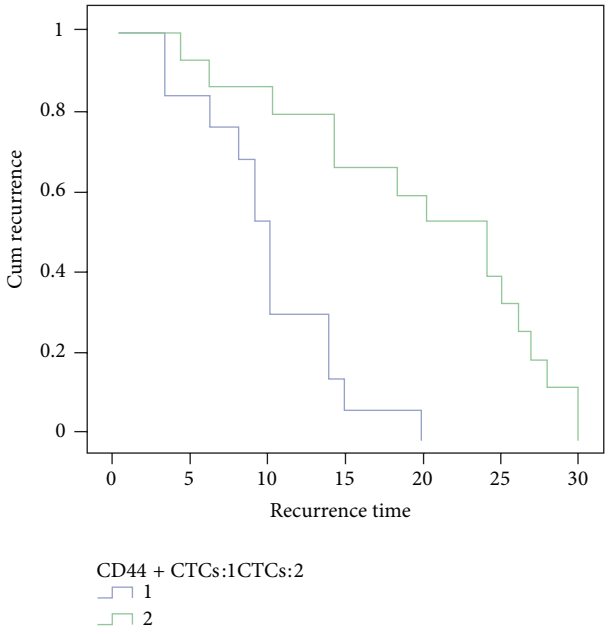

Figure 3: The recurrent time of CD44-positive CTCs group was shorter than that of CTCs group.

on CTCs in gastric cancer and the results from these studies have been inconsistent [12].

Biotechnology advances have allowed the detection and characterization of CTCs in cancer patients. Because CTCs occurat very low numbers, a blood volume of at least 7.5 mL is generally required for analysis. In general, analysis of CTCs involves primary enrichment followed by CTC detection. Enrichment may be achieved using various methodologies based on physical properties and biological properties of CTCs which differentiate them from the normal blood cells [13]. In our research, density gradient centrifugation was used to enrich CTCs. Immunofluorescence was used to identify CTCs, which were defined as CK19 positive (a marker for epithelial tumor cells) and CD45 negative (the common leukocyte antigen), while DNA was detected with DAPI. These approaches have been proven to be both sensitive and effective [14].

Gastric cancer is the most frequent malignancy in the world. Although many advances have been made in the early diagnosis and surgical treatment, patient prognosis remains poor. The major cause of death from GC is the inability to detect and prevent metastasis at an early stage of disease. Several studies investigating the presence of CTCs in gastric cancer patients have been reported in the literature, but both the CTC detection techniques used and the results obtained were heterogeneous [15–17]. And most of these studies focused on the sensitivity and specificity of CTCs isolation, as well as the relationship between CTCs and cancer relapse.

CTCs could be regarded as progenitors of cancer relapse. However, the presence of CTCs in the circulation is not sufficient to initiate metastasis because only a minority of the CTCs may possess the stem cell-like properties required to reseed or metastasize to distant organs. This has led to the hypothesis that CTCs may have the hallmarks of cancer stem cells (CSCs) which could allow them to form a tumor at a distant site. Recent studies have demonstrated that stem cell markers are frequently overexpressed in CTCs [18, 19]. Sun et al. have reported that the presence of circulating stem cell-like epithelial cell adhesion molecule-positive (EpCAM) tumor cells is associated with a poor prognosis for hepatocellular carcinoma patients following curative resection [20].

Therefore, we hypothesized that identifying the stem cell-like CTC subpopulation would provide more prognostic information than CTC quantitation alone. In our present study, we tested whether CTCs with CSCs properties play a crucial role in the spread of cancer in GC patients.

Zhang et al. and Takaishi et al. have demonstrated that CD44-positive gastric cancer cells exhibit the properties of self-renewal and the ability to produce differentiated progeny, both of which are consistent with a CSC phenotype [7, 21]. Accordingly, we used CD44 as a putative stem cell marker to identify CTSC in this study.

In our prospective study of 45 GC patients, we found that the presence of CTCs was correlated with tumor metastasis and recurrence. 27 of 45 GC patients were identified as CTCs positively by immunofluorescent technology. Among them, 19 and 15 patients have developed lymph node and distant metastasis, respectively. Recurrence was observed in 15 of 27 CTCs-positive patients. This data suggest that the presence of CTCs is a potential indicator of poor prognosis for GC patients. These results are in agreement with other reports in the literature for both gastrointestinal and other [22, 23]. Based on these results, we carried out double immunofluorescent staining to determine if CD44-positive CTCs, with a more stem cell-like phenotype, represent a more aggressive subset of CTCs. The presence of CTCs is known to be necessary but not sufficient for the initiation of metastasis because only a minority cells possess the stem cell-like properties necessary to survive and reseed a tumor at a distant site. Thus, detection of CD44-positive CTCs might serve as a novel marker for clinically undetectable metastases and recurrence risk for GC patients. Our data indicate that patients with CD44-positive CTCs were more likely to develop metastases and experience disease recurrence than patients with only CTCs. Our results show that CD44-positive CTCs were identified in 19 of 27 CTCs-positive patients. Those subpopulations were easily to develop metastasis and recurrence than that only CTCs-positive group. The incidence of lymph node metastasis, distant metastasis, and recurrence for two groups were shown as follows: 14/19 (73.68%) versus 19/27 (70.37%), 12/19 (63.16%) versus 15/27 (55.56%), and 13/19 (68.42) versus 15/27 (55.56%), respectively. In addition, the mean time to recurrence was shorter in patients with CD44-positive CTCs. Additionally, we found that CD44-positive CTCs were more often detected in patients with gastric cardia cancer. This could explain the more severe malignancy observed in gastric cardia cancer than in the noncardia GC and should be further investigated.

In conclusion, our data suggest that identifying stem cell-like CTCs would provide more specific prognostic information regarding recurrence risk than merely detecting

CTCs. Whether CTCs from GC patients embed stem cell-like characteristics still requires more extensive prospective studies. To our knowledge, this is the first report to identify the stem cell-like characteristics of CTCs and their prognostic significance in GC patients. Further molecular analysis of CTCs is needed to define possible targets for prevention and potentially treat micrometastasis to improve GC patient outcomes.

Abbreviations

CTCs: Circulating tumor cells
GC: Gastric cancer
CSC: Cancer stem cell
CTSC: Circulating tumor stem cells
PBMCs: Peripheral blood mononuclear cells
PBS: Phosphate buffered saline
DAPI: 4,6-Diamino-2-phenylindole
LCA: Leukocyte Common Antigen.

Conflict of Interests

The authors declare that there is no conflict of interests regarding the publication of this paper.

Authors' Contribution

Man Li and Baogang Zhang contributed equally to this work.

Acknowledgments

The work was supported by grants from the natural fund of Tianjin Medical University (2008ky28) and Tianjin Education Committee Nature fund (20110130).

References

[1] M. E. Han, Y. S. Lee, S. Y. Baek, B. S. Kim, J. B. Kim, and S. O. Oh, "Hedgehog signaling regulates the survival of gastric cancer cells by regulating the expression of Bcl-2," *International Journal of Molecular Sciences*, vol. 10, no. 7, pp. 3033–3043, 2009.

[2] M. Correia, J. C. Machado, and A. Ristimaki, "Basic aspects of gastric cancer," *Helicobacter*, vol. 14, supplement 1, pp. 36–40, 2009.

[3] I. Baccelli, A. Schneeweiss, S. Riethdorf et al., "Identification of a population of blood circulating tumor cells from breast cancer patients that initiates metastasis in a xenograft assay," *Nature Biotechnology*, vol. 31, no. 6, pp. 539–544, 2013.

[4] S. J. Cohen, C. J. Punt, N. Iannotti et al., "Relationship of circulating tumor cells to tumor response, progression-free survival, and overall survival in patients with metastatic colorectal cancer," *Journal of Clinical Oncology*, vol. 26, no. 19, pp. 3213–3221, 2008.

[5] I. Tinhofer, M. Saki, F. Niehr, and V. Budach, "Cancer stem cell characteristics of circulating tumor cells," *International Journal of Radiation Biology*, 2014.

[6] B. Illert, M. Fein, C. Otto et al., "Disseminated tumor cells in the blood of patients with gastric cancer are an independent predictive marker of poor prognosis," *Scandinavian Journal of Gastroenterology*, vol. 40, no. 7, pp. 843–849, 2005.

[7] S. Takaishi, T. Okumura, S. Tu et al., "Identification of gastric cancer stem cells using the cell surface marker CD44," *Stem Cells*, vol. 27, no. 5, pp. 1006–1020, 2009.

[8] S. Meng, D. Tripathy, E. P. Frenkel et al., "Circulating tumor cells in patients with breast cancer dormancy," *Clinical Cancer Research*, vol. 10, no. 24, pp. 8152–8162, 2004.

[9] Z. F. Jiang, M. Cristofanilli, Z. M. Shao et al., "Circulating tumor cells predict progression-free and overall survival in Chinese patients with metastatic breast cancer, HER2-positive or triple-negative (CBCSG004): a multicenter, double-blind, prospective trial," *Annals of Oncology*, vol. 24, no. 11, pp. 2766–2772, 2013.

[10] T. J. Hiltermann, M. M. Pore, A. van den Berg et al., "Circulating tumor cells in small-cell lung cancer: a predictive and prognostic factor," *Annals of Oncology*, vol. 23, no. 11, pp. 2937–2942, 2012.

[11] C. Alix-Panabieres and K. Pantel, "Circulating tumor cells: liquid biopsy of cancer," *Clinical Chemistry*, vol. 59, no. 1, pp. 110–118, 2013.

[12] G. Lurje, M. Schiesser, A. Claudius, and P. M. Schneider, "Circulating tumor cells in gastrointestinal malignancies: current techniques and clinical implications," *Journal of Oncology*, vol. 2010, Article ID 392652, 9 pages, 2010.

[13] C. Alix-Panabieres and K. Pantel, "Technologies for detection of circulating tumor cells: facts and vision," *Lab on a Chip*, vol. 14, no. 1, pp. 57–62, 2014.

[14] Y. Zhang, J. Li, L. Cao, W. Xu, and Z. Yin, "Circulating tumor cells in hepatocellular carcinoma: detection techniques, clinical implications, and future perspectives," *Seminars in Oncology*, vol. 39, no. 4, pp. 449–460, 2012.

[15] A. A. Saad, N. M. Awed, N. N. A. Abd Elkerim et al., "Prognostic significance of E-cadherin expression and peripheral blood micrometastasis in gastric carcinoma patients," *Annals of Surgical Oncology*, vol. 17, no. 11, pp. 3059–3067, 2010.

[16] S. M. Yie, B. Lou, S. Ye et al., "Detection of survivin-expressing circulating cancer cells (CCCs) in peripheral blood of patients with gastric and colorectal cancer reveals high risks of relapse," *Annals of Surgical Oncology*, vol. 15, no. 11, pp. 3073–3082, 2008.

[17] T. Koga, E. Tokunaga, Y. Sumiyoshi et al., "Detection of circulating gastric cancer cells in peripheral blood using real time quantitative RT-PCR," *Hepato-Gastroenterology*, vol. 55, no. 84, pp. 1131–1135, 2008.

[18] N. Wang, L. Shi, H. Li et al., "Detection of circulating tumor cells and tumor stem cells in patients with breast cancer by using flow cytometry," *Tumor Biology*, vol. 33, no. 2, pp. 561–569, 2012.

[19] P. A. Theodoropoulos, H. Polioudaki, S. Agelaki et al., "Circulating tumor cells with a putative stem cell phenotype in peripheral blood of patients with breast cancer," *Cancer Letters*, vol. 288, no. 1, pp. 99–106, 2010.

[20] Y. F. Sun, Y. Xu, X. R. Yang et al., "Circulating stem cell-like epithelial cell adhesion molecule-positive tumor cells indicate poor prognosis of hepatocellular carcinoma after curative resection," *Hepatology*, vol. 57, no. 4, pp. 1458–1468, 2013.

[21] C. Zhang, C. Li, F. He, Y. Cai, and H. Yang, "Identification of CD44+CD24+ gastric cancer stem cells," *Journal of Cancer Research and Clinical Oncology*, vol. 137, no. 11, pp. 1679–1686, 2011.

[22] S. Matsusaka, K. Chìn, M. Ogura et al., "Circulating tumor cells as a surrogate marker for determining response to chemotherapy in patients with advanced gastric cancer," *Cancer Science*, vol. 101, no. 4, pp. 1067–1071, 2010.

[23] M. Cristofanilli, G. T. Budd, M. J. Ellis et al., "Circulating tumor cells, disease progression, and survival in metastatic breast cancer," *The New England Journal of Medicine*, vol. 351, no. 8, pp. 781–791, 2004.

Hindawi Publishing Corporation
BioMed Research International
Volume 2014, Article ID 803914, 10 pages
http://dx.doi.org/10.1155/2014/803914

Research Article

Epithelial-Mesenchymal Transition Regulated by EphA2 Contributes to Vasculogenic Mimicry Formation of Head and Neck Squamous Cell Carcinoma

Wei Wang,[1,2] Peng Lin,[1] Baocun Sun,[2,3] Shiwu Zhang,[4] Wenjuan Cai,[2,5] Chunrong Han,[2] Li Li,[1] Honghua Lu,[1] and Xiulan Zhao[3]

[1] *Department of Otorhinolaryngology Head and Neck, Institute of Otorhinolaryngology, Tianjin First Central Hospital, Tianjin 300192, China*
[2] *Department of Pathology, Tianjin Cancer Hospital, Tianjin Medical University, Tianjin 300060, China*
[3] *Department of Pathology, Tianjin Medical University, Tianjin 300070, China*
[4] *Department of Pathology, University of Texas, MD Anderson Cancer Center, Houston, TX 77030, USA*
[5] *Department of Pathology, Tianjin First Central Hospital, Tianjin 300192, China*

Correspondence should be addressed to Baocun Sun; baocunsun@gmail.com

Received 1 January 2014; Accepted 5 March 2014; Published 17 April 2014

Academic Editor: Xiaochun Xu

Purpose. Vasculogenic mimicry (VM) was related to invasion and metastasis of head and neck squamous cell carcinoma (HNSCC) patients. This study was designed to investigate the role of EphA2 in VM formation of HNSCC. *Methods*. The SiRNA technique was used to knock down the expression of EphA2 *in vitro*. The ability of cell migration and invasion were measured by transwell and wound healing assays; three-dimensional culture was used to detect the ability of channel-like structure formation; Western blot was used to detect the expression of epithelial-mesenchymal transition- (EMT-) related molecules *in vitro*. Further semiquantitative real-time RT-PCR assays and immunohistochemistry were used to demonstrate expression of EphA2 and EMT-related molecules according to VM presence or not in human tissue. *Results*. Knocking down EphA2 *in vitro* leads to disabled channel-like structure formation, reduction of invasion and migration ability, and reverse of EMT-related markers. Both semiquantitative real-time RT-PCR and immunohistochemistry showed that expressions of EphA2, Twist, and Vimentin were higher in the VM-positive group than in the VM-negative group significantly, while expressions of E-cadherin, claudin4, and DSG-3 were reverse. *Conclusions*. EphA2 played a key role in VM formation of HNSCC through regulation of EMT.

1. Introduction

Head and neck squamous cell carcinoma (HNSCC) is the second main upper respiratory tract tumor following lung cancer by incidence and mortality. The overall survival rate has remained unchanged at approximately 35–70% over the past several decades despite advancements in diagnosis and treatment. It is mainly caused by uncontrolled recurrence and local lymph node metastasis [1]. Thus, there is a demand for the development of new therapeutic targets for HNSCC, taking advantage of the disease's unique qualities.

Traditionally, tumor invasion and metastasis are known to mainly depend on angiogenesis/vasculogenesis. However, the results of studies in HNSCC associating microvessel density and various clinicopathological parameters and/or outcome are still inconclusive [2]. Vasculogenic mimicry (VM) is a new type of blood supplement. It is independent of angiogenesis. VM was constructed by highly invasive and genetically dysregulated tumor cells with a pluripotent embryonic-like genotype [3]. Such tumor cells facilitate plasticity to gain the capability to participate in neovascularization processes combined with extracellular matrix remodeling. Ultimately, a fluid-conducting, matrix-rich meshwork is constructed [4]. It has been earlier described in some mesenchymal tumors [5] and now spread to epithelial carcinomas [4, 6]. VM in synoviosarcoma, rhabdomyosarcoma, and hepatocellular

carcinoma has been reported by the authors' laboratory and collaborators in recent years [7, 8]. Tumors that exhibit VM are related to more aggressive biology and increased tumor-related mortality [9]. We previously identified that VM existed in laryngeal squamous cell carcinoma (LSCC) and contributed to the progression by promoting lymph node metastasis, which was an independent predictor of a poor prognosis of LSCC [10]. However, the pathway through which VM impacts tumor biology remains unclear. Therefore, it is necessary to declare the important biomarkers of VM in HNSCC.

EphA2, an embryonic phenotype, has been confirmed as a key factor promoting VM formation through cell plasticity [11] in melanoma. Wang et al. [12] have demonstrated its application in ovarian cancer by interaction with VEGF-a. However, roles of VM might be variable in different tumors. And whether it plays a specific role in HNSCC remains to be investigated.

In this study, we detected existence of VM in human tissue of HNSCC, as well as in a three-dimensional cell culture. Moreover, further *in vitro* study demonstrated that EphA2 played a key role in VM formation of HNSCC through regulating epithelial-mesenchymal transition (EMT). It may be a potential target molecule for HNSCC therapy in the future.

2. Materials and Methods

2.1. Cell Lines, Culture Conditions, and Reagents. Three human head and neck squamous cell carcinoma (HNSCC) cell lines, Hep-2 (larynx), Tb (tongue), and CNE-2 (nasopharyngeal), were utilized. Hep-2 was obtained from the preclinical medicine cell centre of China Union Medical College. Meanwhile, Tb was presented by the Ninth Peoples' Hospital of Shanghai, and CNE-2 was provided by the Immunology and Biotherapy Laboratory of Tianjin Cancer Hospital. Cells were grown as monolayer in RPMI 1640 supplemented with 10% FBS (Invitrogen) and 0.1% gentamicin sulfate (Invitrogen) at 37°C in a humidified 5% CO_2 atmosphere. The recombinant human epithelial growth factor (EGF) was obtained from R&D Systems (Minneapolis, MN, USA). Alexa 568-phalloidin was attained from Molecular Probes, Inc.

2.2. RNA Interference. Following the manufacturer's instructions, transfection was performed by using Lipofectamine 2000 (Invitrogen) with EphA2-specific siRNA (5′-AATGACATGCCGATCTACATG-3′) and the scramble sequence siRNA (GeneChem, Shanghai, China). Meanwhile, the siRNA construct containing a scrambled sequence was transfected into the cells to generate control cells. The transfected cells were selected on the basis of their resistance to Hygromycin B (BD Biosciences, San Jose, CA, USA). Rescue experiments were carried out for migration, invasion, chemotaxis, and Western blotting analysis. The expression of EphA2 protein was monitored by Western blotting to establish cell lines stably expressed by the mutant proteins.

2.3. Western Blotting Analysis. Western blotting analysis was performed as previously described [13]. The antibodies against EphA2, E-cadherin, claudin4, DSG-3, Twist, and Vimentin were acquired from Santa Cruz Biotechnology, Inc.

2.4. Three-Dimensional Cultures. A total of 100 microliters of Matrigel (Invitrogen) and 100 microliters of cells (5×10^6/mL) were dropped into a 24-well plate and allowed to polymerize for 1 hr at 37°C. Another 100 microliters of culture fluid was added to the well, blended, and incubated for 10 days. Culture fluid was replaced every two days. The culture lasted for about 30 days when cells began to die.

2.5. Wound Healing Assay and Invasion Assay. Wound healing assay was performed as previously described by Guo et al. [14]. The speed of wound closure was monitored by phase-contrast microscopy at 0, 3, 6, 9, 12, and 24 h time points. Chemotaxis assay was performed in a 48-well Boyden chamber as described by Sun et al. [15]. A Boyden chamber invasion assay was performed as previously described by Albini et al. [16].

2.6. Patients and Tumor Samples. This study enlisted a total of 203 patients with histopathologically diagnosed HNSCC and treated at the Tianjin Cancer Hospital's Department of Head and Neck Surgery from January 1990 to January 2003. All the cases have complete data of clinical pathological and follow-up. The Otorhinolaryngology Head and Neck Department of Tianjin First Central Hospital offered fresh freezing tissues. The Tianjin Cancer Hospital's and the Tianjin First Central Hospital's ethics committee approved the study protocol.

2.7. Immunohistochemistry of Monostaining and Double Staining and Regents. Monostaining of EphA2, E-cadherin, claudin4, DSG-3, Twist, and Vimentin and double staining of CD31/periodic acid-Schiff (PAS) for VM were performed as previously described by Sun et al. [17].

The antibodies against EphA2, E-cadherin, claudin4, DSG-3, Twist, and Vimentin were acquired from Santa Cruz Biotechnology, Inc. CD31 was purchased from Zhongshan Golden Bridge Biotechnology Co. Ltd., Beijing, China. The 0.5% periodic acid and Schiff solutions were prepared in Department of Pathology in Tianjin Cancer Hospital.

2.8. Evaluation of the Staining. VM was roughly identified using hematoxylin-eosin staining slides. By subsequent double staining, it can be identified as PAS-positive loops surrounded by tumor cells (not endothelial cells), with or without red blood cells. The above 203 cases of head and neck squamous cell cancer were subsequently divided into two groups: VM positive (43 cases) and VM negative (160 cases). The semiqualitative method recorded by the staining index (SI) [17] was employed to investigate the expression of EphA2, E-cadherin, claudin4, DSG-3, Twist, and Vimentin. The positive index (PI) was employed to evaluate the expression of Twist and Vimentin.

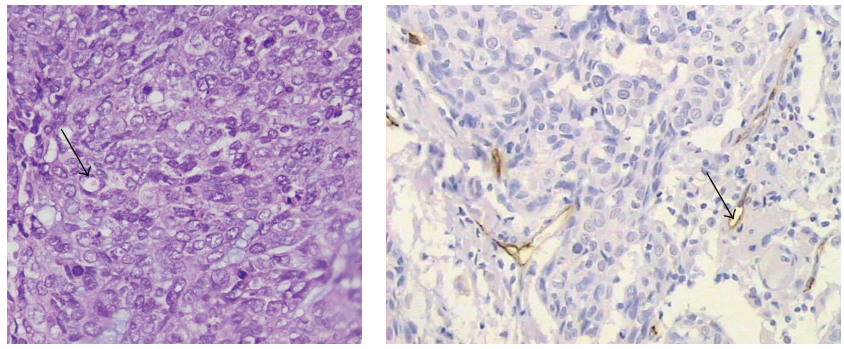

(a) (b)

Figure 1: Identifying VM and EDV by PAS and CD31 double staining ((a), (b)). (a) The VM channel (black arrow) in human sample is formed by head and neck squamous carcinoma cells. There are red blood cells in the center of the channel. PAS-positive substances line the channel and form a basement membrane-like structure (pink) (magnification: ×400). (b) Endothelium-dependent vessels (black arrows) are lined by spindle-shape endothelial cells, which are stained by CD31 (brown). The vessels' basement membrane is positive for PAS staining (pink) (magnification: ×200).

2.9. Quantitative Real-TimeRevers Transcription-Polymerase Chain Reaction Analysis. The real-time RT-PCR analysis was done as described [18]. The results were expressed as n-fold differences in target gene expression relative to the GAPDH, which represents the relative expression value of each sample's targeted gene. The primers of forward and reverse were exhibited below: EphA2 5′-*CCG CAA CAT CCT CGT CAA C*-3′; 5′-*ACA ATG CCA AAG CTC CAC ACG TC*-3′; E-cadherin 5′-*GTG GTC AAA GAG CCC TTA CT*-3′; 5′-*TGG TGC AAC GTC GTT ACG AG*-3′; claudin4 5′-*AGG CCA AGA CCA TGA TCG T*-3′; 5′-*CCA CCA GCG GAT TGT AGA AG*-3′; DSG-35′-*GAT AAT GAA GGC GCA GAT*-3′; 5′-*CCA TAA CCG CTG TCT TTA GAG G*-3′; Twist 5′-*ACA CTA GGC CAC GCA TCT*-3′; 5′-*CTC AGC ATA CCC AAT AGG CA*-3′; Vimentin5′-*GGG AGT CCG CAG TCT TAC GA*-3′; 5′-*TCC AGA CCG AGA AGG CGT AG*-3′; GAPDH 5′-*AGATCCACAACGGATACATT*-3′; 5′-*TATGACAACTCCCTCAAGAT* -3′.

2.10. Statistical Analysis. All analyses were performed using the SPSS software (v.15.0, Chicago, IL). Statistical significance was set at $P < 0.05$. All the results were obtained from at least three separate experiments.

3. Results

3.1. Identification of VM. VM existed in HNSCC (Figure 1(a)). It showed that VM was formed by tumor cells, but not endothelial cells, without hemorrhage, necrosis, or inflammatory cells infiltrating these structures. VM was identified through the detection of PAS-positive loops surrounding tumor cells (not endothelial cells), with or without red blood cells. In CD31-stained slides, there were no positive cells in VM. Recent discoveries in the field of melanoma and ovarian cancer research have suggested that the vasculogenic-like patterned networks formed by tumor cells *in vitro* may account for a subcategory of highly viable, nonangiogenic tumors seen *in vivo* [3, 4]. The endothelium-dependent vessel showed a CD31-positive endothelial cell to form the vessel wall (Figure 1(b)). We also performed three-dimensional cell culture in Matrigel in three HNSCC cell lines, Hep-2, Tb, and CNE-2 cells, to assess their ability to form vasculogenic structure *in vitro*. All of them were able to invariably form vasculogenic-like tube structure. Microscopic observation of the network evolution revealed steady outgrowths which developed into tubular patterns interconnecting spheroidal nests of cells (Figure 2(c)).

3.2. Downregulating the Expression of EphA2 Impaired Channel-Like Structure Formation and the Upregulation of EphA2 Retrieved Its Ability. EphA2 is a transmembrane tyrosine kinase receptor involved in signal-transduction pathways that functions in the regulation of cellular adhesion, migration, and invasion [11, 19]. Overexpression of EphA2 had been observed in many human cancers. The expression of EphA2 in three HNSCC cell lines, Hep-2, Tb, and CNE-2 cells, was first examined by Western blotting. SiRNA technology was applied to inhibit EphA2 expression. A scrambled sequence of siRNA was transfected into the cells to generate control cells, which were designated as scr/HNSCC cells. Later construction of cells overexpressed EphA2 was to build rescued group. Transfected cells were screened for EphA2 expression using Western blotting analysis (Figure 2(a)). The cells were selected by Hygromycin B resistance to establish cell lines that stably downregulated or upregulated expression of EphA2. Following Hygromycin B selection, transfected cells were screened for EphA2 expression using Western blotting analysis. Almost 70–80% of EphA2 protein levels were reduced in siEphA2/HNSCC cells compared with those in scr/HNSCC cells. And the rescued cell appeared to reestablishment of EphA2 in all three cell lines.

To investigate the role of EphA2 in the formation of tubular networks, cells were cultured in Matrigel. Scr/HNSCC cells and rescued cells appeared to form channel-like structures around the 7th day. The presence of a network persisted

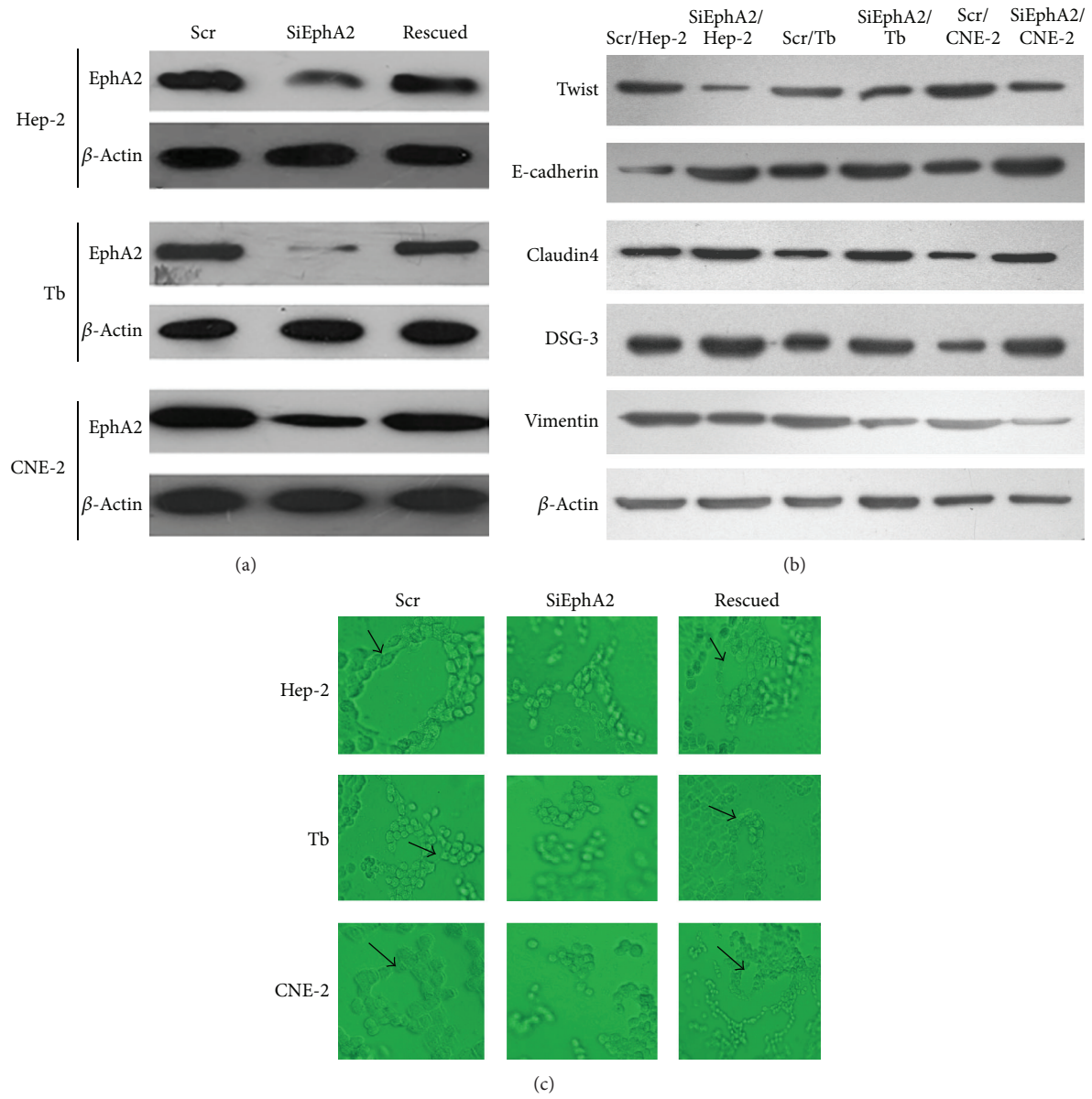

Figure 2: Three-dimension cell culture in three HNSCC cell lines (Hep-2, Tb, and CNE-2) ((a), (b), and (c)). (a) The protein expression of EphA2 was inhibited by siRNA and retrieved after a sequence of overexpression of EphA2 was transfected into siEphA2 cells, which were monitored by Western blotting. (b) Disruption of EphA2 by siRNA leading to the change expression of EMT-related molecules measured by Western blotting. There was a decreasing expression of Twist and Vimentin and an increasing expression of E-cadherin, claudin4, and DSG-3 compared with the control cells ($P < 0.05$). (c) Hep-2, Tb, and CNE-2 cell lines can construct channel-like structures in Matrigel. All cell lines lost the capability to form channel-like structures in Matrigel after EphA2 was knocked down compared with the control cells. And regaining of EphA2 expression reconstructed channel-like networks formation in three cell lines. The black arrows represent the cross-section of the tubular networks, indicating that they contain hollow lumen-like structures (original magnification: ×400).

for about 30 days. Then cells began to die and experiments were generally terminated. The siEphA2/HNSCC cells seemed to fail to construct channel-like structures during this period. Knocking down EphA2 in cell lines showed marked inability to form vasculogenic-like structure compared with control cells, while upregulating EphA2 leads cell lines to regain ability of channel-like networks formation (Figure 2(c)). We suggested that EphA2 may play a key role in VM formation in HNSCC cell lines.

3.3. Downregulating the Expression of EphA2 Impaired Migration and Invasion of HNSCC Cells and Upregulating EphA2 Regained Their Capacity of Migration and Invasion. It has been recognized that VM was associated with tumor invasion and metastasis [9, 20]. EphA2 may be a regulator in VM formation. In order to examine how EphA2 affects cell migration and invasion, we performed wound healing assay and cell chemotaxis assay. Scratch assay, an *in vitro* wound healing assay, is a method for evaluating cell migration capacity. It was

observed that scr/HNSCC cells and rescued cells migrated into the wound and resulted in wound narrowing within 24 h, whereas siEphA2/HNSCC cells were significantly less mobile (Figure 3) as supported by the delay in the mean distance of closure. All the cells were maintained in a medium supplemented with 0.5% FBS to block cell proliferation, which could otherwise account for gap closure. Taken together, our results obviously showed that EphA2 reduction by siRNA impaired the migration and that EphA2 was required for migration of HNSCC cells.

Another method is chemotaxis referring to directional cell movement dependent on a concentration gradient. Robust chemotaxis of the siEphA2/HNSCC cells, scr/HNSCC cells, and rescued cells induced by EGF appeared in a dose-dependent manner, although the chemotaxis of the siEphA2/HNSCC cells was impaired in response to EphA2 reduction. These results revealed that EphA2 was required for HNSCC cell chemotaxis, while a concentration gradient was required for efficient migration in response to EGF (Figure 4(a)). Subsequently, Boden chamber invasion assays were utilized to confirm the three HNSCC lines' different invasive capabilities after EphA2 knockdown. Knockdown of EphA2 in cell lines significantly reduced the invasion capability compared with the control cells (Figure 4(b)), while overexpression of EphA2 retrieved the ability of invasion in all cell lines. Both results indicated that EphA2 knockdown may decrease migration and invasion capabilities of HNSCC cells. We speculated from our study that VM contributed to invasion and metastasis of HNSCC, and EphA2 may play a key role in this process.

3.4. Downregulating the Expression of EphA2 Reversed EMT. Similar to VM, EMT is another phenomenon of acquiring the capability of invasion and metastasis by changing into an embryonic genotype. Recently, it has been consistently demonstrated in epithelial malignancies [21, 22]. It is a type of plasticity during which epithelial cells lose many of their characteristics and acquire properties typical to mesenchymal cells. A key point of EMT is the reduction of cell-cell adhesion by transcriptional repression of cadherins (adherens junctions), occludin and claudin (tight junctions), and desmoplakin (desmosomes) [23–25]. The expression of intermediate filaments is also changing during EMT, such as Vimentin, being typical of mesenchymal cells. In addition, transcription factors, which induced EMT, also play a key role, such as Twist, Snail, Slug, SIP1/ZEB2 (Smad Interacting Protein)/(zinc finger E-box binding homeobox), deltaEF1/ZEB1, and the basic helix-loop-helix (HLH) transcription factor E47. To reveal the role of EphA2 during EMT, we inhibited EphA2 by siRNA to observe changing of EMT-related molecules in three HNSCC cell lines. It was showed that Twist and Vimentin decreased in protein expression, while epithelial adhesion markers E-cadherin, claudin 4, and DSG-3 increased compared with the control cells (Figure 2(b)). It is interesting to speculate that highly aggressive epithelial tumor cells may likewise overexpress the mesenchymal phenotype through the EMT procedure to facilitate VM formatting. EphA2 may impact VM formation through regulating EMT.

3.5. Relationship of VM and Expression of EphA2 and EMT-Related Molecules in HNSCC. To further validate the above conclusion, we detected VM and expression of EphA2 and EMT-related molecules in human samples of HNSCC. Semiquantitative real-time RT-PCR was performed to detect correlated gene expression on 24 cases of frozen tumor tissue (12 VM-positive cases and 12 VM-negative cases). mRNA expression of EphA2 ($P = 0.023$), Twist ($P = 0.001$), and Vimentin ($P = 0.024$) was significantly higher in the VM-positive group than in the VM-negative one, while E-cadherin ($P = 0.035$), claudin4 ($P = 0.034$), and DSG-3 ($P = 0.022$) were significantly lower in the VM-positive group than in the VM-negative one (Figure 5(a)). Furthermore, by immunohistochemistry, EphA2, E-cadherin, claudin4, DSG-3, and Vimentin were found to be expressed in cytoplasm of HNSCC cells. Twist was expressed mainly in the nucleus (Figure 5(d)). The SI of EphA2 ($P = 0.004$) (Figure 5(b)) and PI of Twist ($P = 0.039$) and Vimentin ($P = 0.044$) (Figure 5(c)) were higher in the VM-positive group than in the VM-negative one, while the SI of E-cadherin ($P = 0.044$) (Figure 5(b)), claudin4 ($P = 0.006$), and DSG-3 ($P = 0.032$) were significantly lower in the VM-positive group than in the VM-negative one (Figure 5(c)). We deduced from our study that expressions of EphA2 and EMT-related molecules are associated with VM formation in HNSCC.

4. Discussion

VM refers to the *de novo* generation of tumor microcirculation without participation of endothelial cells. It was first reported in melanoma by Maniotis in 1999 [3]. Previous research has demonstrated existence of VM in most mesenchymal tumors. We first identified that VM existed in squamous cell carcinoma to disclose the secret why we fail to explain invasion and metastasis only by angiogenesis and being inefficient in antiangiogenesis therapy for HNSCC clinically [10]. In this study, we further illustrated that EMT regulated by EphA2 contributed to VM formation in HNSCC. It elucidated the possibility that VM also existed in epithelial neoplasm besides mesenchymal tumors. Our study demonstrates one more time that VM is not an individual event but a general phenomenon during tumor growth, being a functional microcirculation [26].

Tumors with VM have more capacity of invasion and metastasis [9, 20] and predict poor clinical outcome among tumor patients [8]. We posited from our previous study that VM was more likely to contribute to lymph node metastasis and was an unfavorable prognostic factor among LSCC patients (data not shown). Nasu et al.'s [27] and Sood et al.'s [4] study on melanoma cell lines also demonstrated that VM was linked to the aggressive tumor cell phenotype. The highly invasive melanoma cell line was successful in forming VM, while the low-invasive melanoma cell line failed to form VM. Further, our present study explored the mechanism of VM formation in HNSCC. Many factors are necessary in VM formation, including the microenvironment, the interaction between tumor cells and their surroundings, changing to endothelial genotype of the tumor cells, and extracellular

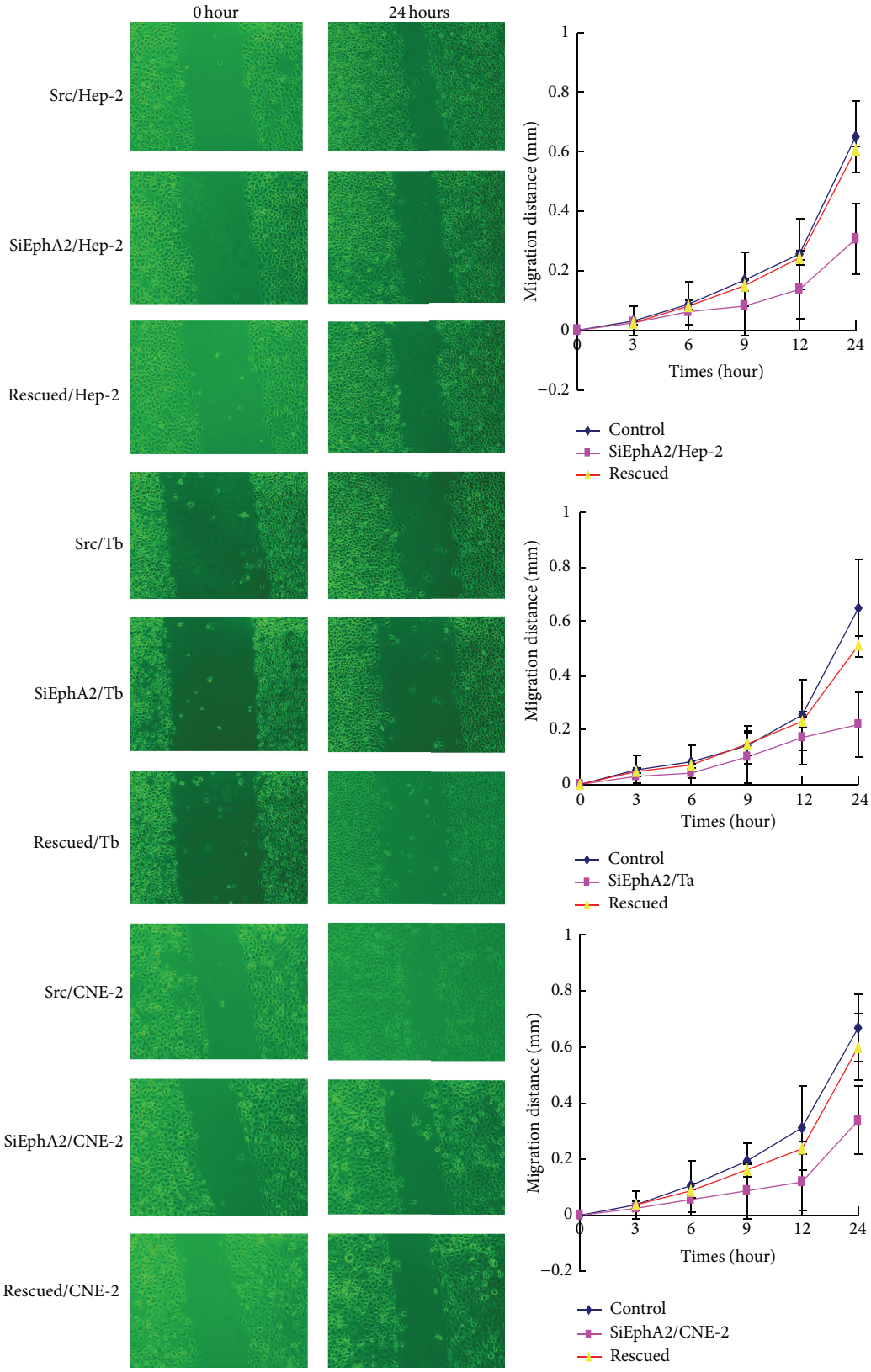

Figure 3: Wound healing assays in HNSCC cell lines. Three HNSCC cell lines knocking down EphA2 strongly reduced the capability of migration compared with the control cells and rescued cells ($P < 0.05$).

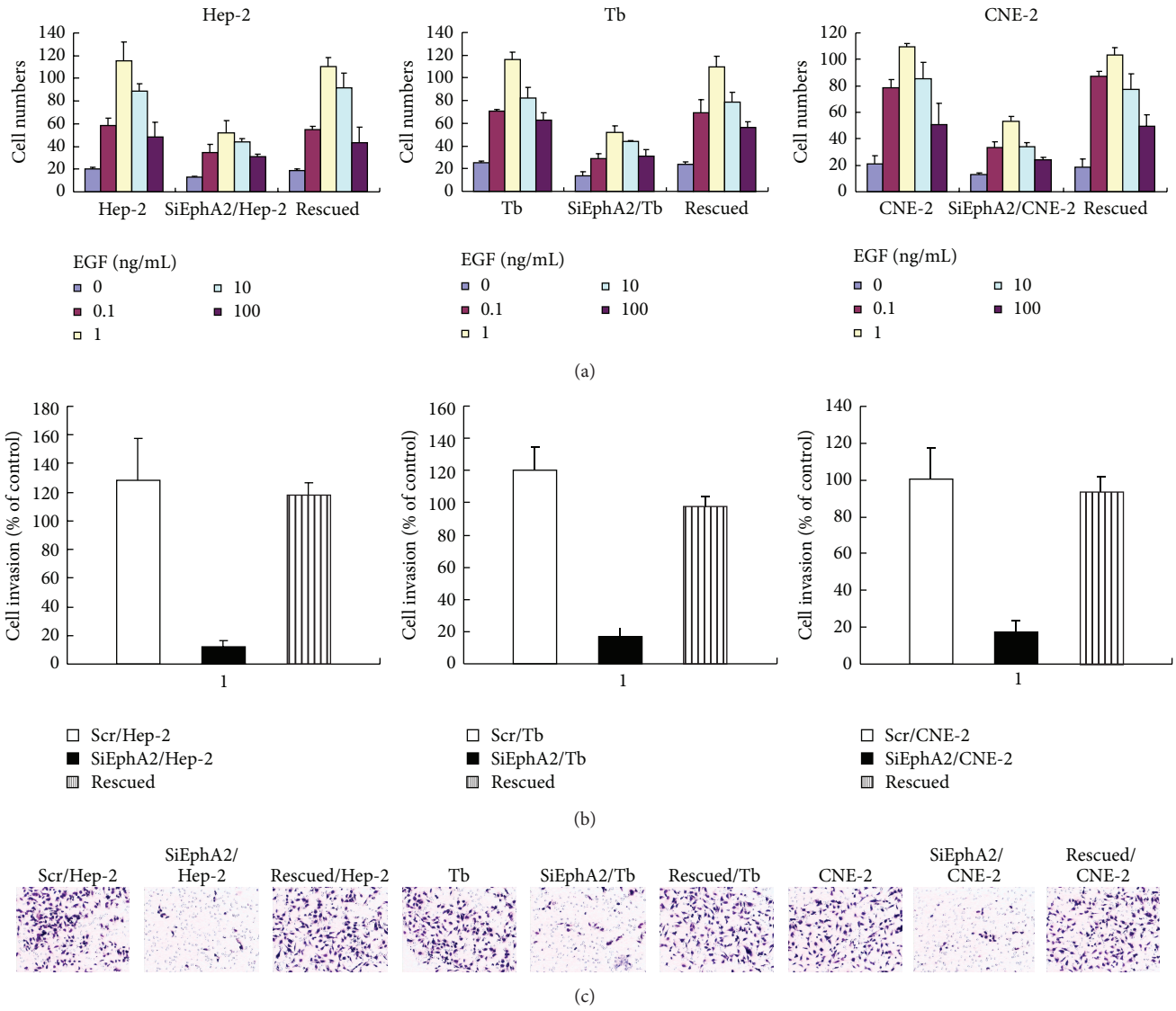

Figure 4: Chemotaxis and invasion assays in HNSCC cell lines. (a) SiEphA2/HNSCC cells, scr/HNSCC cells, and rescued cells induced by EGF appeared in a dose-dependent manner, although the chemotaxis of the siEphA2/HNSCC cells was impaired in response to EphA2 reduction. Chemotaxis assays showed that 1 ng/mL EGF was the optimization concentration for transwell. (b) Invasion assays. There was a remarkably reduced invasion in HNSCC cell lines compared with the control cells and rescued cells ($P < 0.05$).

matrix remodeling. EphA2 was first revealed by Hess et al. [11] which promoted VM formation through dephosphorylation of FAK and remodeling of extracellular matrix in VM formation in melanoma. Our study suggested that EphA2 may be a critical regulator for VM formation, cell migration, and invasion in HNSCC. However, unlike that in melanoma, our study focused on the changing of cell adhesion and cell plasticity regulated by EphA2 in terms of EMT.

Similar to VM, EMT is well correlated with invasion and lymph node metastasis [28]. It is a normal process in embryonic development in which epithelial cells transform into mesenchymal cells. It has likewise been reported to exist in HNSCC. Our study of *in vitro* and human samples demonstrated existence of VM related to the expression of EMT-related molecules. In addition, Maniotis et al.'s [3] analysis *in vitro* through cDNA microarray suggested that melanoma cells overexpressed both epithelial phenotype and mesenchymal phenotype correspondingly. The latter was a type VI collagen, a component of the extracellular matrix which was a major component of VM. It is interesting to speculate that highly aggressive epithelial tumor cells may likewise overexpress the mesenchymal phenotype through EMT during VM formation. Further, our study *in vitro* showed that EphA2 regulated both channel-like tubular formation and expression of EMT-related molecules. Changing of EMT is accompanied by the presence of VM. We conjectured from the above that EMT may be an alternative mechanism of VM formation in epithelial neoplasm. And further investigation is being done to explore new cotherapeutic targets for HNSCC treatment.

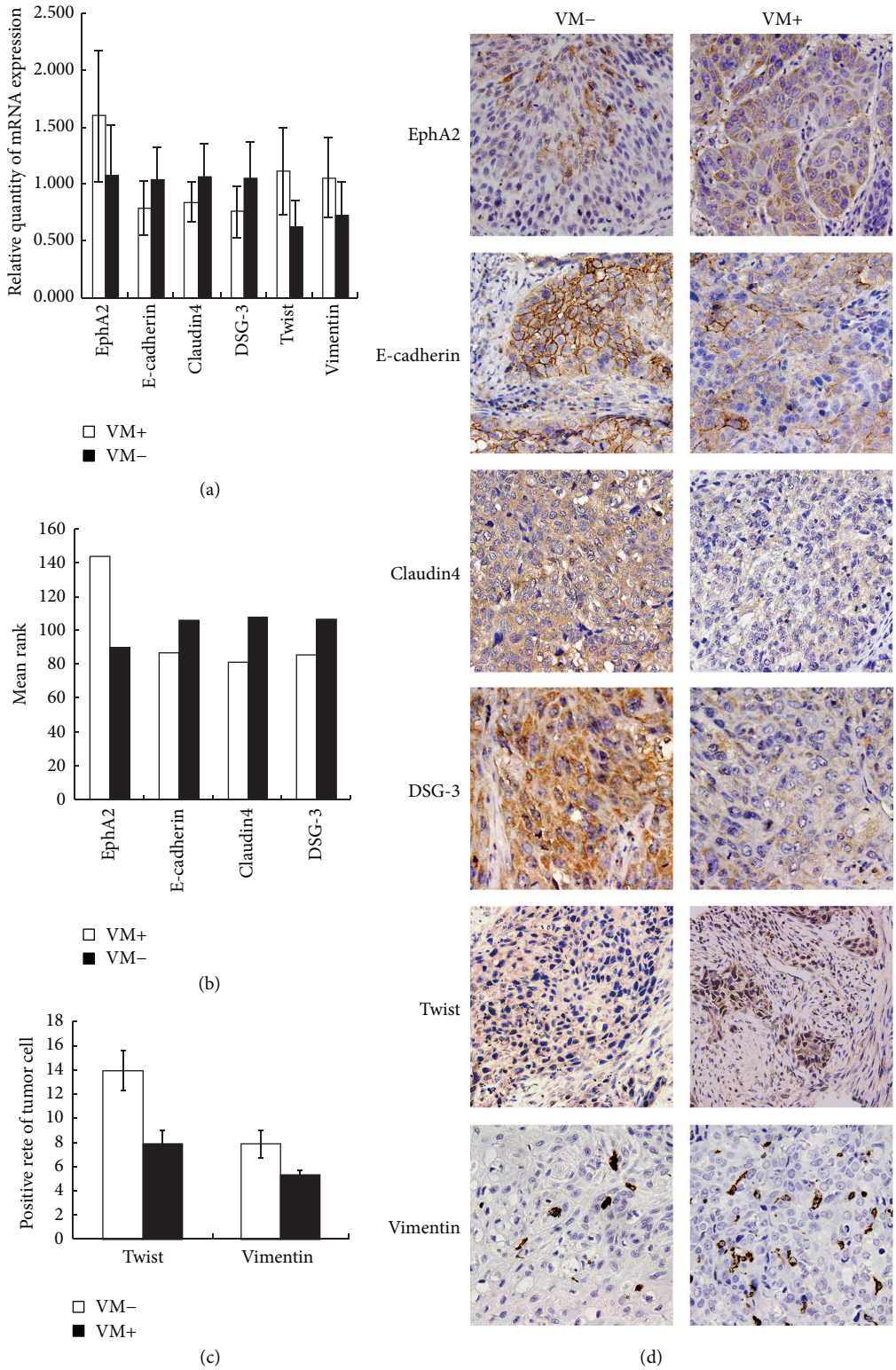

Figure 5: Different expressions of VM-related molecules in HNSCC patients between the VM-positive group and VM-negative group ((a), (b), (c), and (d)). (a) Different mRNA expressions of EphA2 ($P = 0.023$), E-cadherin ($P = 0.035$), claudin4 ($P = 0.034$), DSG-3 ($P = 0.022$), Twist ($P = 0.001$), and Vimentin ($P = 0.024$) between the VM-positive group and VM-negative group. (b) Different protein expressions of EphA2 ($P = 0.004$), E-cadherin ($P = 0.044$), claudin4 ($P = 0.006$), and DSG-3 ($P = 0.032$) between the VM-positive group and VM-negative group by immunohistochemistry. (c) Different protein expressions of Twist ($P = 0.039$) and Vimentin ($P = 0.044$) between the VM-positive group and VM-negative group by immunohistochemistry. (d) By immunohistochemistry, EphA2, E-cadherin, claudin4, DSG-3, and Vimentin were found to be expressed in cytoplasm of HNSCC cells. Twist was expressed mainly in the nucleus.

In summary, EphA2 plays a key role in VM formation in HNSCC through regulation of EMT. EMT may be an alternative mechanism of VM formation in HNSCC different from the mesenchymal tumor which depended more on remodeling of extracellular matrix. Those who are relying on conventional markers of tumor "vascularity" as prognostic markers and who are developing anticancer therapies by targeting angiogenesis should exercise caution concerning VM when interpreting their results. Further, combination of EphA2 and certain EMT-related molecules might be a potential therapeutic target for VM to control invasion and metastasis of HNSCC.

Abbreviations

HNSCC: Head and neck squamous cell carcinoma
LSCC: Laryngeal squamous cell carcinoma
VM: Vasculogenic mimicry
EDV: Endothelium-dependent vessel
EMT: Epithelial-mesenchymal transition
EphA2: Ephrin type-A receptor 2
PCR: Polymerase chain reaction
SI: Staining index
PI: Positive index
DSG-3: Desmoglein-3.

Conflict of Interests

The authors declare that there is no conflict of interests regarding the publication of this paper.

Acknowledgments

This study was supported by Grants from the National Natural Science foundation of China (no. 30830049), International Cooperation Programme of China and Sweden (Grant no. 09ZCZDSF04400), the National Natural Science Foundation of China (no. 81102055), and Tianjin Natural Science Foundation (no. 11JCYBJC10700).

References

[1] D. Chin, G. M. Boyle, S. Porceddu, D. R. Theile, P. G. Parsons, and W. B. Coman, "Head and neck cancer: past, present and future," *Expert Review of Anticancer Therapy*, vol. 6, no. 7, pp. 1111–1118, 2006.

[2] J. J. Homer, J. Greenman, and N. D. Stafford, "Angiogenesis in head and neck squamous cell carcinoma," *Clinical Otolaryngology and Allied Sciences*, vol. 25, no. 3, pp. 169–180, 2000.

[3] A. J. Maniotis, R. Folberg, A. Hess et al., "Vascular channel formation by human melanoma cells *in vivo* and *in vitro*: vasculogenic mimicry," *The American Journal of Pathology*, vol. 155, no. 3, pp. 739–752, 1999.

[4] A. K. Sood, E. A. Seftor, M. S. Fletcher et al., "Molecular determinants of ovarian cancer plasticity," *The American Journal of Pathology*, vol. 158, no. 4, pp. 1279–1288, 2001.

[5] R. Folberg and A. J. Maniotis, "Vasculogenic mimicry," *APMIS*, vol. 112, no. 7-8, pp. 508–525, 2004.

[6] A. K. Sood, M. S. Fletcher, J. E. Coffin et al., "Functional role of matrix metalloproteinases in ovarian tumor cell plasticity," *The American Journal of Obstetrics and Gynecology*, vol. 190, no. 4, pp. 899–909, 2004.

[7] B. Sun, S. Zhang, X. Zhao, W. Zhang, and X. Hao, "Vasculogenic mimicry is associated with poor survival in patients with mesothelial sarcomas and alveolar rhabdomyosarcomas," *International Journal of Oncology*, vol. 25, no. 6, pp. 1609–1614, 2004.

[8] B. Sun, S. Zhang, D. Zhang et al., "Vasculogenic mimicry is associated with high tumor grade, invasion and metastasis, and short survival in patients with hepatocellular carcinoma," *Oncology Reports*, vol. 16, no. 4, pp. 693–698, 2006.

[9] R. Folberg, M. J. C. Hendrix, and A. J. Maniotis, "Vasculogenic mimicry and tumor angiogenesis," *The American Journal of Pathology*, vol. 156, no. 2, pp. 361–381, 2000.

[10] W. Wang, P. Lin, C. Han, W. Cai, X. Zhao, and B. Sun, "Vasculogenic mimicry contributes to lymph node metastasis of laryngeal squamous cell carcinoma," *Journal of Experimental & Clinical Cancer Research*, vol. 29, p. 60, 2010.

[11] A. R. Hess, E. A. Seftor, L. M. G. Gardner et al., "Molecular regulation of tumor cell vasculogenic mimicry by tyrosine phosphorylation: role of epithelial cell kinase (Eck/EphA2)," *Cancer Research*, vol. 61, no. 8, pp. 3250–3255, 2001.

[12] J. Y. Wang, T. Sun, X. L. Zhao et al., "Functional significance of VEGF-a in human ovarian carcinoma: role in vasculogenic mimicry," *Cancer Biology & Therapy*, vol. 7, no. 5, pp. 758–766, 2008.

[13] T. H. Hu, C. C. Huang, L. F. Liu et al., "Expression of hepatoma-derived growth factor in hepatocellular carcinoma: a novel prognostic factor," *Cancer*, vol. 98, no. 7, pp. 1444–1456, 2003.

[14] H. Guo, F. Gu, W. Li et al., "Reduction of protein kinase C ζ inhibits migration and invasion of human glioblastoma cells," *Journal of Neurochemistry*, vol. 109, no. 1, pp. 203–213, 2009.

[15] R. Sun, P. Gao, L. Chen et al., "Protein kinase C ζ is required for epidermal growth factor-induced chemotaxis of human breast cancer cells," *Cancer Research*, vol. 65, no. 4, pp. 1433–1441, 2005.

[16] A. Albini, Y. Iwamoto, and H. K. Kleinman, "A rapid *in vitro* assay for quantitating the invasive potential of tumor cells," *Cancer Research*, vol. 47, no. 12, pp. 3239–3245, 1987.

[17] B. Sun, S. Qie, S. Zhang et al., "Role and mechanism of vasculogenic mimicry in gastrointestinal stromal tumors," *Human Pathology*, vol. 39, no. 3, pp. 444–451, 2008.

[18] Y. H. Wu, Y. W. Cheng, J. C. Tsai, T. C. Wu, C. Y. Chen, and H. Lee, "Reduced XPC messenger RNA level may predict a poor outcome of patients with nonsmall cell lung cancer," *Cancer*, vol. 110, no. 1, pp. 215–223, 2007.

[19] P. Ganju, K. Shigemoto, J. Brennan, A. Entwistle, and A. D. Reith, "The Eck receptor tyrosine kinase is implicated in pattern formation during gastrulation, hindbrain segmentation and limb development," *Oncogene*, vol. 9, no. 6, pp. 1613–1624, 1994.

[20] T. Mäkitie, P. Summanen, A. Tarkkanen, and T. Kivelä, "Microvascular loops and networks as prognostic indicators in choroidal and ciliary body melanomas," *Journal of the National Cancer Institute*, vol. 91, no. 4, pp. 359–367, 1999.

[21] M. A. Huber, N. Kraut, and H. Beug, "Molecular requirements for epithelial-mesenchymal transition during tumor progression," *Current Opinion in Cell Biology*, vol. 17, no. 5, pp. 548–558, 2005.

[22] J. P. Their, "Epithelial-mesenchymal transitions in tumor progression," *Nature Reviews Cancer*, vol. 2, no. 6, pp. 442–454, 2002.

[23] A. Eger, K. Aigner, S. Sonderegger et al., "DeltaEF1 is a transcriptional repressor of E-cadherin and regulates epithelial plasticity in breast cancer cells," *Oncogene*, vol. 24, no. 14, pp. 2375–2385, 2005.

[24] S. Spaderna, O. Schmalhofer, F. Hlubek et al., "A transient, EMT-linked loss of basement membranes indicates metastasis and poor survival in colorectal cancer," *Gastroenterology*, vol. 131, no. 3, pp. 830–840, 2006.

[25] S. Spaderna, O. Schmalhofer, M. Wahlbuhl et al., "The transcriptional repressor ZEB1 promotes metastasis and loss of cell polarity in cancer," *Cancer Research*, vol. 68, no. 2, pp. 537–544, 2008.

[26] A. J. Mueller, D. U. Bartsch, R. Folberg et al., "Imaging the microvasculature of choroidal melanomas with confocal indocyanine green scanning laser ophthalmoscopy," *Archives of Ophthalmology*, vol. 116, no. 1, pp. 31–39, 1998.

[27] R. Nasu, H. Kimura, K. Akagi, T. Murata, and Y. Tanaka, "Blood flow influences vascular growth during tumour angiogenesis," *British Journal of Cancer*, vol. 79, no. 5-6, pp. 780–786, 1999.

[28] M. Mandal, J. N. Myers, S. M. Lippman et al., "Epithelial to mesenchymal transition in head and neck squamous carcinoma: association of Src activation with E-cadherin down-regulation, vimentin expression, and aggressive tumor features," *Cancer*, vol. 112, no. 9, pp. 2088–2100, 2008.